A Constitutive Model for the Compression Behavior of Old Alluvium

by

Maria – Aikaterini Nikolinakou

Diploma, Civil Engineering (1999)
National Technical University of Athens, Greece

Master of Science, Civil and Environmental Engineering (2001)
Massachusetts Institute of Technology, USA

SUBMITTED TO THE DEPARTMENT OF
CIVIL AND ENVIRONMENTAL ENGINEERING
IN PARTIAL FULFILLMENT OF THE REQUIREMENTS FOR THE DEGREE OF
DOCTOR OF SCIENCE IN THE FIELD OF GEOTECHNICAL AND
GEOENVIRONMENTAL ENGINEERING

MASSACHUSETTS INSTITUTE OF TECHNOLOGY

June 2008

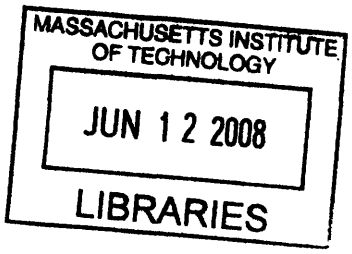

ARCHIVES

Signature of Author.....
Department of Civil and Environmental Engineering
May 21, 2008

Certified by.....
Andrew J. Whittle
Professor of Civil and Environmental Engineering
Thesis Supervisor

Accepted by.....
Daniele Veneziano
Chairman, Departmental Committee for Graduate Students

A Constitutive Model for the Compression Behavior of Old Alluvium

by

Maria – Aikaterini Nikolinakou

Submitted to the Department of Civil and Environmental Engineering
on May 21, 2008, in Partial Fulfillment of the Requirements for the degree of
Doctor of Science in the field of Geotechnical and Geoenvironmental Engineering

ABSTRACT

Old Alluvium is classified as a transported, in-situ weathered tropical soil, and represents a class of geomaterials that have a complex microstructure, including cemented aggregates at the meso-scale and groups of clay stacks at the micro-scale. Despite the presence of significant fractions of nontronite (smectite species), the activity of charged clay particles is initially masked by the aggregation of iron oxides. Compression loading breaks the cementation at the meso-scale and causes physico-chemical changes at the micro-scale, which reveal the expansive characteristics of the clay minerals. It is difficult to achieve a fully disaggregated condition (through mechanical mixing or selective chemical dissolution) and hence, there is little practical value in referencing properties of the intact soil to a hypothetical disaggregated or intrinsic state as proposed for other bonded soils.

The proposed formulation describes the variation of compressibility according to a measure of the microstructural changes using the Cation Exchange Capacity as a state variable. Upon load reversal, a model based on double layer theory is integrated to predict macroscopic volumetric expansion due to the swelling of the nontronitic clay fraction. This behavior is also linked to the Cation Exchange Capacity through the preconsolidation stress level, and hence, can accommodate changes in the clay swelling potential caused by mechanical or physicochemical loading.

The model parameters depend on the compression characteristics of the intact soil, on measurements of the Cation Exchange Capacity in the intact and partially disaggregated states, on the amount of expandable minerals in the microstructure and on the initial hydration of the clay stacks.

Overall, the proposed formulation introduces a new way of modeling the compression of bonded materials with evolving microstructural characteristics, which does not require a unique reference state. It builds the swelling response directly on the physicochemical characteristics of the soil. The thesis also includes an experimental program on block samples obtained from a tunneling project in San Juan, Puerto Rico. The laboratory data was used for the calibration and detailed validation of model predictions. The proposed formulation enables predictions of expected engineering properties through the vertical weathering profile of the Old Alluvium.

Thesis Supervisor: Andrew J. Whittle

Title: Professor of Civil and Environmental Engineering

Acknowledgments

During the course of this dissertation, many many people became part of my academic or personal life and I am grateful to all of them, who in one way or another helped me finish this Thesis and become the person I am today. There are certain people however whom I would particularly like to acknowledge:

Prof. Whittle, my thesis supervisor, who always guided me with clear direction through this modeling task that many times seemed impossible. During my dissertetion years, I have learned a lot through the various research and teaching assignements I did with him

Prof. Einstein, who has always been a great mentor for me, who helped me with the geological understanding of Old Alluvium, and who gave me the opportunity to work with him in his educational projects

Dr. Germaine, who introduced me to the lab-world and helped me with the experiments, and who showed us how to be cheerful under any circumstances

Prof. Ulm, for the most exciting teaching of poromechanics, and his advice on my work

Prof. Kausel, who never missed an opportunity to introduce me to some visiting Professor

Prof. Ochsendorf, who brought me closer to my dream of studying historic structures, and who treated me as if I were his own student

Prof. Tallon, who helped me view engineering through the perspective of an art historian, and who became a good friend even though I doubt we have been more than 50 hours in the same location

The George and Marie Vergottis Foundation for their fellowship support

Prof. Marinos, who is responsible for my career as a Geotechnical Engineer and Dr Koubis, who first made me love Geology

Prof. Gazetas, Gantes, Kavvadas and Boukovalas, who insisted in me going to MIT

Sheila who keeps this group in order (practically and mentally), Alice who took care of us during my first years, Anthee, Pat and Cynthia for their support all these years

Steve Rudolph, who always helps us in the lab

The many geotechnical friends: Sophie, Pong, Engsew, Mike, Sherif, Antonis, Charisis, Naeem, Bruno, Jay, Yvonne, Gonzalo, Ralf, Nuria…

My non geo-friends, and especially Cansu Tunca, Antonino Vaccaro, Midori Taki, Sondra Aiello, Cara DeJong

My long time classmates and friends Kartal Toker, Jean-Louie Locsin, Jianyong Pei and Anamika Prasad.

Carlos and Pilar Regalado, who helped me many times to avoid misery

The many Greeks who never let you feel homesick, and especially George Constantinides, Anna Pisania, Thodoris Konstantakopoulos, and Panos Papapetrou

Dimitris Illiadelis, Simos Gerasimidis and the infamous 533, who took care of me as their big sister

Panagiotis Kavouklis, Yannis Chatzigiannelis, Youli Konstantinopoulou and Christina Samaraki who remained good friends despite the transatlantic distance

Angeliki Stathopoulou and Yannis Papamichail, with whom I share beautiful memories from many parts of the world

Ricardo Garcia, whom I met my 3rd day in Boston and has been my close friend ever since

Rita Sousa, who shares with me the same love for traveling, good food, wine and …tunnels, and has always been patient with my complaining and my crazy ideas

Andrea Adamo, Aristeidis Karalis, Costas Pelekanakis, Luigi Adamo and Jenn Baltz, who were always there for me during the hard times, the miserable times, the hectic times, but also the best times of my life so far

My aunt, who secretly sponsored many of my trips and extracurricular activities

My sisters, Konstantina and Katerina, who came to study in Boston near me.

My parents who always support me no matter the distance or the circumstances.

TABLE OF CONTENTS

LIST OF TABLES

LIST OF FIGURES

1 Introduction

There is an extensive literature of constitutive models describing the behavior of soils. Elaborate generalized models have been formulated for normally and overconsolidated clays (e.g. MIT-E3, Whittle, 1987; MIT-S1, Pestana, 1994; BBM, Alonso et al, 1990) and freshly deposited sands (MIT-S1, Pestana, 1994). Various models have also been developed for bonded soils or soils that possess some kind of structure (Kavvadas & Amarosi, 2000; Cotecchia & Chandler, 2000; Nova et al, 2003; Alonso & Alcoverro, 2002; Chazallon & Hicher, 1998). Significant efforts have also been put into modeling the behavior of expansive soils (BEM, Alonso et al, 1999; Pinyol & Alonso, 2007; Komine & Ogata, 2004; Loret et al, 2002).

Lately, large construction projects in areas with tropical climates, such as the Central and South Americas, or South-East Asia, have established the need to understand and model soils that are the result of tropical weathering actions. Such soils are characterized by complex microstructures, that often contain expansive minerals and include porous systems at the macro and micro-scale that are not necessarily interconnected.

The present research studies the behavior of the Old Alluvium of Puerto Rico, a transported and in-situ weathered tropical soil, and aims to understand and model its behavior in 1-D compression tests. Following the basic lines of thought of model development at MIT, the formulation is based on observations of soil behavior through extensive and careful laboratory testing. Because of the complexity of the soil structure, these observations included not only the macroscopic response of the material to various modes of compressive loading, but also the detailed study of the structure through observations of the microstructure, mineralogical studies and physicochemical loading (Zhang, 2002).

The goal of this thesis is to develop a constitutive compression model that incorporates the microstructure of the soil and addresses the changes caused in the microscale by external macroscopic loading. The model is formulated such that input parameters and state variables can be directly related to macro or micro-characteristics of the material. In this way, the formulation can be applicable not only to the tropical soil from Puerto Rico, but also generally to soils with complex microstructures.

1.1 ORGANIZATION

Chapter 2 addresses the geological characteristics of the Old Alluvium. It first summarizes the mineralogical and microstructural information available on the soil through the laboratory program performed by Zhang (2002). It then discusses the geological background of the material and examines whether its mineralogical content and structure are typical of tropical soils from similar regions. The chapter further discusses some geological processes and mechanisms associated with the formation tropical soils, in order to form a better understanding of the soil microstructure.

Chapter 3 discusses the 1-D consolidation behavior of the Old Alluvium. It summarizes the compression tests performed by Zhang (2002) and by the Author, as part of the present research. It studies the characteristics of the observed compression behavior and compares them with the main features of the response of granular soils, clays and bonded soils; in this way, the relation of the microstructure with the observed macroscopic behavior is better understood. The chapter further discusses the similarities of Old Alluvium compression characteristics with the response of other Old Alluvial soils, some clays with complex microstructure, and some clayey shales.

Chapter 4 introduces the model proposed for the behavior of the Old Alluvium to virgin compression loading. The formulation is based on the MIT-S1 compression model to which it integrates additional variables that aim to represent the changes in the soil microstructure and how these are translated to the macrostructural response. The chapter gives full details of the procedures required to select the input parameters from standard oedometer tests. It then evaluates the performance of the formulation by comparing the model predictions with the available experimental data.

Chapter 5 introduces the proposed swelling model. The formulation derives from the double layer theory, which is directly connected to the physicochemical characteristics of the soil microstructure. The reloading response is also addressed. Again, the chapter provides detailed description for the selection of the required input parameters. Then, it demonstrates the predictive capabilities of the proposed model not only for the Old Alluvium, but also for other materials with similar microstructural characteristics.

Finally, Chapter 6 presents a summary of the thesis, conclusions from the study of the examined soil behavior and recommendations for further research.

1.2 REFERENCES

Alonso E, Vaunat J, Gens A. (1999): "Modelling the mechanical behavior of expansive clays", Engineering Geology, No 54, 173–183.

Alonso E.E., Alcoverro J. (2002): "Swelling and Degradation of Argillaceous Rocks", Proceedings of the 3rd International Conference on Unsaturated Soils, Recife, Brazil, 3, 951-969.

Alonso, E.E., Gens A., Josa A. (1990): "A constitutive model for partially saturated soils", Géotechnique, 40 (3), 405-430.

Chazallon C., Hicher P. Y. (1998): "A constitutive model coupling elastoplasticity and damage for cohesive-frictional materials", Mechanics of Cohesive-Frictional Materials, 3, 41-63.

Cotecchia F., Chandler R.J. (2000): "A general framework for the mechanical behavior of clays", Géotechnique, 50 (4), 431-447.

Kavvadas M., Amorosi, A. (2000): "A constitutive model for structured soils", Géotechnique, 50 (3), 263-273.

Komine H., Ogata N. (2004): "Predicting Swelling Characteristics of Bentonites", Journal of Geotechnical and Geoenvironmental Engineering, 130 (8), 818 – 829.

Loret B., Hueckel T., Gajo A. (2002): "Chemo-mechanical coupling in saturated porous media: elastic–plastic behaviour of homoionic expansive clays", International Journal of Solids and Structures 39, 2773–2806.

Nova R., Castellanza R., Tamagnini C. (2003): "A constitutive model for bonded geomaterials subject to mechanical and/or chemical degradation", International Journal for Numerical and Analytical Methods in Geomechanics, 27 (9), 705-732.

Pestana J.M. (1994): "A unified constitutive model for clays and sands", Sc.D thesis, Massachusetts Institute of Technology, Cambridge, MA.

Pinyol N., Vaunat J., Alonso E. E. (2007): "A constitutive model for soft clayey rocks that includes weathering effects", Géotechnique, 57 (2), 137–151.

Whittle A.J. (1987): "A constitutive model for overconsolidated clays with application to the cyclic loading of friction piles", PhD thesis, MIT, Cambridge, MA.

Zhang, G. (2002): "Laboratory Characterization of a Highly Weathered Old Alluvium in San Juan, Puerto Rico", PhD thesis, MIT, Cambridge, MA.

2 Nature and Structure of the Old Alluvium, Puerto Rico

2.1 INTRODUCTION

This research aims to understand and model the behavior of tropical residual soils that cover most of north-northeast Puerto Rico (Figure 2-1), and underlie major areas of the city of San Juan. The deposits are referred to as Old Alluvium. Figure 2-2 shows a typical vertical profile with plasticity index and SPT blow count (N) data from two phases of the site investigation for the underground construction of the Tren Urbano in Río Piedras (Whittle & Bernal, 2003). For engineering purposes, the Old Alluvium is subdivided into the Upper Clay, Middle Zone and Lower Sand units. The subdivision is based largely on grain size distribution, coloration and stratification of the otherwise highly spatially variable soils. The vertical profile reflects the weathering pattern of the original Pleistocene Alluvium; the heaviest weathering occurs near the ground surface, while there is minimal alteration below the water table in the Lower Sand.

Before major engineering activities took place in San Juan during the late 1990's, there were few reported problems of structures founded on the Old Alluvium. However, earthwork projects had traditionally been careful to control compaction procedures in order to avoid structural breakdown, and foundation stresses were generally small (Whittle and Bernal, 2003). Prior to the construction of Tren Urbano, there was no experience of underground construction in the formation. The ground movements measured during excavation of the tunnels for section 7 of the project (using NATM, EPB and stacked drift methods) greatly exceeded the initial predictions. This led to major revisions in the application of grouting techniques and to an extensive study of the behavior of Old Alluvium (Zhang, 2002).

Mineralogical studies conducted post-facto by Zhang (2002) have revealed the presence of a significant fraction of clay minerals (mainly kaolinite and nontronite) within the Upper Clay and Middle Zone of the Old Alluvium. Furthermore, microscopic observations showed that the intact soil consists of quartzitic grains and cemented clay aggregates, which have their own internal secondary structure.

This chapter summarizes the mineralogical and microstructural information available for the soil. It then discusses the geological background of the material and shows that the mineralogical

observations are typical of tropical soils from similar regions. Further investigation of the geological processes and mechanisms associated with the formation tropical soils, aims to establish a clear understanding of the origin of the soil structure and the factors that can lead to structural breakdown and produce significant changes in macro-scale engineering properties. This understanding is essential for the development of any soil model intending to address the true nature of the material.

2.2 LABORATORY ANALYSES ON OLD ALLUVIUM

The content and nature of the Old Alluvium was extensively studied by Zhang (2002). He used a variety of techniques that can be divided into the following categories:

- X-Ray diffraction, thermal and chemical analyses (including X-ray fluorescence (XRF)), energy dispersive X-ray spectroscopy (EDXS), Cation Exchange Capacity analyses, selective chemical dissolution (SCD), index tests and grain size analyses to determine quantitatively and qualitatively the mineralogical composition of the Old Alluvium, properties of the clay minerals and the general soil structure,
- Environmental scanning electro-microscope (ESEM) observations, to study the material microstructure, and
- Slake tests, to determine the sensitivity of the soil structure to environmental agents.

2.2.1 Mineralogy of the Old Alluvium

Table 2-1 summarizes the findings of the quantitative mineralogical analysis (Zhang, 2002). In the Upper Clay, only about 20% weight is quartz and less than 10% orthoclase. On the other hand there is a significant percentage of clay minerals (54%), namely around 34% kaolinite and close to 20% nontronite (a mineral that belongs to the family of smectites). In addition, there is a presence of 9% by weight iron oxides (around 6% goethite and about 3% hematite), which is significant for these compounds (Schwertmann & Taylor, 1989).

When compared with the Upper Clay, the Middle Zone has a smaller percentage of clay (44% compared to 54% in the UC). The fraction of the swelling minerals is also smaller. In addition, it contains less than half the amount of goethite and no hematite.

Finally, it should be noted that in both layers there is a substantial presence of adsorbed water in the air-dried soil (12.5 and 8.5% weight respectively).

2.2.2 Microstructure of the Old Alluvium

Based on ESEM observations and the results of his experimental work, Zhang (2002) proposed a representative unit volume for the Old Alluvium as shown in Figure 2-3. The main features are as follows:

- At the macro-level (mm level, ref. Figure 2-4) the soil consists of grains, with diameter of about 80-100μm. Some of them are sand (mainly quartz) grains, but about 25% are actually aggregates with their own internal structure. At this macro-level, the solid grains and aggregates are cemented together with iron oxides, forming a relatively stiff matrix. There is a significant inter-aggregate porous system with pore sizes comparable to those of the aggregates (50-100μm, Figure 2-5). The inter-aggregate pores are well connected to each other.
- The aggregates are formed by cementing or bridging together many clay platelets (10-20μm), as shown in Figure 2-6. Again the platelet bridges are made by iron oxides. The aggregates have an internal, intra-aggregate porous system (with pore sizes about 10-20μm). These pores have irregular shapes and most of them are connected to each other with channels. However, some intra-aggregate pores exist isolated from the other void spaces and therefore they cannot exchange pore fluids with the interconnected pore system. No pore size distribution measurements were performed (e.g., Mercury Intrusion Porosimetry), because such methods would create partial breakdown of the structure and hence, yield erroneous results.
- At the micro-level (less than 1μm), the platelets (Figure 2-7 and Figure 2-8) consist of many clay particles stacked in face-to-face configurations. Iron oxides are found to precipitate and thus coat the surfaces of the clay stacks (Figure 2-9, 200nm scale). As discussed in Table 2-1, the mineralogical analyses found that these iron oxides are mainly goethite and hematite. They also showed that both kaolinites and smectites (nontronites) are present in this soil, but their particles cannot be easily identified in the natural state because of the iron oxide coatings. However, once these coatings have been removed using selective chemical dissolution with

DCB[1] treatment, the different clay stacks can be clearly seen (Figure 2-10): the particles of kaolinite appear as near hexagonal and flat plates with irregular shapes, while smectites exist in thin and curved flakes. The imperfectness of the hexagonal shape reflects the low crystallinity of kaolinites.

- In contrast to the Upper Clay (Figure 2-7), the microscopic appearance of Middle Zone (Figure 2-8) is much cleaner; the platelet shape is better distinguished, and the bridges between the platelets are more clearly identified. This observation is in accordance with the mineralogical results that showed a much smaller presence of iron oxides in the Middle Zone.
- With depth, the intensity of weathering decreases; Middle Zone is eventually underlain by Lower Sand, which consists mostly of clean or silty sands. ESEM micrographs obtained from a Lower Sand sample show that there are no connections between particles. Furthermore, there is no coating on the surfaces – as pointed on the figure, the edges of a group of kaolinite particles are clearly discernible.

2.2.3 Slake tests

Zhang (2002) performed slake tests in water, glycerol, DCB (sodium dithionite, sodium citrate, and sodium bicarbonate), NaHMP (sodium hexametaphosphate, $(NaPO_3)_6$) and hydrochloric acid (HCl). These tests are summarized in Figure 2-12. Even though the soil contains significant amount of expansive clay minerals, immersion in water or glycerol (which is used to expand the double layer) produced no response. This led to the conclusion that the clay particles must be disconnected from the macroscopic porous space (Figure 2-3). DCB broke down the external structure of the aggregates, but caused no swelling or dispersion. Only immersion in NaHMP produced observable swelling and a significant increase in the soil volume.

2.2.4 Open questions

The investigations by Zhang (2002) revealed the presence of clayey and swelling minerals in the soil and a complicated structure in the micro-level. Yet, a number of issues require further insight.

[1] DCB: sodium dithionite, sodium citrate, and sodium bicarbonate solutions

The processes that led to the formation of the clay minerals in the soil structure should be identified in order to understand the observed microstructure and the chemical conditions of the local pore environment, which possibly would affect the swelling behavior. In addition, the mechanisms of association of the iron oxides to the soil structure should be investigated in order to explain why the clay minerals appear insensitive to compounds (such as glycerol) known to expand double layers and cause macroscopic volume changes. Finally, it is important to understand how the microstructural composition evolves with depth and whether this characteristic weathering profile should be anticipated in other comparable soil profiles.

2.3 GEOLOGY BACKGROUND

2.3.1 Old Alluvium

'Alluvium' is a general term for all transitory or permanent deposits of water-borne sediments (these can include mixtures of gravels, sands, silts and clays) in stream channels, flood plains or deltaic environments (Stokes & Varnes 1955, Edelman & van der Voorde 1963). The term 'Old Alluvium' usually refers to Pleistocene-age alluvial deposits that are found in river terraces. Soil scientists consider Old Alluvial deposits as 'well-developed soils', which have generally been exposed to subaerial environments (due to sea level change and/or tectonic or isostatic uplift) and hence, may have undergone significant physical and chemical alterations. Geographical location and climate are key factors in determining the extent of these alterations. In the tropics, weathering is so intensive that the original grains of the the Old Alluvium may partially or totally have converted to clays and oxides, resulting in significant changes of the soil structure, texture and behavior; in contrast, in the temperate zones, the alteration process is slow or nonexistent and so the deposits may not undergo much change.

The Old Alluvium deposits in tropical regions are generally characterized by their low natural fertility, the types of dominant clay minerals (kaolinites, smectites, or combinations of the two), low contents of carbonates and organic matter, and a gley-mottling[2] texture.

[2] "Gleying" is defined as localized weathering along shrinkage cracks near the ground surface. (Kaye, 1959). In tropical climates, during the dry period, strong desiccation causes shrinkage cracks near the ground surface. During the subsequent wet period, water penetrates into the cracks, causing the soil to swell locally, and facilitating the dissolution of minerals.

Old Alluvia are found widely in South East Asia (extinct drainage system of the South China Sea; Gupta et al. 1987), in the major river basins of South Asia (Ganges, Brahmaputra and Indus), sub-Saharan Africa (Niger, Congo), and South America (Orinoco), as well as Northern California (USGS maps). Table 2-2 details the occurrence of old alluvia in the world.

2.3.2 Old Alluvium in Puerto Rico

The Old Alluvium in Puerto Rico is distributed over a gently sloping coastal plain located in the central-eastern part of the north coast of the island (Deere 1955, Kaye 1959, Pease & Monroe 1977). In fact, it blankets much of the northeastern coastal plain, higher stream terraces, and part of the central upland (Figure 2-1). In addition, it underlies most of the present-day flood plain sediments of Holocene age (e.g. recent littoral deposits and recent alluvium). The deposits are referred to locally as the Hato Ray Formation because the deposit is well exposed at the surface in the Hato Ray district of San Juan.

According to Briggs (1966), an uplift occurred during the Tertiary (early Miocene) period along an east-west axis through the volcanic and plutonic core of central Puerto Rico. This event raised the limestone stratum above sea level initiating the development of a karst environment. As a result, only major streams could maintain surface valleys, and they carried large amounts of sand (weathered from the andesitic and basaltic volcanic rocks upland) towards the north, to the floodplains and the sea, where the sand was redistributed by longshore (littoral) currents and to some extent by the wind. With further uplift, the surface flow was further reduced and the deposited blanket of sand was left in place, where it was subjected in tropical weathering that altered the less durable grains to kaolinitic clay and other weathering products. Finally, during the Pleistocene, some glacially-controlled advances and retreats in the sea level further affected the blanket sands at lower elevations (although Briggs believes that the effect was minor; see also Monroe, 1980).

An eroded peneplain[3] of Middle Tertiary limestone probably exists beneath the Old Alluvium in San Juan (Figure 2-2), and hence the contact between the two formations is expected to be generally sharp. As the coastal plain was developed through various stream channels, the Old Alluvium deposit is highly variable in thickness, but has a minimum depth of 25 m (Kaye 1959,

[3] A peneplain is an almost featureless plain, the final stage in fluvial or stream erosion.

Pease & Monroe 1977). The variation in thickness may also result from the complex eroded surface of the limestone bedrock on which the Old Alluvium rests unconformably.

2.3.3 Parent material of the original blanket of sand

The territory of Puerto Rico can be divided into three main geographic divisions (Figure 2-1a): 1) a mountainous core that makes up the southern two-thirds of the island, also known as the central upland province; 2) a belt of rugged karst topography in the north-central and northwestern parts of the island; and 3) a discontinuous fringe of relatively flat coastal plains distributed around the island. According to USDA (1978), the Old Alluvium is derived from parent rocks in the central upland province which include:

- Intrusive igneous rocks, mainly granodiorite and quartz-diorite;
- Extrusive basic volcanic rocks, such as lava, tuff, breccia;
- Sedimentary rocks, such as limestone, tuffaceous sandstone and siltstone.

The major rock-forming minerals contained in these rocks in the central upland were summarized in a classic study by Kaye (1959) as follows:

- Sedimentary rocks: calcite, marly clay, quartz, kaolinite;
- Intrusive igneous rocks: albite[4], quartz, augite, chlorite;
- Volcanic rocks: feldspar, quartz, mica, pyroxene, albite, hornblende, chlorite.

2.3.4 Depositional environment

The Old Alluvium was formed through the accumulation of alluvial and colluvial sediments, in a series of coalesced alluvial fans, which are slightly dissected by small streams. The evidence of occasional stratification, sand pockets and lenses, the lack of marine fossils, and the areal relationship with established fluvial deposits suggest very strongly that this formation was originally deposited as a piedmont alluvial plain (Deere 1955). Numerous sea level fluctuations in the Pleistocene glacial epoch caused a complex stream system with meandering stream channels to develop. During periods of glacial retreat, the sea level rose and finer-grained deposition generally occurred. In periods of glacial advance, the sea level fell as water was taken up in expanding glacial ice. As a result, stream gradients and energy increased and caused

[4] Albite is listed, but most likely most felspars are present.

down-cutting through and reworking of previously deposited coastal plain sediments. Therefore, deposition occurred in a fresh water environment in stream channels and river terraces.

2.3.5 Post-depositional processes and timing

After initial deposition, the material became exposed to the atmosphere due to either sea level changes or tectonic uplifts[5]. In the sub-aerial environment, tropical weathering and new soil-forming processes were initiated, causing continuous alteration of the composition, structure and engineering properties of the soils.

Initial alluvial deposition took place in the early Pleistocene (i.e., 1.0 - 1.6 million years ago). The current material consists of thoroughly decomposed sands and gravels with extensive conversion of unstable primary minerals (i.e. except quartz and orthoclase) into clays or other secondary minerals (such as the iron oxides). There is an almost complete lack of relationship with present-day stream alluviation (Kaye 1959). Significant surface erosion may also have occurred in the tropical wet climate (with abundant rainfall and frequent storms).

Desiccation commonly takes place following tectonic uplift or lowering of the groundwater table and is especially common in climates where there is a high rate of evaporation during dry seasons. The upper units of the Old Alluvium (Upper Clay, Figure 2-2) appear to have undergone intensive desiccation, resulting in a well-developed cross-patterned network of shrinkage cracks.

The mineralogical studies on the Old Alluvium showed that the main weathering products are kaolinite and nontronite as the clay fraction, and goethite-hematite as the secondary oxides. The presence of these minerals is not surprising, because they appear as weathering products in other neighboring formations. White et al (1998) have found that the pore water in this region is supersaturated with kaolinite. Buss et al (2005) showed that the nearby upland granitic rocks (Luquillo Mountains, Figure 2-13) contain kaolinite and goethite. Buss et al (2005) also examined the possibility that the local presence of the iron oxides is partially the result of coupling between biological processes and mineral weathering. According to the study, Fe^{+2} can supply micro-organisms with an energy alternative to organic carbon; low carbon contents and

[5] There is no evidence of post-middle Miocene submergence of the northern coastal plain of Puerto Rico, but there is little double that the deposits were affected by eustatic changes of the sea level (Briggs, 1966).

availability could favor autotrophic iron-oxidizing bacteria (Hallbeck & Petterson (1991), Holt at al (1994)). In the uplands of Puerto Rico (Figure 2-13) Fe^{+2} is released upon weathering of hornblende and biotite (minerals abundant in the parent granitic rock). The authors found similar trends for the concentrations of this "bioavailable" iron, cells and iron oxidizing bacteria along the depth of the weathered topmost part of the rock (Figure 2-14). It is not proven whether it is the availability of iron that favors the presence of these autotrophic iron oxidizing bacteria or the bacteria that cause the increase of the bioavailable iron. However, the consumption of Fe^{+2} by the aforementioned bacteria alters its concentration gradients within the weathered profile, therefore it may be playing an important role in the weathering process (Fletcher et al, 2006).

2.3.6 Uniqueness of the Old Alluvium

The depositional environment, post-depositional processes and the weathering products of the Old Alluvium are common in the region of Puerto Rico and typical in tropical soils of similar environments. However, it is the microstructure of Old Alluvium – the way the weathering products are associated – that result in the unique macroscopic response of the material. The following section therefore further investigates the mechanisms that are associated with the weathering products in the Old Alluvium, and hence affect its formation.

2.4 MECHANISMS AFFECTING THE FORMATION OF OLD ALLUVIUM

This section looks into the conditions associated with the formation of clay minerals during weathering, in order to understand the microenvironment preserved locally inside the clay platelets of the Old Alluvium. In addition, it investigates the formation of iron oxides and the mechanisms of their association with the soil skeleton components, in order to explain why Old Alluvium in its natural state appears to be isolated from actions of the macroscopic environment.

2.4.1 Formation of clay minerals: kaolinite and smectite

The formation of clay minerals in the tropics, where temperatures are high, is affected by the interaction with water through two main processes: the modification of the parent rocks and

leaching. The final formation products depend on the amount of the local rainfall and its annual pattern.

The formation of smectites is favored in environments rich in basic cations (Ca^{+2}, Mg^{+2}), and the principal requirement is that the parent rock contains sufficient amounts of basic cations (such parent rocks are basalts, shales, limestones or volcanic ash rocks). Therefore, the leaching of the weathering products should be at a minimum, so that this high concentration of cations is maintained.

As listed in section 2.3.3, the parent materials at the upland parts of Puerto Rico are indeed rich in basic cations. Furthermore, the tropical climate of the region is characterized by rainfall seasons followed by dry periods during which evaporation is intense and drainage at a minimum, resulting in soil solutions concentrated in silica and basic cations. Therefore the geological and climatic conditions in the region of deposition of the Old Alluvium favor the presence of smectitic minerals as in-situ weathering products.

Usually such weathering processes result in smectitic minerals, which are not flocculated, but have rather parallel configuration and minimal interlayer distances due to the high concentration of cations in the vicinity. However there is a great inherent potential for swelling, should the concentration of cations decrease (for example with addition of distilled water).

High rainfall, evenly distributed throughout the year, induces soil solutions with low concentrations of silica and basic cations that favor the formation of kaolinite minerals. Similar conditions can also be achieved in humid tropics (alternative wet and dry seasons) in the parts of the landscape where drainage is unrestrained (for example at sloping terrains).

Therefore, smectites are associated with poorly drained environments (lowlands, or low permeability zones like faults), while they appear more as transitory weathering products in well-drained areas with intense leaching. Under the latter conditions they are unstable and they are commonly altered to kaolinite. There is also evidence that an intermediate product of formation of kaolinite from smectite can be interstratified kaolinite and montmorillonite (Borchardt, 1989); such interstratifications have been observed in natural soils (Sudo & Hayashi, 1956; Skharov & Drits, 1973) and are, most probably, the result of improvement in drainage.

In contrast to smectites, that require particular formation conditions, kaolinites and iron oxides (hematite) or oxyhydroxides (goethite) are common weathering products of tropical soils.

As discussed above, studies in the upland areas of San Juan have encountered high concentrations of kaolinite and goethite in the weathered horizons of the parent granitic rocks. Typically, such weathering products are soils characterized by micro aggregates (of 10-200μm dia) formed by kaolinite particles associated with edge to face contacts, which are very stable due to thin coatings of iron oxides (Figure 2-15). They are often referred to as pseudo sand/silts, and they have a double porosity system, consisting of a large inter-aggregate porosity at the micrometer scale and an intra-aggregate micro-porosity at the submicron scale (Righi & Meunier, 1995). Therefore, in spite of their large clay content, they remain highly permeable.

2.4.2 Formation of iron oxides.

Iron is released during weathering through mechanisms of protolysis[6] and oxidation. The liberated iron may be oxidized immediately if oxygen is present, or migrate until it reaches an oxygenated zone. The other possibility is that oxidation takes place in the silica structure itself, with a resulting charge imbalance that weakens the structure and facilitates its breakdown. Once released, Fe^{3+} will immediately hydrolyze when it comes in contact with H_2O. Thus, depending on the conditions of the surrounding environment, the iron in an oxide may undergo variable periods of immobilization and mobilization which may be cyclic over quite short times. This may lead to characteristic spatial patterns of low and high concentrations of Fe oxides at various scales, from the micro-scale of an aggregate (μm or mm), to that of a horizon (cm or m), or a soil profile (m). Iron oxides are characterized by a significant surface charge, which depends on concentration of H^- or OH^- in the solution.

When oxidized, iron can assume the form of an oxide (for example Fe_2O_3: hematite), a hydroxide ($Fe(OH)_3$), or an oxyhydroxide (e.g. FeOOH; goethite).

Goethite (FeOOH) is an iron oxide that occurs in almost every type soil and climatic region. On the other hand, the association of goethite with hematite (Fe_2O_3) is a very common feature in the tropical zones. Hematite soils are rarely completely free of goethite; hematite is actually an anhydrated form of goethite:

$$Fe_2O_3 + H_2O \rightarrow 2FeOOH \qquad (2.1)$$

[6] A reaction that transfers protons (hydrons)

From a chemical point of view, the goethite – hematite ratio depends on the conditions of the above reaction, mainly its free energy and the activity of water[7]. Various data are available for the free energy of this reaction varying from +1.7 to -0.4 kJ/mol. For example, negative values indicate a higher stability of goethite at a water activity of 1 (distilled water). However, as the H_2O activity decreases below unity, hematite becomes increasingly more stable. The relative stability is also referred to depend on particle size (Langmuir & Whittemore, 1971). Another variable is the content of foreign ions, particularly Al^{2+} substituting for Fe^{3+} in the mineral structure. Calculations using existing thermodynamic data show that Al substitution decreases the equilibrium H_2O activity, and therefore increases the stability of hematite relative to goethite.

From a geotechnical point of view, the goethite – hematite ratio is affected by various pedo-environmental factors, such as the initial valence of the Fe source, its concentration in solution, pH, oxidation potential (Eh), temperature, soil water activity, soil organic matter, Al activity in the soil solution, and ionic environment (Schwertmann & Taylor, 1989). More specifically, the goethite-hematite ratio decreases with increasing soil temperature and increases as pH decreases. Soil moisture and drainage conditions may also influence the ratio; in various cases hematite is abundantly found in the drier parts of a weathered soil layer, while it is completely absent in the less drained parts of the same soil horizon. Many examples can be found in the literature; Curi & Franzmeier, (1984) report a 176m toposequence[8] of Oxisols[9] in central Brazil, where the upland drier parts are red and strongly hematitic, while the valley soils are yellow, and hematite free. In the highly desiccated coastal plain of N. Carolina, redder soils dominate at the dry plateau edges, and yellowish brown ones are found on the plateau itself (Daniels et al, 1975). The Alfisols[10] on the terraces of the river Guadalquivir (Spain) were found hematitic when well drained, but contained only goethites when imperfectly drained (Pena & Torrent, 1984). These trends have

[7] Water activity is a measure of how efficiently the water present can take part in a chemical (or physical) reaction. It depends on the water composition and temperature.

[8] Toposequence is a sequence of related soils that differ primarily because of topography being a soil-formation factor.

[9] Oxisols are very weathered soils that within at least the first 2m below the surface are characterized by the absence of weatherable primary minerals, the presence of kaolinites, quartz, and iron/aluminium oxides (hence the name), the absence of water dispersible clay and the presence of low CEC and small amounts of exchangeable bases (Oxford Dict. of Earth Sc.). They are mostly present in the tropics.

[10] Alfisols are mineral soils characterized by clay enriched or argilitic horizons. They are derived from base-rich parent materials (Oxford Dict. of Earth Sc.). They form in semiarid to humid areas, and are rich in aluminium and iron (hence the name). Alfisols occupy around one tenth of the Earth's ice-free land surface.

been partially reproduced in the lab (Torrent et al, 1982). Figure 2-16 shows a schematic representation of the mentioned processes and factors that influence the formation of goethite vs. hematite; however the representation assumes that hematite forms from ferrihydrite ($5Fe_2O_3.9H_2O$), which has not been found to be in close association with hematite in tropical soils.

2.4.3 Mechanisms of association of iron oxides to the clay surfaces

Iron oxides associate with the clay mineral surfaces through processes of aggregation and cementation (Schwertmann & Taylor,1989). In the cementation process, Fe-oxides fill portions of the pores between the matrix particles; this way aggregates are formed, which often have sizes comparable to sand particles and extend considerably within the soil structure. Aggregation is understood as the association of the soil matrix particles into groups by minute particles of Fe-oxides. The resulting aggregates form not so much through crystal growth but more through an attraction between the positively charged Fe-oxide particles and the negatively charged clay silicates. Hence, aggregated cations mask the true physicochemical properties of the clay surfaces.

The nature of aggregation is not completely understood, but Yong et al (1987) argue that the mechanism of association of the iron oxides on the clay surfaces is dictated by their electric charge and hence based on Coulombic forces rather than on coherence through the formation of a chemical bond ("chemisorption"). Similarly, Blackmore (1973) suggests that aggregation is the result of cohesion between films, or parts of films of iron oxide formed on the clay surface; those films are being formed by the attachment of positively charged ions on the negatively charged clay surfaces (Coulombic bonding).

Aggregation differs from cementation in that association is not resulting from crystal growth (hence permanent), but is controlled by physicochemical factors and therefore it can be reversed. For example, because the charge of Fe-oxides is pH dependent, aggregation should also be pH dependent. Yong & Ohtsubo (1987) observed that ferrihydrite ($5Fe_2O_3 \cdot 9H_2O$) was precipitated onto kaolinite surfaces only when precipitation occurred under acid conditions. As shown in Figure 2-17 (upper part), kaolinite-ferrihydrite complexes formed at $pH < 5$ are extremely stable, even if the pH value is subsequently increased. However, if the initial pH is high (bottom part of the figure, $pH_0 = 9.5$) the ferrihydrite seems to be established as a separate phase, independent of

the kaolinite, without being adsorbed onto the kaolinite. Lowering the pH to 4.1 resulted in some ferrihydrite being absorbed on the faces of the kaolinite particles, but nevertheless a significant proportion of the ferrihydrite remained as a separate phase not interactive with the kaolinite surface charge effects. Similarly, Greenland et al (1968) studied the artificial precipitation of iron hydroxides on well-crystallized kaolinites and observed that higher pH values resulted in increasing amounts of non-associated iron.

Blackmore (1973) showed that the amount and timing of the addition of the iron oxides is decisive to whether the oxides will aggregate very strongly, or not at all. He treated 3 types of clays (kaolinite, illite and bentonite) with hydrolyzing[11] ferric chloride ($FeCl_3$) to artificially induce aggregation. During the dehydration part of this process, films of the iron oxides squeeze between neighboring clay crystals, as they orient parallel to each other. The aggregation is indicated macroscopically by the color change of the clay (from grey/white to yellowish); the permanence of this color change even after severe dispersion of the aggregates suggests that the film of the hydrous oxide over the clay surface can be very adhesive. Figure 2-18 shows the effect of the amount of iron oxides present in the stability of aggregation. This amount is expressed as the weight of oxide per unit weight of clay. When more than a certain amount of oxides is added, the resulting aggregation is very stable and resistant to dispersants. As expected, because kaolinite particles are thicker, fewer oxides are needed to achieve strong aggregation. To a first order estimate, an oxide to clay weight ratio of 0.6 is required for bentonite[12] to produce a monomolecular layer of oxide over the particle surface. The same ratio for kaolinite (10 times thicker than bentonite) would be 0.06. The experimental results (Figure 2-18) showed similar values. However, bentonite demonstrated strong bonding with iron oxide amounts much less than those theoretically required for saturated aggregation.

Other factors that affect the amount of aggregation were explored by Rengesamy & Oades, (1977). Using data from synthetic iron oxides, they concluded that the effectiveness in aggregating increases with decreasing crystallinity. They also found that at high surface areas only small additions of Fe oxides were sufficient to effectively promote aggregation of silt particles. Very small but highly charged iron oxides seem to be particularly effective. Cambier

[11] Hydrolysis is a chemical reaction in which a chemical compound splits with the addition of water.

[12] Bentonite has single crystals, about 1nm thick, while the iron coating is assumed to be 0.3 nm thick on each side of the particle (ignoring the edges)

and Prost (1981) also report that they had to remove only a small portion of the total Fe-oxides in order to disperse a ferralitic soil from Senegal.

The above studies show that the part of iron oxides responsible for aggregation is probably the amorphous or poorly crystallized fraction; furthermore, a much lower amount than that required for cementation is sufficient to produce very resistant bonds.

2.4.4 Mechanisms of disassociation of iron oxides from the clay surfaces

The presence of iron oxides, especially when aggregated on the clay surfaces, can create very resistant soil structures. Mechanisms that destroy this association can be catastrophic for the stability of the soil structure.

Iron oxides can be removed from the clay surfaces using chemical treatments (for example EDTA (disodium salt of ethylenediamine tetraacetic acid), or NaHMP (sodium hexametaphosphate, $(NaPO_3)_6$)). In nature, one of the known mechanisms of removal of iron oxyhydroxides is strong desiccation (Righi & Meunier, 1995). Some removal has also been observed through extended mechanical mixing (Schwertmann & Taylor, 1989).

2.4.5 Observed effects of iron oxides on the behavior of various clays

There are a number of examples where the presence of iron oxides has been found to interact with the physico-chemical activity of clays and hence suppress macroscopic volume changes.

Righi & Meunier (1995) discuss that kaolinite crystal blocks exhibit a far lower cation exchange capacity than pure kaolinite due to the presence of iron oxides. They refer to the study by Pedro et al (1976), which demonstrated the role of iron-oxyhydroxides in the inactivation of kaolinite by chemically removing the iron compounds from the soil sample (using NH_4 oxalate in the dark). After the treatment, the usual properties of kaolinite were restored, the CEC was greatly improved, and the soil swelled and shrank normally. A significant observation in this study is that the chemical treatment only removed a small fraction of the iron oxyhydroxides – the amorphous or poorly crystallized one; however, as mentioned in section 2.4.3, this is the crucial fraction that is responsible for the micro-aggregate stability and the masking of the clay activity.

Keren (1986) reports a similar masking of the physicochemical activity in montmorillonite, however the mineral treatment was done using hydroxyl aluminum polymers. The study found that the polymers existed as gibbsite islands (of about 15nm diameter), randomly distributed in the interlayer space. The positively charged polymers had precipitated on the planar surfaces of the negative charged clay surfaces and were blocking their exchange potential, and hence altering both chemical and physical properties of the soil (cation exchange capacity, ion exchangeability, swelling, clay dispersion, soil permeability). Again, only a small amount of polymers were sufficient for the observed changes.

Yong & Ohtsubo (1987) also showed that the ferrihydrite precipitated onto kaolinite led to a reduction of the total net negative charge of the clay particles and that the amorphous iron (Fe) and aluminum (Al) compounds (in their wet state) formed a highly hydrated gel with a three-dimensional structure that linked the clay particles.

Lambe (1960) noted that clay minerals can intergrow and/or aggregate to form larger and less plastic particles and found that the most important agent in natural soils that have aggregated fines were iron oxides. He specifically studied the effect of aggregants (ammonium chloride), cementation (with lime) and dispersants (sodium tetraphosphate) on the shear behavior of a stiff sensitive clay from Outardes, Quebec, with apparent cementation between the clay particles. The results of the study are illustrated in Figure 2-19. Figure 2-19(a) shows that the presence of aggregants increased the soil shear strength, and had an effect more significant than that of the lime cementation. Figure 2-19(b) shows that the aggregant also increased the stress-strain modulus. In both cases, the dispersant had the opposite effect. However, neither the aggregant nor the dispersant caused any change on the friction angle (Figure 2-19(c)).

McKyes et al (1974) observed that the Champlain sea clays have amorphous coatings of iron oxides (among others) that contribute to a bonded structure; once this structure is destroyed (through extensive shearing) the clay turns into a very sensitive one.

Finally, Kenney et al (1967) studied Labrador clay, which is a Canadian reddish, homogeneous, quick clay, which was originally deposited in a marine environment and chemically altered in situ[13]. The natural structure contains iron oxides, which seem to form some

[13] Labrador clay mainly consists of fine grained mica (50%), feldspar (25%), chlorite (15%), and quartz (10%)

kind of cementation. Once they are removed (after treatment with EDTA[14]), the soil exhibits a lower preconsolidation pressure and a softer response. It is interesting to note that the EDTA technique removed 70% of the removable iron, and this amounted to only 0.8% of the dry soil weight.

2.5 NEW ASSUMPTIONS ON THE MICROSTRUCTURE OF OLD ALLUVIUM

The Old Alluvium contains clay minerals and iron oxides as a result of its geologic history. Following the investigation in paragraph 2.4 some important new assumptions can be made about its microstructure:

- The formation mechanisms of smectitic minerals discussed above (section 2.4.1) permit the following two assumptions for the intra-platelet microspace: (i) the smectitic minerals exist in a face-to-face orientation, and (ii) the pore water associated with these mineral stacks (their local micro-porosity system) has a different salinity than the macroscopic pore water, as it is most probably rich in cations. As a result, a large part of the negative surcharge of the clay faces is satisfied by the presence of the intra-platelet cations and the Double Layer length is reduced; thus the swelling potential of the minerals is suppressed. It should be expected thought that if this local porosity gets connected to the macroscopic porous space and the associated pore water concentration dilutes, the swelling potential will automatically increase, following the increase in the value of the Double Layer length.
- At the macro (μm to mm) scale, iron oxides precipitate between the grains or aggregates and form cementation, which provides a strong bonding between the soil particles.
- At the micro level, some fraction of the iron oxides (the amorphous phase) aggregate onto the clay minerals. As the nature of the association is mostly electrostatic, the bond locks a high percentage of the negative surface charge of the clay to equilibrate the large positive charge of the iron oxide compound. In this way, aggregation reduces the Cation Exchange Capacity of the clay minerals and therefore masks its macroscopic physicochemical characteristics. This assumption is clearly supported by the fact that during the slake tests (Zhang, 2002) samples treated with DCB, a chemical that breaks down the cementation, produced only big pieces of

[14] EDTA: disodium salt of ethylenediamine tetraacetic acid

clay, but did not disperse the aggregates. On the other hand, samples treated with NaHMP, a chemical that affects the aggregation, disintegrated and expanded significantly.

- Because the mechanism of aggregation is electrostatic, its stability depends on the oxide maintaining its positive charge. Therefore, any changes in the pore water that can increase the pH can jeopardize the strength of the aggregation. Given the aforementioned high concentrations of cations in the local intra-platelet porosity, it is possible that any mechanical action that would break the micro-pore isolation could also weaken the aggregation of the iron oxides.
- In minerals with high surface areas only small amounts of iron oxides are sufficient to promote effective aggregation. Figure 2-18 superimposes on the data from Blackmore (1973) the weight of iron oxides relative to that of clays present in the Old Alluvium. In the Upper Clay, the ratio would imply an 85% aggregation, if the clay fraction were pure kaolinite, and a 55% aggregation, if it were pure bentonite. The corresponding values for the Middle Zone are about 60% and 40% respectively. Given the soil contains both kaolinite and nontronite, it can be assumed that a large amount (more than 60% for the UC) of the clay is strongly aggregated.

The above assumptions have a very important implication: The Old Alluvium has a significant swelling potential, which is concealed in its natural state because of three independent but interrelated mechanisms: (i) the face-to-face orientation of the clay minerals, (ii) the local micro-pore water rich in cations and (iii) the aggregation of iron oxides. As a result, the apparent isolation of the swelling minerals is not mechanical but rather physicochemical. The iron oxides do not necessarily need to form a continuous coating around the clay minerals and consequently the breakdown of the soil structure is a result of both mechanical damage and electro-chemical changes facilitated by the mechanical damage.

Finally, the geologic review in this chapter showed that neither the mineralogy nor the weathering processes in the Old Alluvium are unique. Similar combinations of swelling minerals and (iron) oxides should be expected in other Old Alluvia or tropical soils in general. The following chapter will illustrate that there are indeed a number of soils (or weak rocks) that have a comparable engineering response. Understanding and modeling the behavior of Old Alluvium will therefore benefit the study of soils well beyond the area of Puerto Rico.

2.6 REFERENCES

Blackmore A.V. (1973): "Aggregation of clay by the products of iron III hydrolysis", Australian Journal of Soil Research, 11 (1), 75-82

Borchardt G. (1989): Smectites, Chapter 14 in Minerals in soil environment, 2nd edition, SSSA Book Series, No1, Dixon J.B., Weed S.B. (editors).

Briggs R.P. (1966): "The blanket sands of northern Puerto Rico", Transactions of the 3rd Caribbean Geology Conference, Geol. Surv. De., Kingston Jamaica, 60-68

Buss H.L., Bruns, M.A., Schultz, M.J., Moore J., Mathur C.F., Brantley S.L. (2005): "The coupling of biological iron cycling and mineral weathering during saprolite formation, Luquillo Mountains, Puerto Rico", Geobiology, 3, 247–260

Cambier P., Prost R. (1981): "Etude des associations argile-oxyde: Organization des constituents d'une materieau ferralittique", Agronomie, 1, 713-722

Curi, N. and Franzmeier, D.E (1984): "Toposequence of Oxisols from the central plateau of Brazil", Soil Science Society of America Journal, 48, 341-346.

Daniels, R.B., E.E. Gamble, and C.S. Holzhey (1975): "Thick Bh horizons in the North Carolina Coastal Plain: Morphology and relation to texture and ground water", Soil Science Society of America Proceedings, 39, 1177–1181.

Deere, D. U. (1955). Engineering Properties of the Pleistocene and Recent sediments of the San Juan Bay Area, Puerto Rico. Ph.D. Thesis, University of Illinois, Urbana.

Dixon, J.B. (1989): Kaolin and Serpentine group minerals, Chapter 10 in Minerals in soil environment, 2nd edition, SSSA Book Series, No1, Dixon J.B., Weed S.B. (editors).

Edelman, C. H. & van der Voorde, P. K. J. (1963). Important characteristics of alluvial soils in the tropics. Soil Science, 95, 258-263.

Fletcher R.C., Buss H.L., Brantley S.L. (2006): "Physical–chemical feedbacks between atmospheric oxygen and bedrock weathering during steady-state spheroidal weathering", Earth and Planetary Science Letters, 244 (1-2), 444-457.

Greenland D.J., Oades J.M. (1968): Iron Hydroxides and clay surfaces", 9th International congress of soil science, Adelaide, 1, 657-668.

Gupta, A., Rahman, A., Wong, P.P., & Pitts, J. (1987) The Old Alluvium of Singapore and the extinct drainage system to the South China Sea. Earth Surface Processes and Landforms, 12, 259-275.

Hallbeck L., Pedersen K. (1991): "Autotrophic and mixotrophic growth of Gallionella ferruginea", Journal of General Microbiology, 137, 2657–2661.

Holt J.G., Krieg N.R., Sneath P.H.A., Staley J.T., Williams S.T. (1994): "Bergey's Manual of Determinative Bacteriology", Williams & Wilkins, Baltimore, MD.

Kaye, C.A. (1959) Coastal Geology of Puerto Rico: (A) Geology of the San Juan Metropolitan Area. Geological Survey Professional Paper 317. US Government Printing Office, Washington, D.C.

Kenney T.C., Moum J., Berre T. (1967): "An experimental study of bonds in a natural clay", Proceedings of the geotechnical conference, Oslo, 1, 65-69

Keren R. (1986): "Reduction of the CEC of montmorillonite by take-up of hydroxyl Al polymers", Clays and Clay Minerals, 34, 534-538.

Lambe, T. W. (1960): A mechanistic picture of shear strength in clay, Research Conference on Shear Strength of Cohesive Soils, New York, 555–580.

Langmuir D., Whittemore D.O. (1971): "Variations in the stability of precipitated ferric oxyhydroxides", in Non-equilibrium systems in natural water chemistry, Gould R.F. (editor), Advanced Chemistry Series, 106, 209-234.

Loiselle A., Massiera M., Sainani U.R. (1971): "A Study Of The Cementation Bonds Of The Sensitive Clays Of The Outardes River Region", Canadian Geotechncal Journal, 8, 479-498

McKyes E., Sethi A., Yong R.N. (1974): "Amorphous coatings on particles of sensitive clay soils", Clays and Clay minerals, 22, 427-433

Monroe W.H. (1980): "Geology of the Middle Tertiary Formations of Puerto Rico", Geological Survey Professional Paper 953. US Government Printing Office, Washington, D. C.

Murphy, S.F., S.L. Brantley, A.E. Blum, A.F. White, H. Dong. (1998): Chemical weathering in a tropical watershed, Luquillo Mountains, Puerto Rico: II. Rate and mechanism of biotite weathering. Geochim. Cosmochim. Acta, 62, 227-244.

Pease, M. H. Jr. & Monroe, W. H. (1977). Geologic Map of the San Juan Quadrangle, Puerto Rico. Washington, D.C., US Geological Survey.

Pedro et al, 1976: "Recherches sur la constitution et la genese des terra roxa etsrucurada du Brasil". Ann. Agron, 27, 265-294.

Pena E., Torrent, J. (1984). Relationships between phosphate sorption and iron oxides in Alfisols from a river terrace sequence of Mediterranean Spain. Geoderma, 33, 283-296.

Rengesamy P., Oades J.M. (1977): "Interaction of monomeric and polymeric species of metal ions with clay surfaces; II. Changes in surface properties of clays after addition of iron (III)", Australian Journal of Soil Research, 15, 235-242.

Righi D., Meunier A. (1995): "Origin of clays by rock weathering and soil formation", Chapter 3 in Origin and mineralogy of clays, Velde B., editor, Springer.

Sakharov B.A., Drits V.A. (1973): "Mixed layer kaolinite-montmorillonite: a comparison of observed and calculated diffraction patterns", Clays and Clay Minerals, 21, 15-17.

Schwertmann U., Taylor R.M. (1989): Iron Oxides, Chapter 8 in Minerals in soil environment, 2nd edition, 1, Dixon J.B., Weed S.B. (editors), SSSA Book Series.

Shirlaw J.N., Hencher S.R., Zhao J. (2000): "Design and construction issues for excavation and tunneling in some tropically weathered rocks and soils", in: H. Rahardjo, D.G. Toll, and E.C. Leong (eds.), Unsaturated Soils for Asia. Proceedings of the Asian Conference on Unsaturated Soils, Singapore.

Stokes, W. L. & Varnes, D. J. (1955). Glossary of Selected Geologic Terms. Colorado Scientific Society Proceedings, 16, Denver, Colorado.

Sudo T., Hayashi H. (1956): "A randomly interstratified kaolin-montmorillonite in acid clay deposits in Japan", Nature, 178, 1115-1116.

Torrent J., Guzman R., Parra M.A. (1982): "Influence of relative humidity on the crystallization of Fe(III) oxides from ferrihydrite", Clays and Clay Minerals, 30 (5), 337-340.

USDA – US Department of Agriculture (1978). Soil Survey of San Juan Area of Puerto Rico. Published by the US Department of Agriculture.

WCC (1997) Supplemental Site Investigation Reports for Tren Urbano Section 7, Woodward-Clyde Consultants, 2 Vols.

White A.F., Blum A.E., Schulz M.S., Vivit D.V., Stonestrom D.A., Larsen M., Murphy S.F., Eberl D. (1998): "Chemical weathering in a tropical watershed, Luquillo Mountains, Puerto Rico: I. Long-term versus short-term weathering fluxes", Geochimica et Cosmochimica Acta 62, 209–226.

Whittle A.J., Bernal J. (2003): "Stacked Drift Construction of a Large Cavern in Weathered Alluvium", Proceedings of the Soil and Rock America Conference, MIT, Cambridge MA, 2, 2315-2322.

Yong R.N., Ohtsubo M. (1987): "Interparticle Action and Rheology of Kaolinite-Amorphous Iron Hydroxide (Ferrihydrite) Complexes", Applied Clay Science, 2, 63-81.

Zhang, G. (2002): Laboratory Characterization of a Highly Weathered Old Alluvium in San Juan, Puerto Rico. PhD thesis, MIT, Cambridge, MA.

Zhang G., Germaine J.T., Whittle A.J. Ladd, C.C. (2004b) "Soil structure of a highly weathered old alluvium", Géotechnique, 54 (7), 453–466.

Zhang G., Whittle A. J., Germaine J. T., and Nikolinakou M. A. (2006): "Characterization and Engineering Properties of The Old Alluvium in Puerto Rico", 2nd Int. Workshop on Characterization and Engineering Properties of natural soils, Singapore, 4, 2557-2590.

Mineral	Fraction in air-dried UC (%wt)	Fraction in oven-dried UC (%wt)	Fraction in air-dried MZ (%wt)	Fraction in oven-dried MZ (%wt)
Adsorbed water	12.43	0.0	8.39	0.0
Quartz	19.42	22.18	29.0	31.66
Orthoclase	8.19	9.35	15.44	16.86
Kaolinite	29.46	33.64	21.01	22.93
Nontronite	17.65	20.16	11.98	13.08
Goethite	5.11	5.83	2.39	2.61
Hematite	2.76	3.15	0.0	0.0
Montmorillonite	0.0	0.0	2.05	2.24
Illite	0.0	0.0	2.75	3.0
Pyrophyllite	0.0	0.0	2.75	3.0
Muscovite	trace	trace	trace	trace
Total	95.02	94.31	95.76	95.38

Table 2-1: Summary of the fractions of all minerals in the old alluvium; UC = Upper Clay, MZ = Middle Zone (Zhang, 2002).

Africa	Asia	South America
Nigeria, Niger River	Indonesia: Java, Borneo, Sumatra	Venezula, Orinoco
Tanganyika, Great Ruaha River	Burma, Irriwaddy Delta	Guianas
Belgian Congo, Lufira Valley	India: Ganges, Brahmaputra River	Colombia
Northern Rhodesia, Kafue Flats	Pakistan	Puerto Rico[b]
Nyasaland, Shire Valley	New Guinea	
	Singapore[a]	
	Malaysia[a]	

[a]: Gupta et al. (1987); Shirlaw et al. (2000), [b]: Kaye (1959).

Table 2-2: Occurrence of old alluvia throughout the world (except noted, all are from Edelman & van der Voorde, 1963).

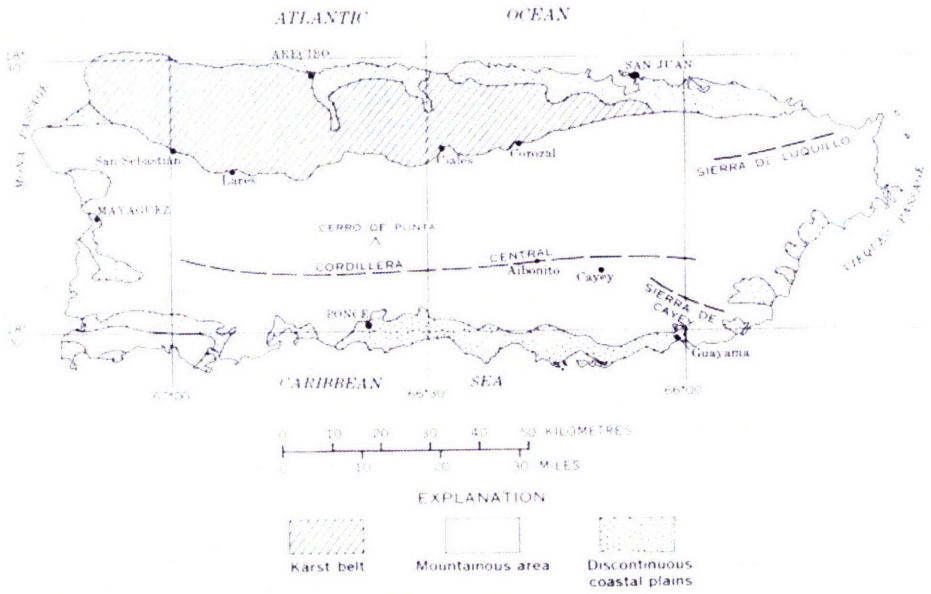

(a) Principal physiographic divisions of Puerto Rico (Pease & Monroe 1977).

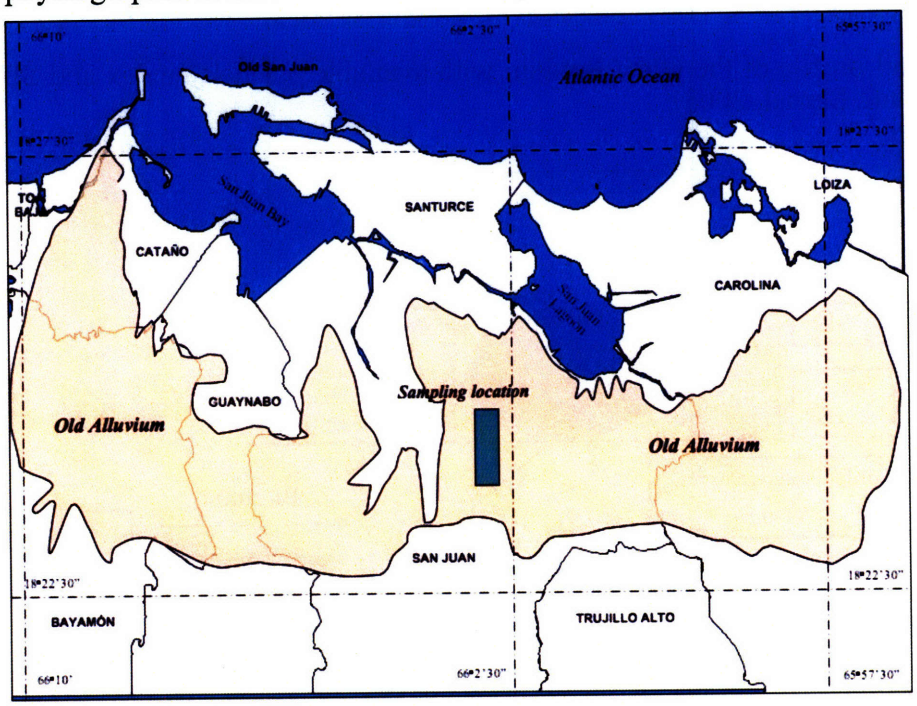

(b) Location of the Old Alluvium deposits in San Juan (samples obtained from tunneling project in Río Piedras).

Figure 2-1: The Old Alluvium in Puerto Rico (Zhang et al, 2006).

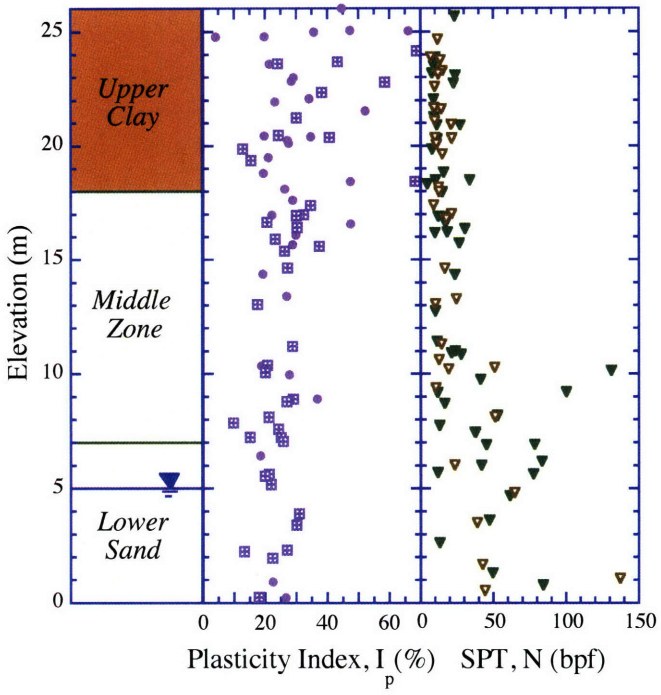

Figure 2-2: Soil profile of the Old Alluvium with available plasticity index and SPT blow count data (Whittle and Bernal, 2003).

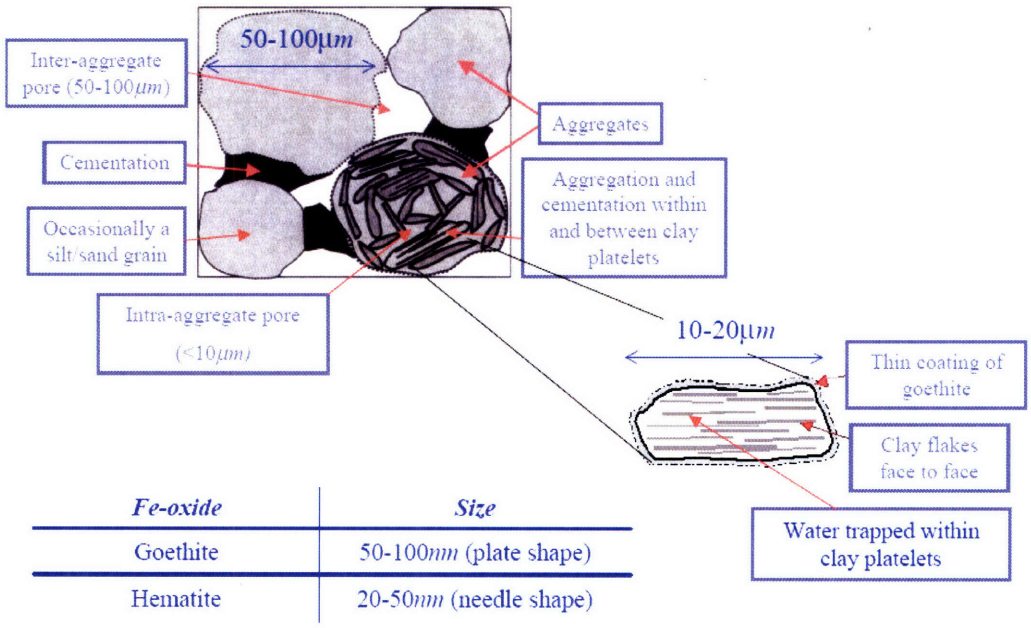

Figure 2-3: Schematic of the microstructural unit cell of Old alluvium (Zhang, 2002).

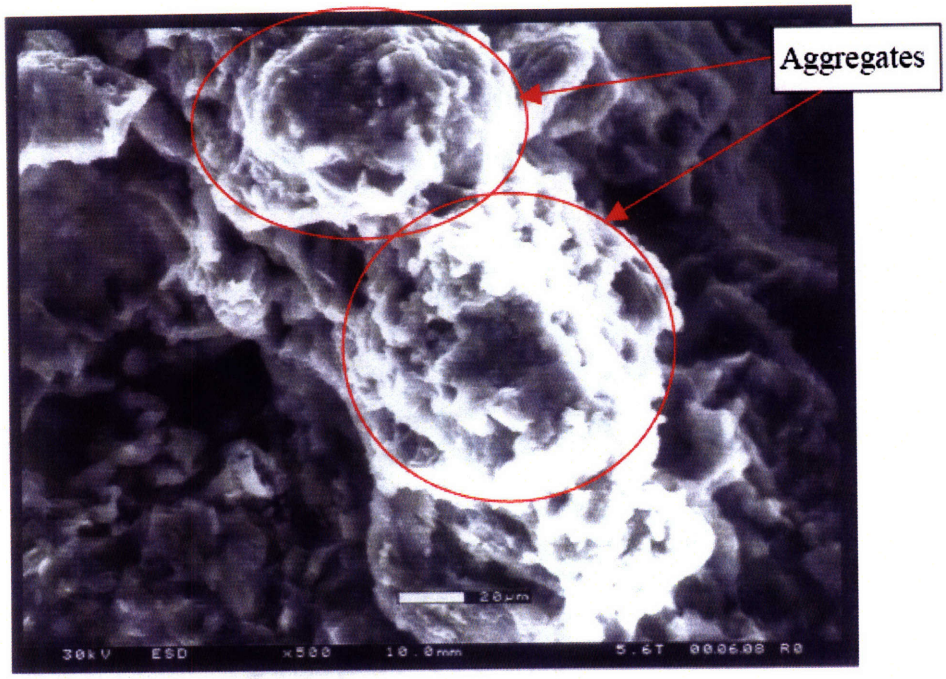

Figure 2-4: ESEM micrograph of intact Upper Clay sample showing the aggregates and connections between aggregates (Zhang 2002).

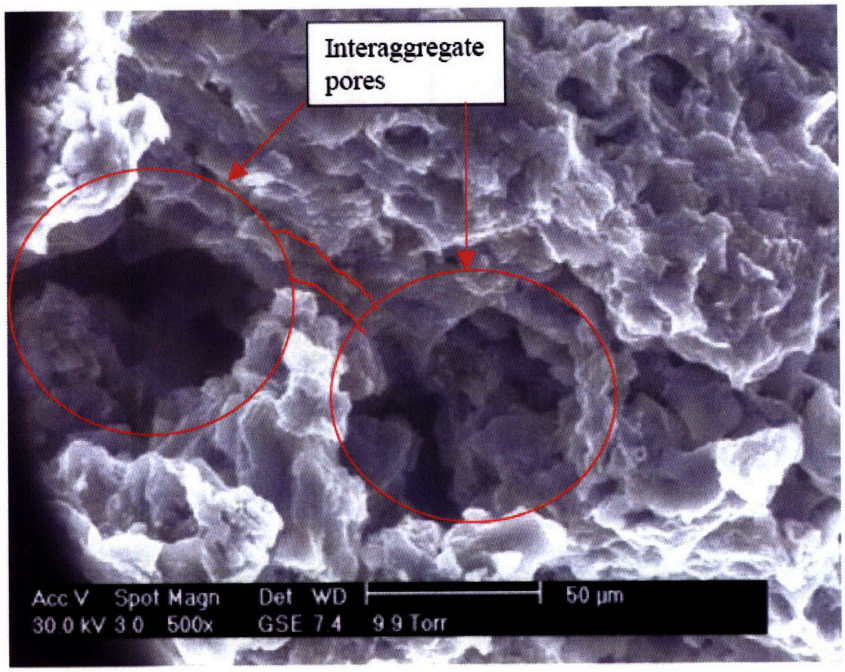

Figure 2-5: ESEM micrographs of an Upper Clay sample showing the features of void space with inter-aggregate pores and intra-aggregate pores (Zhang, 2002).

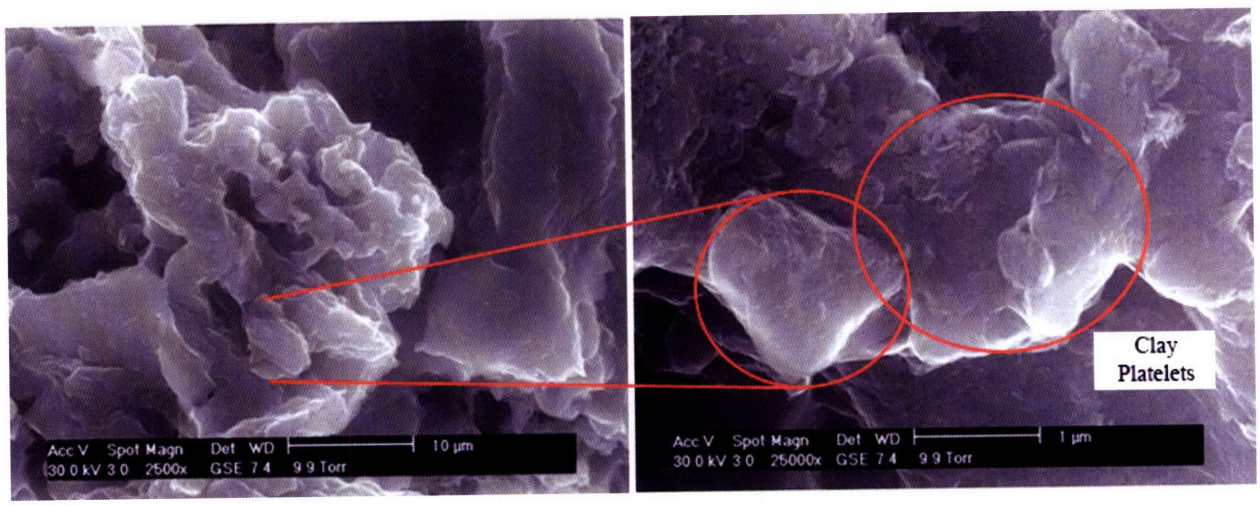

Figure 2-6 (left) and Figure 2-7 (right): ESEM micrographs of intact soil samples (Upper Clay) showing a network of clay platelets on a 10µm scale (left) and the actual clay platelets on a 1µm scale (Zhang, 2002).

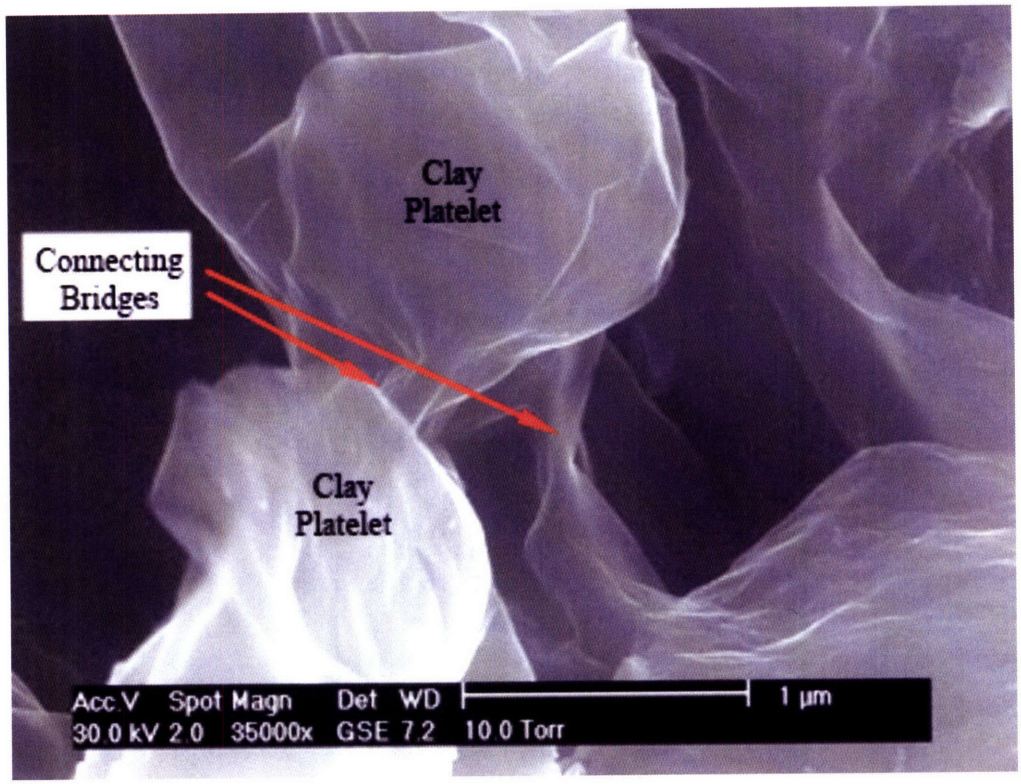

Figure 2-8: ESEM micrograph of a Middle Zone intact soil sample showing the clay platelets and the inter-platelet connecting bridges (Zhang, 2002).

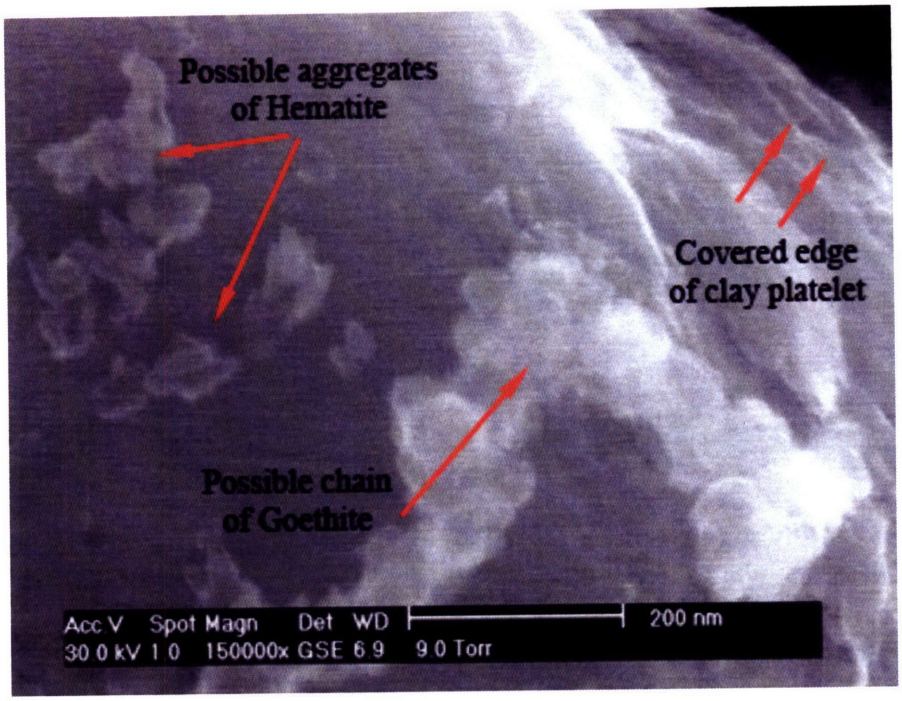

Figure 2-9: ESEM micrographs of intact soil samples (Upper Clay), showing the possible forms of iron oxide coating (Zhang, 2002).

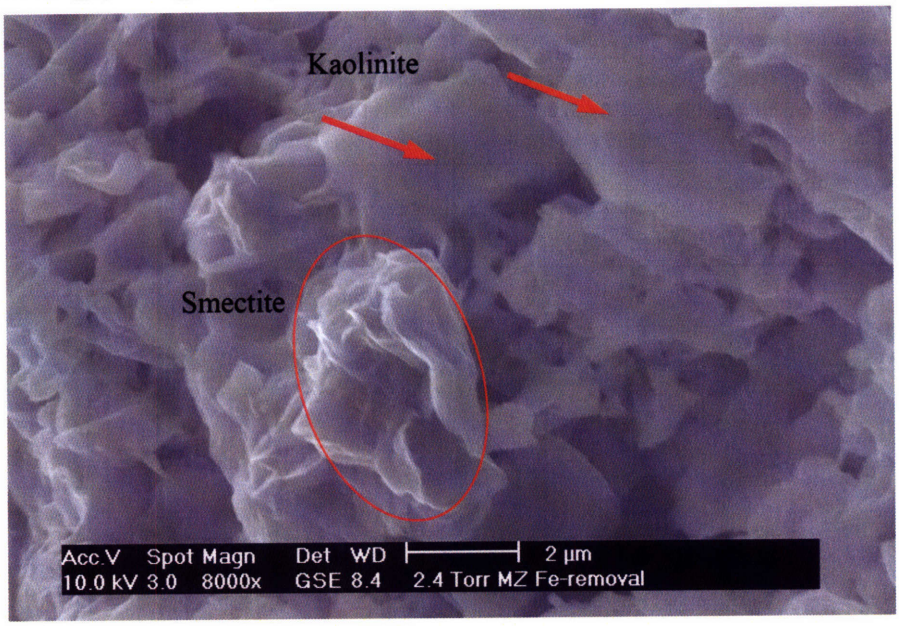

Figure 2-10: ESEM micrograph of a DCB-treated Middle Zone sample: the particles inside the ellipse are smectite, while those pointed with an arrow are kaolinite (Zhang, 2004b).

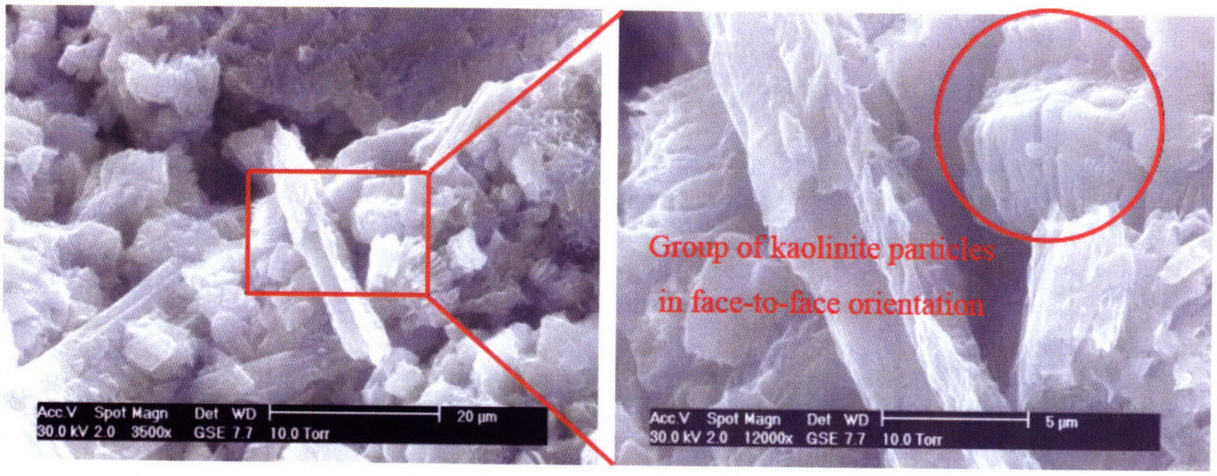

Figure 2-11: ESEM micrograph of a Lower Sand sample. There are no connection bridges and no coating of particles; hence a kaolinitic platelet (in circle) is clearly discernible (Zhang, 2004b)

Solution	Slaking response	Final sample condition	Solution change
Water	No reaction	Same as intact	No change
Glycerol	No reaction	Same as intact	No change
DCB	Very slow cracking; no swelling; no dispersion	Red color disappeared; sample became dark gray; fractured into big pieces	Became yellow, but still transparent
NaHMP	Quick self-peeling; observable swelling; slight dispersion	Totally disintegrated into large aggregates; huge volume increase	A little bit of suspension; semi-transparent
HCl	Slow microcracking; no swelling; no dispersion	Keeps intact shape but with microcracks	Light yellowish; still transparent

(after 2 days)

(after 7 days)

(after 2 days)

Figure 2-12: Slake tests on Old Alluvium (Zhang, 2002).

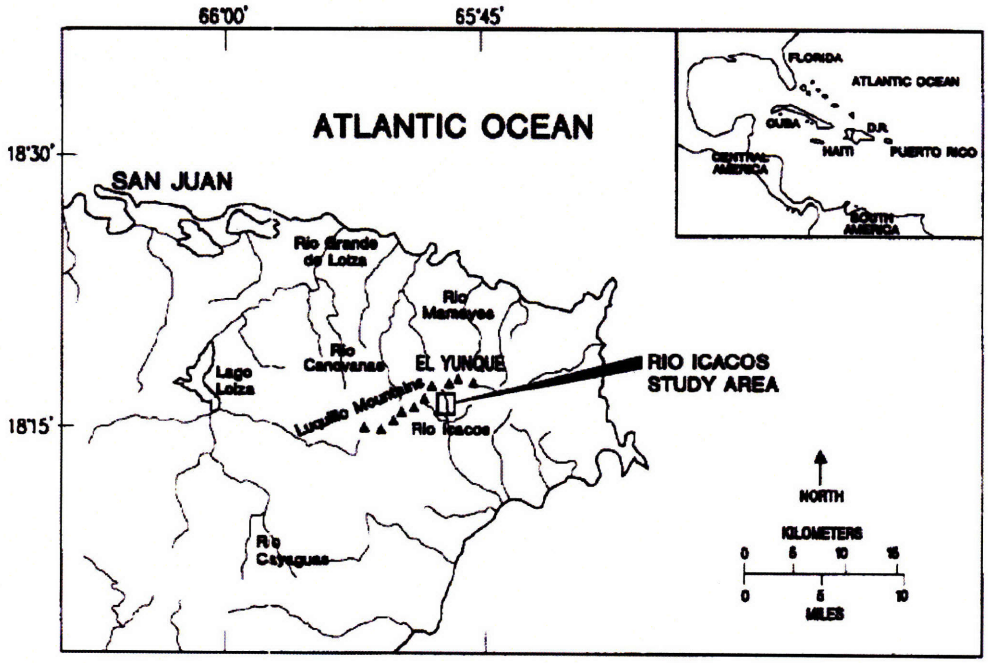

Figure 2-13: Location of Luquillo Mountains study area (Murphy et al (1998); same study area as Buss et al (2005), White et al (1998)).

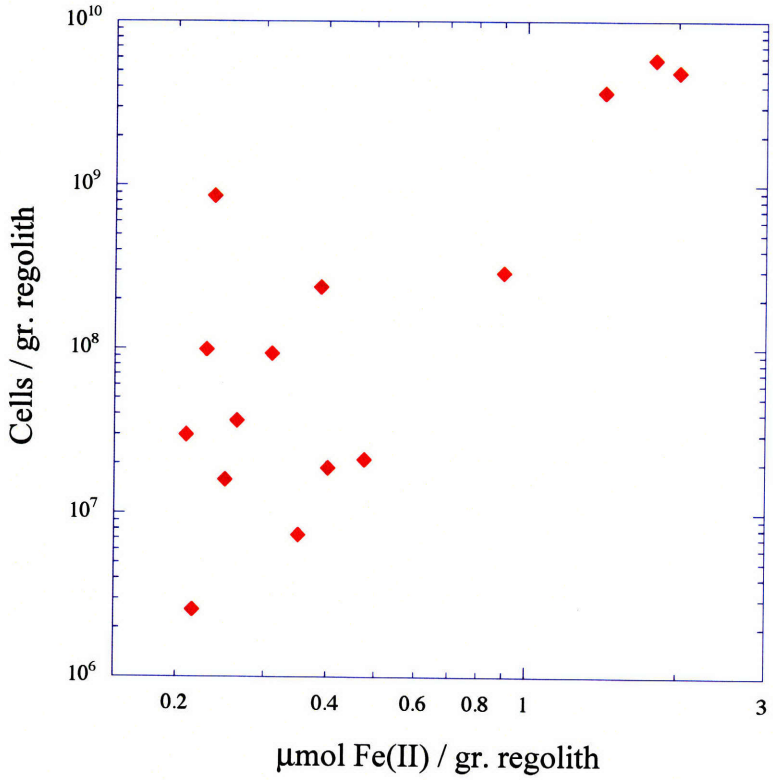

Figure 2-14: Correlation between direct cell counts vs. the amount of iron present in a gram of regolith (after Buss, 2005).

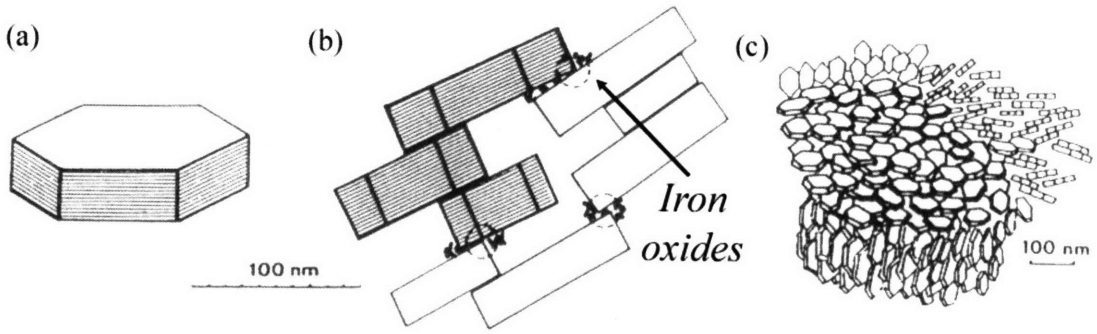

Figure 2-15: Kaolinite particles aggregated because of iron oxides. a) Kaolinite crystal. b) particle aggregate composed of kaolinite crystals connected at plate ends. c) micro-aggregate structure made of edge-face crystal associations. After Righi & Meunier (1995).

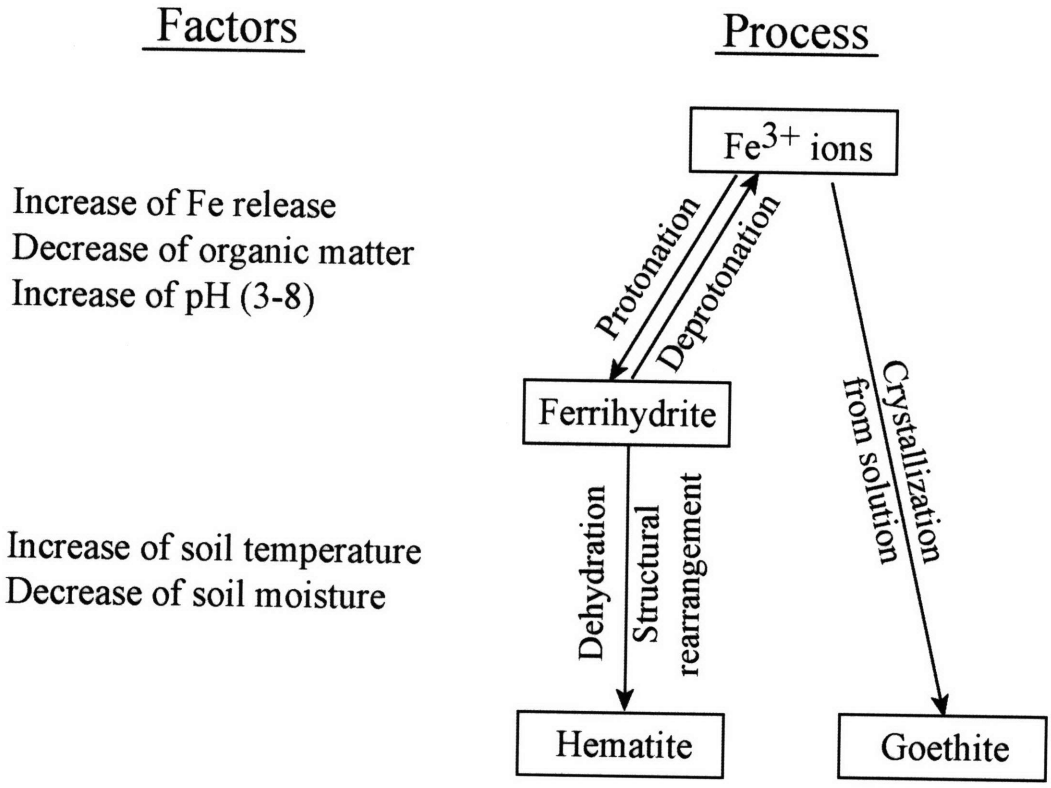

Figure 2-16: Hematite and goethite: Schematic representation of their competitive process of formation and factors influencing it (Schwertman & Taylor, 1989).

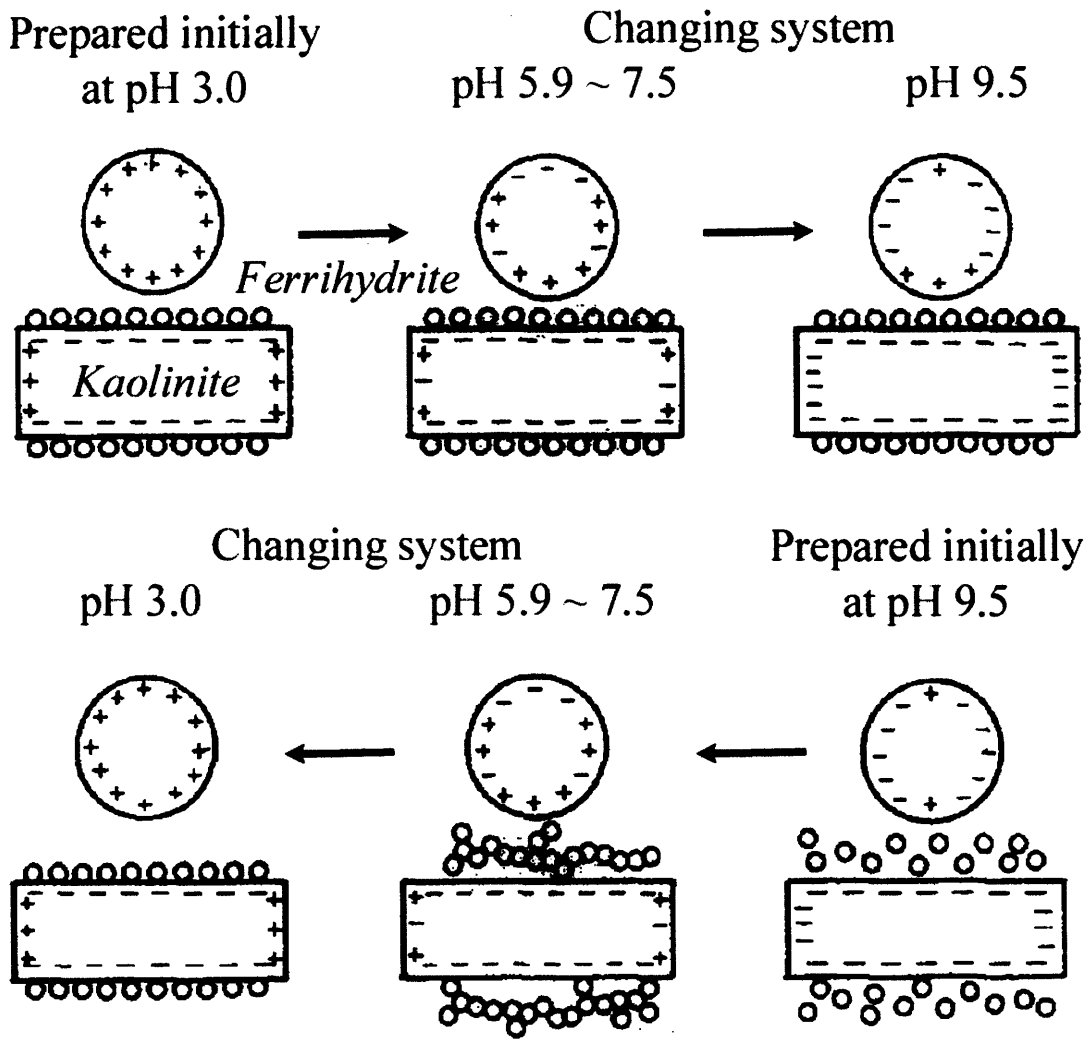

Figure 2-17: Schematic diagram of kaolinite-ferrihydrite associations for the complexes prepared initially at pH 3.0 and 9.5 and subsequently brought to other pH levels. In the first case, the associations were very stable and not sensitive to changes of the pH level. In the second case the degree of associations depends on lowering the pH levels. The circles above each association show the charge of the iron oxide under the specific pH value (Yong et al, 1987).

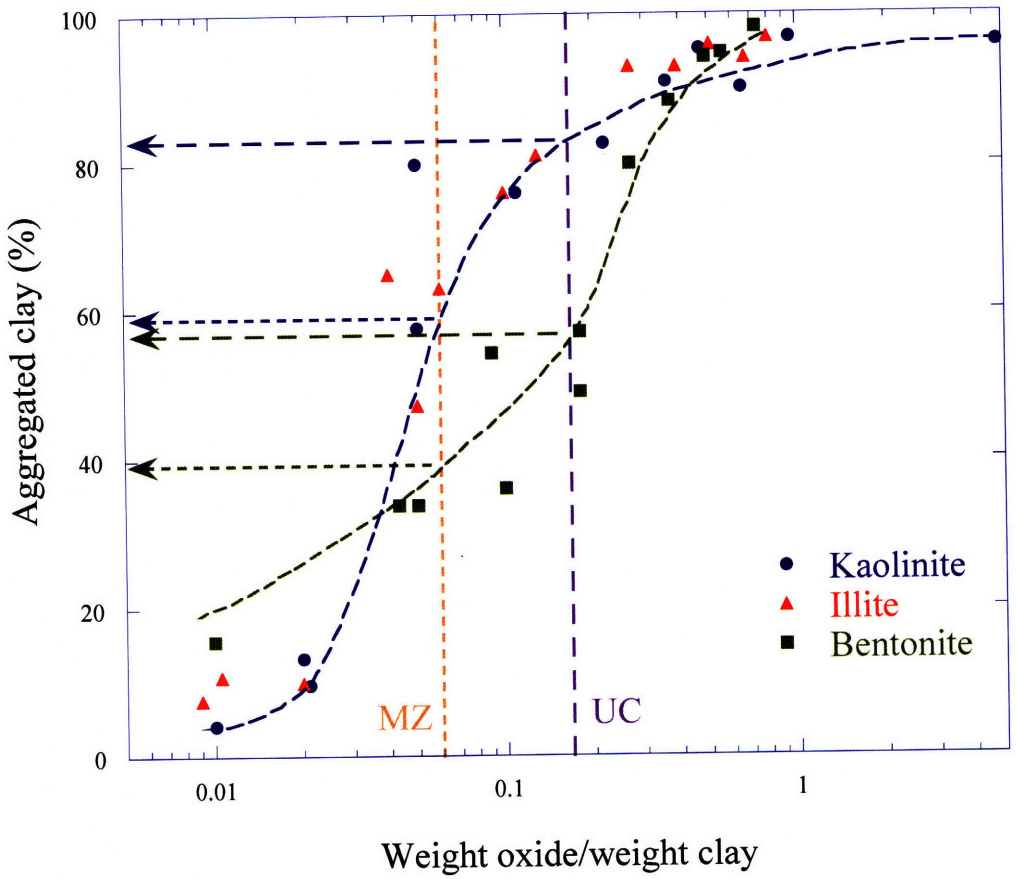

Figure 2-18: Clay still aggregated after a dispersion treatment as a function of hydrous iron oxide ratio (reproduced from Blackmore, 1973). The vertical lines show the level of the corresponding ratios for Upper Clay (UC) and Middle Zone (MZ) layers of Old Alluvium.

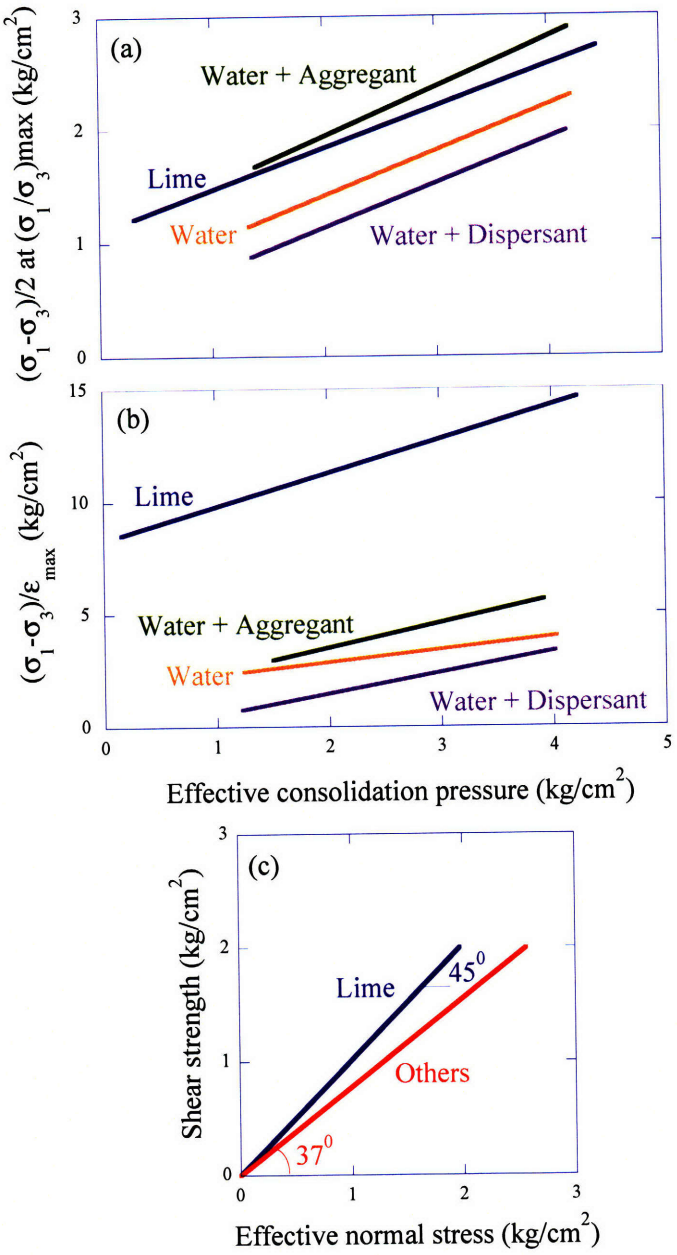

Figure 2-19: Effects of aggregants, dispersants and cementation on strength properties: (a) on shear strength; (b) on stress-strain modulus; (c) on friction angle. The aggregant used was a quarternary ammonium chloride and the dispersant sodium tetraphosphate (Loiselle et al, 1971, after Lambe, 1960).

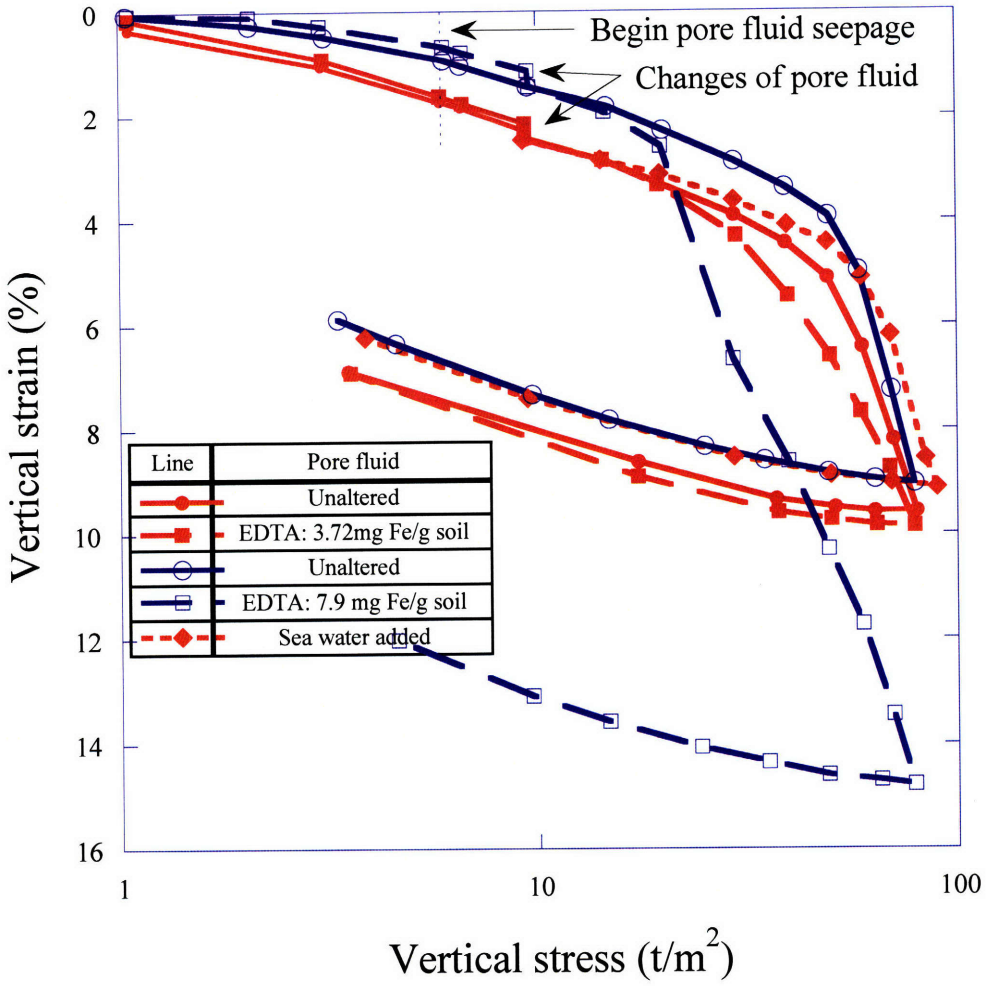

Figure 2-20: effect of EDTA on compression behavior of Labrador clay (Kenney, 1967).

3 Compression behavior of the Old Alluvium

3.1 INTRODUCTION

The previous chapter has shown that the Old Alluvium of Puerto Rico has a complex microstructure with physical characteristics that don't often coexist in sedimentary soils. The intact structure resembles a cemented granular soil consisting of quartz and silt-sized aggregate particles. The particles are lightly cemented by iron oxides, which are also responsible for stabilizing the aggregates. The aggregates are comprised of clay particles including a substantial fraction of a smectitic species (nontronite). Although the intact soil is stable, disaggregation can be induced by mechanical mixing and/or chemical treatment.

This chapter describes the 1-D consolidation behavior of the Old Alluvium. As the material has features of granular soils (macroscopic presence of quartz-aggregate grains), of bonded soils (iron oxide cementation), and of clays (clayey minerals, inherent swelling potential due to the geologic formation), it is interesting to compare its response to the behavior of more familiar sedimentary soils. The chapter builds on prior studies by Zhang (2002) and includes results of further tests by the Author to provide more detailed information from which to construct a constitutive model.

3.2 EXPERIMENTAL PROGRAM

3.2.1 Introduction

Zhang (2002) studied the consolidation behavior of the Old Alluvium using block samples obtained during construction of the stacked drift cavern for the Río Piedras station in San Juan. Laboratory tests were carried out in both conventional oedometer and high pressure consolidometer devices. From the available results, four tests are believed to provide reliable data. Table 3-1 summarizes the location of the block samples, the initial conditions and the loading-unloading sequence of each test.

The Author has conducted a new experimental program to investigate in more detail the compression behavior of Old Alluvium (Table 3-2). The main goals of this program were:

- to study the breakdown of the material at high stresses and investigate whether it is possible to define an intrinsic state for the destructured/disaggregated soil, as reported by others (e.g., Burland, 1990; Gens & Nova, 1993).
- to investigate how the swelling properties of the soil vary with the level of maximum loading applied on the soil.
- to examine the unloading and re-compression behavior under repeated loading cycles.

3.2.2 Experimental procedures

The 1-D compression behavior of the Old Alluvium was studied using two different devices:

1) The standard incremental oedometer device with dead loads. Tests followed well-developed and published techniques (e.g., Lambe, 1951). The stress limit of this device is around 30 ksc[15].

2) A modified Baldwin high force universal loading frame with automated feedback control[16] (Zhang, 2002). This load frame is configured with two load cells in order to achieve high resolution control at low and high pressure ranges. The current system was able to apply and maintain constant loads in the range 0.45 to 29,000 kg (i.e. equivalent to pressures up to 640 ksc).

In both cases, the load increment ratio, LIR = 1, and each load was maintained long enough to ensure the End of Primary Consolidation. The End-of-Primary time varied significantly during the test and especially between loading and unloading paths. The samples were inundated with distilled water, except test 102, which was inundated with glycerol.

The experimental setup followed the general guidelines presented by Zhang (2002). All of the test specimens were cut from Block B7[17] (Sample U5, Sub1), which was collected from a depth of 6m (Upper Clay). The block was still in a very good condition preserving its natural moisture content, it showed no cracks or detectable disturbance in the X-Ray photographs, and had a generally homogeneous macrostructure with minimal white venations. As noted by Zhang (2002) the physical orientation of the block samples was not recorded during field sampling and hence, there is no account of anisotropy characteristics.

---

[15] ksc is used as the main stress unit so stress levels are automatically normalized by atmospheres (σ/p_a)

[16] The Baldwin frame is generally used for testing rocks, concrete or other materials at MIT.

[17] Block 7 was extracted in June 1999 from the stacked drift cavern for the Rio Piedras station in San Juan.

As with the samples in the previous experimental program, trimming and cutting proved especially challenging. Prior experience has shown that the presence of quartzitic grains causes rapid deterioration of the teeth of regular bandsaw blades. Therefore, trimming was carried out using saws with carbide-tipped blades. Manual cutting was necessary as the material is variably brittle. Trimming of the specimen followed the guidelines proposed by Zhang (2002). Trimming (preliminary and final) of the sample into a cylinder required a sharp straight-edged knife and special care was exercised not to fracture the soil or detach surface wedges.

All the specimens were initially loaded up to 2 ksc, unloaded and inundated with water (or glycerol) under conventional dead load application[18]. As shown in Table 3-2, the natural specimens were not saturated. Hence attention was paid to prevent swelling when water was added to the specimen, in order to minimize microfabric changes during the inundation; initial loading to the level of 2 ksc was chosen for this purpose. In cases where expansive strains started to occur, the vertical consolidation stress was increased without waiting for the end of primary consolidation.

The current test program (Table 3-2) comprised of two pairs of tests (SJ1 and SJ2; 101 and 102), each including one standard oedometer (low pressure) and one high pressure compression test.

Sample SJ1 was consolidated in the standard oedometer; initially it was compressed to 2 ksc, unloaded to 0.25 ksc and inundated with distilled water. It was then consolidated up to a maximum stress of 16 ksc with one cycle of unload-reload. Sample SJ2 was also initially loaded to 2 ksc, unloaded to 0.25 ksc and inundated in a classical oedometer. After being transferred to the high pressure load frame, it was compressed to a maximum vertical stress of 512 ksc, unloaded to 0.5ksc, reloaded and finally unloaded up to 32 ksc[19].

The second set of tests, 101 and 102[20], were both inundated in the standard oedometer frame. Sample 101 was then transferred to the high pressure frame where it was compressed to a maximum vertical stress of 635 ksc with uloading – reloading cycles at 160 ksc, 320 ksc and 635

[18] As the inundation of the specimens destined for the high pressure load frame took place under dead load, some discrepancies exist in the strain measurements at the stress level of 2ksc, caused by transferring the sample between the two loading frames, and by the change in the data acquisition system.

[19] Specimen SJ1 and SJ2 were prepared by Ian Whitehead.

[20] Specimen 101 and 102 were prepared by Guoping Zhang, who was also responsible for the initial increments (up to 160ksc for 101).

ksc (2 cycles). It was finally unloaded to 5 ksc. Speciman 102 was consolidated in the classical oedometer to a maximum stress of 26 ksc, with one unload-reload cycle at 11 ksc, and 4 unloading-reloading cycles at 26 ksc, followed by a final unloading to 0.6 ksc. The distinctive feature of test 102 is the use of glycerol as the pore fluid in order to produce maximum expansion of the double layer in the microstructure. As discussed in Chapter 2, Old Alluvium in its natural state is not affected by the presence of glycerol – which is used to expand the double layer – because the swelling potential is masked by the soil structure and the presence of iron oxides. Because this protection is destroyed during breakdown, glycerol was used as a pore fluid to determine at which stress level and with what rate the soil swelling potential is released.

3.2.3 Discussion of results

Figure 3-1 summarizes the compression data for the tests performed by Zhang (2002) and Figure 3-2 the ones performed by the Author, using a loge-logσ'_v state space. This space provides a better linearization not only for sands and clays, but also for soil mixtures (Pestana & Whittle, 1995). Unless noted differently, all plots have the same axis scales, ranging from 10^2 to 10^3 ksc for the vertical stress and from 0.12 to 1.2 for the void ratio.

The common observation from all tests is that the Old Alluvium exhibits a significant compression under vertical loading, reaching up to 40% strain in the high-pressure tests. Furthermore, despite the large compressive forces applied and the extent of void ratio changes, there is a significant volumetric recovery during unloading, and some even samples swell back to their initial void ratios.

Tests also appear to have a characteristic apparent yield stress or preconsolidation pressure, which is in the order of 5 to 8 ksc for the Upper Clay samples, and 35 ksc for the Middle Zone sample (test Oed 8). In some cases this characteristic stress marks an abrupt break in the compression curve (for example test 101), while in other cases the transition to the higher compressibility regime is more gradual (for example oed13, Figure 3-1c).

Tests 101 and SJ2 revealed that there is a gradual increase in the amount of expansion, following the increase in the applied vertical stress. This can be observed in Figure 3-2b,c. Furthermore, Figure 3-3 plots the amount of recovered volumetric strain obtained during each of the unloading paths of test 101. The figure shows that unloading from high stresses (more than

100 ksc) results in much greater volumetric expansion (20% recovered strain) than unloading from lower stresses levels (less than 60 ksc – 5% recovered strain).

Unloading-reloading cycles show a stable pattern of volume change, and they are identical for the same load reversal levels; there seems to be, in other words, a memory of this reversal stress that defines the unloading-reloading behavior.

Reloading is characterized by significant hysteresis and an apparent yield stress that is lower than that of the first loading curve (at a level of 3-4 ksc). Figure 3-4 demonstrates the amount of hysteresis by plotting the accumulated strain energy[21] for the four unloading/reloading cycles in test 101.

In test 102, glycerol was used as a pore fluid[22]. However, the amount of swelling observed is still dictated by the maximum vertical stress and is of comparable magnitude with the corresponding stress levels in the rest of the tests, that are inundated with distilled water (see also Figure 3-13, which discusses the recovered volumetric strain for all the tests). As discussed in Chapter 2, the intact Old Alluvium material is not affected by the presence of glycerol during slaking tests. The results of test 102 indicate that the maximum load applied to the sample (30 ksc) was not sufficient to destroy the structure protecting the expansive clay minerals.

Figure 3-5 plots the values of the vertical coefficient of consolidation, c_v, for tests SJ2 and 101. The reported values were calculated using the log-time method. In both cases, the coefficient decreases significantly over the course of the test (4 orders of magnitude, from c_v = O[10^{-2} cm^2/sec] to O[10^{-6} cm^2/sec]). More importantly, it can be observed that the value of c_v does not only decrease during loading (solid lines in the figure) but also by about an order of magnitude during unloading (dashed lines in the figure).

Figure 3-6 plots the hydraulic conductivity against void ratio for the same tests. The values of the hydraulic conductivity, k, were obtained using the calculated coefficient of consolidation, c_v, and compressibility parameter m_v. There is again a net reduction in k, in the range of 4 orders of magnitude during each test, from O[10^{-5} cm/sec] to O[10^{-9} cm/sec]. However, in contrast to c_v,

[21] Strain energy for 1-D consolidation tests is defined as the work per unit volume (Ladd, 2001):

$$SE = \int \sigma'_v \, d\varepsilon_n = \sum (\sigma'_{v,ave} \Delta\varepsilon_n), \text{ where } \varepsilon_n \text{ is the natural strain}$$

[22] As already discussed, glycerol as pore fluid aids to immediately expand the double layer to its full length.

the conductivity increases during the unloading branches of each test. As a result, the permeability-void ratio relation is characterized by two parallel families of lines, one for the loading and one for the unloading paths. Along these paths, the hydraulic conductivity values range between 10^{-5} and 10^{-9} cm/sec.

The mineralogical and microstructural analysis of the Old Alluvium (Chapter 2) has shown that the material has features in common with granular soils, with clays and with cemented soils. Its behavior is hence expected to exhibit similarities with all of the above soil types. It is therefore most appropriate to discuss the above observations of the compression tests in parallel with the established frameworks of behavior for sands, clays, and finally for bonded soils. In this way, the unique features of Old Alluvium can be better identified.

3.3 GRANULAR MATERIALS AND OLD ALLUVIUM

It has been made clear that the Old Alluvium is not a cohesionless soil, however it contains a significant fraction of quartz minerals and aggregates of comparable size. Specifically, particle size analyses have shown (Zhang, 2002; Chapter 2) that the Upper Clay (at a depth of 3.7m) contains 20% quartz (and other sand size particles), while the Middle Zone consists of 30% quartz. Sands generally exhibit a smaller range of particle sizes and have a much simpler mineralogy than residual soils. However, it is certainly possible that the Old Alluvium shows behavior common with granular soils.

3.3.1 Compression behavior of cohesionless soils

Figure 3-7 shows the typical behavior of freshly deposited cohesionless soils in one-dimensional compression, plotted in the e-logσ'_v space. The specimens have been "freshly" deposited by means of pluviation or undercompaction at a range of initial densities (expressed by initial void ratios, e_0). The figure demonstrates the key characteristics of compression behavior for cohesionless soils:

- regardless of the initial formation density, specimens of the same sand exhibit the same behavior at high compression stresses and converge to a unique void ratio-stress relationship referred to as the Limiting Compression Curve (LCC). Pestana & Whittle (1995) showed that this curve can be described by a linear relationship in a loge-logσ' space.

- there is no clear distinction between an initial purely elastic response and the particle crushing at high stresses – instead, there is a gradual transition to the LCC region accompanied by significant plastic strains.

There is a general agreement in the literature (e.g. Roberts and DeSouza, 1958) that the principal mechanism that controls the soil response at high stresses (LCC region) is particle crushing[23], while at low stress levels the volume changes are due to the elastic response of the soil skeleton and sliding and rolling or particles (particle rearrangement). The transition between the low and high stress region therefore depends on how much rearrangement the structure can accommodate and on how prominent are the individual particles to breakage.

Figure 3-8 plots the results of the compression tests on the Old Alluvium, in the loge-logσ'_v space. The data are grouped according to the sample depth. One can see that there is generally a uniform behavior for each depth group, especially at high stresses (marked with the shaded band on the figure). However, the compression behavior of Old Alluvium presents some differences from the standard framework for granular materials:

- The Limiting Compression Curve is not unique at high stresses. The compressibility parameter (ρ_c) increases with depth in the ground.
- For each depth group, the Limiting Compression Curve is not well linearized in the loge-logσ'_v space. Instead, the compressibility (ρ_c) appears to increase with the level of stress. This is illustrated by the dotted line in Figure 3-8, which aligns only with a small part of the LCC for test 101.
- All samples exhibit a characteristic yield stress in the range of 5 to 8 ksc. This value is low relative to what is usually observed in sandy materials but is comparable to the values reported for angular particles. Figure 3-7 shows that very angular (calcareous and feldparitic) sands exhibit a yield stress in the range of 10-20 ksc, while quartzitic sands with rounded particles show a yield stress in the order of 200 ksc.
- The mode of transition to the high stress region is not the same in all cases – for example, as mentioned before, sample 101 exhibits a more abrupt transition than oed13.

The observed differences can possibly be attributed to the nature of the Old Alluvium and especially to the fact that compression stresses change the apparent soil mineralogy, as well as

[23] The term particle crushing is collectively used to describe all aspects of breakage and fragmentation.

that samples have variable composition of quartz and aggregates. The following section examines the factors that affect the compression behavior of granular soils aiming to understand how they may relate to the observed behavior of Old Alluvium.

3.3.2 Factors affecting the compression behavior of cohesionless materials

Based on the above observations and further investigation reported by Pestana (1994), the factors that affect the compression behavior of cohesionless soils can be summarized as follows:

1. Intrinsic (Material) Factors:

   1.1. Formation density and initial particle arrangement (fabric); these are particularly important in the low stress regime. In the case of weathered soils such as the Old Alluvium, they may vary irregularly with depth and within the same horizon, because they depend on the local intensity of weathering agents, the amount of mineral leaching etc. Such variations can explain the lack of relationship between void ratio and depth observed in Figure 3-8.

   1.2. Mineralogy; mineral particles with high tensile strength have higher resistance to fracturing, which is the mechanism of 1-D compressibility in the LCC region. As an example one can compare in Figure 3-7 the different response between the quartz particles of the Ottawa sand and the shell fragments of a calcareous sand (Quiou Sand). It has been discussed that in Old Alluvium high stresses break the aggregates and reveal clay platelets. As the Limiting Compression Curve depends on the soil mineralogy, it is anticipated that its characteristics would change as soil structure breaks down and different minerals become active.

   1.3. Grain characteristics, including particle size, angularity and gradation; these affect the onset as well as the development of the crushing, as stresses concentrate more through angular contact points. Sands with large and angular particles exhibit crushing earlier and are characterized by a gradual transition to the LCC regime, while fine sands with round particles exhibit a much more pronounced yield. Old Alluvium consists of both solid quartz grains and aggregates in non-uniform distribution within its presence. It is therefore possible that samples from the same horizon or even the same block to have different percentage of quartz vs. aggregates present, and hence to exhibit varying

resistance to fracturing. This could explain the observation in Figure 3-8 that each sample has a different transition to the high stress region.

2. External Factors:

   2.1. Effective stress on the soil skeleton and shear stress ratio; even though hydrostatic and one-dimensional compression are characterized by qualitatively similar behavior, the presence of shear stresses in 1-D compression enhances particle crushing (Datta et al., 1979; DeBeer, 1963; Vesic & Barksdale, 1963).

   2.2. Time dependent behavior; particle crushing is a time dependent phenomenon. Therefore, creep characterizes the behavior of the LCC regime even for dry uniform sands. It is highly possible that the compression response of the Old Alluvium is time dependent, however such behavior has not been studied so far.

   2.3. Interstitial fluids; the pore fluid can promote particle fracturing, by reducing the surface energy required for the propagation of a crack. Water for example can cause particle breakage through loss of cohesion due to mineral surficial energy reduction (Vutukuri & Lama, 1978); through suction reduction (Vutukuri & Lama, 1978); through expansion of clay minerals (De Alba & Sesana, 1978; Delgado et al., 1982)]; or through stress corrosion (Atkinson & Meredith, 1987). The factors are more significant for materials with large particles (broken rocks, granular fills for dams), because such particles are statistically prone to have more flaws. Chapter 2 discussed that the Old Alluvium contains clay minerals that are initially isolated in groups containing different interstitial fluid. The mechanical effect of pore fluids may therefore be important, and it will be further investigated below.

   2.4. Temperature effects, which have not been considered to date.

3.3.3 Particle crushing

In the general framework of granular material compression, particle crushing is significant, not only because it controls the soil response at high stress levels, but also because it becomes a crucial mechanism to be described in materials with grains that have an internal structure (aggregates), and therefore break and alter the overall particle size distribution. Mineralogical studies (Zhang 2002) have shown that in the Old Alluvium loading reduces the amount of silt-

sized particles and increases that of clay-sized particles, due to the breakdown of the silt-sized aggregates. Therefore, observations and studies on particle crushing of pure sands could benefit the modeling of microstructural evolution in the Old Alluvium during compression.

Several authors have reported tests under high stress levels to study particle crushing and the nature of the transition to its regime. These include Terzaghi and Peck (1948), De Souza (1958), Harremoes (1959), Roberts (1964), DeBeer (1963), Hagerty et al (1993) and Nakata et al (2001a,b). Stress levels vary in the order of 10^3 ksc, with Hagerty et al (1993) reporting a compression stress of 6.89×10^3 ksc. The studies showed that crushing is more extensive in angular, rough-surfaced particles, and in poorly graded materials. Furthermore, the stress level of the apparent yield (the onset of particle crushing) depends little on mineralogy, increases with increasing relative density and decreasing mean particle size, and decreases with particle angularity. For very angular particles the yield point is difficult to identify. Hagerty et al (1993) also postulated that at very high stresses the amount of crushing decreases, and the material exhibits a pseudo-elastic compression behavior, but with much higher stiffness than its initial state.

Based on these observations, the Old Alluvium should be expected to exhibit an apparent break point at a stress level that increases with decreasing void ratio, mean particle size and particle angularity. Indeed, the sample from the Middle Zone (oed 8), which has a much lower initial void ratio, has a much higher apparent yield stress (compare 35 ksc to 5-8 ksc). Variations in the percentage of quartz vs. aggregate particles present can account not only for the different yield stress levels, but also for the smoother or more abrupt transitions observed.

More relevant to the Old Alluvium are natural materials whose microstructure is altered by particle crushing such that their response at high pressures is also affected. Such materials include pyroclastic weak rocks, (Cecconi & Viggiani, 2001), carbonate sands (Coop, 2000), calcarenites (Lagioia & Nova, 1995) and compacted decomposed granite (Fukumoto, 1990). For example, Cecconi et al (2002) performed chemical micro-analyses on samples of a pyroclastic deposit from Central Italy (Pozzolana Nera) and concluded that the soil bonds are made of the same constituents as the grains and therefore bond deterioration and grain crushing during first loading are indistinguishable mechanisms. In the Old Alluvium, high stress loading causes more complicated changes than particle or bond crushing. However, the above studies provide helpful insights for the modeling of the microstructural evolution, as shown in Chapter 4.

Finally, there are cases in which particle breakage is aided significantly by the presence of pore water. This role of pore fluids is important in the Old Alluvium, since microstructural research has concluded (Chapter 2) that isolated pore spaces with different salinity exist within the soil microstructure.

Among the various ways water can interfere with the particles (mentioned in 3.3.2) stress corrosion is most relevant. The mechanism is named as such, because water can act as a corrosive agent and the stressed areas close to the tip of a micro-crack are much affected by this corrosive agent than the less-stressed material away from the tip. Recently, Oldecop and Alonso (2001, 2003) studied the effect of stress corrosion on particle breakage in rockfills. They observed that increasing the Relative Humidity (RH) increased the apparent compressibility, until its maximum value at saturation. Also, beyond an apparent "yield stress", increase of the relative humidity under constant loading resulted in a sudden strain increase ("jump"), such that irrespectful of the stress history or the mode of RH increase, samples with the same RH exhibited the same compressibility under compression (Figure 3-9). Hence, any situation leading to a change in water content of the particles could be enough to trigger collapse deformations and to increase the material compressibility against further loading. Furthermore, saturation of the particles seemed sufficient to produce the same collapse deformation as full flooding.

Therefore, the compression behavior during particle crushing is controlled by the level of the applied stress and also by changes in relative humidity (or suction); breakdown/collapse can occur as an increment of strain not related to an increment in load, but rather to an increment in the relative humidity. As discussed in Chapter 2, the Old Alluvium is characterized by at least two levels of porosity (e.g. macro and micro pores), and the pore fluid in the micropores has probably a higher salinity than the bulk water in the macropores. When a connection is established between the two porous spaces, osmotic changes will take place, and hence stress corrosion is a potential mechanism aiding to the macrostructural breakdown and the increase of the material compressibility.

3.3.4 General remarks regarding granular materials

In its initial, intact state, the Old Alluvium has features of a granular material, and its response to compression loading is affected by the factors that control particle rearrangement at low stresses and particle crushing at high stresses. Particle crushing is particularly important,

because by breaking down the aggregate structure, it reveals the initially concealed clay minerals.

The constitutive framework for granular soils can provide the basis for modeling the compression behavior, however is not sufficient to describe materials like the Old Alluvium. The non-uniform distribution of solid particles and aggregates within the soil structure (due to weathering) results in different patterns of particle rearrangement within the same soil. Furthermore, the response at high stresses (Limiting Compression Curve) is re-defined continuously, because breakdown does not only crush the soil particles, but also alters the apparent mineralogy. To accommodate these new needs, a granular framework should be enhanced to account for changes in the microstructure.

3.4 CLAYEY MATERIALS AND OLD ALLUVIUM

3.4.1 Compression behavior of clays

The consolidation of clay suspensions is characterized by a virgin compression line (VCL) illustrated in Figure 3-10 in loge-logσ'_v space, which provides a better linearization, as shown in the figure, which plots over more than 7 cycles of stress. Intact clay specimens exhibit initially much lower compressibility but eventually converge into this virgin compression line. The observed yield point is known as "preconsolidation" pressure, and it is often noted as σ'_p. Sample disturbance may significantly affect the initial part of the loading curve, up to the preconsolidation pressure. Figure 3-11 shows the 1-D compression behavior of an intact Boston Blue Clay sample, and notes the estimated initial stress and void ratio (σ'_{v0}, e_0), and the preconsolidation pressure, σ'_p.

Preconsolidation can be the result of one of four basic mechanisms (Ladd, 1999). Pure mechanical mechanisms include unloading due to erosion or physical removal of the overburden materials, and result in a constant ratio σ'_p/σ'_{vo} within an 1-D soil profile. Physico-chemical processes (carbonation, Al/Fe oxides aggregation) result in natural cementation associated with higher values of σ'_p but an erratic OCR profile in the soil. The preconsolidation pressure is also

altered by desiccation (drying due to evaporation or freezing, resulting in erratic σ'_p profiles) and aging (1-D drained creep, which produces a constant σ'_p/σ'_{vo}).

Unloading results in expansion of the soil, however, the strain recovered is much smaller than the strain caused by the compression loading (Figure 3-11). This difference in compressibility indicates that the virgin compression behavior involves irreversible plastic strains. Upon reloading, sedimented clays present only a small hysteresis with regard to the unloading curve, and there is a clear memory of the preconsolidation as the behavior converges towards the virgin compression line (Figure 3-11).

Idealized 1-D models introduce the compression index, C_c, to describe the slope of the virgin compression line, and the swelling (or expansion) index, C_s, to describe the behavior during unloading and reloading cycles[24]. These are shown in Figure 3-11. The Figure demonstrates that in these simple 1-D models three variables (σ'_p, C_c, C_s) are sufficient to describe the volumetric changes during compression, unloading and reloading of the clay.

Table 3-3 summarizes characteristic values that would have been attributed to the Old Alluvium samples, had it been a conventional clay material. Examining the behavior of Old Alluvium within a clay framework yields many interesting observations:

- The soil appears to be overconsolidated. However, the notion of preconsolidation pressure could be misleading. As discussed before, the quartz particles and aggregates are believed to dominate the behavior at low stresses, while the clay minerals appear to be concealed and inactive within the microstructure. Hence the change in compressibility is not strictly the result of mechanical unloading or physicochemical action between clay particles (mechanisms of preconsolidation stress), but also probably the initiation of disaggregation and particle crushing (presence of a yield stress). Barksdale & Blight (1997) similarly discuss that the equivalent preconsolidation pressure observed in the compression behavior of a residual andesitic lava is a measure of the strength of the interparticle and intermineral bonds remaining in the soil after weathering rather than just a traditionally defined preconsolidation pressure. Mesri and Adbel-Ghaffar (1993) have compiled an extensive database on the relationship between cohesion intercept and preconsolidation pressure of stiff natural clays and

[24] In the ε_v-logσ'_v space, the notation CR and RR is used for the compression and swelling index respectively.

clayey shales (Figure 3-12). For the Old Alluvium, triaxial tests (Zhang, 2002) on samples from block B7 (depth 6m, Upper Clay) showed a cohesion intercept $c'_{(6m)} = 0.26$ ksc, while a triaxial test on a deeper sample (12m depth, Middle Zone) yielded $c'_{(12m)} = 0.24$ ksc. From tests 101/SJ2 (also on block B7), $\sigma'_{p(6m)} \approx 7$ ksc, and from oed8 $\sigma'_{p(12m)} \approx 35$ ksc. Hence, $(c'/\sigma'_p)_{(6m)} = 0.037$ and $(c'/\sigma'_p)_{(12m)} = 0.007$, which are also plotted on Figure 3-12. The Upper Clay measurements fall within the envelope proposed by Mesri and Adbel-Ghaffar (1993), but also the Middle Zone ones are still within the range of the reported data. The comparison demonstrates that even though the Old Alluvium is characterized by a combination of small cohesion and high preconsolidation values, it correlates with the available data on overconsolidated clays and some clayey shales.

- The amount of volumetric expansion gradually increases with the level of preconsolidation. This can be seen directly from the compression tests (Figure 3-2), and is further demonstrated by Figure 3-13, which plots the recovered volumetric strain during unloading from all available tests. The figure shows that unloading from stresses lower than 60 ksc leads to moderate volumetric expansion (8-12% recovered volumetric strain). Unloading from higher stresses (more than 100ksc) causes much more significant volumetric changes (up to 25%). To further demonstrate this observation, Figure 3-14 plots the values for the compression indexes C_c and C_s (see also Table 3-3). Given the significant change in compressibility during a single test, the figure differentiates between results below and above 100 ksc. The data shows that the compression index C_c is generally smaller in the higher stress regime, while index C_s increases. Furthermore, the C_s/C_c ratio is as high as 0.4, instead of 0.1 to 0.2 usually reported for clays.
- Figure 3-13 also shows that the rate with which strain is recovered is higher at higher "preconsolidation" stresses. In addition, it indicates that the rate of strain recovery is unique for each stress level in the first compression curve.
- At high stresses, the repeated cycles of unloading and reloading show the same pattern of volume change: unloading from the same "preconsolidation" pressure results in almost identical behavior during unloading. It is unclear from the available data at which stress level the amount of volume change stabilizes. Tests 101 and SJ2 suggest that this happens at about 80 ksc (Figure 3-2, Figure 3-3, and Figure 3-13).

- Reloading produces a large amount of hysteresis (see Figure 3-4) and is characterized by a smoother transition to the high stress compression behavior. Such a hysteresis, and the presence of an apparent "yield" stress are not common in clay behavior.
- In all cases, reloading brings the soil back to the same state (stress and void ration) on the first primary loading curve, and there appear to be no irrecoverable strains from the unloading-reloading cycle. The soil appears to keep a memory of the maximum effective stress applied on it.
- As shown in Figure 3-5, the coefficient of consolidation during a single test decreases four orders of magnitude, and it does decrease during unloading. Figure 3-15 shows the changes observed in c_v during loading cycles on Boston Blue Clay; in contrast to the Old Alluvium, the coefficient of consolidation decreases only one order of magnitude. Similarly, Figure 3-16 shows the evolution of hydraulic conductivity for Boston Blue Clay and test 101. Compared to Boston Blue Clay, changes in the Old Alluvium appear dramatic. The observation that the coefficient of consolidation, as well as the hydraulic conductivity of the Old Alluvium decrease substantially during compression suggests that the initial macroscopic porous space collapses due to loading. During unloading, the macroscopic void ratio increases as does the hydraulic conductivity; however, the coefficient of consolidation continues to decrease. This fact is related to the soil compressibility and that suggests that the flow associated with the clay minerals (flow in the microscopic intra-platelet porous spaces) is restricted, and thus delays the consolidation process. It is postulated that this restriction is a result of the swelling that takes place within the platelets, creating a widened double layer space around the clay minerals.

The above-discussed observations indicate that in general, aspects of clay behavior become important for the Old Alluvium as the structure breaks down and the clay minerals become active. The full swelling potential of the material is not readily available initially, but is revealed gradually. The observations support the assumption formulated in Chapter 2, that the Cation Exchange Capacity and hence the double layer length of the smectitic minerals in the microstructure of the Old Alluvium are initially suppressed by the soil structure and the presence of the iron oxides.

As the swelling potential is revealed, it is probable that the response of the Old Alluvium become sensitive to those factors that affect the compression of clays.

3.4.2 Factors affecting the compression response of sedimented clays

The factors affecting the compression response of sedimented clays can be generally categorized as mechanical and physico-chemical (Olson & Mesri, 1970, Pestana, 1994) and depend greatly on the stress history of the deposit. Particle rearrangement, sliding between particles, deformation (including bending of the plate shaped clay minerals) and rupture of particles are mechanical processes that influence the compression behavior at large loading stresses. Physico-chemical mechanisms, on the other hand, are mainly associated with surface force interactions between the clay minerals and the pore water system, especially the double-layer (osmotic) repulsive forces. Thus, the compression behavior at large stresses is affected by the clay mineralogy, the pore water electrolyte concentration, and the temperature conditions of the test. Pestana (1994) offers a comprehensive study of the effect of these physico-chemical factors, which is summarized here with Figure 3-17 and Figure 3-18. Figure 3-17 compares the response of kaolinite, illite and calcium montmorillonite, hydrated with distilled water. The different surface areas of the minerals affect the formation void ratios, and therefore the location of the virgin compression line (limiting compression curve on the figure). The slopes of the lines also vary; the compression coefficient in the plotted scale (ρ_c in the MIT-S1 framework, see Chapter 4) is 0.16 for the kaolinite, 0.19 for the illite and 0.22 for the montmorillonite; Pestana further reports values up to 0.6 for some montmorillonites. Figure 3-18 shows the effects of the cation valence, the electrolyte concentration and pH on the compressibility of montmorillonite. Variation in the electrolytic concentration has hardly any effect on calcium montmorillonite but causes large changes in the formation density and subsequently on the overall compressibility of the sodium montmorillonite. In both cases though the slope of the virgin compression line is unaltered.

In relation with the behavior of Old Alluvium, the above findings indicate that the observed increase in the slope of the Limiting Compression Curve (Figure 3-8) may well be the result of the change in active mineralogy, as the soil structure breaks down. In addition, changes in the electrolyte concentration – induced by linking the macroscopic pore space to the high salinity microscopic space – can also cause large changes in the compressibility response.

3.4.3 Examples of clays with behavior similar to Old Alluvium

There are examples of clays that do exhibit large swelling although the primary loading produces very small compression strains. Data from Burland (1990) show that the swelling coefficient, C_s, of 3 clays increases significantly during subsequent unloading cycles and reaches values comparable to those of Old Alluvium (Table 3-4).

Figure 3-19 plots oedometer tests on Todi clay, an intensively fissured, heavily overconsolidated medium plastic lacustrine clay with 3-5% clay fraction, 19% water content, 50% liquid limit and 28% plasticity index (Calabresi & Scarpelli, 1985). The swelling results in significant volume change and the soil compressibility is much higher during reloading. Alonso (2002) observes that there is a distinct "yield" stress during first loading that is much higher than the apparent yield stress during reloading and concludes that it is not only the loading at high stresses but also the extensive swelling that damage the soil structure and transform the natural material to an extent that erases the maximum previous preconsolidation stress. A similar decrease in the apparent yield stress during reloading is also observed in the Old Alluvium (tests 101 and SJ2 in Figure 3-2).

There are also examples where a change in salinity of the pore water can lead to swelling behavior similar to that of Old Alluvium. For example, Figure 3-20 shows the swelling of Bisaccia clay. Bisaccia is a very active smectitic clay of marine origin, containing 30% smectitic minerals, 10% kaolinite and 20% illite, and has a liquid limit of 110% and a natural salt content of 3g/l (Alonso, 2002; DiMaio et al, 2004). The clay samples were reconstituted with and immersed in a 1 M NaCl solution, then exposed to distilled water at 2 different stress levels during unloading. When the exposure took place at the end of unloading (at 0.1ksc) the soil instantaneously swelled to a little above the initial void ratio. On the other hand, when the exposure took place at higher stresses (10ksc) the immediate swelling was small, but the soil eventually swelled dramatically (Picarelli & al, 2000). Alonso (2002) interprets this behavior as a result of easier access of the distilled water to the clay minerals, as the structure progressively rearranges during swelling. DiMaio (2004) also reports values of the coefficient of consolidation for Bisaccia clay. Figure 3-21 shows that increasing the salinity of the pore fluid leads to a significant decrease of the coefficient of consolidation during unloading (more than 2 orders of magnitude).

3.4.4 General remarks on clay behavior and Old Alluvium

The structure of the Old Alluvium is far more complicated than most sedimented clays. The significant volume changes that occur during unloading are due to the presence of smectitic minerals (nontronite fraction), therefore the unloading behavior of the Old Alluvium is affected by the mechanical and environmental factors that control the response of clays.

An important observation of this section is that microstructural arrangements can have a significant effect on the compression/swelling response of materials that contain clay minerals. Clays with unusual behavior (that are rather unsystematically reported) could be better understood if the macroscopic observations were linked to their microstructure.

3.5 BONDED SOILS AND OLD ALLUVIUM

The mineralogical analyses, as well as the ESEM observations on the Old Alluvium (Chapter 2) show that the soil is initially cemented, with iron oxides forming connecting bridges between the quartz grains and the aggregates. Furthermore, the aggregates themselves consist of a cemented network of platelets.

Beyond similarities with granular or clayey materials, the intact Old Alluvium is a bonded soil, and should be expected to behave as such during the first loading. This section looks into the nature of bonded soils and the macroscopic response that is induced by compression loading, in order to investigate to what extend the Old Alluvium behaves according to the frameworks established for these materials.

3.5.1 Introduction and definition of bonded soils

Most soils present some form of structure in their natural state. There is extensive reference for structure in soft clays (Mesri, 1975; Tavenas & Leroueil, 1990), stiff clays and clay shales (e.g. Calabresi & Scarpelli, 1985; Burland, 1990; Burland et al., 1996; Cotecchia, 1996, Cafaro, 2001; Alonso, 2002), granular soils (e.g. Mitchell & Solymar, 1984; Coop & Atkinson, 1993), residual soils (e.g. Vaughan, 1988; Wesley, 1990; Zhang 2004b) and weak weathered rocks (e.g. Eliot & Brown, 1985; Addis & Jones, 1990; Sekiguchi et al, 1985, Lagioia & Nova, 1993). In most cases, the term "structured soil" or "bonded soil" is used to describe the presence of any form of structure within the soil.

Mitchell (2005, 1976), also Lambe & Whitman (1969), Burland (1990), Leroueil & Vaughan (1990) all define soil structure as the combination of fabric (arrangement of particles) and interparticle bonding. However, as Cotecchia & Chandler (1997) noted, bonding is not necessarily a solid link; especially in clays, it can be the result of various phenomena such as electrostatic, electromagnetic or other forces acting to connect the soil particles. Therefore, the nature, amount and strength of bonding are influenced by the soil mineralogy, the water chemistry during deposition, the pressure, temperature and organic content; it also depends on mechanical conditions such as deposition and consolidation rates and strain paths.

3.5.2 Nature of bonding

Bonding is a micromechanical feature of bonded soils, which alters the nature of particle interactions and thus affects significantly the mechanical response of the soil at the macroscopic level.

Natural soils are known to develop bonding through mainly two distinct processes: precipitation of material to (sedimentary) deposits and weathering of parent rocks, mostly igneous crystalline ones (Tamagnini, 2002).

Precipitation can be concurrent with deposition or be post-depositional, and is often associated with diagenesis and gravitational compaction. Hence bonding tends to increase with time. Various processes belong to this category, including:

- cementation due to chemical precipitation of carbonates, gypsum, iron or aluminium oxides and hydroxides at particle contacts
- cold welding due to high pressure
- solution and precipitation of silicates at intergranular contacts
- thixotropy in fine-grained soils[25]
- ageing effects
- coalification of organic sediments due to development of aliphatic chains in molecules
- combinations of the above

[25] The term "thixotropy" is used to describe a strength increase with time at constant composition (Lambe & Whitman, 1969). Thixotropy is completely reversible upon further loading.

Weathering leads to breakdown of parent rock material through mechanical and/or chemical degradation and hence to the formation of residual soil deposits. Factors that facilitate weathering include crystal dissolution, chemical reactions, and thermal straining (Mitchell, 2005). As extensively discussed in Chapter 2, various environmental agents (temperature and chemical composition of the pore water) act on the less chemically stable minerals (felspar, mica) and transform them into more stable ones (kaoline, illite). In the intermediate stage, bonding and structure are present due to crystallization associated with the formation of new minerals and the precipitation of salts and oxides; some unaltered minerals and part of the initial structure are also encountered. Mechanisms such a drying cycles can lead to further aggregation of the product clay particles with the generation of van der Waals bonds, which are usually strong and difficult to reverse (Burland, 1990). In the final product, most of the original minerals (except mainly quartz) have been decomposed or disintegrated. In addition, some of the newly formed minerals are removed by leaching, leading to a gradual increase in porosity. Extreme drying can further dissolve bonds by inducing strong acidity on the clay surfaces. Therefore, weathering aids the formation of bonded soils from solid rocks, but it can eventually destroy their structure.

3.5.3 Bonding and macroscopic behavior

The presence of bonds in a soil affects significantly its macroscopic behavior. In detail, it is usually observed that (Leroueil & Vaughan, 1990; Tamagnini, 2002):

- the soil exhibits a more pronounced yield, whether in compression, unloading or shear
- because of the strength of bonds and the open nature of the material (increased void space due to the structure between the particles), these soils exhibit a flexible skeleton and an elastic behavior up to the critical (yield) load (Bjerum, 1967)
- at a given void ratio during virgin compression, bonded clays exhibit higher stresses than are possible for the equivalent unbonded material. This is illustrated in Figure 3-22, using data from the Bothkennar clay[26]. As also shown in the figure, in many cases the compression curve eventually converges towards that of the unbonded material
- the shear strength increases

[26] Bonding of Bothkennar clay is formed by aluminosilicates and iron compounds.

- in many cases, bonding builds tensile strength and 'true' cohesion
- under shear loading the material response usually changes from brittle/dilatant to ductile/contractant behaviour as confining stress increases
- after yielding, bond effects tend to decrease
- in soils containing expansive minerals, removal of bonds usually causes increase in the amount of swelling (during unloading)
- when bonds are fragile in nature, or the skeleton has no solid arrangement, sudden or fast destructuration can lead to unstable soil behavior and collapse. This phenomenon is encountered in quick clays, because their mineral grain skeleton has an extremely open arrangement, "like a card house built up of thin plate-like particles" (Bjerum 1967).

The above observations, and especially the fact that many bonded soils appear to approach the behavior of their unbonded equivalent with the breakdown of structure, have led to a generally accepted pattern of studying bonded materials with reference to their destructured or intrinsic states. Intrinsic states refer to properties of reconstituted soils, where the structure has been entirely removed. According to Burland (1990) this state can be achieved by thoroughly mixing the natural soil at a water content between w_L (liquid limit) and 1.5 w_L. The intrinsic properties can then be obtained through one-dimensional consolidation, and with pore water chemistry similar to that of the natural pore water.

In most practical cases, the destructuration process is gradual and the final state not always clear. Thus, using the reconstituted material as a reference state has offered many advantages. In addition, a vast amount of experimental data (e.g. Burland, 1990) has always justified this approach. Figure 3-22 introduces this principle. After significant loading, the behavior of the natural intact clay samples converges to that of the reconstituted clay. This principle has influenced the majority of constitutive models for bonded soils (Chapter 4).

3.5.4 Breakdown of soil structure

Structure can be removed from a soil through mechanisms that either break the bonds or remove them from the soil skeleton. These mechanisms can be the result of geological processes, excessive loading, chemical actions, or environmental activity. In more detail:

- The main geological process that destroys soil structure is weathering; the alteration of minerals and the eventual leaching of weathering products usually weaken any form of soil structure.
- Loading destroys bonds mechanically. Even 1-D compression or consolidation loading past the soil yield strength is capable or breaking down or disassociating the bonding developed between the soil particles. Shearing (either in compression or in tension) naturally damages interparticle bonding.
- Unloading can also destroy structure very effectively, especially in soils containing expansive minerals; the strains induced by swelling are sufficient to break down most of the bonding (Leroueil & Vaughan, 1990; Burland, 1990)
- Cyclic loading, even in small levels of stress, accelerates the destruction of bonds, as expansive pressures are exerted on a skeleton already weakened by loading, and vice versa.
- Chemical actions can dissolve and carry away bonds, leaving behind a rather collapsible material. The most common chemical action is the leaching of cementing agents, for example soluble $CaCo_3$ found in calcareous soils or in carbonate bonding. However, recalling that bonds are not necessarily solid links, this category may include any action that would disrupt the forces established between particles; for example change in the chemistry of pore water, or addition of highly valenced agents.
- Cyclic climatic loading (seasonal water content changes, dry and wet cycles) is also responsible for significant bond damage, as it combines mechanical effects (expansion and contraction) with chemical changes due to variation of water content and electrostatic forces that can develop during dry conditions. Again, the presence of expansive minerals is very favorable to the destruction process. Cafaro & Cotecchia (2001) showed that several drying-wetting cycles are capable of cause a progressive destruction for an overconsolidated stiff marine clay from South Italy[27], while drying can eventually cause the same damage as mechanical loading, but at a much slower rate (Figure 3-23).
- Seasonal climatic loading, namely freezing, that induces expansive strains.

[27] Montemesola clay, composed mainly of illite (50-70%), kaolinite (10-25%), ferriferous chlorites (10-20%) and Montmorillonite (5-10%). Carbonate bonding is present due to diagenesis.

3.5.5 Old Alluvium as a bonded soil

The Old Alluvium exhibits macroscopically many of the characteristic observations discussed above. There is a pronounced "yield", that defines two distinct regions during compression loading, one of low relative compressibility (low stress range) and one with much higher relative compressibility (high stress range – see Figure 3-8). As the structure breaks down, the compressibility further increases. Furthermore, unloading causes increased amounts of volume change.

The structural breakdown of the Old Alluvium in 1-D consolidation loading is the result of a combination of these mechanisms. Compression loads mechanically break down the cementation between grains and aggregates, and between platelets within the aggregates. Physico-chemical loading, caused by changes in the pH and the salinity of the micro-pores when the distilled water in the macroscopic pore space gets access to these pores, affects the iron oxide disaggregation. Furthermore, the extensive volumetric expansion during unloading imposes stresses that facilitate the mechanical breakdown of the cementation.

It is very difficult to fully disaggregate the Old Alluvium. Figure 3-24 compares the compression behavior of intact samples with material that has been reconstituted from bucket samples at water content $w = 1.5w_L$[28]. The relative response is different from what it is generally reported for bonded soils (Figure 3-22), i.e. the compression of intact samples does not converge towards the response of the reconstituted samples. The intact samples exhibit much lower compressibility at all stress levels.

Recalling the prior discussion of material microstructure (Chapter 2), compression of Old Alluvium not only breaks cementing bridges between or within the aggregates, but also reveals a different mineralogical composition, and therefore alters the character of the soil (by increasing the activity of the clay fraction). Furthermore, as discussed in Chapter 2, bonding does not only originate from precipitation, but is also due to electrochemical forces. Hence, the amount or resistance of bonding is not only a function of the mechanical loading, but also of various physico-chemical factors, like the local (microstructural) water chemistry, or the compounds present. As a result, it is highly probable that the manual disaggregation of the reconstituted samples in Figure 3-24 did not have the same effect on the microstructure as the mechanical

[28] The state of disaggregation is not defined in these tests. Later tests by Zhang (2004b) showed than even blending of Old Alluvium in a mixer for 30 min was still generating mechanical disaggregation.

loading of the intact samples. Different loading conditions won't necessarily lead to the same ('reference") destructured state; referring to a reconstituted state is not appropriate for the Old Alluvium.

This is not the first case that such an observation is made. Mitchell (1976) thought that reconstituted behavior should depend on the strength of the pre-existing units and the mixing effort. Cotecchia and Chandler (1997) used electron microscopic images of Pappadai[29] clay to show that the reconstituted samples exhibit a sedimentation structure that differs from that of the natural soil. Fearon & Coop (2002) also investigated the effect of different reconstitution energies on the soil microstructure and its Atterberg limits. The studied materials are from the Sicilide Unit (Argille Scagliose, South Italy), which contains scaly clays, intensely fissured marls and clay shales inter-bedded chaotically. Some samples were reconstituted traditionally (through thorough mixing at $1.2\text{-}1.5w_L$) and some were repeatedly minced (passed several times through an industrial food mincer). Figure 3-25 shows SEM pictures from the natural, reconstituted and minced material. The natural sample (Figure 3-25a) contains aggregates of clay particles greater than 2μm, irregularly arranged. In the reconstituted (Figure 3-25b) the material is finer and more homogeneous but composite particles can still be seen (although they tend to be smaller than the natural). The minced sample (Figure 3-25c) has very different fabric: no composite particles can be seen and the clay mineral sheets exhibit a clear orientation. These microstructural images show that classic reconstitution efforts did not provide the energy essential to break the microstructure of the clay aggregates, and only mincing managed to destroy the intra-particle bonds.

3.5.6 General remarks on bonded soils and Old Alluvium

The Old Alluvium is a bonded soil but its structure is the result of both precipitation of cementing agents and electro-chemical associations in the scale of the clay minerals. Hence, its response to compression loading depends on the mechanical as well as physico-chemical characteristics of the soil skeleton and its environment.

The behavior of the Old Alluvium indicates that a new distinction should be made when studying bonded soils. Traditionally, these materials are assumed to have a reconstituted state,

[29] Liquid limit 65%; Plastic limit 30%; and 12% smectite content.

which is unique and can be reached after extensive loading. This approach has been able to describe successfully the behavior of the first type of structured materials (diagenesis of sedimented soils), the bonding of which is caused by crystallization and precipitation of cementing agents. The case of Old Alluvium shows that there are natural materials that do not have a clearly defined or unique reconstituted state, because their structure is the result of mineral alterations and physico-chemical forces, and hence depends on the micro-environmental conditions and is subject to further changes. Referring to a reconstituted state for such materials is not appropriate; instead, a framework is required that would map the microstructural changes due to a specific mode of loading/disaggregation.

3.6 CLAYEY SHALES AND OLD ALLUVIUM

Shales are sedimentary rocks and so are formed under totally different geological conditions than the Old Alluvium – which is the product of transportation and weathering processes. Hence any relation between the two materials is not immediately obvious. However, there are examples of clayey shales that exhibit a macroscopic response in both compression loading and unloading similar to that of Old Alluvium. Therefore, it is of interest to investigate possible links between the mechanical response of these two classes of materials.

3.6.1 Examples of compression behavior in certain clayey shales

Figure 3-26 plots oedometer test results (in the same loge-logσ'_v axes used throughout this chapter) for four clayey shales – Intact Pierre Shale, Intact Fort Union Shale, Intact Bearpaw Shale and Culebra Shale[30]. The samples have initial void ratios comparable to those of the Old Alluvium (various depths). Pierre and Fort Union Shale intact samples are compressed up to 320 ksc and during this initial loading they exhibit an apparent yield stress at 20-30 ksc respectively, and a significant compressibility thereafter. Unloading causes large expansive strains and results in void ratios similar or even larger than the initial one. The intact Bearpaw Shale sample is

[30] At the reported locations (Figure 3-26) the following information was available:
Pierre Shale: w_l= 36%-113%, w_p = 20-62%, I_p = 113%, 12%-40% montmorillonites and Fe/Mn oxide cementation (Diaz & Fernando, 1987; Tourtelot, 1962)
Bearpaw Shale: w_l= 80%-150%, w_p = 18-27%, I_p = 140%, 50% clay (Diaz & Fernando, 1987; Peterson, 1958)
Fort Union Shale, w_l = 89% and Plasticity Index I_p = 69% (Diaz & Fernando, 1987)

loaded to lower stress levels (up to 45 ksc), but like the other shale specimen it exhibits an apparent yield stress (at 3 ksc) and significant expansion during unloading.

Figure 3-27 plots tests on saturated samples of natural Laviano "scaly" clay shale, a highly tectonized shale with a dense network of polished shearing planes, 24% clay fraction and 24% plasticity index. The maximum vertical stress is 90 ksc. It can be observed that the amount of recovered strains during unloading increases with the maximum compression stress level, a feature which is similar to the expansion behavior of the Old Alluvium.

3.6.2 Microstructure of the materials

Clayey shales include clay minerals, often montmorillonitic ones. Yet, there hasn't been a well accepted theory as to why the overall macroscopic behavior of some clayey shales seems to be dominated by the montmorillonitic response (extensive swelling), despite the general macrostructure. The most plausible explanation is based on studies of the shales' microstructure. Pye & Krinsley (1983) have shown using backscattered electron microscopy that the clay minerals in shales are often present as clay stacks which may range in size up to 150 μm. Seedsman (1987) studied a set of shales from the Coal Measures of the Bowen Basin, Queensland, and concluded that although crystalline swelling of individual montmorillonite particles is at a very small scale (< 1 nm), when the same strain is developed in clay stacks composed even partially of montmorillonite sheets, it may lead to very large deformations. Figure 3-28 shows the photograph of a large clay stack – approximately 12.5μm in thickness. With the assumption that the montmorillonite phase is in the two-layer state with a basal spacing of 1.55 nm, the author estimated that the stack is composed of approximately 8300 illite layers and 2800 montmorillonite layers[31]. He further concluded that the deformations of the clay stacks could have a significant macroscopic influence. Collapse of the montmorillonite sheets from a two-layer to a one-layer hydration state can cause irreversible damage to the Shale fabric and hence reduce its tensile strength. The study showed that even though one cycle of relative humidity is not producing significant effects in the macroscopic strength, repeated unloading cycles result in extended damage.

[31] Seedsman however notes that stacks as large as the one shown in Figure 3-28 are not common in the shale as a whole, partly because of the low clay content (30--40%) and partly because of the dominance of discrete illite and kaolin in the clay-size fraction.

As discussed above, any direct comparison between these Shales and Old Alluvium is not possible. However, the two materials share a common microstructural characteristic; they both include stacks of swelling clay minerals in compacted parallel orientation. Therefore they both have an inherent potential for swelling which – in the intact state – is restricted by their macroscopic structure.

Alonso (2002) attributes the extensive swelling of shales to the destruction of the rock bonds around the clay sheets (see Figure 3-28), during initial loading to very high stresses; hence, during unloading, when stresses are released, swelling may take place since it is not restrained by the mineral structure. Loading on the Old Alluvium causes more extensive changes than mechanical cracking. However, during unloading the response of the soil is controlled by the same microstructural characteristics as in shales. The modeling of swelling in clayey shales (see Chapter 4) can therefore provide helpful guidelines for understanding the behavior of the Old Alluvium.

3.7 OTHER OLD ALLUVIA

Old Alluvia, defined as transported and in-situ weathered soils, can be encountered in many parts of the world, such as South and South East Asia, sub-Saharan Africa, and South America (Chapter 2). It is possible that Old Alluvia with similar parent materials and similar transportation and weathering conditions would have behavior comparable to that of the Old Alluvium in San Juan.

For instance, recent construction projects in Singapore have resulted in the study of a local Old Alluvium, as its presence caused various problems. During tunneling, the initially hard and stable material deteriorated overnight, after being exposed to air and water and required stabilization through chemical grouting to permit further excavation. However, unweathered parts of the material provided a stable face for tunneling even below the water table (Shirlaw et al, 2000). Chiam et al, (2003) and Chu et al (2003) also report clogging on TBM machines and slope failures.

Figure 3-29 shows on a map of SE Asia the additional land present during Pleistocene and the old drainage system, which is associated with the deposition of this Old Alluvium. The parent material appears to be mainly granite and feldspars eroded from mountains of what is now

Malaysia and Indonesia (Shirlaw et al, 2000). The majority of the initial deposits consisted of round quartz particles, and 10% fresh feldspars. Since deposition, they have been cemented and later have been subjected to tropical weathering. The resulting present soil has similar mineralogy with the one in Puerto Rico. It consists mainly of quartz, kaolinite, smectite and iron oxides. According to Gupta et al (1987), smectites account for about 50% of the clay fraction. The microstructure is also comparable, as the iron oxides act as cementation agents. However, clay minerals are reported to form coatings around the particles and available studies have not revealed any groups of clay platelets in the microscale. Compression tests defined yielded values between 0.08 and 0.1 for compressibility index C_c, and between 0.02 and 0.04 for swelling index C_s. These values are within the expected limits for clayey soils. However, the available tests do not exceed 25ksc in compression levels; experience with the Old Alluvium in San Juan has shown that higher stresses and different loading modes may cause significant breakdown, and thus alter the compressibility and swelling parameters. Further testing is required to understand the potential behavior of the Old Alluvium in Singapore.

3.8 SUMMARY

In this chapter the compression behavior of the Old Alluvium was presented and discussed in comparison with the established behavior frameworks of three soil groups: cohesionless soils, sedimentary clays and bonded soils. The material exhibits similarities to all three categories - sands, clays and bonded materials, but neither framework is capable of describing entirely its observed behavior.

The response of the Old Alluvium to compressive loads has several distinctive features: during loading the compressibility evolves continuously leading to strains up to 40%. The swelling potential also increases and so unloading from higher stresses leads to significant volumetric expansion. However, swelling strains seem to be reversible – at least at the macroscopic level. It is also observed that unloading/reloading cycles from the same reversal stress are identical, an indication that the changes occurring during loading are halted during the unloading/reloading cycles.

It was extensively discussed in Chapter 2 that the Old Alluvium has a complex and rather unstable microstructure, consisting of clay platelets connected together into aggregates that are

further cemented between them and with quartz grains. External actions, such as mechanical loading, or changes in the chemical environment, can disrupt this structure by destroying the cementation or the intra-aggregate bonds. Hence, a successful understanding and modeling of the macroscopic compression behavior needs to be linked to the changes occurring in the micro-scale structure. A framework for granular materials could serve as a modeling basis, since initially the soil resembles a structured granular material; however, measurements of compressibility are not constant material parameters, but rather state variables that need to be updated following the changes in the microstructure and the exposure of clay minerals. Similarly, the variables defining the volumetric changes during unloading/reloading cycles need to be updated to reflect the degree of association of the iron oxides to clay surfaces and the release of the swelling potential of the clay minerals. Finally, due to the nature of the changes in the microstructure – which are both mechanical and chemical – there is not a unique reconstituted or intrinsic state of the material; structural degradation needs to be mapped dynamically in relation with the applied loading path.

The Old Alluvium in Puerto Rico exhibits a behavior pattern much different than what has been typically discussed in soils. The changes occurring in the microstructure during loading call for a model that would incorporate the evolution of the soil parameters. The presence of other Old Alluvia in the world as well as examples of materials with similar microstructure, or analogous macroscopic response signify than construction in more than one geographic region can benefit from such a modeling approach.

3.9 REFERENCES

Addis M. A., Jones M. E. (1990): "Mechanical behaviour and strain rate dependence of high porosity chalk", Proceedings of the International Chalk Symposium, Brighton, 111-116.

Alonso E. (1998): "Modelling expansive soil behaviour", Proceedings of the 2nd International Conference on Unsaturated Soils, Beijing, China, 2, 37-70.

Alonso E.E., Alcoverro J. (2002): "Swelling and Degradation of Argillaceous Rocks", Proceedings of the 3rd International Conference on Unsaturated Soils, Recife, Brazil, 3, 951-969.

Atkinson B. K., Meredith P. G. (1987): "The theory of subcritical crack growth with applications to minerals and rocks", Fracture mechanics of rock (ed. B. K. Atkinson), Academic Press, London, 111-166.

Banks D.C., Strohm W.E., DeAngulo M., Lutton R. (1975): "Study of Clay Shale Slopes along the Panama Canal", Technical Report S-70-9, Report 3 of a Series, U.S. Army Engineer Waterways Experiment Station, Vicksburg, Mississippi.

Barksdale R.D., Blight G.E. (1997): "Compressibility and settlement of residual soils", Chapter 8 in Mechanics of Residual Soils, G.E. Blight, Balkema.

Bjerrum L. (1973): Problems of soil mechanics and construction on soft clays", State-of-the-art report, Proceedings, 8th International Conference of Soil Mechanics and Foundation Engineering, Moscow, Vol III, 111-159.

Bjerrum L., Kenney T.C. (1967): "Effect of structure on the Shear Behavior of Normally consolidated Quick Clays", Proceedings of the geotechnical conference, Oslo, 1, 19-27.

Burland J. B., Rampello S., Georgiannou V. N., Calabresi G. (1996): "A laboratory study of the strength of four stiff clays", Géotechnique, 46 (3), 491-514.

Burland J.B. (1990): "On the compressibility and shear strength of natural clays", Géotechnique, 40 (3), 329-378.

Cafaro F., Cotecchia F. (2001): "Structure degradation and changes in the mechanical behaviour of a stiff clay due to weathering", Géotechnique, 51 (5), 441-453.

Calabresi G., Scarpelli G. (1985): "Effects of swelling caused by unloading in overconsolidated clays", Proceedings 11th ICSMFE, 2, 411-414.

Cecconi M., DeSimone A., Tamagnini C., Viggiani G.M.B. (2002): "A constitutive model for granular materials with grain crushing and its application to a pyroclastic soil", International Journal for Numerical and Analytical Methods in Geomechanics, 26 (15), 1531-1560.

Cecconi M., Viggiani G.M.B. (2001): "Structural features and mechanical behaviour of a pyroclastic weak rock", International Journal for Numerical and Analytical Methods in Geomechanics, 25 (15), 1525–1557.

Chiam S.L., Wong K.S., Tan T.S., Ni Q., Khoo K.S., Chu J. (2003): "The Old Alluvium", Underground Singapore 2003 Engineering Geology Workshop.

Chu J., Goh P.P., Pek S.C., Wong I.H. (2003): "Engineering properties of the Old Alluvium soil", Underground Singapore 2003 Engineering Geology Workshop.

Coop M. R., Atkinson J. H. (1993): "The mechanics of cemented carbonate sands", Géotechnique, 43 (1), 53-67.

Coop M.R. (2000): "The influence of particle breakage and state on the behaviour of sands", International Workshop on Soil Crushability, IWSC'99, Yamaguchi, Japan.

Coop M.R., Atkinson J.H. (1993): "The mechanics of cemented carbonate sands", Géotechnique, 43 (1), 53–67.

Cotecchia F., Chandler R. J. (1997): "The influence of structure on the pre-failure behaviour of a natural clay", Géotechnique, 47 (3), 523-544.

Cotecchia F., Chandler R. J. (1998): "One-dimensional compression of a natural clay: structural changes and mechanical effects", Proceedings, HSSR '98, Napoli, 1, 103-114.

Cotecchia F., Chandler R.J. (2000): "A general framework for the mechanical behavior of clays", Géotechnique, 50 (4), 431-447.

Cotecchia, F. (1996). The effects of structure on the properties of an Italian pleistocene clay. PhD thesis, University of London.

Datta M., Gulhati S.K., Venkatappa Rao G. (1979): "Crushing of calcareous sands during shear", Proceedings, 11th Offshore Technology Conference, Houston, 3, 1459-1467.

Daupley X. (1997): "Etude du potentiel de l'eau interstitielle d'une roche argileuse et des relations entre ses propriétés hydriques et méchaniques, Thèse Doctoral. Ecole Nationale des Mines de Paris.

De Alba E., Sesana, F. (1978): "The influence of expansive minerals on basalt behavior", Proceedings of the international congress of engineering geology, Madrid, 107-116.

De Souza J. M. (1958): "Compressibility of sand at high pressure", MS thesis, Massachusetts Institute of Technology, Cambridge, Massachusetts.

DeBeer E. E. (1963): "The scale effect in the transposition of the results of deep sounding tests on the ultimate bearing capacity of piles and caisson foundations", Géotechnique, 13 (1), 39-75.

Delgado Rodriguez J., Veiga Pinto A., Maranha das Neves, E. (1982): "Rock index properties for prediction of rockfill behavior", Memoria No 581, Laboratorio Nacional de Engenharia Civil, Lisboa.

Di Maio C., Santoli L., Schiavone P. (2004): "Volume change behavior of clays: the influence of mineral composition, pore fluid composition and stress state", Mechanics of Materials 36, 435–451.

Diaz C., Fernardo A. (1987): "An experimental investigation of the engineering behavior of natural shales", PhD Thesis, University of Illinois at Urbana-Champaign.

Eliot G. M., Brown E. T. (1985): "Yield of a soft, high-porosity rock", Géotechnique, 35 (4), 413-423.

Fearon R.E., Coop M.R. (1999): "The stiffness behaviour of a structurally complex clay", Problematic Soils 1998, Yanagisawa W., Moroto N., Mitachi T. (eds), Balkema, Rotterdam, 611–614.

Fearon R.E., Coop M.R. (2002): "Reconstitution: what makes an appropriate reference material?" Géotechnique, 50 (4), 471–477.

Fleming R.W., Spencer G.S., Banks D.C. (1970): "Empirical study of behavior of clay shale slopes", NCG Technical Report No 15 (2 vols.), U.S. Army Engineer Nuclear Cratering Group, Livermore, California.

Fukumoto T. (1990): "A grading equation for decomposed granite soil", Soils and Foundations, 30 (1), 27–34.

Germaine J.T. (2008): Personal Communication: CRS tests on Boston Blue Clay.

Germaine J.T. and Ladd C.C. (1988): "Triaxial testing of saturated cohesive soils", Advanced Triaxial Testing of Soil and Rock, ASTM STP 977, R.T. Donaghe, R.C. Chaney, and M.L. Silver (eds.), 421-459.

Hagerty M. M., Hite D. R., Ullrich C. R, Hagerty D. J. (1993): "One-Dimensional high pressure compression of granular media", Journal of Geotechnieal Engineering, 119 (1), 1-18.

Hall E. B., Gordon B. B. (1963): "Triaxial testing with large-scale high pressure equipment", Laboratory Shear Testing of Soils; Special Tech. Publication No. 361, ASTM, Philadelphia, Pa. 315-328.

Harremoes P. (1959): "Compressibility of ground sand at high pressures", MS thesis, Massachusetts Institute of Technology, Cambridge, Massachusetts.

Jamiolkowski M., Ladd C.C., Germaine J.T., Lancellotta R. (1985): "New developments in field and laboratory testing of soils", Proceedings, 11th International Conference of Soil Mechanics and Foundation Engineering, San Francisco, I, 57-153.

Kabbaj M., Tavenas F., Leroueil S. (1988): "In-situ and laboratory stress–strain relationships", Géotechnique, 38 (1), 83–100.

Kenney T.C., Moum J., Berre T. (1967): "An experimental study of bonds in a natural clay", Proceedings of the geotechnical conference, Oslo, 1, 65-69.

Kenney, T. C. (1967): "The influence of mineral composition on the residual strength of natural soils", Proceedings of the geotechnical conference on the shear strength properties of natural soils and rocks, Oslo, 1, 123-129.

Kjaernsli B., Sande A. (1963): "Compressibility of some coarse-grained materials", Proceedings, European Conference in Soil Mechanics and Foundation Engineering, Weisbaden, Germany, 245-251.

Ladd C.C. (1999): Advanced Soil Mechanics – Lecture notes, Massachusetts Institute of Technology, Cambridge, MA.

Ladd C.C. (2001): Soil Behavior – Lecture notes, Massachusetts Institute of Technology, Cambridge, MA.

Lade P.V., Yamamuro J.A., Bopp P.A. (1996): "Significance of particle crushing in granular materials", Journal of Geotechnical Engineering, 122 (4), 309-316.

Lagioia R., Nova R. (1993): "A constitutive model for soft rocks", Geotechnical engineering of hard soils-soft rocks, 625-632.

Lagioia R., Nova R. (1995): "An experimental and theoretical study of the behaviour of a calcarenite in triaxial compression", Géotechnique, 45 (4), 633-648.

Lambe T.W. (1951): Soil Testing for Engineers, John Wiley & Sons, Inc., New York.

Lambe T.W.,Whitman R.V. (1969): Soil Mechanics, John Wiley & Sons, Inc.

Leroueil S., Vaughan P.R. (1990): "The general and congruent effects of structure in natural soils and weak rocks", Géotechnique, 40 (3), 467–488.

Lutton R.J., Banks D.C. (1970): "Study of Clay Shale Slopes along the Panama Canal, Report 1, East Culebra and West Culebra Slides and the Model Slope", Technical Report S-70-9, Report 3 of a Series, U.S. Army Engineer Waterways Experiment Station, Vioksburg, Mississippi.

Mesri G. (1975): Discussion, Journal of Geotechnical Division, ASCE, 101, GT4, 409-412.

Mesri G., Abdel-Ghaffar M.E.M. (1993): "Cohesion intercept in effective stress-strability analysis", Journal of Geotechnical Engineering, 119 (8), 1229-1249.

Mesri G., Godlewski P.M. (1977): "Time and stress compressibility inter-relationship", Journal of Geotechnical Engineering, ASCE, 111 (4) 444-464.

Mesri G., Lo D.O.K. (1989): "Subsoil Investigation: The weakest link in the analysis of test fills", in The Art and Science of Geotechnical Engineering at the Dawn of the 21st century; a volume honoring Ralph B. Peck; Prentice Hall, 308-335.

Mesri G., Olson R.E. (1971): "Consolidation charactyeristics of Montmorillonite", Géotechnique, 21 (4), 341-352.

Mitchell J. K., Solymar Z. V. (1984): "Time-dependent strength gain in freshly deposited or densified sand", Journal of Geotechnical Engineering division, ASCE, 110, No. GT11, 1559-1576.

Mitchell J.K., Soga K. (2005): Fundamentals of Soil Behavior, John Wiley & Sons, New York, N., 3rd edition.

Nakata Y., Hyodo M., Hyde A.F.L., Kato Y., Murata H. (2001a): "Microscopic particle crushing of sand subjected to high pressure one-dimensional compression", Soils and Foundations, 41 (1), 69-82.

Nakata Y., Kato Y., Hyodo M., Hyde A.F.L., Murata H. (2001b): "One dimensional compression behaviour of uniformly graded sand related to single particle crushing strength", Soils and Foundations, 41 (2), 39-51.

Nikolinakou M.A., Whittle A.J. (2008): "Predictions on boundary value problems for deep excavations in Berlin Sand, using the MIT-S1 model", in final preparation.

Nobari E. S., Duncan J. M. (1972): "Effect of reservoir filling on stresses and movements in earth and rockfill dams", University of California, Department of Civil Engineering, Report No. TE-72-1.

Oldecop L.A., Alonso E.E. (2001): "A model for rockfill compressibility", Géotechnique, 51 (2), 127-139.

Oldecop L.A., Alonso E.E. (2003): "Suction effects on rockfill compressibility", Géotechnique, 53 (2), 289-292.

Olson R.E., Mesri G. (1970): "Mechanisms controlling compressibility of clays", Journal of Soil Mechanics and Foundation Division, ASCE, 96, (SM6), 1863-1878.

Pestana J. M., Whittle A. J. (1995): "Compression model for cohessionless soils", Géotechnique, 45 (4), 611-631.

Pestana J.M. (1994): "A unified constitutive model for clays and sands", Sc.D thesis, Massachusetts Institute of Technology, Cambridge, MA.

Peterson R. (1958): "Rebound in Bearpaw shale", Geologic Society of America, Bulletin, 69, 1113-1124.

Picarelli L. (1991): Discussion on the paper: "The general and congruent effects of structure in natural soils and weak rocks" by S. Leroueil and P.R. Vaughan, Géotechnique, 40 (2), 281-284.

Picarelli L., Olivares L., DiMaio C., Urcioli G. (2000): "Properties and behaviour of tectonized clay shales in Italy", The Geotechnics of Hards Soils Soft Rocks, Balkema, 1211-1214.

Pye K., Krinsley D.H. (1983): "Interlayered clay stacks in Jurassic shales", Nature, 304, 618-620.

Roberts J.E. (1964): "Sand Compression as a factor in oil field subsidence", PhD Thesis, MIT, Cambridge, MA.

Roberts J.E., DeSouza J.M. (1958): "The compressibility of sands", Proceedings, ASTM, 58, 1269-1277.

Rocchi G., Fontana M., Da Prat M. (2003): "Modeling of natural soft clay destruction processes using viscoplasticity theory", Géotechnique, 53 (8), 729–745.

Seedsman R.W. (1987): "Strength implications of the crystalline and osmotic swelling of clays in shales", International Journal of Rock Mechanics, Mineral Sciences and Geomechanics, Abstracts, 24 (6), 357-363.

Sekiguchi H., Nishida Y., Matsumoto T., Uesawa M. (1985): "Charecterization of a diatomaceous mudstone by elastoplasticity", Proceedings of the 5th International Conference of Numerical Methods in Geomechanics, Nagoya, 437-444.

Sheahan T.C., Germaine J.T., Ladd C.C. (1990): "Automated triaxial testing of soft clays: an updated commercial system", ASTM Geotechnical Testing Journal, 13 (3), 153-163.

Shirlaw J.N., Hencher S., Zhao J. (2000): "Design and construction issues for excavation and tunneling in some tropically weathered rocks and soils", Proceedings of the GeoEng2000 International Conference on Geotechnical, Geological Engineering, Melbourne, Australia.

Tamagnini C., Castellanza R., Nova R. (2002): "A Generalized Backward Euler algorithm for the numerical integration of an isotropic hardening elastoplastic model for mechanical and chemical degradation of bonded geomaterials", International Journal for Numerical and Analytical Methods in Geomechanics, 26 (10), 963-1004.

Tavenas F., Leroueil S. (1990): "Laboratory and in-situ stress-strain-time behaviour of soft clays", International Symposium on Geotechnical Engineering of Soft Soils, Mexico City, 2.

Terzaghi K. (1960): "Discussion on Salt Springs and Lower Bear River dams", Transactions, ASCE 125 (2), 139-148.

Terzaghi K., Peck R. B. (1948): Soil mechanics in engineering practice, John Wiley & Sons, New York, N.Y.

Tourtelot H.A. (1962): "Preliminary investigation of the geologic setting and chemical composition of the Pierre Shale, Great Plains Region, U.S. Geol. Survey Professional Papers, 390.

Vaughan P. (1997): "Engineering behaviour of weak rocks: Some answers and some questions". Geotechnical Engineering of Hard Soils-Soft Rocks, Balkema, 1741-1765.

Vaughan P. R. (1988): "Characterizing the mechanical properties of in-situ residual soils", Proceedings, Second International Conference on Geomechanics in Tropical Soils, Singapore, 2, 469-487.

Vesic A., Clough G. W. (1968): "Behavior of granular materials under high stresses", Journal of Soil Mechanics and Foundation Divisions, 94 (3), 661-668.

Vesic A.S., Barksdale R. D. (1963): Discussion on "Test methods and new equipement", ASTM STP 361, 301-305.

Vutukuri V. S., Lama R. D. (1978): "Handbook on mechanical properties of rocks", Claustahl: Trans. Techical Publications.

Wesley L. D. (1990): "Influence of structure and composition on residual soils", Journal of Geotechnical Engineering division, ASCE, 116 (4), 589-603.

Zhang G., Germaine J.T., Whittle A.J. Ladd, C.C. (2004b) "Soil structure of a highly weathered old alluvium", Géotechnique, 54 (7), 453–466.

Zhang G., Germaine J.T., Whittle A.J., Ladd C.C. (2004a): "Index properties of a highly weathered old alluvium", Géotechnique, 54, (7), 441–451.

Zhang, G. (2002): "Laboratory Characterization of a Highly Weathered Old Alluvium in San Juan, Puerto Rico", PhD thesis, MIT, Cambridge, MA.

Robinet J.C., Pakzad M., Jullien A., Plas, F. (1999): "A general model for expansive and non expansive clays", International Journal for Numerical and Analytical Methods in Geomechanics, 23, 1319-1335.

Test	Sample location		Sample depth (m)	Initial density (g/cm^3)	Initial water content, w_0 (%)	Initial void ratio, e_0	Initial degree of saturation S (%)	Test Frame	Pore Fluid	Max stress, σ'_{vmax} (ksc)	Complete unloading from σ'_{vmax}	Unload-Reload cycles at σ'_v (ksc):
	Unit	Block										
Oed07	UC	B3-S1	1.22	1.82	27.00	0.86	83.0	HP	Water	230.6	Yes	30
Oed11	UC	B3-S2	1.22	1.9	27.18	0.8	91.1	Std.	Water	30.0	Yes	2 8
Oed13	UC	B3-S6	1.22	1.71	26.86	0.9	80.0	HP	Water	457.2	No	-
Oed08	MZ	B1-S2	10.67	2.08	15.63	0.48	86.2	Std.	Water	288.0	Yes	30 30

Note: HP: High pressure loading frame; Std.: Standard oedometer load frame.

Table 3-1: Summary of consolidation tests run by Zhang (2002)

Test	Sample location		Sample depth (m)	Initial density (g/cm^3)	Initial water content, w_0 (%)	Initial void ratio, e_0	Initial degree of saturation S (%)	Test Frame	Pore Fluid	Max stress, σ'_{vmax} (ksc)	Complete unloading from σ'_{vmax}	Unload-Reload cycles at σ'_v (ksc):
	Unit	Block										
SJ1	UC	U5	6	1.74	32.55	1.04	83.6	Std.	Water	16	Yes	2 16
SJ2	UC	U5	6	1.77	33.95	1.03	88.2	HP	Water	511.5	Yes	2 16 511.5
101	UC	U5-S1	6	1.75	38.62	1.13	91.8	HP	Water	634.8	Yes	20.3 158.7 317.4 634.8 (x2)
102	UC	U5-S2	6	1.81	40.23	1.07	100	Std.	Glycerol	288.0	Yes	11.4 25.8 (x4)

Note: HP: High pressure loading frame; Std.: Standard oedometer load frame.

Table 3-2: Summary of new consolidation tests.

Test	Sample depth (m)	Insitu stress σ'_{v0} (ksc)	Prec. pres. σ'_{p} (ksc)	Test Frame	Ave. C_c 10-100 ksc	Ave. C_c 100-1000 ksc
Oed07	1.22	0.22	8	HP	0.25	0.24
Oed11	1.22	0.23	6.1	Std.	0.25	-
Oed13	1.22	0.21	7.2	HP	0.26	0.23
Oed08	10.67	2.22	35	HP	0.29	0.24
SJ1	6	1.04	1.9	Std.	0.35	-
SJ2	6	1.06	7.8	HP	0.3	0.27
101	6	1.05	5	HP	0.39	0.30
102	6	1.09	5.5	Std.	0.35	-

Note: HP: High pressure loading frame; Std.: Standard oedometer load frame.

Test	σ'_{rev} (ksc)	C_s	σ'_{rev} (ksc)	C_s	σ'_{rev} (ksc)	C_s	σ'_{rev} (ksc)	C_s	σ'_{rev} (ksc)	C_s	σ'_{rev} (ksc)	C_s
Oed07	30	0.06	231	0.11								
Oed11	8	0.01	30	0.05		0.09						
Oed13	457	0.06										
Oed08	30	0.04	30	0.03	288	0.13						
SJ1	2	0.02	16	0.08	16	0.08						
SJ2	2	0.02	16	0.12	511	0.13	511	0.10				
101	20	0.09	159	0.14	317	0.14	635	0.14	635	0.13	635	0.13
102	11	0.05	26	0.07	26	0.06	26	0.06	26	0.06	26	0.07

Table 3-3: Characteristic values of the clay framework for Old Alluvium tests. Multiple C_s values reflect multiple unloading cycles.

Soil	w_o (%)	w_L (%)	I_p (%)	σ'_{rev} (ksc)	C_s	σ'_{rev} (ksc)	C_s	σ'_{rev} (ksc)	C_s
Boom Clay	25-32	59-79	27-50	60	0.067	80	0.098	122	0.159
Gault Clay	20-30	75-80	30-50	70	0.040	70	0.046	70	0.085
Todi Clay	17.5	57.9	28.1	130	0.099	130	0.112	115	0.117

Table 3-4: Swelling coefficients of 3 natural clays during unloading cycles (data from Burland, 1990; Burland et al, 1996; Robinet et al, 1996; Mesri et al, 1993).

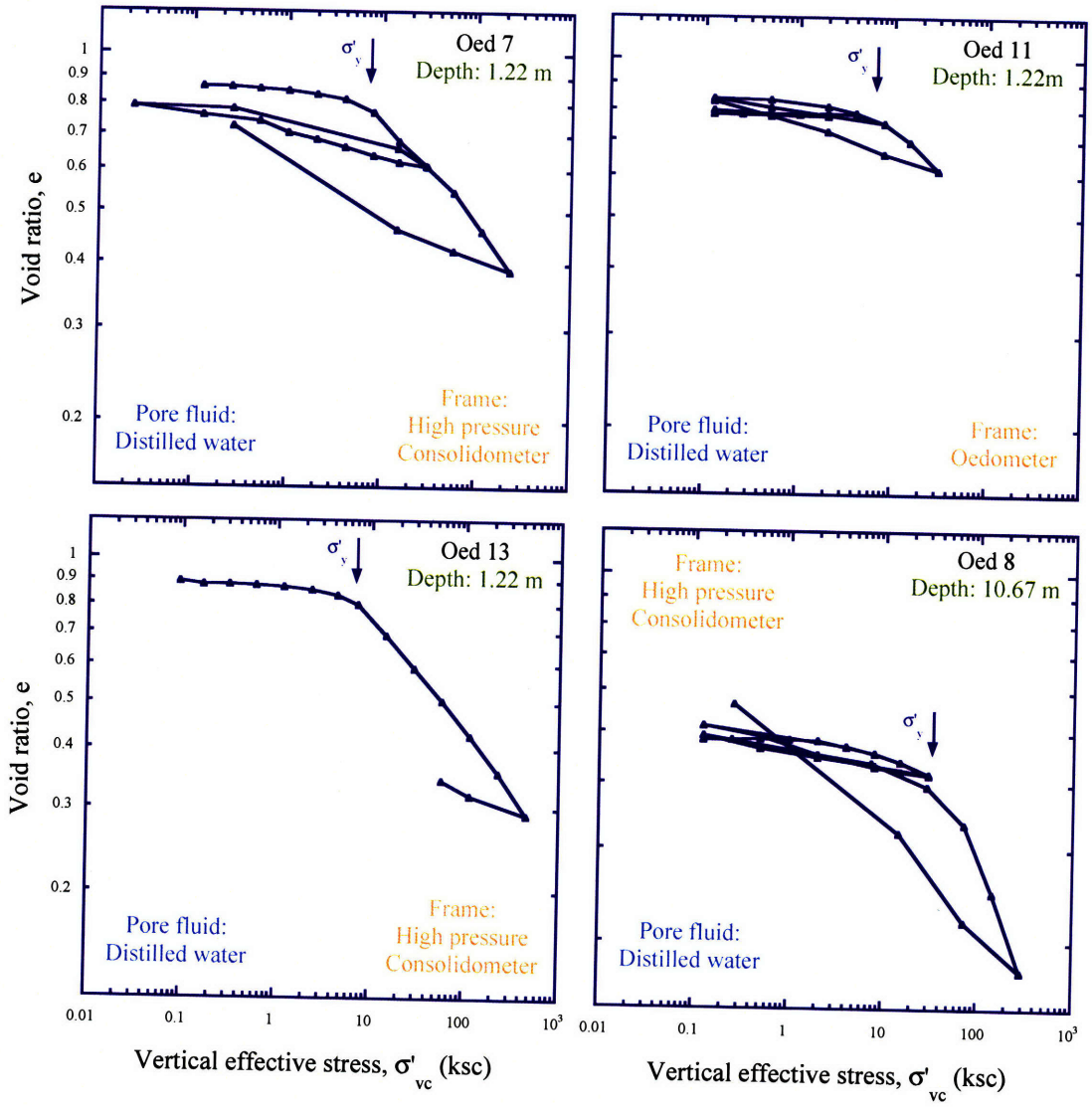

Figure 3-1: Compression tests on the Old Alluvium performed by Zhang (2002).

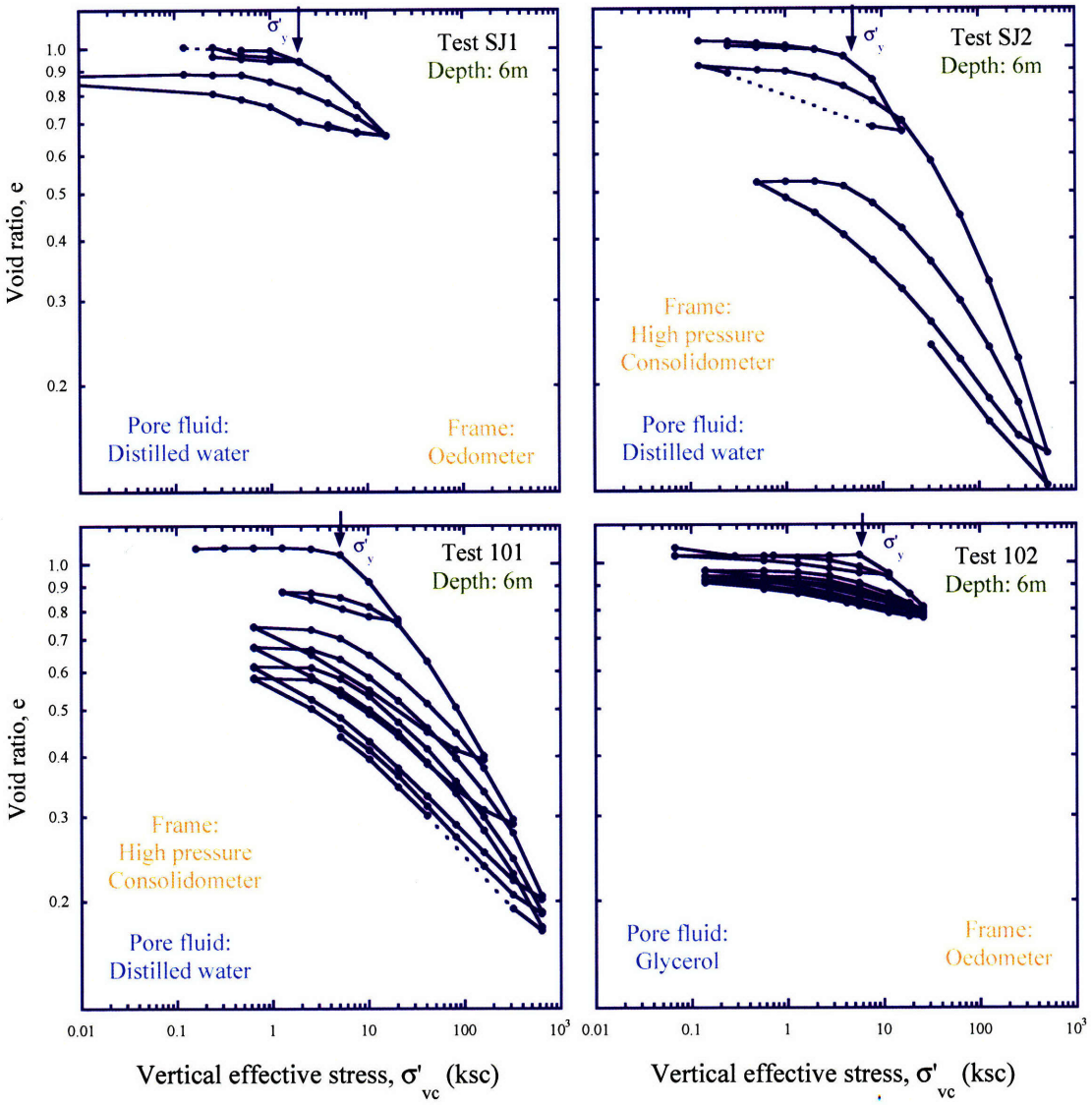

Figure 3-2: New compression tests on the Old Alluvium.

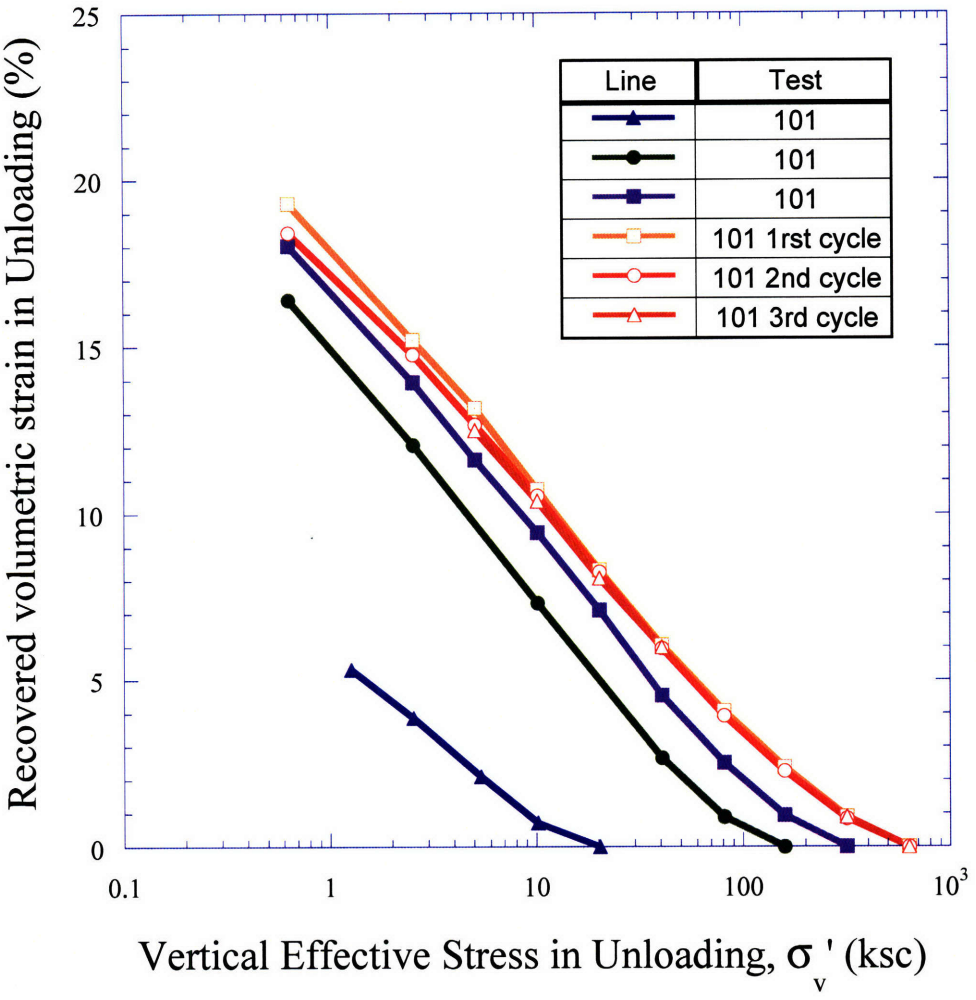

Figure 3-3: Recovered volumetric strain (strain at load reversal – current strain) during unloading for test 101.

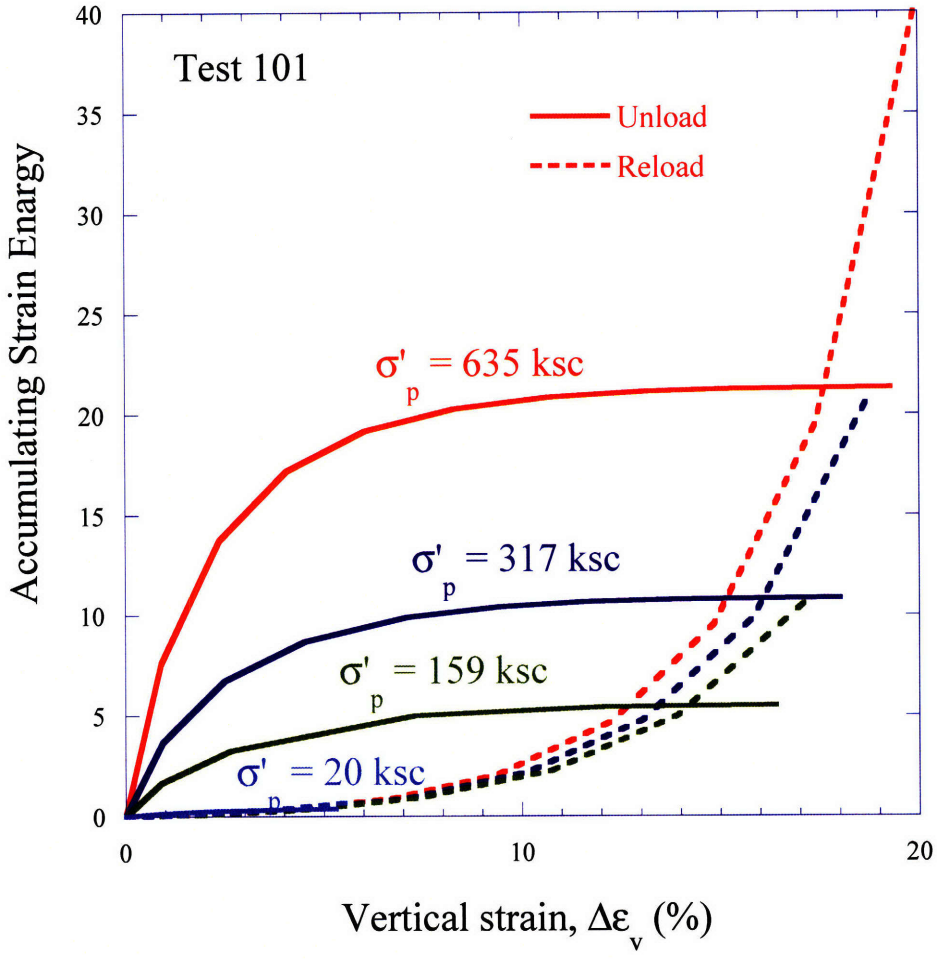

Figure 3-4: Accumulating strain energy during the unloading/reloading cycles of test 101.

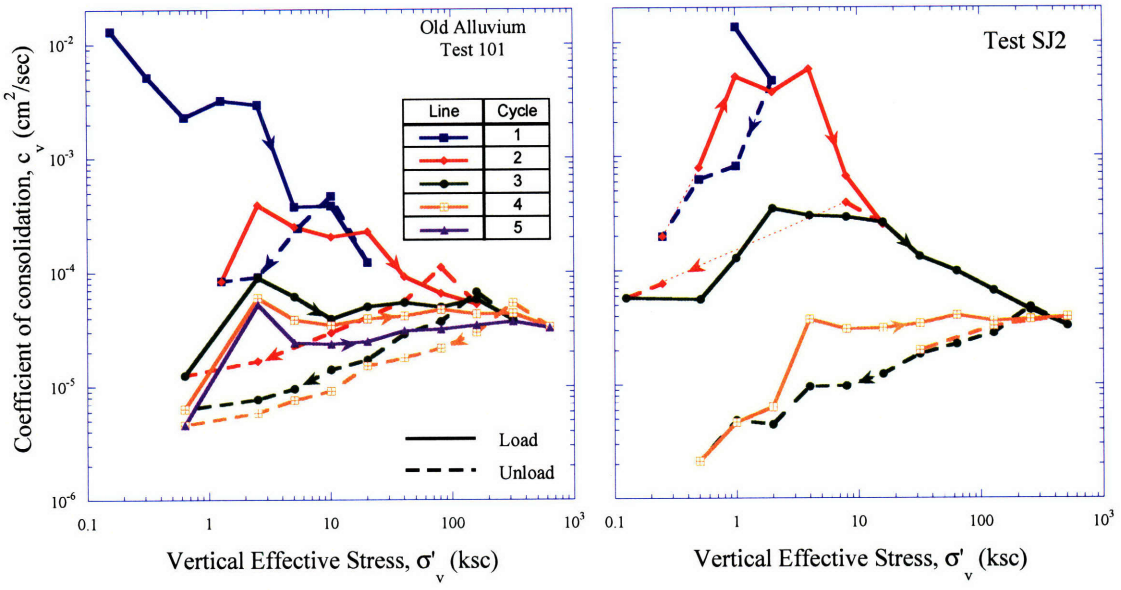

Figure 3-5: Evolution of the coefficient of consolidation during loading-unloading cycles for tests 101 and SJ2. Solid lines correspond to increase of vertical stress (loading/reloading), while dashed lines correspong to unloading.

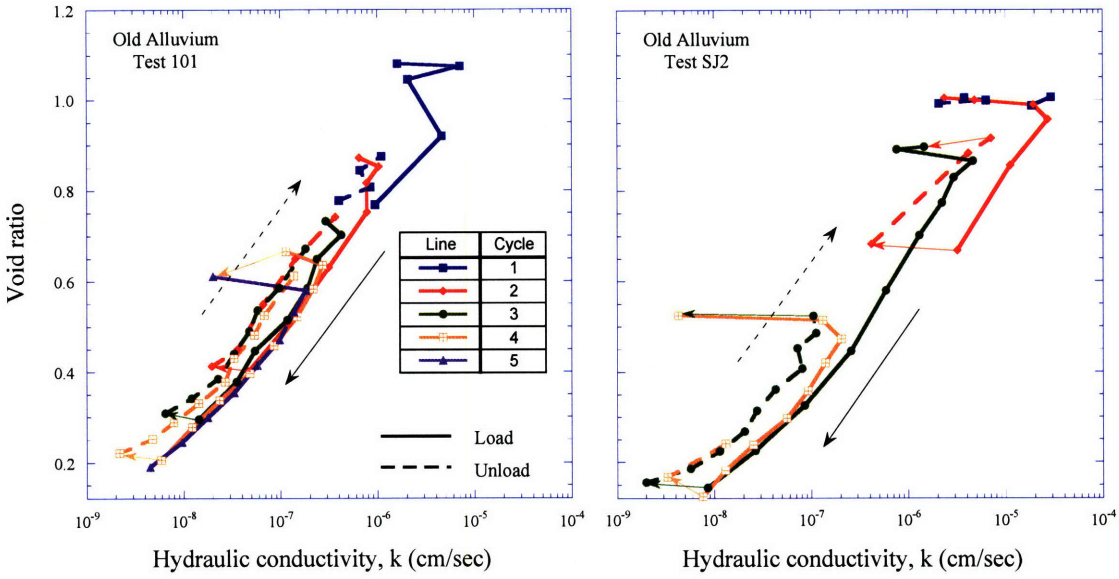

Figure 3-6: Evolution of the hydraulic conductivity during loading-unloading cycles for tests 101 and SJ2. Solid lines correspond to increase of vertical stress (loading/reloading), while dashed lines correspond to unloading.

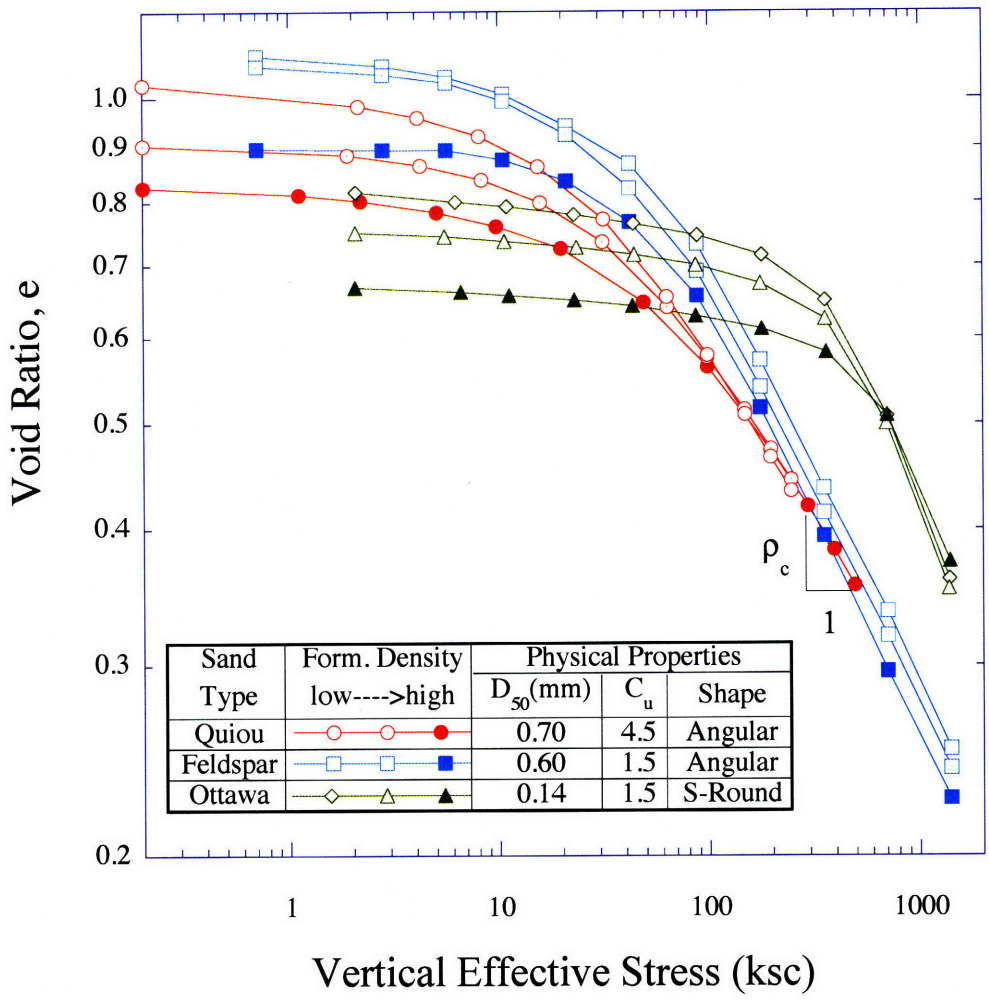

Figure 3-7: Typical behavior of freshly deposited cohesionless soils in 1-D compression (after Pestana, 1994).

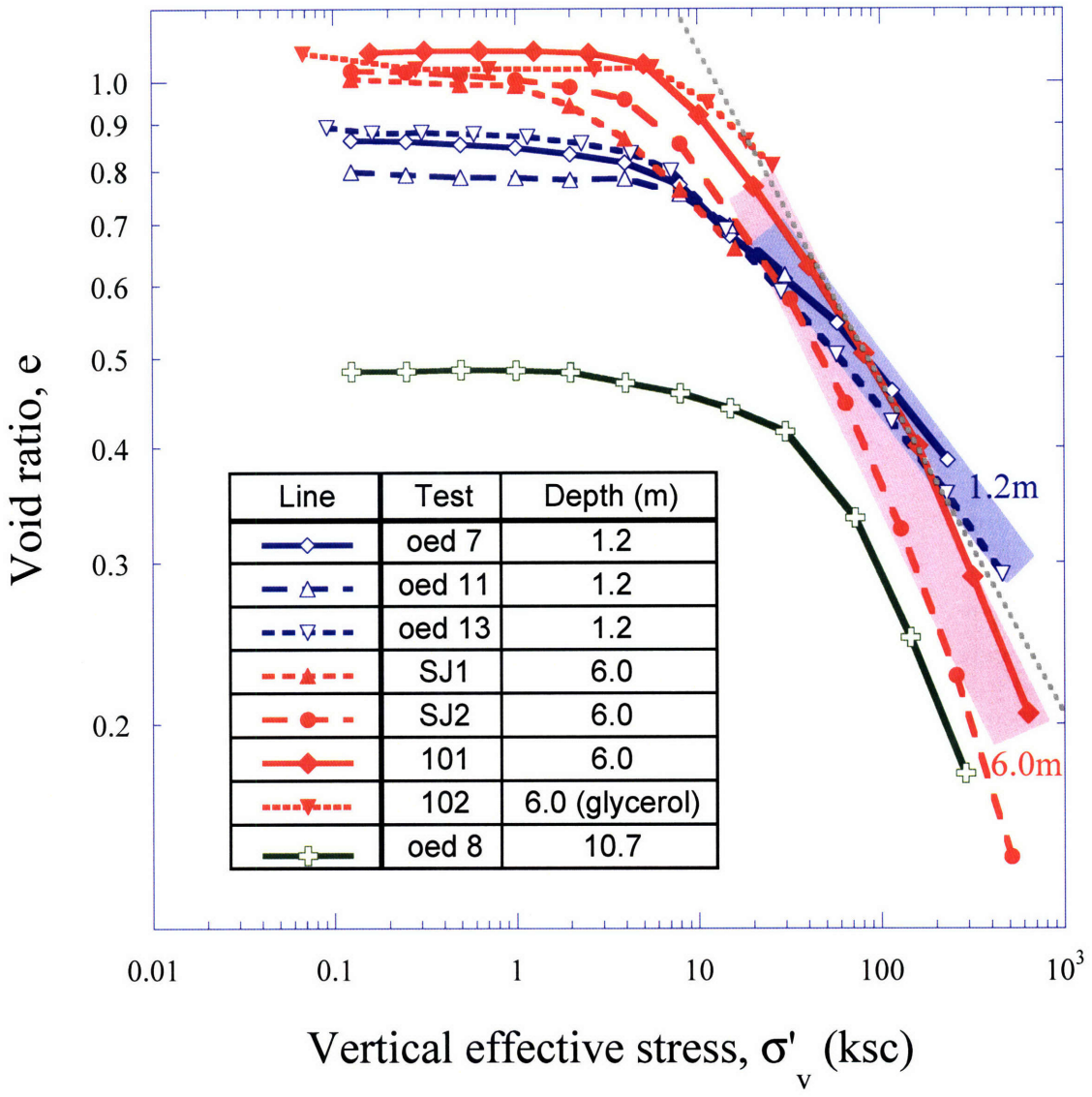

Figure 3-8: Compression tests on the Old Alluvium; figure shows only data for first (virgin) compression and groups results according to the sample depth (Data for oed 7,8,11,13 from Zhang, 2002).

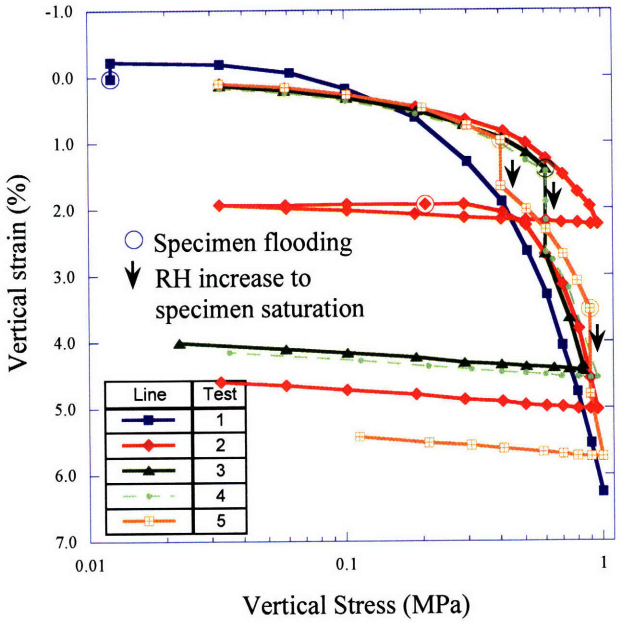

Figure 3-9: Effect of Relative Humidity changes and flooding on rockfill compressibility. Open circles indicate the stress level of flooding for each test and step changes in vertical strain correspond to increase of RH to saturation. Test 4 is same as Test 3 but with controlled flooding (after Oldecop & Alonso, 2001).

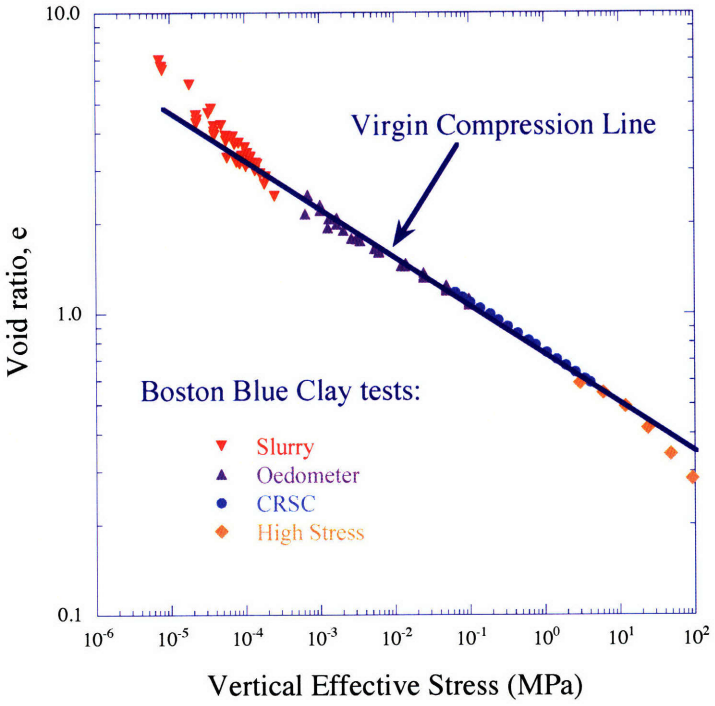

Figure 3-10: Compression behavior of Boston Blue Clay showing data from slurry, oedometer, CRS and high stress tests.

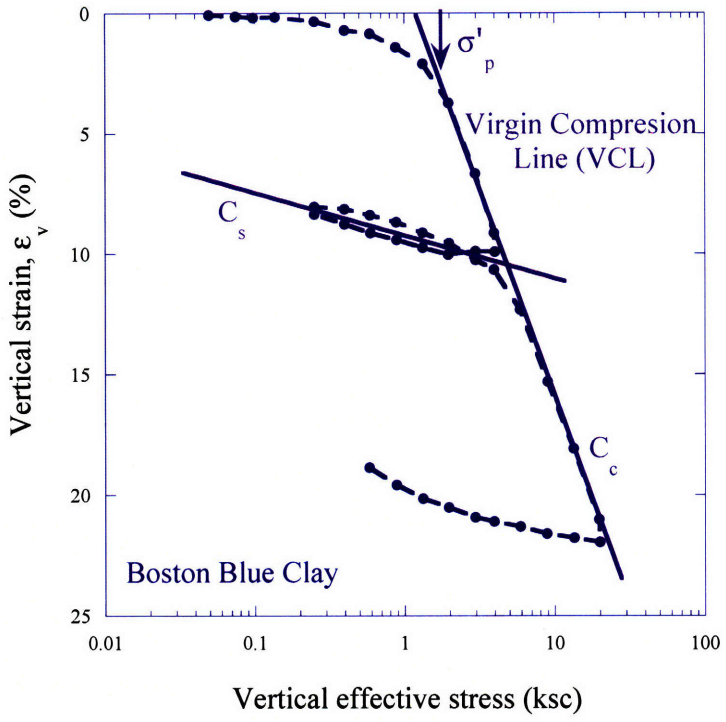

Figure 3-11: Compression behavior of an intact Boston Blue Clay sample (Maine Illitic clay of low plasticity). The figure also shows the parameters of an idealized 1-D model (preconsolidation pressure (σ'_p), compression index C_c and swelling index C_s).

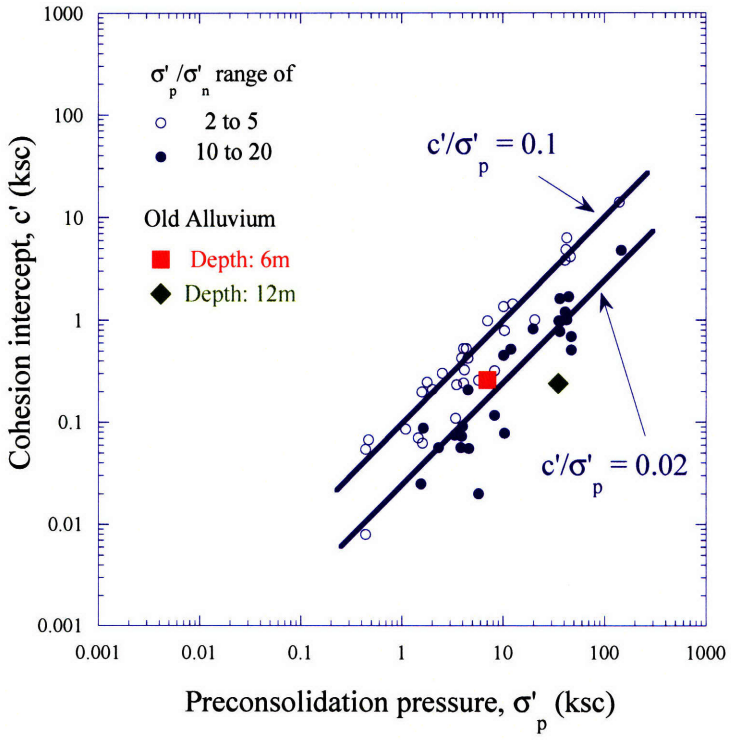

Figure 3-12: Relationship between preconsolidation pressure and cohesion intercept, after Mesri and Abdel-Ghaffar (1993).

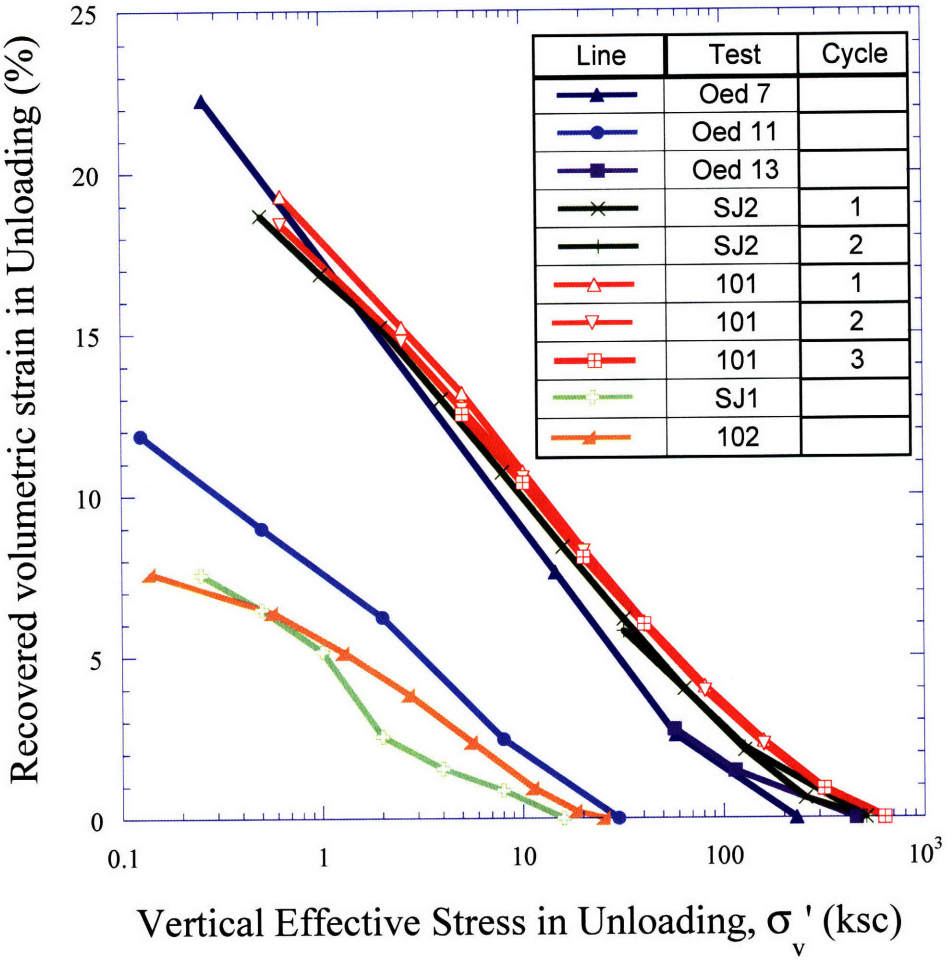

Figure 3-13: Recovered volumetric strain (strain at load reversal – current strain) during unloading from the maximum compression stress of all available tests.

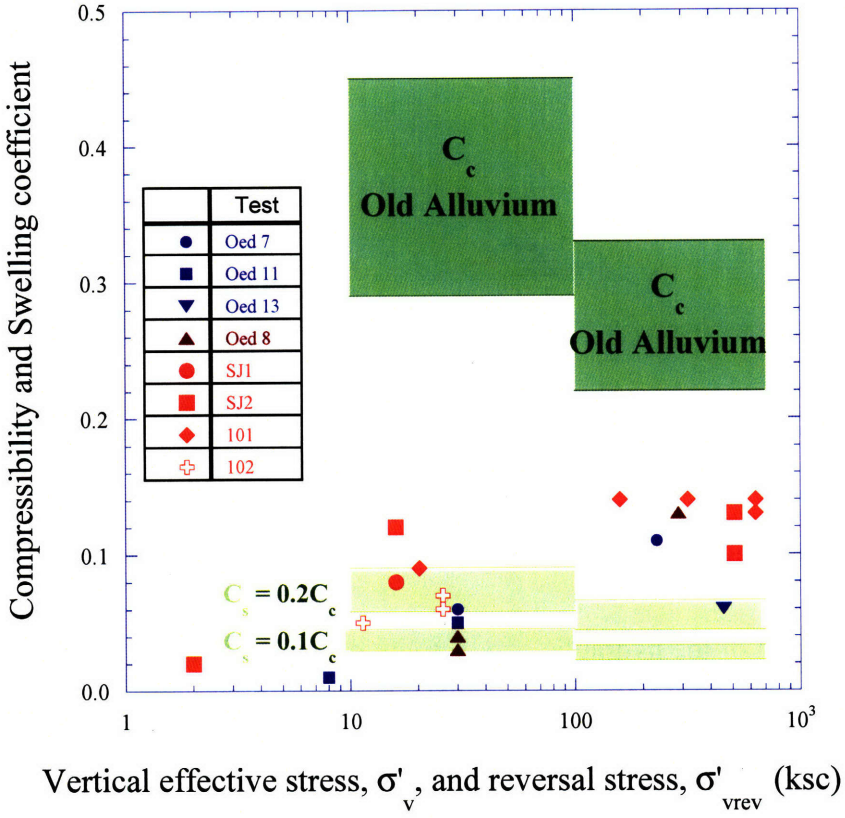

Figure 3-14: Observed range of values for the compression index C_c and observed values for index C_s, based on data from all available tests on Old Alluvium.

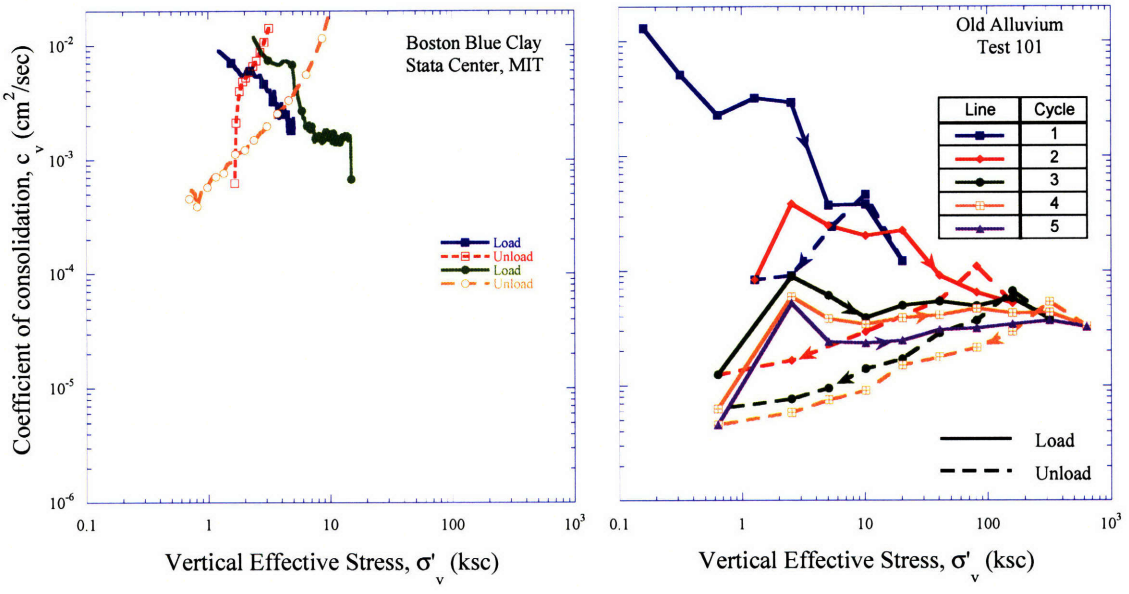

Figure 3-15: Evolution of the coefficient of consolidation during loading-unloading cycles for Boston Blue Clay and Old Alluvium. Solid lines correspond to increase of vertical stress (loading/reloading), while dashed lines correspond to unloading (Data on BBC from Germaine, 2008).

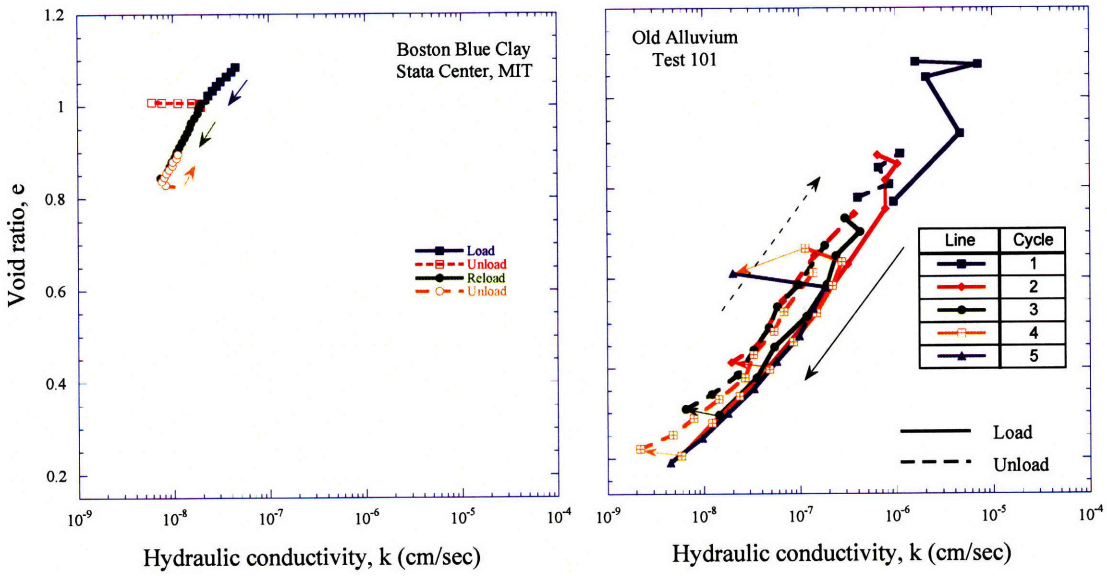

Figure 3-16: Evolution of the hydraulic conductivity during loading-unloading cycles for Boston Blue Clay and Old Alluvium. Solid lines correspond to increase of vertical stress (loading/reloading), while dashed lines correspond to unloading (Data on BBC from Germaine, 2008).

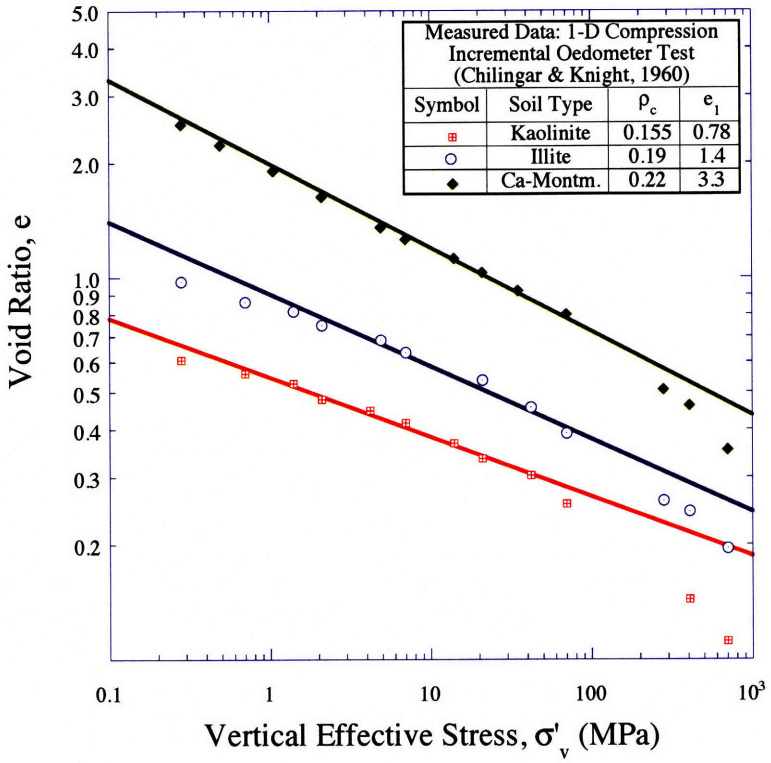

Figure 3-17: Effect of clay mineralogy on the compression behavior (after Pestana, 1994).

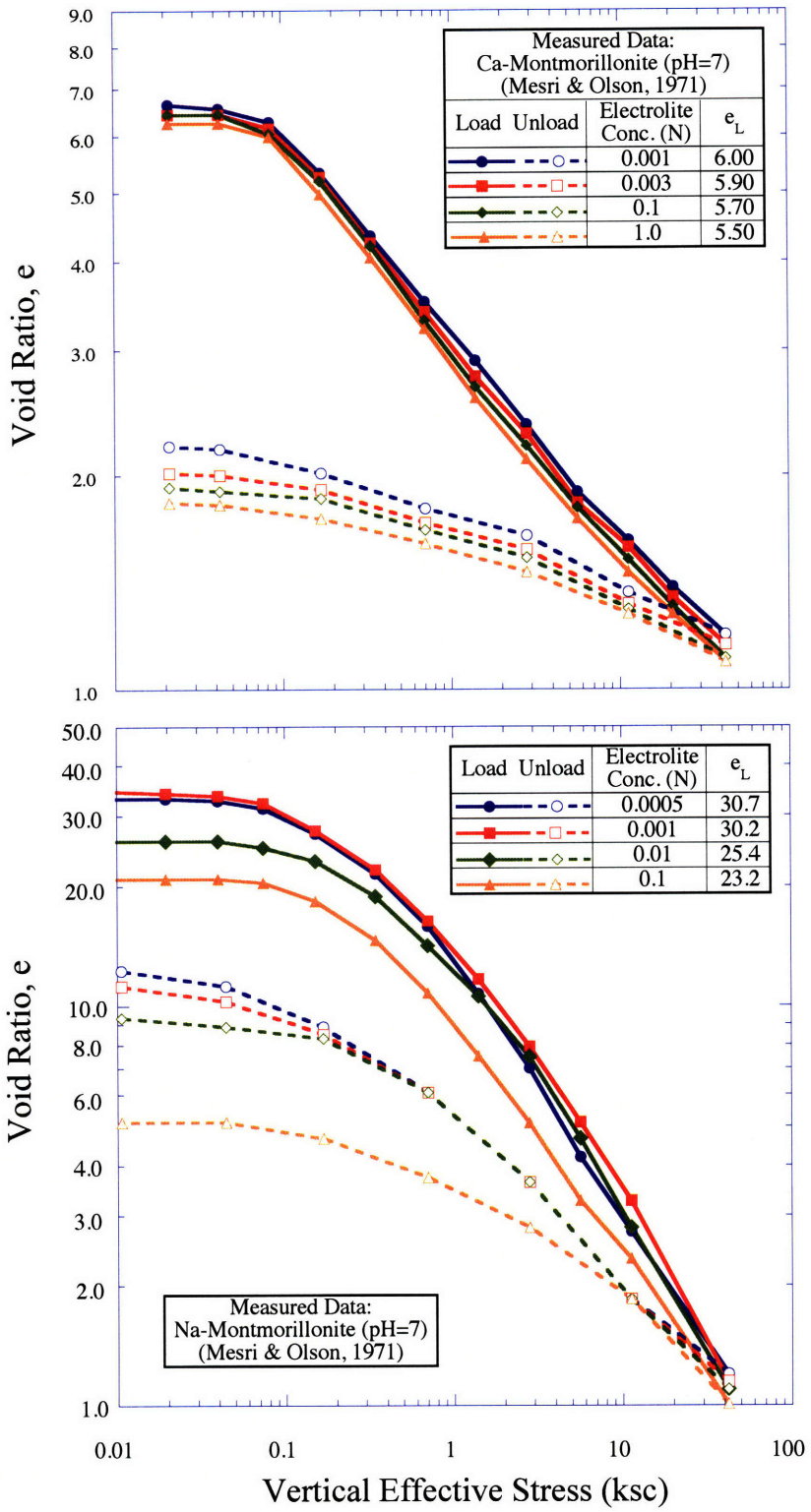

Figure 3-18: Effect of electrolyte concentration and ion valence on the compression behavior of montmorillonites (after Pestana, 1994).

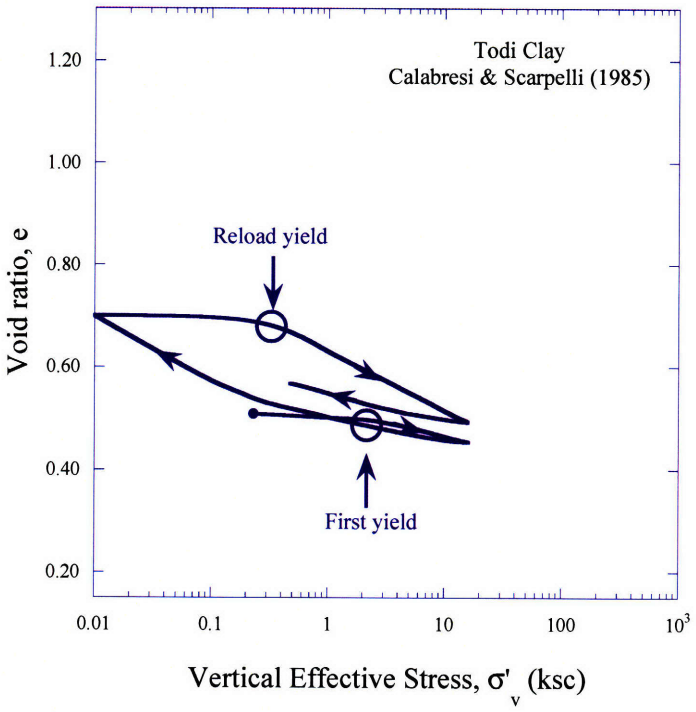

Figure 3-19: Oedometer tests on intact and reconstituted Todi clay (after Calabresi & Scarpelli, 1985).

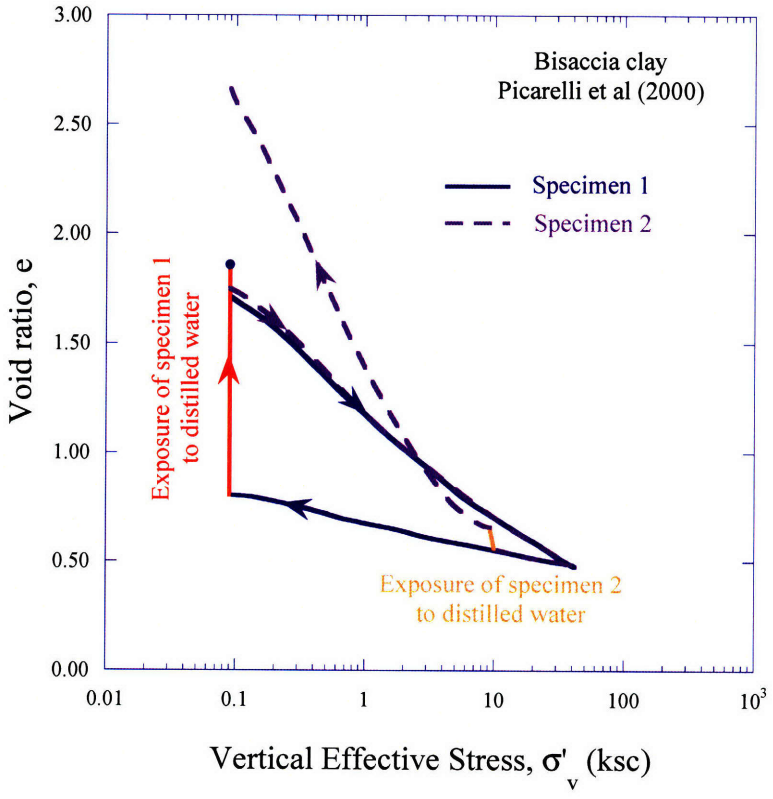

Figure 3-20: Swelling of Bisaccia clay with exposure to distilled water at 2 different stress levels (after Picarelli et al, 2000).

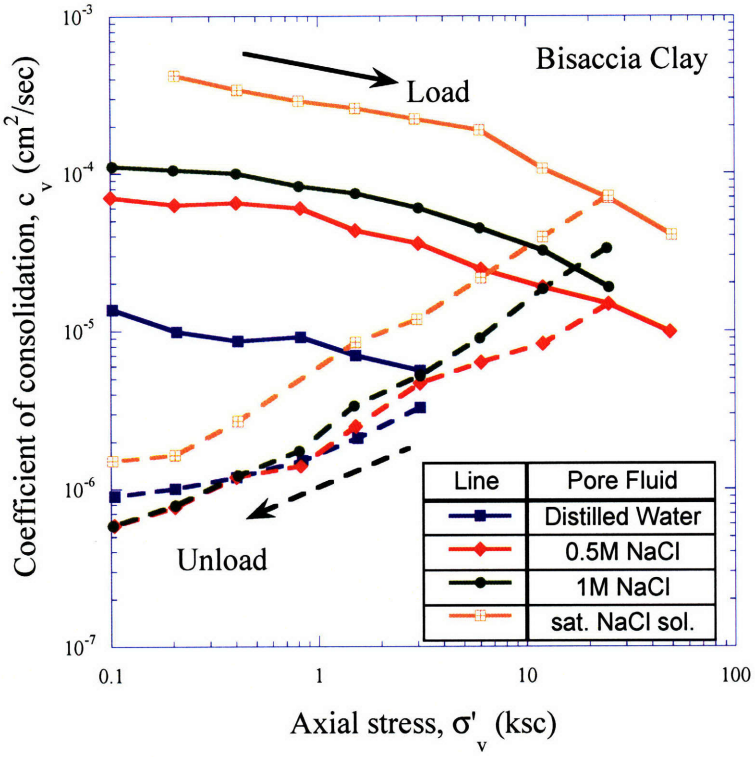

Figure 3-21: Coefficient of consolidation of Bisaccia clay for different values of pore fluid salinity (DiMaio, 2004).

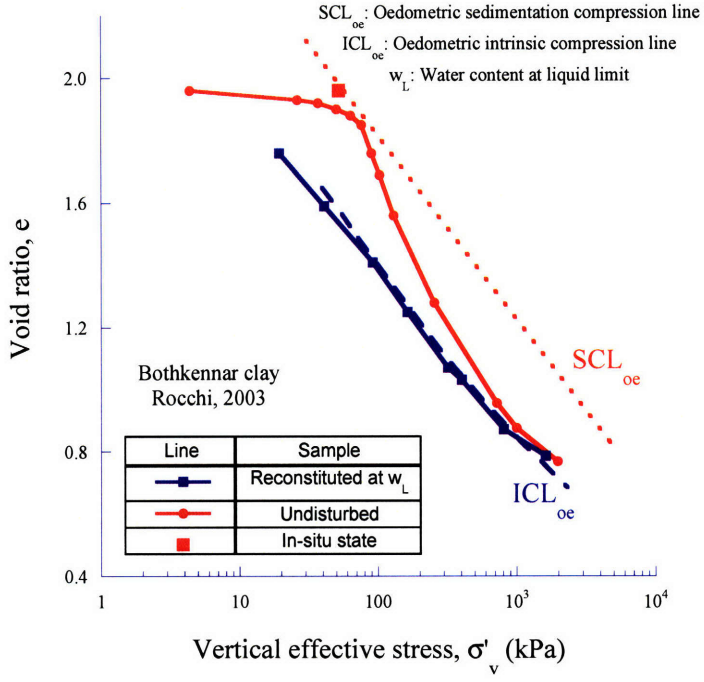

Figure 3-22: Data from Bothkennar clay illustrating the typical behavior of a bonded soil and the intrinsic properties principle: after significant loading the natural clay behavior converges to that of the reconstituted. (data after Rocchi, 2003; for in-depth discussion of the SCL and ICL lines, see Burland, 1990).

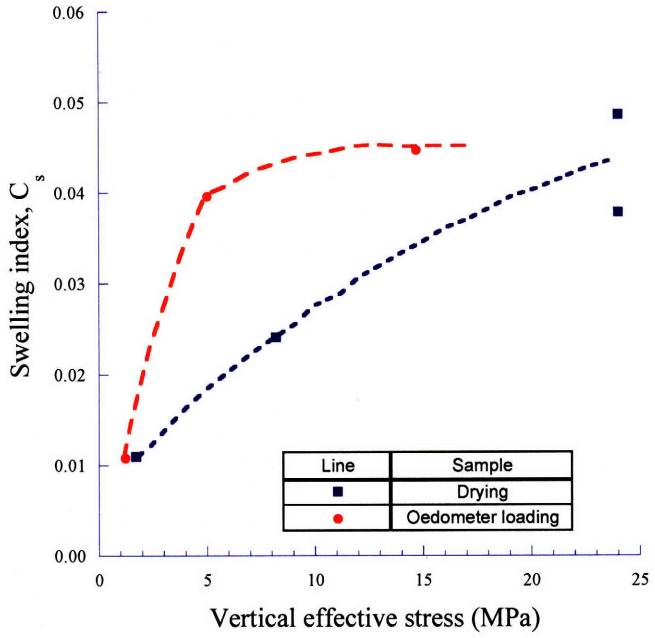

Figure 3-23: Effect of oedometer loading and drying on the swelling capacity of Montemesola clay (after Cafaro & Cotecchia, 2001). Note: C_s defined in terms of specific volume.

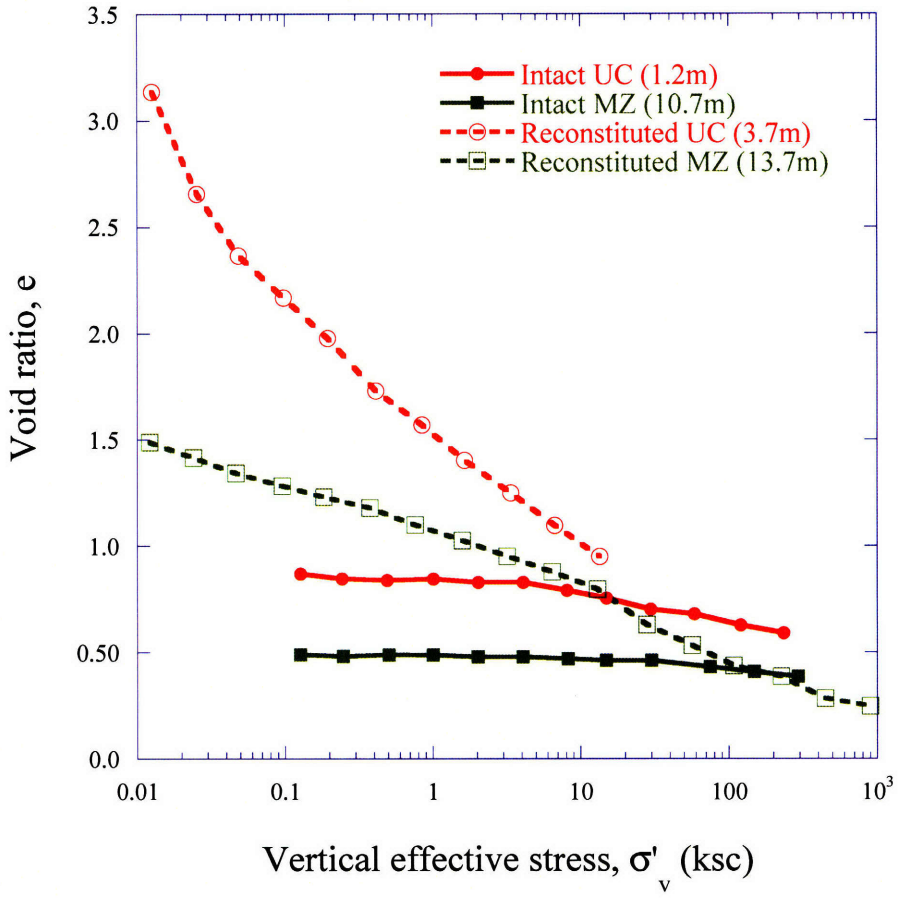

Figure 3-24: Compression behavior of mechanically resedimented Old Alluvium (Zhang, 2002)

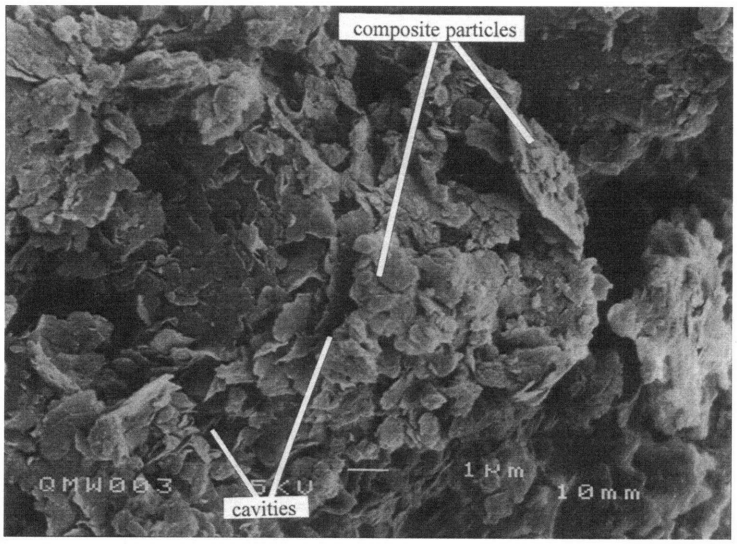

(a)

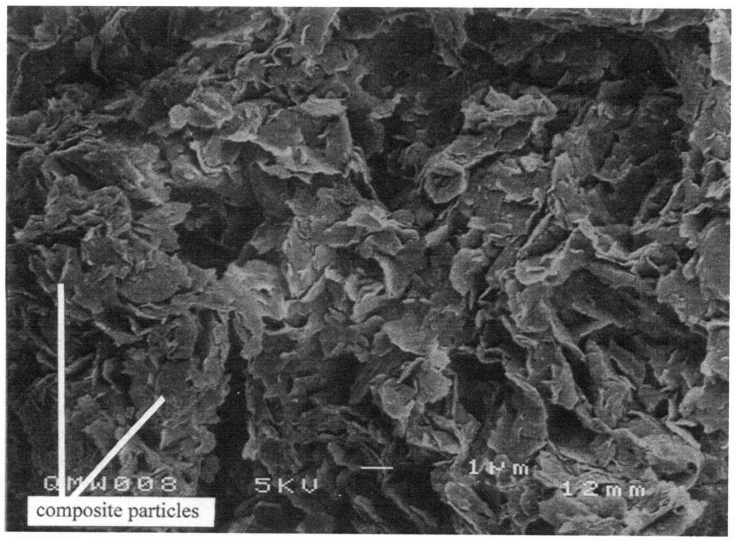

(b)

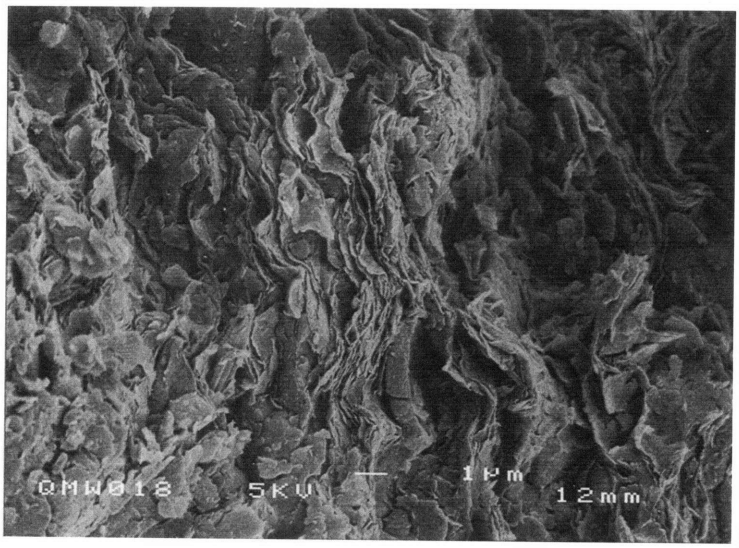

(c)

Figure 3-25: SEM images of natural, reconstituted, and minced Argille Scagliose (Fearon & Coop, 2002).

Shale	w_l (%)	w_p (%)	I_p (%)	Clay fraction	Cementation
Pierre	36-113	20-62	113	12-40% montm.	Fe/Mn Oxide
Fort Union	89		69		
Culebra					
Bearpaw	80-150	18-27	140	50% clay	

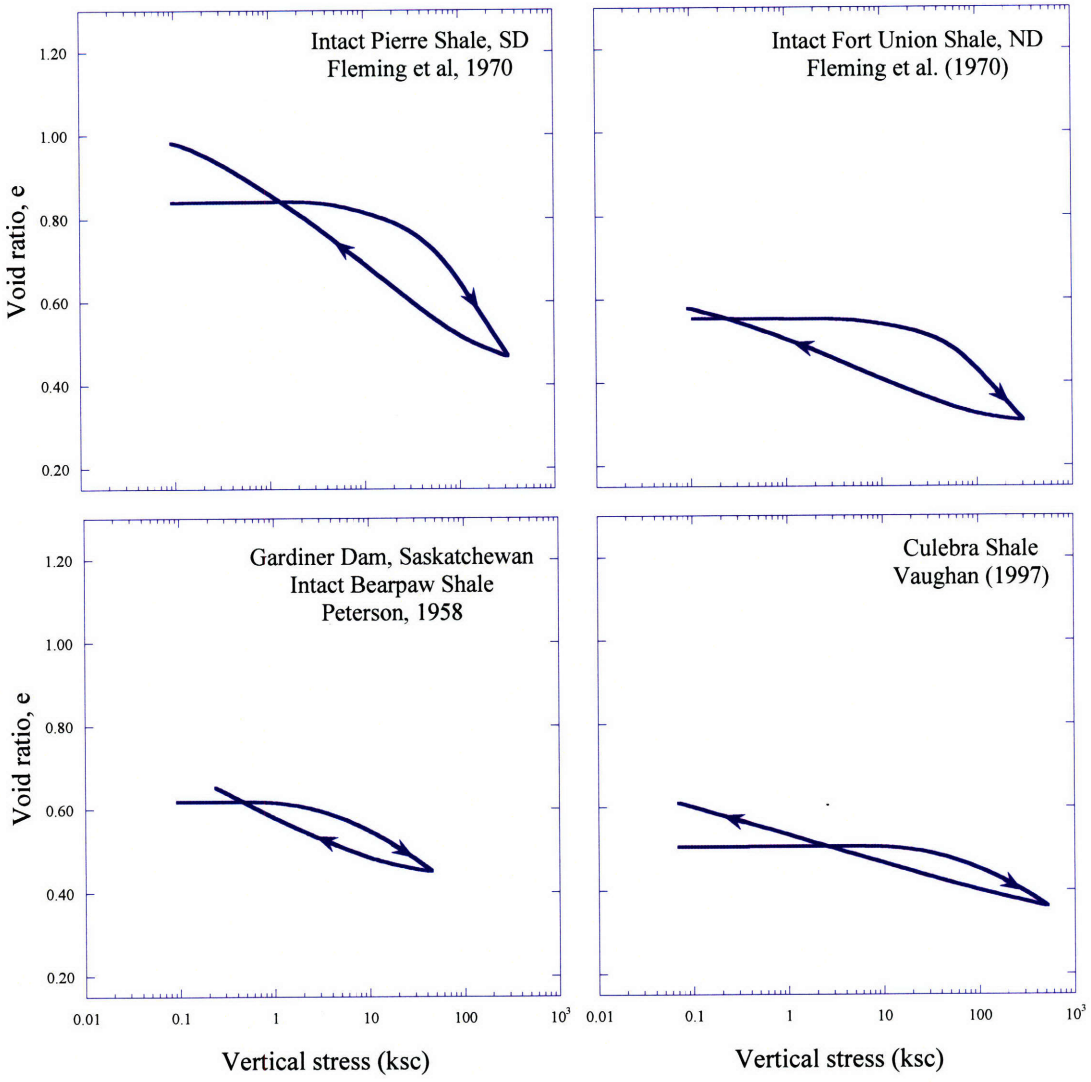

Figure 3-26: Oedometer results for 4 clayey shales (Diaz & Fernando, 1987).

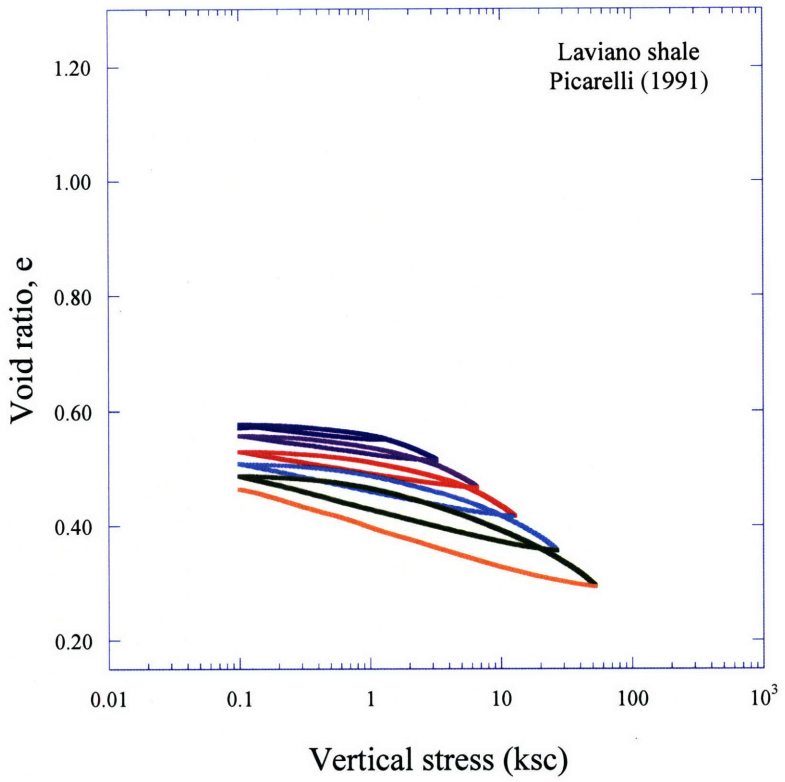

Figure 3-27: Oedometer test on natural Laviano clay Shale (after Picarelli, 1991).

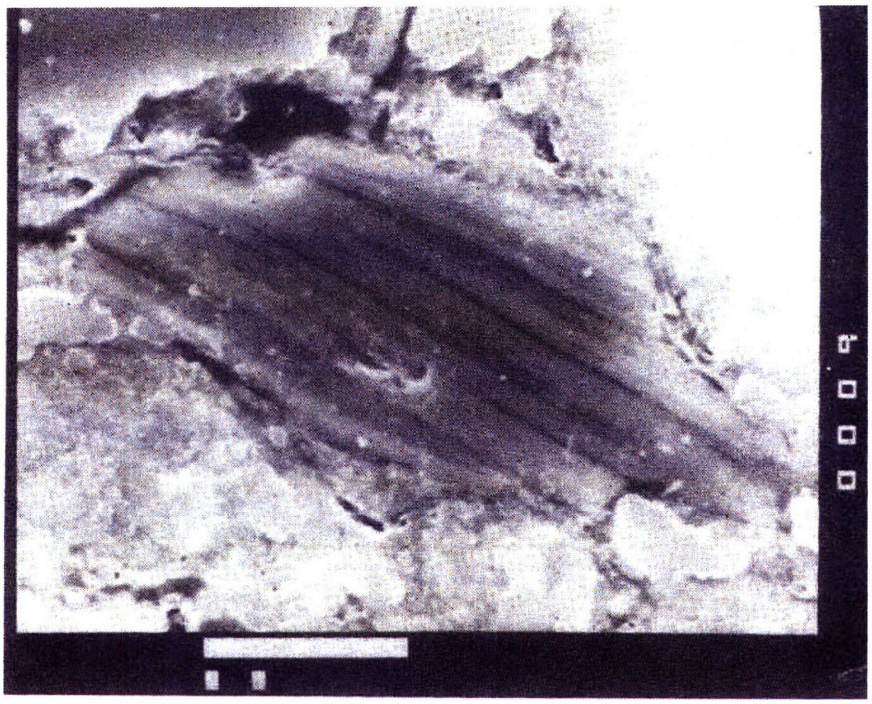

Figure 3-28: Clay stacks in "Coal Measures" shale (Seedsman, 1987, picture from Alonso, 2002).

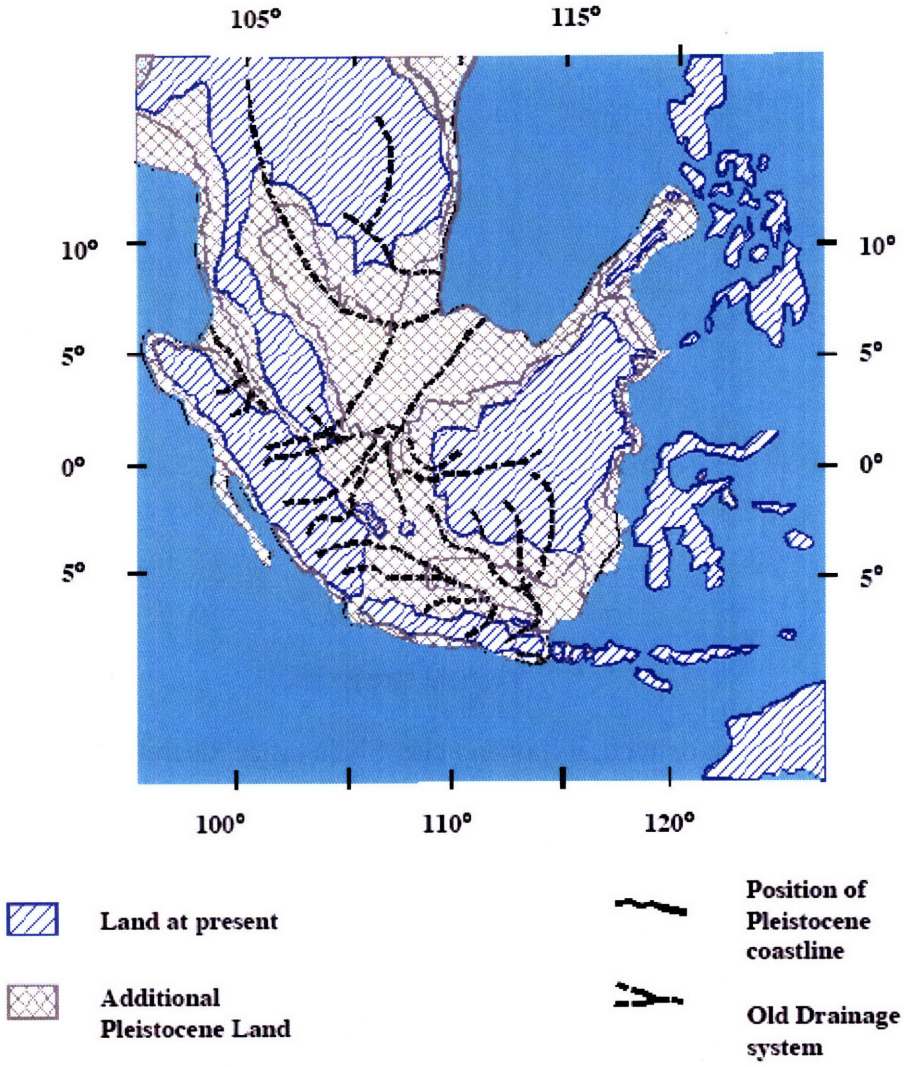

Figure 3-29: Map of SE Asia showing the additional land present during Pleistocene and the Old Drainage system (Shirlaw et al, 2000).

3.10 APPENDIX 3.I

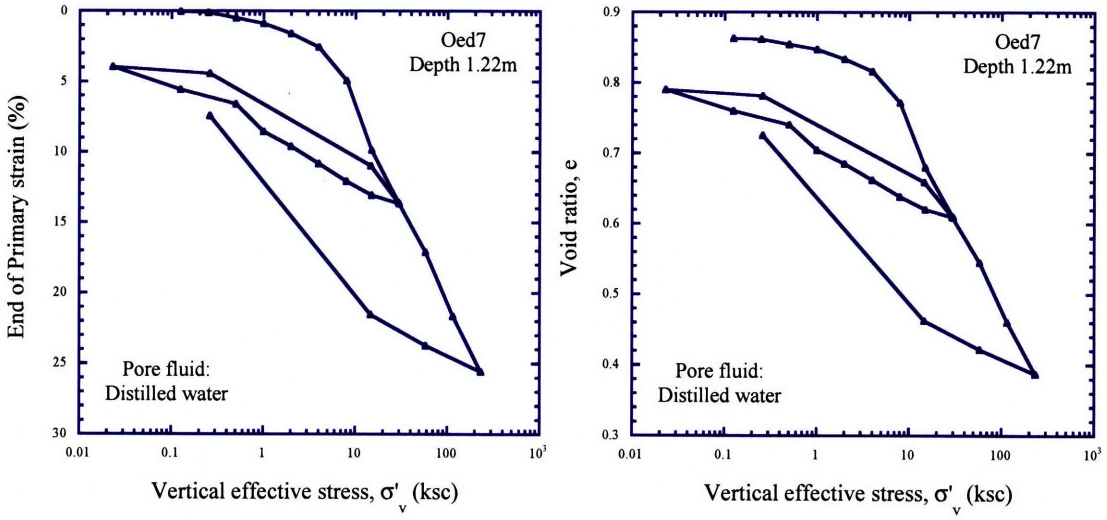

(a) Test Oed 7: Standard oedometer

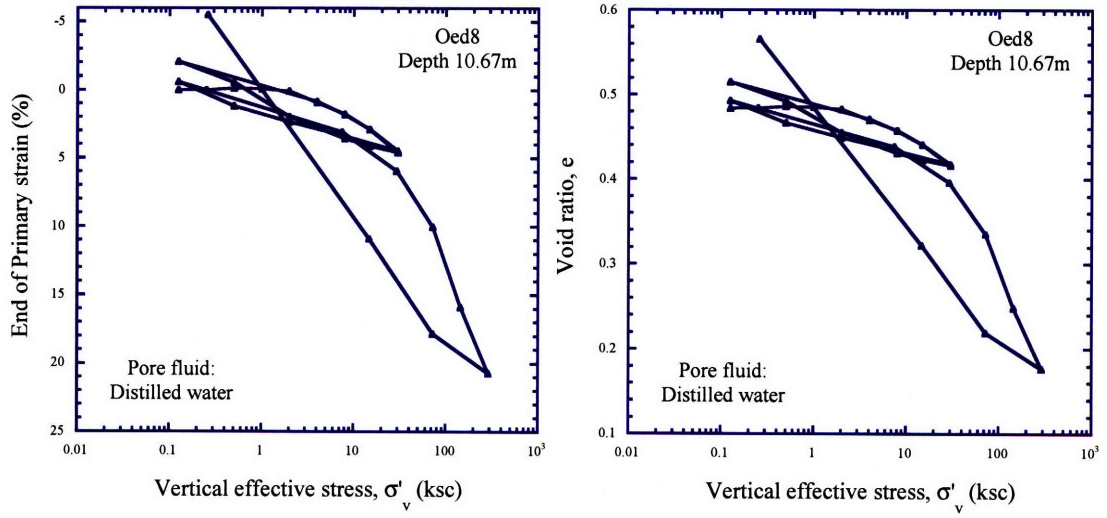

(b) Test Oed 8: High pressure consolidometer

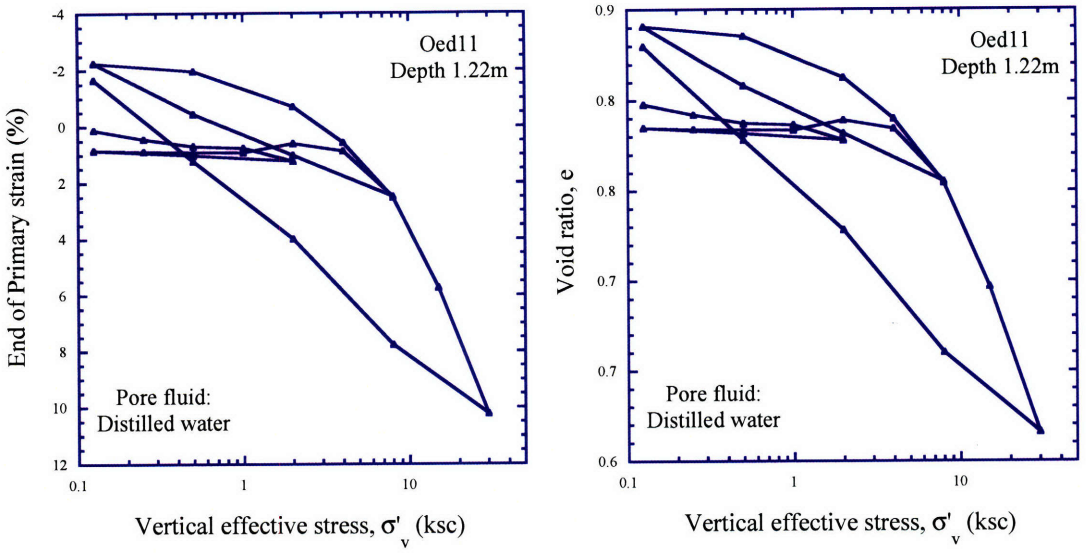

(c) Test Oed 11: Standard oedometer

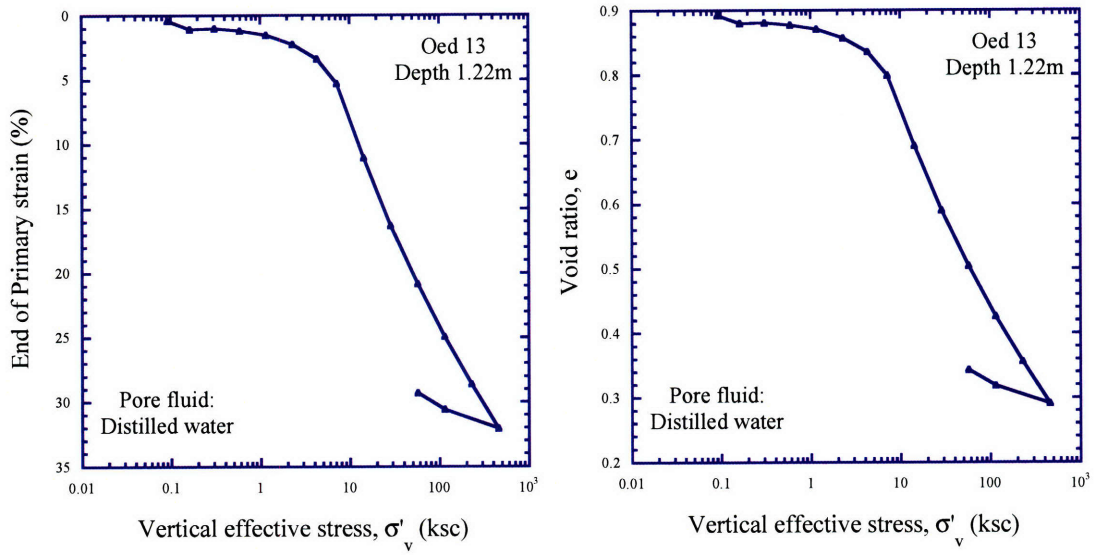

(d) Test Oed 13: High pressure consolidometer

Figure 3.I-1: Tests on Old Alluvium performed by Zhang (2002).

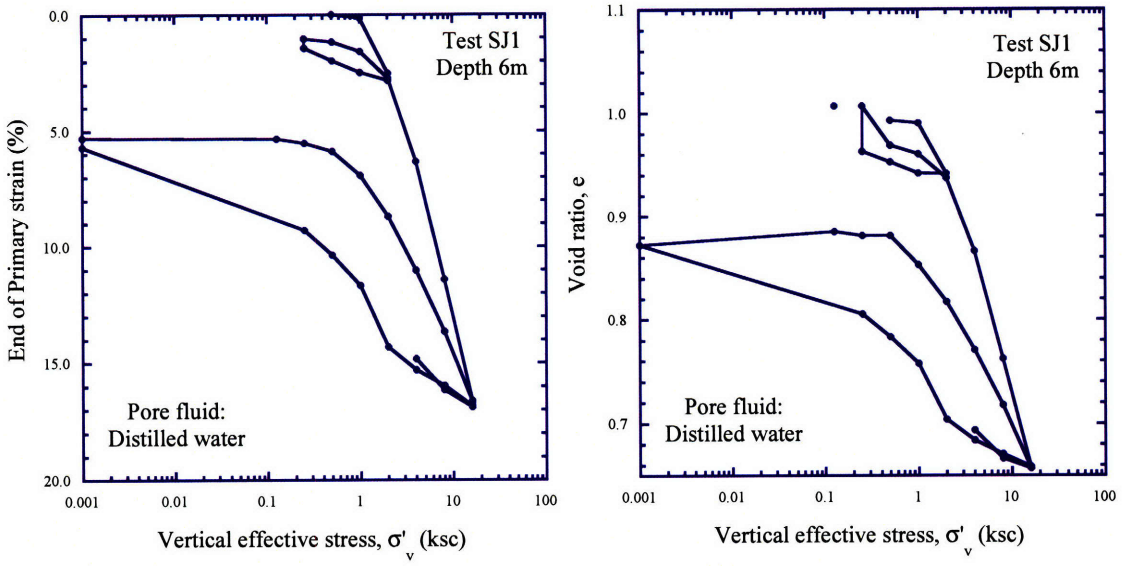

(a) Test SJ1: Standard oedometer

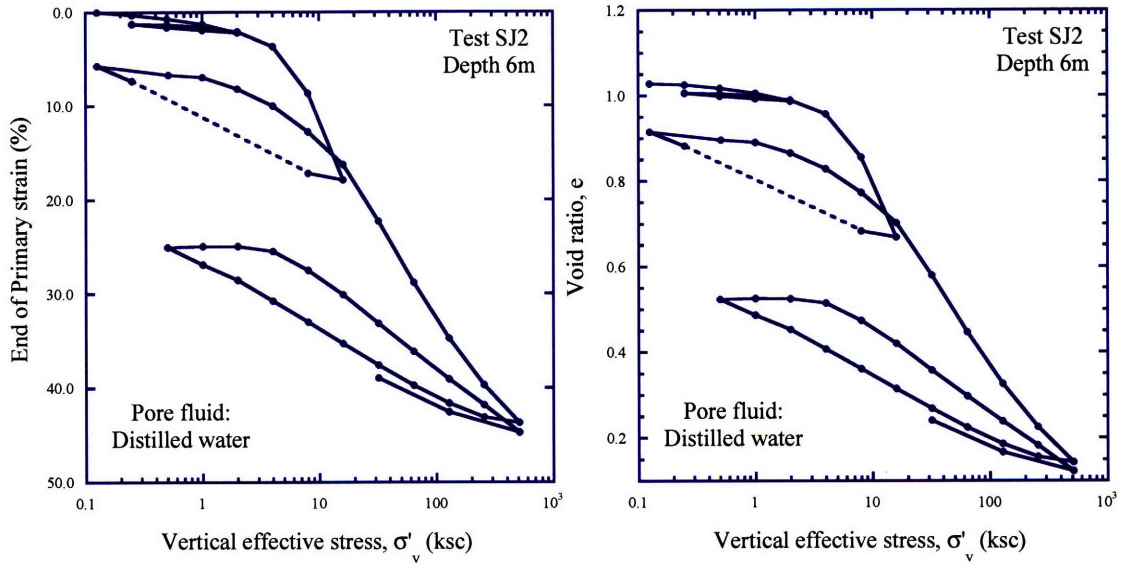

(b) Test SJ2: High pressure consolidometer

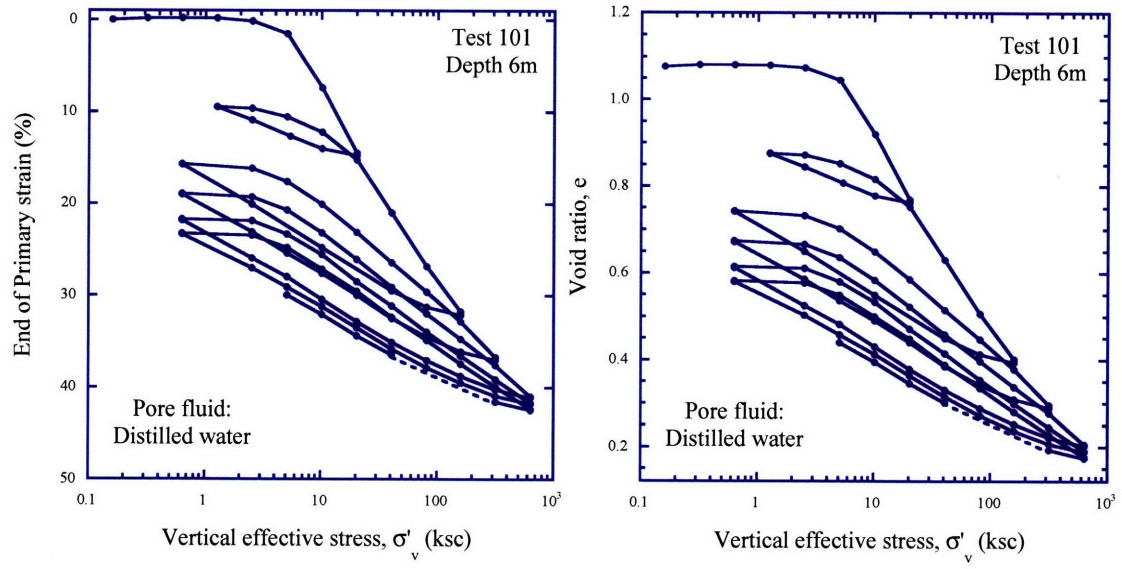

(c) Test 101: High pressure consolidometer

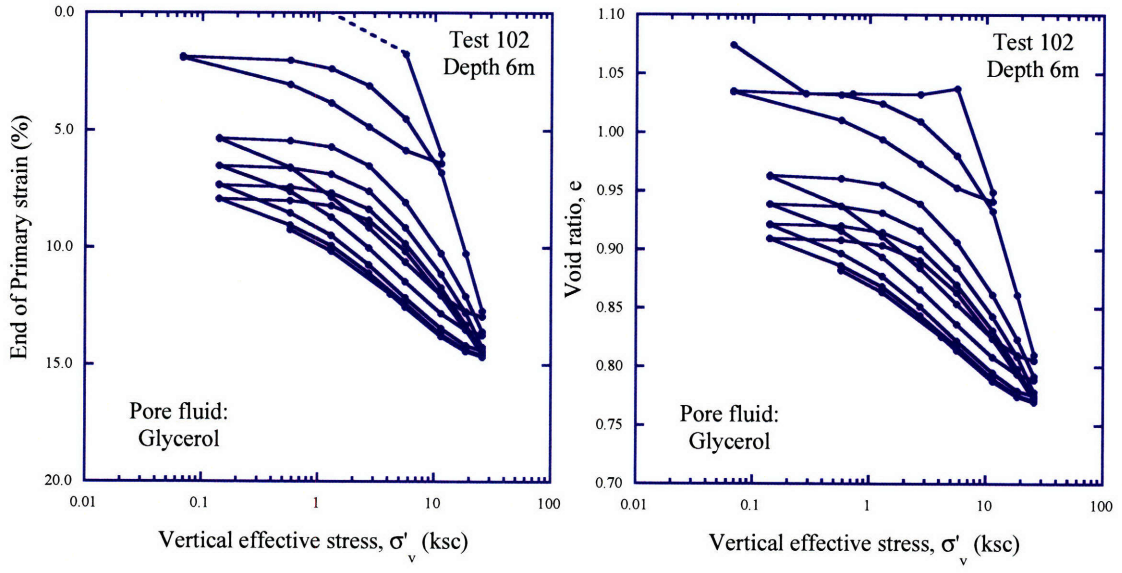

(d) Test 102: Standard oedometer

Figure 3.I-2: Tests on Old Alluvium performed by the Author.

4 Model for virgin compression loading

4.1 INTRODUCTION

The response of the Old Alluvium in compression loading (i.e., first loading) has distinct characteristics at both the macroscopic and microscopic scale (Chapter 3): on the macro-scale, the intact material is a bonded soil with a complex internal structure, which breaks down during loading; on the micro-scale, not only are bond elements destroyed, but a different mineralogical composition is revealed.

This chapter initially reviews the most relevant constitutive formulations for bonded geomaterials in an effort to highlight useful approaches for the modeling of Old Alluvium and identify their limitations. A new formulation is proposed to describe the response of the intact Old Alluvium in compression loading. The formulation introduces variables that represent microstructural changes and their effects on macrostructural response.

4.2 MODELING OF BONDED SOIL BEHAVIOR

4.2.1 Overview

The importance of including the effect of soil structure into constitutive models has been identified quite early (since the late 1970's, e.g. Nova, 1977; Wilde, 1977), but it wasn't until the 1990's that the principles of damage type models were systematically applied in soil modeling. According to Kavvadas & Amarosi (2000), there have been historically three types of procedures to include structural effects in soil modeling:

- The refinement of the "small strain" response, by incorporating stiffness non-linearity in the "elastic" domain (e.g. Dafalias & Herrmann, 1980; Jardine et al., 1986, 1991; Whittle & Kavvadas, 1994).
- The refinement of the material's memory of its stress history, by adding a number of "yield" or "history" surfaces, which record key characteristics of the stress path (e.g. Mroz et al., 1978, 1979; Prevost, 1978; Hashiguchi, 1985).

- The description of the effects of material structure by a damage type mechanism, which permits one to reduce the size of the yield surface due to bond degradation (Kavvadas, 1995; Lagioia & Nova, 1995; Muir Wood, 1995; Chazallon & Hicher, 1998).

Modeling the effect of bonding on the behavior of soils has traditionally involved the introduction of an additional set of bond-related properties and state variables. Most models link the evolution of a "bonding" to some form of plastic strain rate, and correlate the current state of the material to a reference state. As introduced above, most researchers have used the reconstituted or intrinsic state of the soil as a reference state. Alternatively, Desai (1996) proposed a more generalized formulation that assumes that the deforming material is a mixture of parts in two reference conditions, the relatively "intact" and the "fully adjusted" state, and hence the observed behavior can be expressed in terms of the behavior in each of these states.

Gens and Nova (1993) formed the conceptual basis for modeling the behavior of bonded soils by proposing the variation of the size and location of the yield surface for various degrees of initial bonding, b_0. Figure 4-1(a) shows that bonding not only increases the size of the yield surface (p_∞), but also introduces a tensile strength, p_t:

$$p_\infty = p_c(1+b) \tag{4.1}$$

$$p_t = p_c a_t b \tag{4.2}$$

where p_c is the size of the reference surface (Figure 4-1a), a_t an input parameter defining the tensile strength and b a state variable of the amount of bonding. Bonding degrades exponentially with plastic strains:

$$\begin{aligned} b &= b_0 e^{-(h-h_0)} \\ h &= h_1 \int d\left|\varepsilon_s^{\,p}\right| + h_2 \int d\left|\varepsilon_v^{p}\right| \end{aligned} \tag{4.3}$$

where ε_s^p, ε_v^p are the plastic shear and volumetric plastic strains and h_1, h_2 are input parameters, the role of which is to control the relative rate of bond degradation with regard to the plastic strain components. With this formulation, bond degradation (and subsequent softening) due to the increased stress levels is connected to the direct hardening caused by the same increase in loading. The framework uses the intrinsic unbonded properties as the reference state. Figure 4-1(b) plots a series of compression curves obtained for different degrees of bonding.

This parametric study shows that the presence of bonds increases the yield strength of the material, but eventually all compression lines converge to the response of the unbonded soil.

Following a large number of models during the course of the 1990s, Kavvadas & Amorosi (2000) presented a model that aimed to unify all processes that lead to soil structure, from overconsolidation, to cement bonds and ageing. The model has two characteristic surfaces, an internal plastic yield envelope and an external bond strength envelope, hence differentiating between plastic yielding and destructuring (Figure 4-2). The internal surface (PYE) defines the border between elastic and plastic states, hence plays the role of the classical `yield surface'. The external surface (BSE) is controlled by the amount of available bonding, which can be the pre-consolidation pressure in the case of overconsolidated clays or the strength of the cementation bonds in cemented clays or thixotropic bonds in aged clays. The size of the BSE changes according to:

$$\dot{\alpha} = \alpha\left[\left\{\left(\frac{1+e}{\lambda-\kappa}\right)-\zeta_v \exp(-\eta_v,\varepsilon_v^p)\right\}\dot{\varepsilon}_v^p + \left\{\theta_q - \zeta_q \exp(-\eta_q,\varepsilon_q^p)\right\}\dot{\varepsilon}_q^p\right] \tag{4.4}$$

where α is the major semi-axis of the BSE surface, e the current void ratio, ε_v^p and ε_q^p are the plastic volumetric and deviatoric strain components, λ,κ are standard compression parameters (from Critical State Soil Mechanics), and ζ_v, η_v, θ_q, ζ_q, and η_q parameters that control the volumetric/deviatoric structure degradation. Therefore, plastic strains modify this external surface if bond degradation occurs, but they can also occur at stress states inside the external surface, affecting only the internal yield envelope (Figure 4-2). Figure 4-3 shows the application of the formulation to Vallericca clay, a stiff overconsolidated medium plasticity marine clay with 30% carbonate bonding. The model aims to capture the effect of soil structure and of microstructural changes (i.e., removal of bonding) to the compression and shear behavior of the material.

Cotecchia and Chandler (2000) introduced the ratio of the yield stress of a structured soil to the corresponding stress (same specific volume, Figure 4-4) of the reconstituted/intrinsic state as a means of normalizing the behavior of natural clays. The ratio is called "Stress Sensitivity", S_t. Figure 4-4a illustrates that this ratio is constant for both isotropic and K_0 conditions and hence, is a universal measure of the initial microstructure. The authors discuss that the same ratio relates the undrained strength of a bonded and a reconstituted soil (consolidated at the same water

content). Figure 4-4b illustrates that since both the preconsolidation pressure and the peak undrained strength ratios between the natural and reconstituted material are the same, the yield surface of any structured state can be constructed from the reconstituted state based on the Sensitivity ratio. In other words, S_t is the characteristic measure of the soil structure.

Chazallon & Hicher (1998) proposed modeling bond deterioration through damage theory. Their model uses energy arguments to couple elastoplasticity and damage, and expresses damage through changes in the elastic properties that happen according to a thermodynamically acceptable damage energy release rate. This damage energy release rate is defined as a function of the elastic strains:

$$Y = \frac{1}{2}\underline{\underline{\varepsilon}}^e : \underline{\underline{C}} : \underline{\underline{\varepsilon}}^e \tag{4.5}$$

and the evolution of damage is associated with the loading function:

$$f_D(Y,D) = F_D(Y) - D \tag{4.6}$$

where D is the damage variable ranging from 0 (no damage) to 1 (all bonds destroyed).

The approach further considers that material behavior changes from elastoplastic to elastic as the soil becomes strongly cemented. Similarly, Carol et al (2001) used damage theory to model anisotropic damage degradation.

Nova et al (2003) proposed an elastoplastic strain-hardening model for the mechanical and chemical degradation of soils. The evolution of bonding due to mechanical effects follows the general principles of Gens & Nova (1993). The novelty of the 2003 formulation was the introduction of a variable that is responsible for non-mechanical effects, such as chemical dissolution, temperature, time of exposure to weathering agents, or intensity of the chemical attack. Adopting the notation of Figure 4-5(a), the weathering effects are introduced heuristically:

$$p_m = P_m(\varepsilon^p)Y(X_d) \tag{4.7}$$

where p_m is the additional size of the yield surface introduced by bonding, P_m is a function controlling the dependence on plastic strains, and $Y(X_d)$ is the weathering function. The effect of weathering on the yield surface is illustrated in Figure 4-5. The variable X_d is a scalar parameter that varies in a parabolic function:

$$Y(X_d) = (1 - X_d)^2, \; 0 \leq X_d \leq 1 \tag{4.8}$$

with $X_d = 0$ corresponding to the intact state and $X_d = 1$ to the fully weathered state. The rational for using a parabolic form for the weathering function is that intensive weathering is expected to have more effect on the intact than on a highly weathered state of a material, in terms of yield strength. The weathering function is completely uncoupled from the variables describing the mechanical degradation, it does not affect other parameters like the elastic modulus or the friction angle, and can produce damage in the presence or absence of plastic flow[32]. Figure 4-5 shows an example of the model performance for the case of chemical weathering. A silica sand cemented with lime is loaded and then subjected to acid flow. Figure 4-5c illustrates the stress path with the associated deterioration of the yield locus, as well as the plastic potential and plastic flow direction. Figure 4-5d-f plot the evolution of the axial effective stress, the axial strain and the hardening parameters with the amount of weathering (parameter X_d).

4.2.2 Bonded soil models and Old Alluvium

Among these models, the formulation by Kavvadas & Amorosi (2000) is one of the most elaborate, incorporating anisotropic bond degradation and various shearing modes. In addition the Nova (2003) model establishes an efficient way of modeling non-mechanical effects in degradation. However, like all models of this family, both formulations address soil materials where bonding is developed between an otherwise unaltered (intact) soil skeleton. As a result, even in the cases that chemical as well as mechanical processes are included, the discussed models only capture the removal of the interparticle structural elements and they maintain a constant reference to a unique intrinsic state.

The limitation of these formulations with regard to the Old Alluvium is that they cannot address changes in the soil skeleton itself, which could lead (Chapters 2 and 3) to varying mineralogical or chemical content in the microstructure, and hence to different behavior during unloading (swelling) or subsequent loading.

[32] The weathering function has a role similar to that of the accumulated mass transfer of adsorbed water, in the theory of chemoplasticity developed by Hueckel et al. (2002), which is discussed later in Chapter 5.

4.2.3 A Model for clayey shales

Alonso & Alcoverro (2002) proposed a model that does link bond evolution with changes in soil microstructure. The objective of the research was to model the swelling of clayey shales, that contain expandable clay stacks initially restricted by the encircling rock mass (see section 3.6). Hence the bonds themselves are of a mechanical nature (bonding between rock grains or rock crystals), but their disruption reveals a microstructure of different mechanical properties.

The model has two components, one at the macro level and one at the micro level. At the macro level the formulation follows Gens and Nova (1993) for bonded materials. However, part of the macroscopic plastic strain is the result of reversible volumetric deformations at the micro level.

At the micro level, bonding evolves as an exponential function of strain, similar to equation (4.3):

$$b = b_i e^{-h_1 \int |d\varepsilon_v^p| - h_2 \int |d\varepsilon_s^p|} \tag{4.9}$$

where b_i is the initial amount of bonding, $\varepsilon_v^p, \varepsilon_s^p$ the plastic volumetric and deviatoric strains respectively and h_1, h_2 input parameters fitted to describe the assumed rate of bond destruction. Figure 4-6(a) shows an example of the accumulated plastic volumetric strains for three different rates of debonding. Deformations are computed as a function of the confining stress, the current amount of bonding and a microstructural stiffness that also depends on the bonding. Micro-level deformations are translated into macroscopic plastic strains through an empirical transfer function proposed by Alonso (1998):

$$f = f_0 + f_1 \left(1 - \frac{\sigma'}{\sigma'_{ob}} \right)^{n_D} \tag{4.10}$$

where σ' is the current stress, σ'_{ob} the yield stress in compression (preconsolidation stress), and f_0, f_1 and n_D parameters that control the influence of micro-strains on the macrostructure. These parameters are selected based on the available swelling data; for example, function f_0 is selected so that the calculated behavior fits the swelling curve immediately upon load reversal, while n_D controls the effect of the unloading stress ratio σ'/σ'_{ob}, and so is selected at lower stress levels. The role of this transfer function is discussed in more detail in Chapter 5. The contribution of the micro-deformations to the plastic strains modifies the apparent stiffness both

during unloading and during subsequent re-loading, resulting in larger swelling deformations and a more compressible response during reloading. An example of the performance of the model can be seen in Figure 4-6(b).

As discussed in section 3.6, the Old Alluvium and some clayey shales have certain common microstructural characteristics, which affect their response in compression loading. The formulation by Alonso and Alcoverro (2002) is very useful for the modeling of the compression behavior of the Old Alluvium, as it links bond evolution with changes in the soil microstructure, and translates reversible strains in the micro-scale with irrecoverable macroscopic deformations. However the proposed transfer function cannot easily be linked to the physical processes that occur in the microstructure of the Old Alluvium and the macroscopic model assumes a unique fully damaged state.

4.2.4 A model for pyroclastic materials

In Old Alluvium, bond deterioration, aggregate breakdown and grain crushing during first loading are difficult to distinguish. These microstructural changes bear some resemblance to the breakdown of soils with bonds having the same material as the skeleton grains, because in both cases there is no clear distinction between cementation and soil grain crushing. Cecconi et al (2002) attempted to model the behavior of such granular materials (specifically pyroclastic weak rocks) under compression loading that induces grain crushing. They based their approach on Virgin Compression Line observations by Coop (2000) and on the fact that finer granular materials exhibit lower friction angles (Herle et al, 1999; Miura et al, 1997). The main characteristics of the formulation are shown in Figure 4-7. The model allows the friction angle to change (decay) with the evolving grain size distribution. The stress ratio at zero dilatancy, M is considered an internal variable, which degrades with accumulated plastic strain:

$$\dot{M} = -\rho_M (M - M_{crit})\left(\left|\dot{\varepsilon}_v^p\right| + \xi_M \dot{\varepsilon}_s^p\right) \tag{4.11}$$

The grain size distribution is also linked to the location of the virgin compression line, through variable b, which represents the ratio between the current size of the yield locus in isotropic compression and the yield surface corresponding to the stable, fully degraded material (p_s, Figure 4-7):

$$\dot{b} = -\rho_b (b-1)\left(\left|\dot{\varepsilon}_v^p\right| + \xi_b \dot{\varepsilon}_s^p\right) \tag{4.12}$$

$$\dot{p}_s = -\rho_s p_s \left(\left|\dot{\varepsilon}_v^p\right| + \xi_s \dot{\varepsilon}_s^p\right) \tag{4.13}$$

where ρ_s, ρ_b, ρ_M *and* ξ_s, ξ_b, ξ_M are constants which are determined by comparing predicted and observed responses along drained and undrained triaxial compression paths.

The model has a mathematical structure very similar to the formulation given by Gens and Nova (1993), as it assumes a virgin state for the intact material and another of the fully degraded state after grain crushing, and interpolates between the two with internal variables that evolve during the loading process. However, the variable b in this formulation represents the evolution of the grain size distribution. This modeling approach is very useful, as it introduces the notion of evolution of material parameters (such as the friction angle and the location of the virgin compression line). Nevertheless, it is not directly applicable to Old Alluvium, as it doesn't accommodate changes in the activity of clay minerals, which are important for the modeling of the unloading response, and it involves many input constants, which are difficult to relate to the nature of the soil. Finally, as in other cases, it assumes a known destructured state as a reference.

4.3 MIT COMPRESSION MODEL

The MIT compression model (Pestana, 1994; Pestana & Whittle, 1995) is a formulation built for cohesionless materials and sedimentary clays. In the present model it is used as the basis for modeling the compression behavior of Old Alluvium, and hence is described here in detail.

The compression model uses four input parameters and incorporates the void ratio (measure of density) as a separate state variable.

4.3.1 Compression model for sands

According to Pestana & Whittle (1995), sand specimens compressed from different initial formation densities approach a unique limiting compression curve (LCC) at high stress levels, which can be described by a linear relationship in a loge-logσ' space. Pestana (1994) developed a compression model, which is capable of accurately describing the behavior of freshly deposited cohesionless soils over a wide range of stresses and densities. The model came to fill a gap in the

modeling of granular materials, as previous approaches (for example bi-linear models used in the framework of critical state soil mechanics (Schofield & Wroth, 1968) or power law models (Janbu, 1963; Lade, 1977) did not consider density as a state variable of the soil and had not managed to successfully capture the progressive development of irrecoverable deformations during first loading.

It has already been discussed in Chapter 3 that the response at low pressure levels is caused by elastic deformation of the soil skeleton and by particle rearrangements (sliding, rolling and activation of new contacts), while at high pressures (LCC regime), deformation is controlled by particle crushing. Hence, irrecoverable, plastic strains develop throughout first loading.

At high stresses, the limiting compression curve is described by its slope ρ_c and a reference stress, σ_{ref} at unit void ratio, as is shown in Figure 4-8. The slope, ρ_c, depends slightly on the material mineralogy, while the reference stress is highly affected by the particle size; Figure 4-9 shows that σ_{ref} tends to increase with particle size.

The incremental elastoplastic effective stress - strain relationship is given by:

$$\dot{\varepsilon} = \frac{e}{1+e}\left[\frac{\delta_b^{\theta}}{C_b(\sigma'/p_a)^{1/3}} + \frac{\rho_c}{\sigma'/p_a}(1-\delta_b^{\theta})\right]\frac{\dot{\sigma}'}{p_a}$$
$$\dot{\varepsilon}^e = \frac{e}{1+e}\left[\frac{1}{C_b(\sigma'/p_a)^{1/3}}\right]\frac{\dot{\sigma}'}{p_a} \qquad (4.14)$$

where:

- $\dot{\varepsilon}$ and $\dot{\varepsilon}^e$ are the increments of the total and elastic volumetric strains;
- e is the current void ratio;
- σ' is the mean effective stress and p_a the atmospheric pressure;
- C_b is an input parameter that is related to the elastic tangent bulk modulus K^e. The later is expressed as a separable function of the mean effective stress and the current void ratio and in general increases with confining stress and density:

$$\frac{K^e}{p_a} = C_b\frac{1+e}{e}\left(\frac{\sigma'}{p_a}\right)^{1/3} \qquad (4.15)$$

Figure 4-10 shows a conceptual representation of the evolution of the tangent bulk modulus for a compression test. In the low stress region the modulus depends on the formation density, while at high stresses (LCC region) deformations are controlled by particle crushing and the bulk modulus is independent of the formation conditions. The transition to this unique relationship in the LCC regime can be either smooth (more angular particles) or abrupt (finer, ground particles), approximating a yield point where the bulk modulus is discontinuous.

- δ_b is a measure of the dimensionless distance between the current mean effective stress and the equivalent mean effective stress, σ'_b, on LCC, at the same void ratio (Figure 4-8). δ_b is given by:

$$\delta_b = 1 - \frac{\sigma'}{\sigma'_b}, \quad 0 \le \delta_b \le 1; \quad \sigma'_b = \sigma'_{ref}\left(\frac{1}{e}\right)^{1/\rho_c} \tag{4.16}$$

- θ is the fourth input parameter, which describes the smoothness of the transition between the low and high stress regimes. Figure 4-11 shows the effect of θ on both the evolution of the bulk modulus and the elastoplastic transition in the loge-logσ' space. The parameter depends on (increases with) the particle angularity, as illustrated in Figure 4-12, which plots sands of different angularities with the value of θ that best describes their transition to the LCC regime.

Guidelines for the proper selection of the model's input parameters, along with the laboratory tests required, are detailed in Pestana (1994), Pestana & Whittle (1995, 1999), and are summarized here in Table 4-1.

4.3.2 Compression response of clays

As discussed in Chapter 3, the virgin consolidation line of reconstituted clay specimens can also be well described by a linear relationship in the loge-logσ' space (Figure 4-13). It is therefore qualitatively similar to the limiting compression curve for sands and can be represented by the compression model of equation (4.14). For the case of clays, mineralogy is the principal factor affecting the slope, ρ_c, of the LCC, and the reference stress, σ'_{ref}, is controlled not only by the grain size distribution (characterized now by the clay fraction) but also by the physico-chemical characteristics of the pore fluid/environment (dielectric constant, concentration of dissolved electrolyte, valence of adsorbed cations and pH).

4.4 DEVIATION FROM EXISTING MODEL BEHAVIOR

Based on the observations made in Chapter 3, it is expected that the MIT compression model cannot successfully describe the behavior of Old Alluvium. Indeed, Figure 4-14 plots test 101 with a MIT-S1 prediction fitted for the lower stress levels. The prediction is in very good agreement with the data up to a stress level of about 80ksc. At higher vertical stresses, the measured data deviate from a linear Limiting Compression Curve (in loge – logσ' space) and the actual behavior is characterized by a much higher compressibility, ρ_c.

Various parts of the data can be fitted with different sets of compression input parameters (ρ_c, σ_{ref}) that define the location of the Limiting Compression Curve. Figure 4-15 shows that such a set can be found to fit the final as well as intermediate parts of the experimental curve for test 101; in fact, any intermediate part could be fitted with input values varying between the initial and final parameter sets.

Such variation in the input parameters can be justified when their physical meaning within the MIT compression soil model is considered. Pestana (1994) has concluded the following:

- For sands, particle mineralogy has little influence on the location of the limiting compression curve (i.e., ρ_c and σ_{ref} are largely independent of mineralogy).
- In contrast, for reconstituted clays, mineralogy is the principal factor affecting the slope of the LCC, ρ_c.
- ρ_c is also significantly affected by the relative activity of the clay, R_A:

$$R_A = 1\text{-}w_p/w_L \qquad (4.17)$$

where w_p = plastic limit and w_L = liquid limit of the clay.

Figure 4-16 shows that the parameter increases with increasing activity, and varies between 0.12 for kaolin ($R_A = 0.26$) and as high as 0.60 for Na-Montmorillonite ($R_A = 0.95$).

- The particle size (characterized by D_{50}) has a significant effect on σ_{ref} for both sands and clays. (Figure 4-9). In the case of sands, the reference stress increases with finer particles, as larger particles are prone to crush at lower stresses due to larger contact stresses, and increased likelihood of flaws (Billam, 1971, Marsal, 1967).

- For clayey materials, the reference stress (location of normally consolidated line) is also affected by the formation structure (flocculated vs. dispersed) and the chemical composition of the pore fluid.
- Finally, particle angularity influences both parameters.

Mineralogy and microstructure tests on the the Old Alluvium (Chapter 2) have shown that clay minerals exist but are hidden in the initial, structured form of the soil. Once mechanical disaggregation occurs, the clay minerals actively affect the behavior of the material, producing the following effects:

- Initially the soil appears to be a sand-like material and ρ_c is unique and independent of the breakdown. At high stresses, after the structure has been significantly disrupted, there is notable change in the clay activity, and the macroscopic response is affected by the presence of the clay minerals. At this new stage both the mineralogy and the relative activity affect the value of ρ_c, and since they evolve due to continuous breakdown (progressive disaggregation), the parameter ρ_c is also expected to increase in magnitude.
- Similarly, the presence of clay particles at the later stages of the test is expected to increase the value of the reference stress.

Based on these observations, a constitutive model aiming to describe the compression behavior of the Old Alluvium should be able to vary the Limiting Compression Curve from one that corresponds mostly to sandy materials to one that characterizes more clay-like behavior.

4.5 PROPOSED MODEL

4.5.1 Tracking changes during breakdown

Compression of the the Old Alluvium involves particle rearrangement and crushing, as well as mechanical disaggregation, removal of cementation bonds and most importantly disassociation of the iron oxide aggregation from the clay stacks. As a result, there is a progressive increase in clay activity, as clay minerals start to interact actively with the porous environment.

The rate at which this disaggregation happens, however, is not directly known. The only available microstructural information exists at the beginning (intact state) and end of the

compression tests. There is some evidence that the change is gradual. The expansive minerals (particularly nontronite) are responsible for much of the observed swelling deformations, hence the amount of recovered volumetric strain during unloading from a specific stress level can be used as an indication of the amount of "revealed clay". Test 101 includes measurements of recovered strains for unloading at a range of pre-consolidation pressures. Figure 4-17, that plots the strain recovered in unloading for these different preconsolidation levels, σ'_p, illustrates that there is a significant increase in the amount of recovered strain for σ'_p = 60-200ksc, and a smaller increase for σ'_p >200ksc.

Based on these observations, it is speculated that iron oxide disaggregation occurs mainly within a small range of stress levels (approximately 60-200ksc). In other words, the release of the clay physicochemical properties happens slowly initially, and then within a fairly small range of stress levels most of the clay becomes readily interactive with its environment. Much less pronounced changes occur thereafter. It is hence proposed to track the microstructural changes during breakdown with a sigmoid-type function.

4.5.2 Representation of the clay actively present in the soil

The amount of recovered volumetric strain is a good indication of the amount of active clay minerals present in the soil structure. This behavior can be quantified through the use of Cation Exchange Capacity (CEC) as a surrogate parameter.

Cation Exchange Capacity (CEC) is defined as the amount of exchangeable cations that a clay mineral can adsorb at a specific pH. Readily exchangeable cations are the ones that can be replaced easily by leaching with a solution containing other cations of higher replacing power than the adsorbed cation[33]. Effectively, CEC is a measurement of the total unbalanced negative electric charges present in the soil. These negative charges can be the result of isomorphous substitution of aluminum or silicon atoms at the mineral sheets, of broken bonds at the edges and external surfaces, or of the dissociation of accessible hydroxyl (OH^-) groups (replacement of H^+

[33] Brief summary on cation replaceability: In general, ions with higher valence are held more tightly, while small cations tend to displace large cations; however cations with lower replaceability may replace others with higher one by mass action, if their concentration is relatively high (Mitchell, 1976).

by other cations). The negative charges from the last 2 mechanisms are pH dependent, and therefore sensitive to environmental changes.

In any case, the Cation Exchange Capacity is a measure of the interlayer spaces that are available to exchange cations and it depends on the type and the amount of clay minerals present (unbalanced negative charge), as well as on the concentration of cations in the pore fluid and their electrovalence. The units used for the Cation Exchange Capacity are milliequivalents (meq) per 100 grams of dry clay[34].

There are several methods for the determination of Cation Exchange Capacity, and no one method can be employed reliably for all clays. However, a method that is used more efficiently for many clay minerals is based on saturation, primarily with barium as the index cation, and is advantageous because CEC does not dependent on the pH of the saturation (for most minerals).

Zhang (2002) measured the Cation Exchange Capacity of Old Alluvium in both its intact state and after removal of the iron oxides. He used a simple barium chloride method after Hendershot and Duquette (1986). The iron oxides were removed using DCB (sodium dithionite – citrate – bicarbonate mixture). The results in Table 4-2 show that the chemical treatment caused a notable increase in the value of the CEC for both the Upper Clay and the Middle Zone. However, the change is more pronounced for the Upper Clay, a result expected as the upper stratum of the soil contains more clay minerals.

The Cation Exchange Capacity is employed as the variable to quantify the active clay minerals in the microstructure, and so, according to the discussion in 4.5.1, its evolution is described with a sigmoid-type function of the applied (preconsolidation) stress level:

$$CEC = CEC_i + \frac{1}{2}(CEC_i - CEC_f)\left(1 + \tanh\left(\frac{\sigma' - \sigma'_m}{\sigma'_m - \sigma'_o}\right)\right) \tag{4.18}$$

where CEC_i and CEC_f are the cation exchange capacities of the intact soil and of the soil after chemical disaggregation (i.e. after removal of the iron oxides), σ'_o and σ'_m are values of the preconsolidation pressure marking the onset of microstructural degradation and at maximum rate of degradation, respectively. This is illustrated in Figure 4-18.

[34] Equivalent weight is the combined weight of an element; the number of equivalents is defined as weight of element/atomic weight. (Mitchell, 1976)

The stress levels σ'_m and σ'_o can be inferred from a high stress compression test. The value of σ'_o corresponds to the departure from a linear Limiting Compression Curve relation. For example, Figure 4-19 shows that in test 101 (material from depth 6m), this deviation occurs at a stress level of σ'_o= 80ksc. The stress level corresponding to the maximum rate of degradation (and hence of the CEC increase) can be interpreted from Figure 4-17 as σ'_m= 250ksc. It will be discussed in Chapter 5 that any available data on the amount of volumetric expansion can improve the selection of parameter σ'_m. Based on the chosen values and the initial and final CEC values given in Table 4-2, one can predict how the cation exchange capacity of The Old Alluvium changes during compression. The calculated values are plotted in Figure 4-18: the CEC of the soil starts increasing after the compression load has reached 80ksc, and it approaches its final value at an estimated stress level, σ'= 450ksc.

4.5.3 Evolution of compression parameters

At low compression stresses, the soil is regarded as a granular material; therefore the values for both the compressibility parameter (ρ_c) and the reference stress (σ_{ref}) are fitted based on the intact soil behavior, following the compression model of Pestana and Whittle (1995).

As discussed in section 4.5.1 the parameters defining the high stress compression behavior of Old Alluvium should evolve following the increase of the Cation Exchange Capacity. There are no data indicating a direct relationship between the (instantaneous) slope of the Limiting Compression Curve (ρ_c) and the cation exchange capacity. However, ρ_c is significantly affected by the relative activity of the clay (section 4.4 and Figure 4-16). Based on the microstructural and mineralogical observations on Old Alluvium (Chapter 2), as well as its macrostructural response during unloading, it can be assumed that the initial activity of the material is low (little volumetric expansion; close to the response of Illites and Kaolinites in Figure 4-16), but eventually it increases towards that of montmorillonites (significant volumetric expansion, but not as high as that of pure sodium montmorillonites, for example). Based on information on Atterberg limits (Zhang, 2002), the expected variation of ρ_c for different degrees of disaggregation is plotted in Figure 4-20. It is inferred that for the case of Old Alluvium the

compressibility coefficient ρ_c can be related to the relative activity R_A with an almost 1:3 slope in the plotted $\log_{10}(R_A)$-$\log_{10}(\rho_c)$ space.

Since Cation Exchange Capacity is used as the variable to represent the evolution of clay activity during compression (and associated disaggregation) of the Old Alluvium, it is proposed that the change of the compressibility coefficient ρ_c is analogous to the increase in the Cation Exchange Capacity values:

$$\rho_c = \rho_{c,i}\left(\frac{CEC}{CEC_i}\right)^n \tag{4.19}$$

where ρ_{ci} and CEC_i are the compressibility and the cation exchange capacity of the intact soil respectively. Parameter n controls the relative rate of change between CEC and ρ_c and so is introduced to reflect the slope in the $\log_{10}(R_A)$-$\log_{10}(\rho_c)$ space (i.e. n = 0.3, c.f. Figure 4-20). It therefore generalizes the use of equation (4.19) for soils other than Old Alluvium, the compressibility of which may be affected by the relative activity in a different way (Figure 4-20).

The reference stress, σ_{ref}, is assumed to vary in a similar fashion:

$$\sigma_{ref} = \sigma_{ref,i}\left(\frac{CEC}{CEC_i}\right)^n \tag{4.20}$$

where $\sigma_{ref,i}$ is the reference stress of the intact material.

Figure 4-21 plots values of ρ_c and σ_{ref} calculated according to equations (4.19) and (4.20). The compressibility parameters increase following the selected evolution pattern of the Cation Exchange Capacity.

4.6 INPUT PARAMETERS SELECTION

The proposed compression model incorporates the four input parameters of the MIT compression model (ρ_c, σ'_{ref}, θ and C_b) and it introduces five more (CEC_i, CEC_f, σ'_o, σ'_m, and n) to capture the behavior of soils with varying amounts of active clayey minerals.

Table 4-3 summarizes the input parameters for the new compression model. In more detail:

- C_b defines the elastic bulk modulus at small strain levels. It can be estimated using measurements of 1) volumetric stress-strain behavior in hydrostatic unloading; 2) one-dimensional unloading with lateral stress measurements; and 3) small strain elastic shear modulus. However, due to inaccuracies in small strain measurements in triaxial tests, it would ideally be determined by Resonant Column or in-situ cross-hole or down-hole measurements of the shear modulus from elastic shear wave velocity. Reported values of C_b are 800±100 for clean uniform sands and 400-500 for low plasticity clays, although the value would decrease with increasing plasticity.

  The Old Alluvium initially consists of quartz particles and similarly sized aggregates; hence the intact state is expected to have C_b values similar to those of sands. A value of $C_b = 950$ is selected.

  However, higher values are expected before the yield stress due to the presence of cementation. Dvorkin et al. (1999) showed that the elastic (compression) modulus of epoxy cemented glass beads increases by a factor of two when the cement concentration in the pore space increases from 0 to 10% (amount enough to fill the space around grain contacts). The notable characteristic of Old Alluvium though is that beyond the yield point the void ratio changes significantly. As a result, the elastic bulk modulus increases by a factor of 3 between 5ksc and 30ksc (selected stress levels before and after the yield point) for a constant value of C_b. It is hence not trivial the net increase in elastic modulus due to cementation.

  Dvorkin at al (1991,1994) proposed an approach to update the elastic parameters based on the amount and geometry of the cementation present (Appendix 4.I). Even though the approach cannot be directly applied to Old Alluvium (it assumes that the skeleton consists of solid grains and there is substantial amount of cementation to be considered as a continuous foundation), it can help estimate an increased value of C_b for the low stress, pre-yield locus.

  In conclusion, a 25% increase is C_b is assumed to reflect the presence of cementation. Hence, with the selected value of $C_b = 950$ (not considering cementation), a value of $C_{b,i} = 1200$ is proposed for the initial intact skeleton before the transition to the Limiting Compression Curve. A step change between $C_{b,i}$ and C_b is applied at the end of this transition ($\delta_b = 1$ in equation (4.16)). It should be noted that the elastic deformations are small and not observed

directly from the macroscopic strains measured in oedometer tests. Bender element data could provide more accurate information on the bulk modulus changes during compression.

- Parameter θ describes the compression behavior during the transition to the Limiting Compression Curve, so it defines the first loading curve at the transitional regime. Selection of this parameter is based on the available compression data and follows the guidelines for MIT-S1 compression model. As discussed before (4.3.1) θ depends on the angularity of the soil particles. High angularity results in an abrupt transition to the LCC regime (analogous to a "yield stress") and θ is small (closer to 0.1). Rounded particles have a much smoother transition and θ becomes larger. Figure 4-22 shows example predictions with variable θ values.
- $\rho_{c,i}$, and $\sigma_{ref,i}$ define the Limiting Compression Curve of the initial, undestroyed material. $\rho_{c,i}$ describes the slope of the curve, which is a straight line in a a $\log_{10}e$-$\log_{10}\sigma'$ space, and $\sigma_{ref,i}$ references its location (it is the mean effective stress at unit void ratio). They can be fitted in the compression test data before the onset of significant disaggregation. Figure 4-14 shows an example of the selected compression parameters for the intact material. Note that the four input parameters discussed so far (C_b, θ, $\rho_{c,i}$, and $\sigma_{ref,i}$) are identical in physical meaning (and required selection procedures) to C_b, θ, ρ_c, and σ_{ref} in the MIT-S1 compression soil model.
- CEC_i and CEC_f are the values of the cation exchange capacity of the soil at the beginning and at the end of the test accordingly. Typical values of the Cation Exchange Capacity are often reported for common minerals. They vary from 3-10meq/100g for Kaolinites to up to 80-120meq/100g for Montmorillonites. The CEC of nontronite is at the highest side of this range, having values between 110-150 meq/100g. However, the actual value depends on environmental conditions, and in the case of soils like Old Alluvium it cannot be estimated from these values, but it has to be measured directly. A commonly used procedure to determine the cation exchange capacity of a soil is the barium chloride method (Hendershot & Duquette, 1986). The initial value, CEC_i, can be directly defined from the intact material. The final value would ideally be measured on the tested soil at the end of the compression. However this would require individual measurements for every test. In practice, CEC_f can be determined from a specimen treated chemically to remove the aggregation and cementation agents and bonds. This will provide a representative mean value for the disaggregated soil.

- σ'_o is the stress level that marks the onset of significant breakdown and of changes in the microstructural level of the soil. σ'_o is the parameter that controls the point at which the CEC – and subsequently ρ_c – will begin to increase with a significant rate. It can therefore be determined from first loading compression data as the stress level at which the compression behavior at high stresses deviates from the traditional Limiting Compression Curve. This is illustrated in Figure 4-19 for test 101. Figure 4-23 shows the effect of σ'_o on the evolution of CEC values and Figure 4-24 plots the corresponding compression predictions. Even though the differences in the Cation Exchange Capacity are pronounced, the effect of σ'_o on compression behavior is quite small. However, the importance of σ'_o as input parameter will be demonstrated when studying the swelling behavior (see section 5.4.3), which is strongly related to the values of the CEC.
- σ'_m is the stress level at the maximum rate of Cation Exchange Capacity change (Figure 4-18). Hence, it controls the range of stresses along which changes in the soil happen with significant rate. This range of stresses can be defined by looking at the maximum swelling data (for example Figure 4-17), provided that the compression tests include unloading-reloading cycles at regular stress levels. It could also be estimated by the rate of curvature change of the first loading compression curve. Figure 4-25 shows the effect of σ'_m on the evolution of CEC values and Figure 4-26 plots the corresponding compression predictions. It can be seen that σ'_m affects the predictions for both the CEC and the compression behavior; and similarly to σ'_o, it is expected to influence the swelling calculations.
- Finally, n is a factor that controls the evolution of the compression parameters with respect to CEC changes. The value of n can be determined based on data that associates compressibility and Cation Exchange Capacity, or some measure of clay activity, such as the Relative Activity. This procedure was discussed in Figure 4-20. Figure 4-27 shows how n affects the calculated compressibility at high stress levels.

4.7 MODEL PREDICTIONS ON THE COMPRESSION BEHAVIOR OF OLD ALLUVIUM

4.7.1 Study on the available tests

There are compression test data for Old Alluvium from depths 1.2m (Upper Clay, tests 7, and 13), 6m (Upper Clay, tests 101 and SJ2) and 10.7m (Middle Zone, test 8). Based on the discussion in Chapters 2 and 3, the degree of weathering and hence the soil consistency vary with depth, therefore it is expected that some of the input parameters may also vary with depth.

Based on the above discussion, the model is calibrated with test 101, since this provides the most available data for the parameter selection. Figure 4-28 plots the calculated compression response. The figure illustrates that the model is capable of describing the continuing change in compressibility caused by microstructural changes (compare with Figure 4-14).

Specimen SJ2 was obtained from the same depth as 101, hence its response should be well described by the same set of input parameters. Figure 4-29 illustrates that the model succeeds in predicting the evolution of compressibility, however the data exhibits a less pronounced yield and a smaller reference stress than those described by the model. These deviations are most probably the result of spatial variability within the weathered soil. For example, smaller content of quartz particles, which are more brittle than the clay aggregates, would result in a more gradual transition to LCC (higher θ value).

Specimens oed7 and oed13 were obtained from a shallower depth (1.2m). Because weathering is more intense closer to the surface, the soil is expected to have higher percentage of clay minerals but also of cementing agents. The intact material is expected to contain more aggregates (which are brittle) hence $\rho_{c,i}$ and $\sigma_{ref,i}$ should be lower. However, since there is also more cementation, the difference in the values is not that pronounced. Breakdown is also expected to start at lower stress levels (lower value of σ'_o) and take place over larger range of stresses (higher value of σ'_m). It should be noted that as discussed in section 4.6, σ'_o and σ'_m have little effect on the compression predictions, but need to be selected properly to account for the evolution of the apparent clay activity. Figure 4-30 plots the predicted response for test oed7 and Figure 4-31 for test oed13. It can be seen that model describes well the observed compression behavior.

Specimen oed8 was obtained from a greater depth (10.7m), within the Middle Zone (MZ). Mineralogical analyses and microscopic observations performed on material obtained from a depth of 13.7m (Zhang, 2002) showed that the soil is less weathered, and contains more quartz, less clay minerals and less iron oxides than the sample used in test 101 (6m depth). Hence, compared to the values calibrated on test 101, the compressibility of the intact material is expected to decrease while the yield strength to increase (ρ_c to decrease and hence σ_{ref} to decrease, due to the high yield stress). Cation Exchange Capacity measurements showed a higher initial value but smaller overall change. Since the amount of cementation is lower, the evolution of the CEC would probably take place within a smaller range of stresses. Hence, σ'_m should be less than the corresponding one at 6m. Figure 4-32 plots the calculated response for test 8. The yield strength is indeed much higher, but the specimen exhibits a sudden and substantial increase in compressibility, which is not expected given the higher quartz content in the Middle Zone. Unfortunately, no other compression data are available for deeper samples, and it is not clear if this test is truly representative.

4.7.2 Predictions of the compression behavior through the weathering profile

The Old Alluvium, being a tropical in-situ weathered soil, is characterized by spatial variability that is not always consistent with depth – as an example, the specimens from 6m depth have a higher initial void ratio than the ones from 1.2m depth, even though the opposite trend would be expected. However, the degree of weathering does decrease with depth, and so certain assumptions can be made about the variation of the material input parameters:

- The compressibility of the intact soil ($\rho_{c,i}$) decreases, because it contains a higher percentage of quartz and less of the more compressible aggregates. The change in $\rho_{c,i}$ however is not very pronounced, mainly because the amount of cementing agents also decreases.
- The yield strength increases with depth because of the higher percentage of quartz.
- The transition to the LCC region becomes more gradual as the amount of brittle aggregates decreases. Therefore, θ increases with depth. It should be noted that this transition can be locally affected by a higher or lower quartz vs. aggregate ratio in the sample.
- The initial cation exchange capacity, CEC_i, increases with depth, as there is less aggregation on the clay platelets to mask their physicochemical activity.

- The range of cation exchange capacity change decreases with depth, since the actual amount of clay minerals (that are masked and then revealed) decreases; so the final CEC value is expected to decrease.
- As weathering is more intense at shallower depths, the onset of degradation is expected to take place at lower stress levels, so σ'_o should increase with depth. On the other hand, σ'_m is expected to decrease because the range of CEC values also decreases.
- Finally parameter n is constant, as the type of minerals within the microstructural aggregates does not change and so the correlation between compressibility and cation exchange capacity is the same.

Table 4-4 shows the selected variation of input parameters with depth, based on the above discussion, information from the existing data and the assumption of a simple linear mode of change. Note that the void ratio is shown to decrease with depth, although, as already discussed, it is possible it varies irregularly within the profile

Figure 4-33 plots predictions for various depths of the response of the Old Alluvium to compressive loads. The most intensively weathered material from the shallower depths has a small yield strength and a compressibility that increases notably with mechanical disaggregation. As the depth increases, the degree of weathering generally decreases, and so the soil has a denser structure, higher yield strength and a stiffer response. Furthermore, Figure 4-34 shows how the Cation Exchange Capacity evolves during the simulated behavior. In the most weathered materials CEC increases over a wide range of stresses, while as the degree of weathering decreases, the overall CEC change decreases and this takes place within a smaller stress range. Finally, Figure 4-35 evaluates the selected parameter variation by comparing the predicted behavior with the available data from each depth.

4.8 SUMMARY

Existing models for structured soils cannot successfully address the compression of the Old Alluvium. Their main limitations arise from the fact that are based on the assumption of removal of interparticle bonding elements from an otherwise unaltered soil skeleton, and so require a constant reference to a unique intrinsic state. Therefore, they are unable to incorporate structural

changes that happen in the micro-scale, such as the revelation of new minerals or the variation of their surface properties.

This chapter presented the formulation of a new compression model that is able to predict the observed macroscopic response of the Old Alluvium to virgin compression loading. The strength of the model lies in the fact that it links the substantial increase in compressibility to the physicochemical processes that occur in the microstructure.

The model is based on the MIT-S1 compression formulation, to which it adds the flexibility of varying the Limiting Compression Curve from one that corresponds mostly to sandy materials to one that characterizes more clayey ones. In addition, it introduces the Cation Exchange Capacity as a state variable that maintains information of the clay activity in the microstructure. The latter is very important for the prediction of the soil swelling behavior, as it will be discussed in Chapter 5.

The new formulation requires 9 input parameters. The first 4 are inherited from the previous MIT compression model; 2 require knowledge of the Cation Exchange Capacity before and after mechanical disaggregation; 2 more define the stress levels along which most of the structural changes take place; and the last one is associated with the evolution of compressibility. The model was structured so that the input parameters can be directly related to the nature of the soil.

The proposed model is not specific to the Old Alluvium. The ability to incorporate an evolution in compressibility and trace changes in the microstructure, as well as an input set of measurable soil properties add versatility to the formulation and may provide essential components to the modeling not only of other Old Alluvia, but also of clayey materials with evolving physicochemical characteristics in the microstructure.

4.9 REFERENCES

Alonso E.E. (1998): "Modelling expansive soil behaviour", Proceedings of the 2nd International Conference on Unsaturated Soils, Beijing, 2, 37-70.

Alonso E.E., Alcoverro J. (2002): "Swelling and Degradation of Argillaceous Rocks", Proceedings of the 3rd International Conference on Unsaturated Soils, Recife, Brazil, 3, 951-969.

Billam J. (1971): "Some aspects of the behavior of granular materials at high pressure", Proc. of the Roscoe memorial symposium, Ed. R. H. Parry, Cambridge University, 69-80.

Carol I., Rizzi E., Willam K. (2001): "On the formulation of anisotropic elastic degradation. I. Theory based on a pseudo-logarithmic damage tensor rate. II.Generalized pseudo-Rankine model for tensile damage", Int. J. of solids and structures, 38, 491-546.

Cecconi M., DeSimone A., Tamagnini C., Viggiani G.M.B. (2002): "A constitutive model for granular materials with grain crushing and its application to a pyroclastic soil", International Journal for Numerical and Analytical Methods in Geomechanics 26 (15), 1531-1560.

Chazallon C., Hicher P. Y. (1998): "A constitutive model coupling elastoplasticity and damage for cohesive-frictional materials", Mechanics of Cohesive-Frictional Materials, 3, 41-63.

Coop M.R. (2000): "The influence of particle breakage and state on the behaviour of sands", International Workshop on Soil Crushability, IWSC'99, Yamaguchi, Japan.

Cotecchia F., Chandler R.J. (2000): "A general framework for the mechanical behavior of clays", Géotechnique, 50 (4), 431-447.

Dafalias Y. F., Herrmann L. R. (1980): "A bounding surface soil plasticity model", International Symposium of Soils under Cyclic Transient Loading, Swansea, 1, 33-345.

Desai S., Toth J. (1996): "Disturbed state constitutive modeling based on stress-strain and non destructive behavior", International Journal of Solids and Structures, 33 (11), 1619-1650.

Dvorkin J., Nur A., Mavko G. (1991): "The effect of cementation on the elastic properties of granular material", Mechanics of materials 12, 207-217.

Dvorkin J., Nur A., Yin H. (1994): "Effective properties of cemented granular materials", Mechanics of materials 18, 351-366.

Dvorkin J., Nur A., Berryman J..(1999): "Elastic moduli of cemented sphere packs", Mechanics of materials 31, 461-469.

Gens A., Nova R. (1993): "Conceptual bases for a constitutive model for bonded soils and weak rocks", Geotechnical engineering of hard soils-soft rocks, 485-494.

Germaine J.T. (1982): "Development of the Directional Shear Shell for measuring cross-anisotropic clay properties", ScD Thesis, Massachusetts Institute of Technology, Cambridge, MA.

Germaine J.T. (2008): Personal communication

Hashiguchi K. (1985): "Two- and three-surface models of plasticity" Proceedings, 5th International Conference on Numerical Methods in Geomechanics, Nagoya, 125-134.

Hendershot, W.H., Duquette, M. (1986): "A simple barium chloride method for determining cation exchange capacity and exchangeable cations". Soil Science Society of America Journal, 50, 605-608.

Herle I., Gudehus G. (1999): "Determination of parameters of a hypoplastic constitutive model from properties of grain assemblies", Mechanics of Cohesive-Frictional Materials, 4, 461–486.

Janbu N. (1963): "Soil compressibility as determined by oedometer and triaxial tests", Proceedings, 3rd European Conference on Soil Mechanics and Foundations Engineering, Weisbaden, I, 19-25.

Jardine R. J., Potts D. M., Fourie A. B., Burland J. B. (1986): "Studies of the influence of non-linear stress-strain characteristics in soil-structure interaction", Géotechnique, 36 (2), 377-396.

Jardine R. J., St John H. D., Hight D. W., Potts D. M. (1991): "Some practical applications of a non-linear ground model", Proceedings, 10th European Conference on Soil Mechanics and Foundations Engineering, Florence, I, 223-228.

Kavvadas M. (1995): "A plasticity approach to the mechanical behaviour of bonded soils", Proceedings, 4th International Conference on Computational Plasticity, Barcelona.

Kavvadas M., Amorosi, A. (2000): "A constitutive model for structured soils", Géotechnique, 50 (3), 263-273

Ladd C.C. (1999): Lecture notes, Massachusetts Institute of Technology, Cambridge, MA.

Ladd C.C., Foott R., Ishihara K., Schlosser F., Poulos, H.G. (1977): "Stress-Deformation and Strength Characteristics," *State-of-the-Art Report, Proc. 9th ICSMFE*, Tokyo, 2, 421-494.

Lagioia R., Nova R. (1995): "An experimental and theoretical study of the behaviour of a calcarenite in triaxial compression", Géotechnique, 45 (4), 633-648.

Loret B., Hueckel T., Gajo A. (2002): "Chemo-mechanical coupling in saturated porous media: elastic–plastic behaviour of homoionic expansive clays", International Journal of Solids and Structures 39, 2773–2806.

Marsal R.J. (1967): "Large scale testing of rockfill materials", ASCE Journal of Soil Mechanics and Foundation Division, 93(SM2), 27-43.

Mitchell J.K., Soga K. (2005): Fundamentals of Soil Behavior, John Wiley & Sons, New York, N.Y; first edition 1976.

Miura K., Maeda K., Toki S. (1997): "Method of measurement for the angle of repose of sands", Soils and Foundations, 37 (2), 89–96.

Mroz Z., Norris V. A., Zienkiewicz O. C. (1978): "An anisotropic hardening model for soils and its application to cyclic loading", International Journal for Numerical and Analytical Methods in Geomechanics, 2, 203-221.

Mroz Z., Norris V. A., Zienkiewicz O. C. (1979): "Application of an anisotropic hardening model in the analysis of elasto-plastic deformation of soils", Géotechnique, 29 (1), 1-34.

Muir Wood D. (1995): "Kinematic hardening model for structured soil", Proceedings of the international symposium on numerical models in geomechanics, Davos, 83-88.

Nikolinakou M.A., Whittle A.J. (2008): "Predictions on boundary value problems for deep excavations in Berlin Sand, using the MIT-S1 model", in final review for submission.

Nova R, Castellanza R. (2001): "Modelling weathering effects on the mechanical behaviour of soft rocks", International Conference on Civil Engineering, Bangalore, India, 157–167.

Nova R. (1997): "On the modeling of the mechanical effects of diagenesis and weathering", ISRM News Journal 4 (2), 15–20.

Nova R., Castellanza R., Tamagnini C. (2003): "A constitutive model for bonded geomaterials subject to mechanical and/or chemical degradation", International Journal for Numerical and Analytical Methods in Geomechanics, 27 (9), 705-732.

Pestana J. M., Whittle A. J. (1995): "Compression model for cohessionless soils", Géotechnique, 45 (4), 611-631.

Pestana J.M. (1994): "A unified constitutive model for clays and sands", Sc.D thesis, Massachusetts Institute of Technology, Cambridge, MA.

Pestana J.M., Whittle A.J. (1995): "Compression model for cohesionless soils", Géotechnique, 45 (4), 611–631.

Pestana J.M., Whittle A.J. (1999): "Formulation of a unified constitutive model for clays and sands", International Journal for Numerical and Analytical Methods in Geomechanics, 23 (12), 1215–1243.

Prevost J. H. (1978): "Plasticity theory for soil stress-strain behaviour", Journal of Engineering Mechanics Division, ASCE, 104 (5), 1177-1194.

Roberts J.E. (1964): "Sand Compression as a factor in oil field subsidence", PhD Thesis, MIT, Cambridge, MA.

Schofield A., Wroth C.P. (1968): Critical State Soil Mechanics, McGraw Hill, London.

Terzaghi K., Peck R.B., Mesri G. (1996): "Soil Mechanics in Engineering Practice", Wiley Interscience.

Timoshenko S.P., Goodier J.N. (1970): Theory of elasticity, McGraw Hill.

Whittle A. J., Kavvadas M. (1994): "Formulation of the MIT-E3 constitutive model for overconsolidated clays", Journal of Geotechnical Engineering division, ASCE, 120 (1), 173-198.

Zhang, G. (2002): "Laboratory Characterization of a Highly Weathered Old Alluvium in San Juan, Puerto Rico", PhD thesis, MIT, Cambridge, MA.

Nova, R. (1977): "On the hardening of soils", Archwm Mech. Stosow, 29 (3), 445-458.

Wilde, P. (1977): "Two-invariants-dependent model of granular media", Archwm Mech. Stosow 29 (4), 799-809.

Zreik D. (1994): "Behavior of cohesive soils and their drained, undrained and erosional strength at ultralow stresses", PhD thesis, Massachusetts Institute of Technology, Cambridge, MA.

Parameter	Physical meaning	Test required	Method of determination
ρ_c	Compressibility of freshly deposited sands at large stresses	Hydrostatic or 1-D compression test (in triaxial or oedometer apparatus)	Slope of the compression curve at high stresses, in a $\log_{10}e$-$\log_{10}\sigma$' space.
σ_{ref}/pa	Reference stress for the location of the limiting compression curve		Reference effective stress at unity void ratio for the limiting compression curve (straight line in the above loge-logσ' space).
θ	Parameter describing the compression behavior of sands in the low stress transitional regime		Compression data at the transitional regime between low stresses and stresses in the Limiting Compression Curve regime.
C_b	Small strain compressibility at load reversal.	Resonant Column or in-situ crosshole.	Direct measurement (or estimate) of G_{max} from elastic shear wave velocity.

Table 4-1: Input parameters for the MIT-S1 compression model for sands (Pestana, 1994).

Sample	CEC (meq/100g clay)
Natural UC (w/ Fe Oxides)	29.13
DCB treated UC (FE Oxides removed)	52.12
Natural MZ (w/ Fe Oxides)	35.58
DCB treated MZ (FE Oxides removed)	45.34

Table 4-2: Cation Exchange Capacity of natural and DCB treated Old Alluvium samples (depth: 4m - Zhang, 2002).

Parameter	Physical meaning	Test required	Method of determination
C_b	Small strain compressibility of load reversal.	Resonant Column or in-situ crosshole.	Direct measurement (or estimate) of G_{max} from elastic shear wave velocity.
θ	Parameter describing the compression behavior of sandy materials in the low stress transitional regime	Hydrostatic or 1-D compression test (in triaxial or oedometer apparatus)	Compression data at the transitional regime between low stresses and stresses in the Limiting Compression Curve regime.
$\rho_{c,i}$	Compressibility coefficient defining the large stress limiting compression curve of the initial material, before breakdown		Slope of the compression curve in a $\log_{10}e$-$\log_{10}\sigma'$ space, at high stresses, but before significant breakdown
$\sigma_{ref,i}/pa$	Reference stress for the location of the limiting compression curve of the initial material, before breakdown		Reference effective stress at unity void ratio for the "initial" limiting compression curve.
CEC_i	Cation Exchange Capacity (CEC) of the intact material	Test to measure CEC (for example Barium Chloride method)	Direct measurement.
CEC_f	Cation Exchange Capacity (CEC) of the material after bonds/aggregation has been removed		Direct measurement; chemical removal of aggregation and bonds.
σ'_o/pa	Stress level at onset of significant breakdown	Hydrostatic or 1-D compression test (in triaxial or oedometer apparatus)	Stress level at which compression behavior deviates from the classical limiting compression curve.
σ'_m/pa	Stress level at midway of the material breakdown		Estimation from compression curve or swelling data.
n	Factor relating the rates of change of CEC and the compression parameters		Data relating compressibility and clay activity measures (Relative activity, CEC)

Table 4-3: Input parameters for the proposed compression model.

Parameter	2m	4m	6m	8m	10m	12m	14m
C_b	950	950	950	950	950	950	950
θ	0.2	0.22	0.24	0.26	0.28	0.3	0.32
$\rho_{c,i}$	0.28	0.275	0.27	0.265	0.26	0.255	0.25
$\sigma_{ref,i}$/pa	5.5	5	4.5	4	3.5	3	2.5
CEC_i	29	(29) 30	31	32	33	34	35
CEC_f	52	(52) 51	50	49	48	47	(45) 46
σ'_o/pa	60	70	80	90	100	110	120
σ'_m/pa	350	300	250	200	150	150	150
n	0.3	0.3	0.3	0.3	0.3	0.3	0.3
Void Ratio	1.1	1.0	0.9	0.7	0.5	0.4	0.3

To account for the presence of cementation $C_{b,i} = 1200$ at stress levels below the yield point.

Table 4-4: Selected variation of input parameters with depth, for the Old Alluvium.

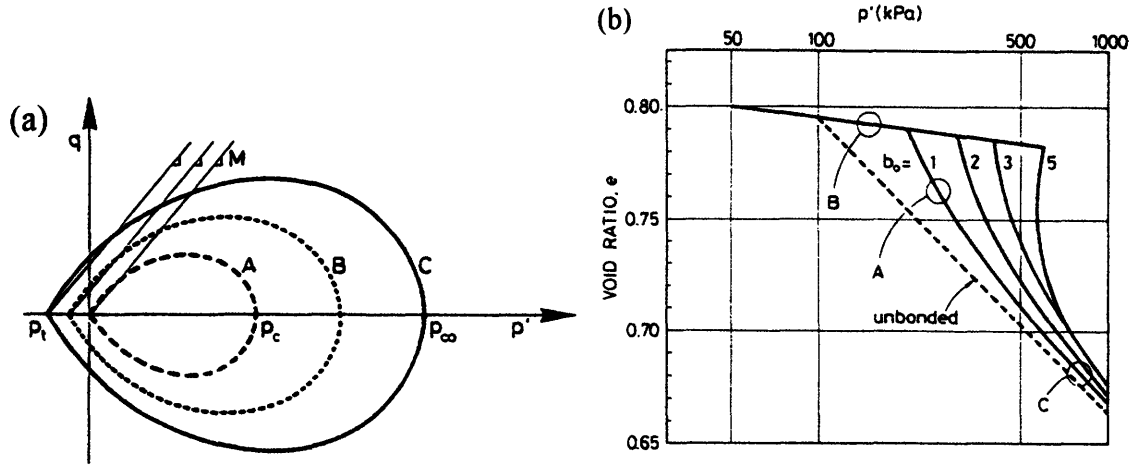

Figure 4-1 (a): Successive yield surfaces for increasing degree of bonding; surface A corresponds to the unbonded material, C to the fully bonded state and B to an intermediate bonded state; (b): Isotropic consolidation curves predicted for different degrees of bonding (after Gens & Nova, 1993).

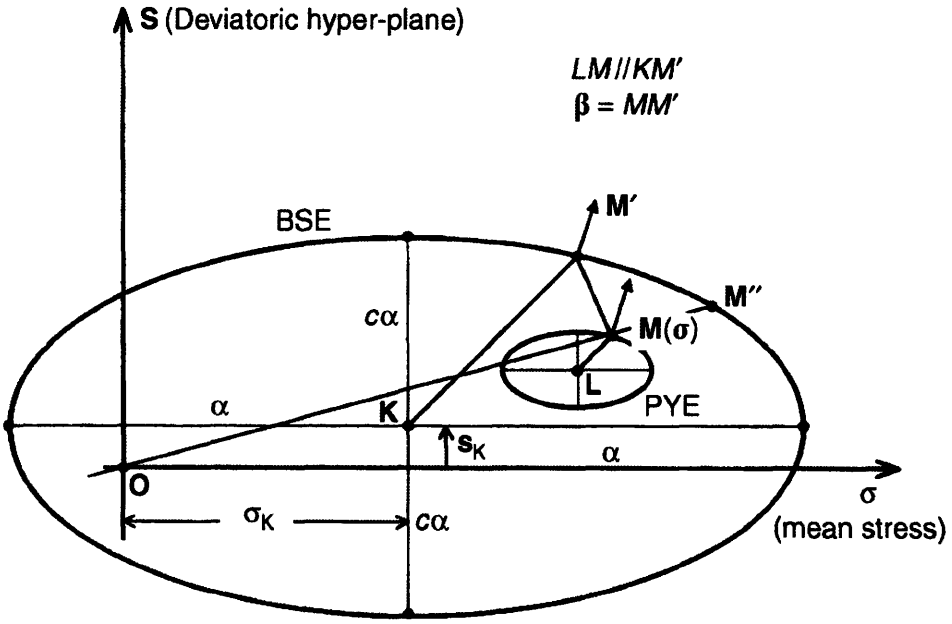

Figure 4-2: Internal Plastic Yield Envelope (PYE) and external Bond Strength Envelope (BSE) of the model proposed by Kavvadas & Amorosi (2000). For material states on the BSE, plastic strains induce bond degradation and the two characteristic surfaces are in contact at the point corresponding to the current stress state (M≡M') and the position of the center of PYE (L) is dictated by the position of the center of BSE (K). When plastic strains do not affect the state of bonds, the current state is on the PYE surface (M) and the motion of L is such that the PYE moves towards point M', which is the conjugate of the current state M on the BSE surface.

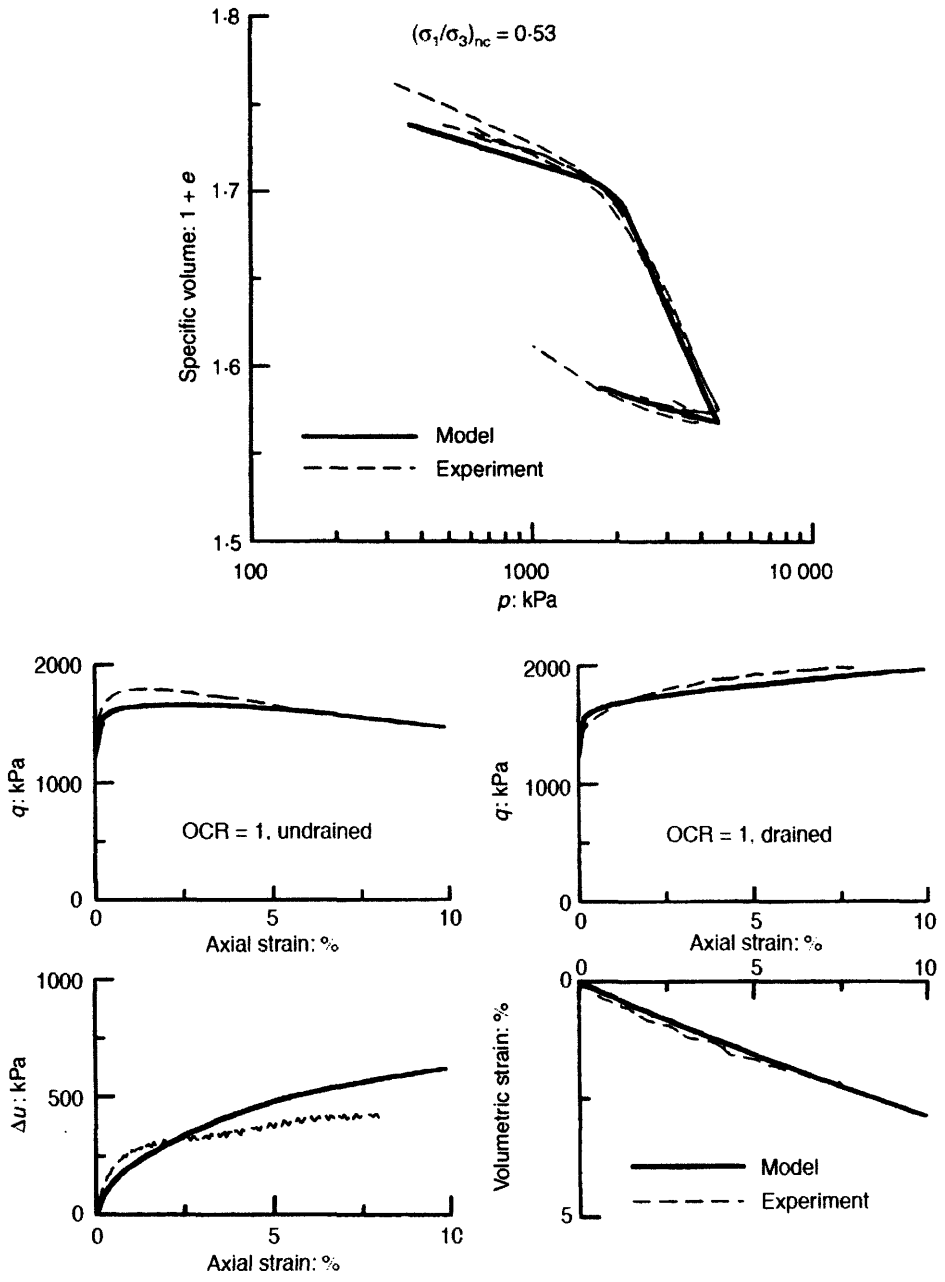

Parameter	Value	Parameter	Value	Parameter	Value
κ^*	0·013	ζ_v	5	x	1
α^*	103	η_v	50	ψ	0·1
λ	0·118	ζ_q	3	γ	14
c	0·85	η_q	0·5	ξ	0·005

Figure 4-3: Application of the model proposed by Kavvadas & Amorosi (2000) to anisotropically consolidated Vallericca clay: comparison between measured data and model predictions for the compression behavior and drained and undrained compression tests. Input parameters were calibrated using triaxial test data.

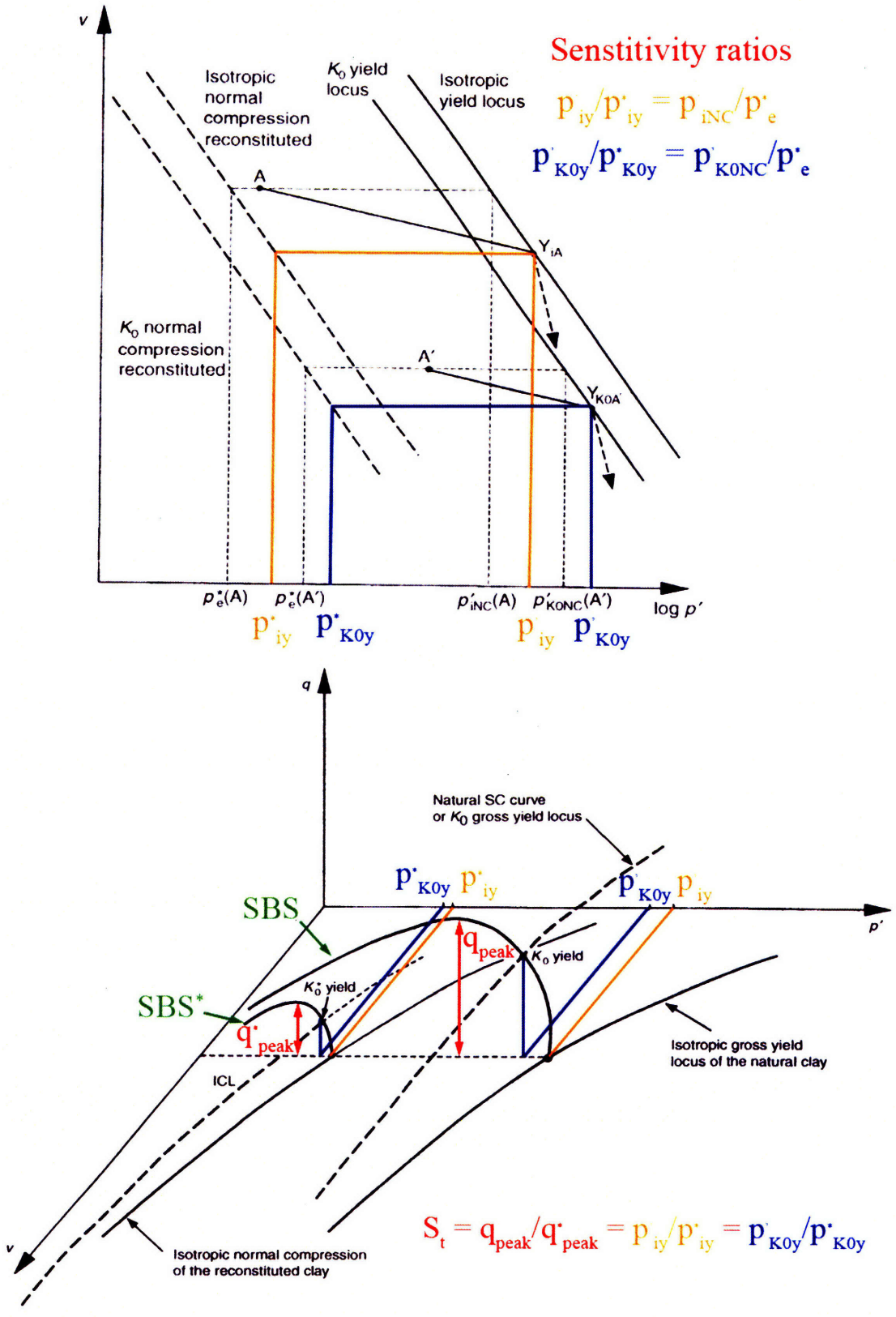

Figure 4-4: Stress sensitivity principle, after Cotecchia & Chandler (2000).

(a) Yield loci for various degrees of weathering

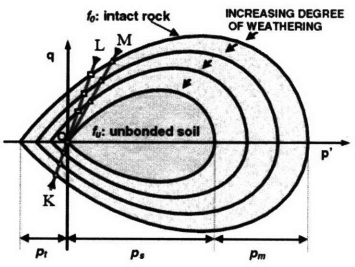

OK: decay of tensile strength
OL: decay of uniaxial compression
OM: decay of elastic threshold in oedometer test

(b)

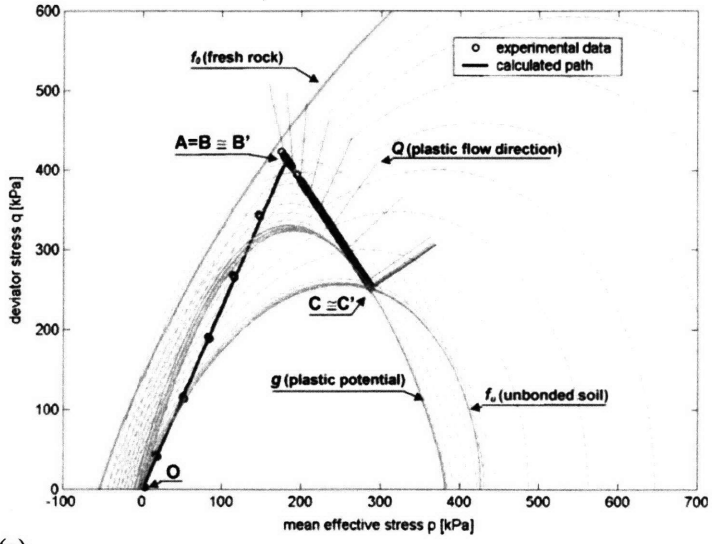

(c)

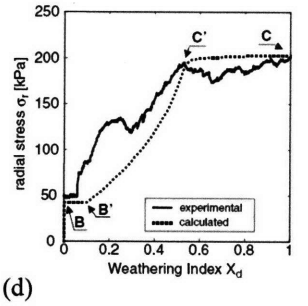

(d)

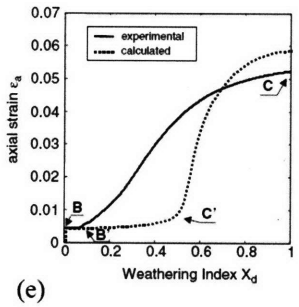

(e)

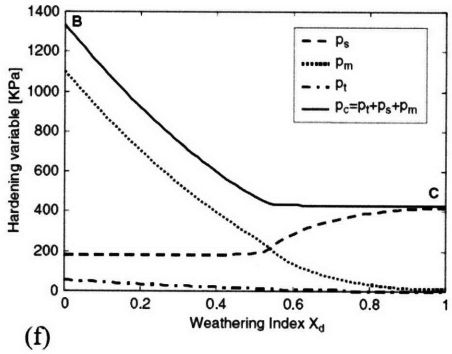

(f)

Figure 4-5: Illustration of the chemical weathering formulation proposed by Nova et al (2003): (a) Yield loci corresponding to different degrees of weathering, and notation; (b) Schematic representation of chemical weathering experiment on cemented silica sand; (c) experimental points and model simulation (stress path, evolution of yield surface, plastic potential and plastic flow direction); (d) evolution of radial effective stress with weathering; (e) evolution of axial strain with weathering; (f) evolution of hardening variables with weathering (after Nova et al, 2003).

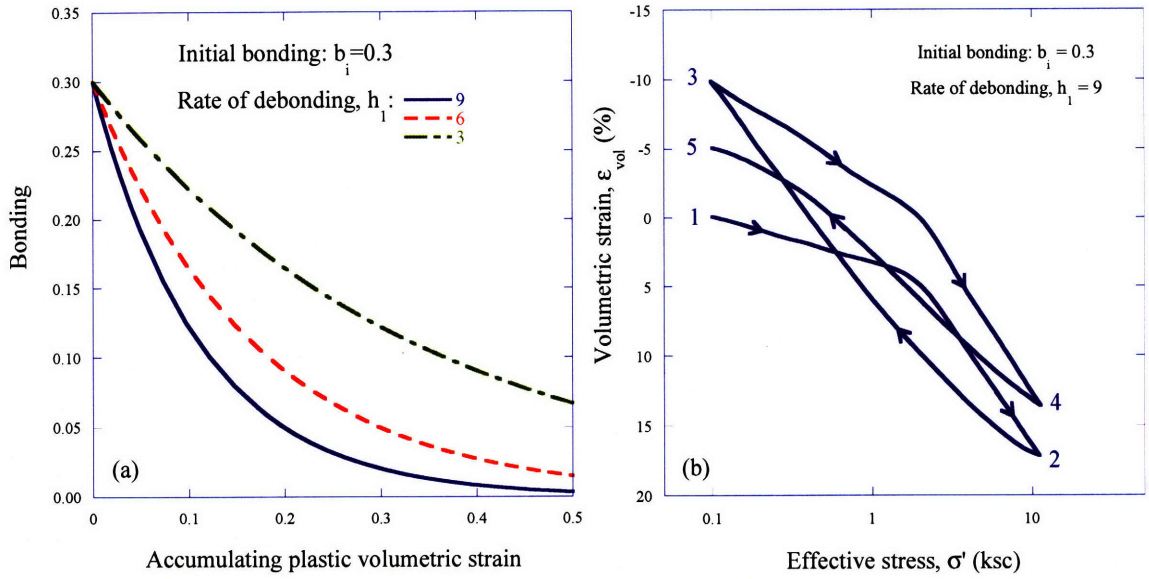

Figure 4-6: Model proposed by Alonso & Alcoverro (2002): (a) Evolution of bonding as an exponential function of plastic volumetric strain; (b) Macroscopic response of a bonded soil to two cycles of loading-unloading.

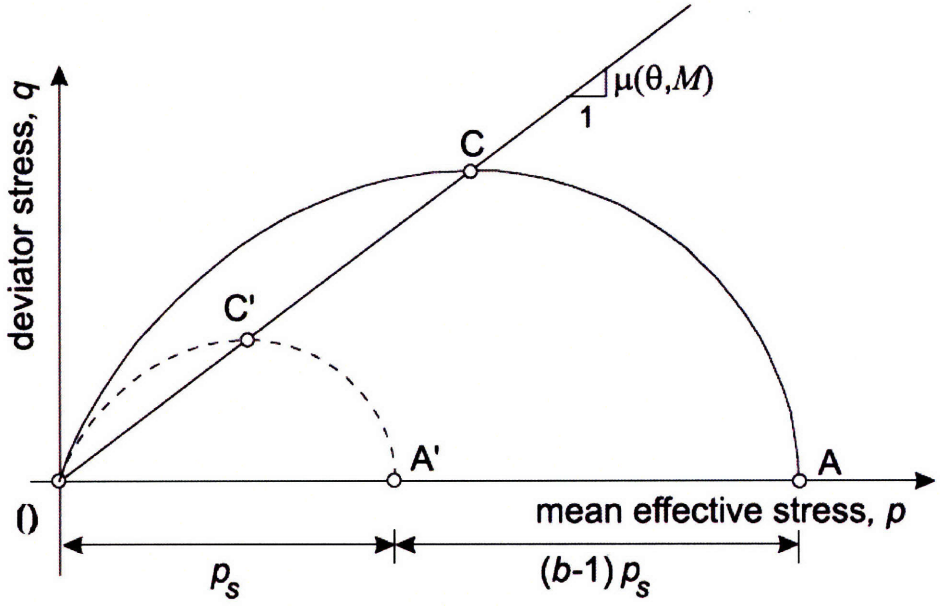

Figure 4-7: Yield surface of the Cecconi et al. (2002) model.

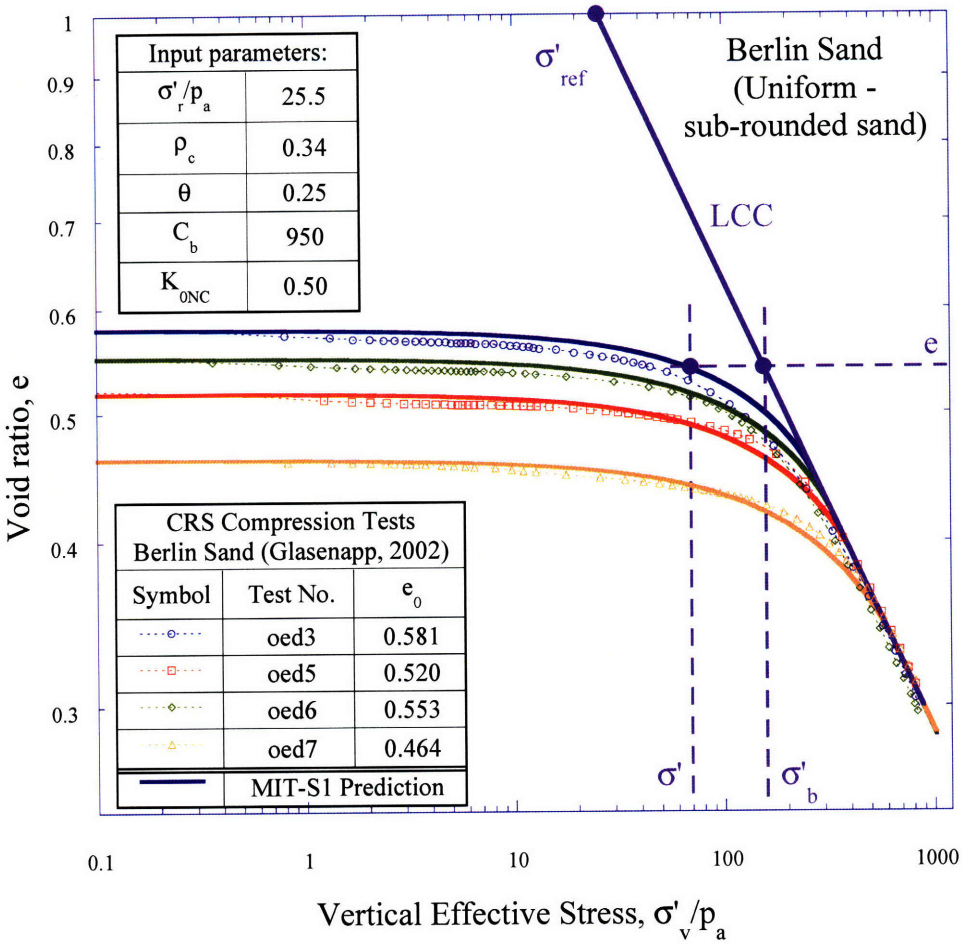

Figure 4-8: Limiting Compression Curve and input parameters in MIT compression model; Data from Berlin Sand (Nikolinakou & Whittle, 2008).

Abbreviation	Sand name	Abbreviation	Sand name
Qtu	Uniform Ottawa S.	Ha	Hawaiian
Qtg	Graded Ottawa S.	Hk	Hokksund
Qzu	Ground Quartz	M	Mol
D	Ground Dolomite	MF	Manchester Fine
F	Ground Feldspar	P	Pennsylvania
CR	Chattahoochee R.	Q	Quiou
DB	Dog's Bay	SR	Sacramento R.
G	Glauconite	Ti	Ticino
HR	Ham River	To	Toyoura

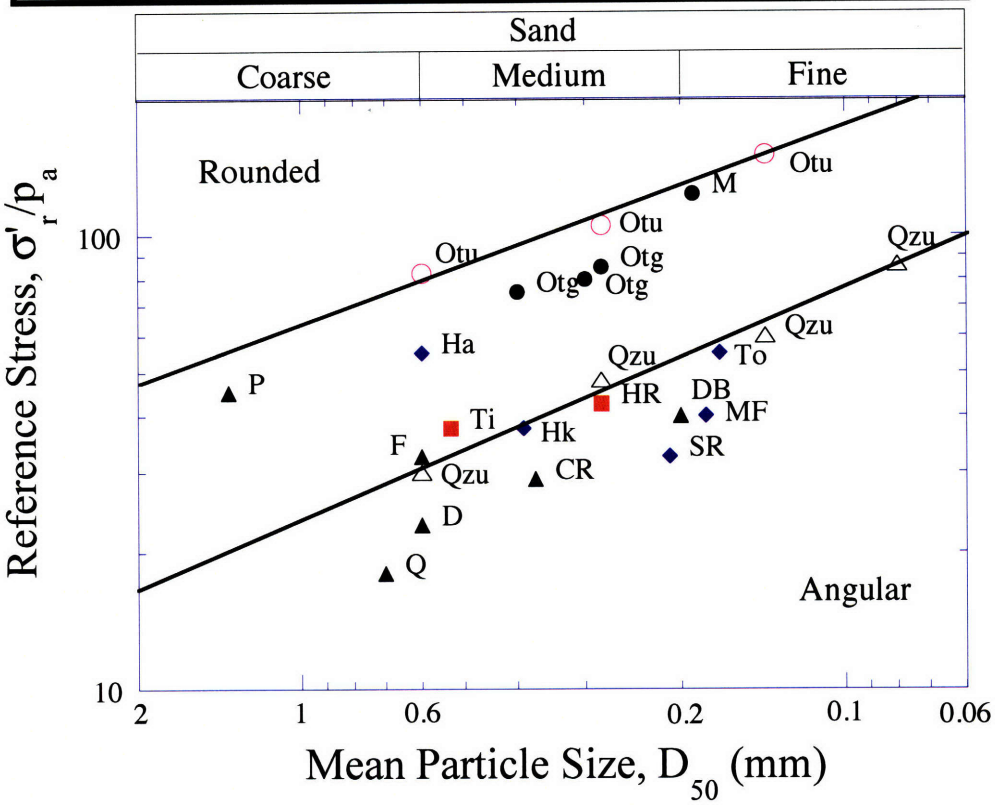

Figure 4-9: Effect of the particle size on the reference effective stress, σ'_r (after Pestana, 1994).

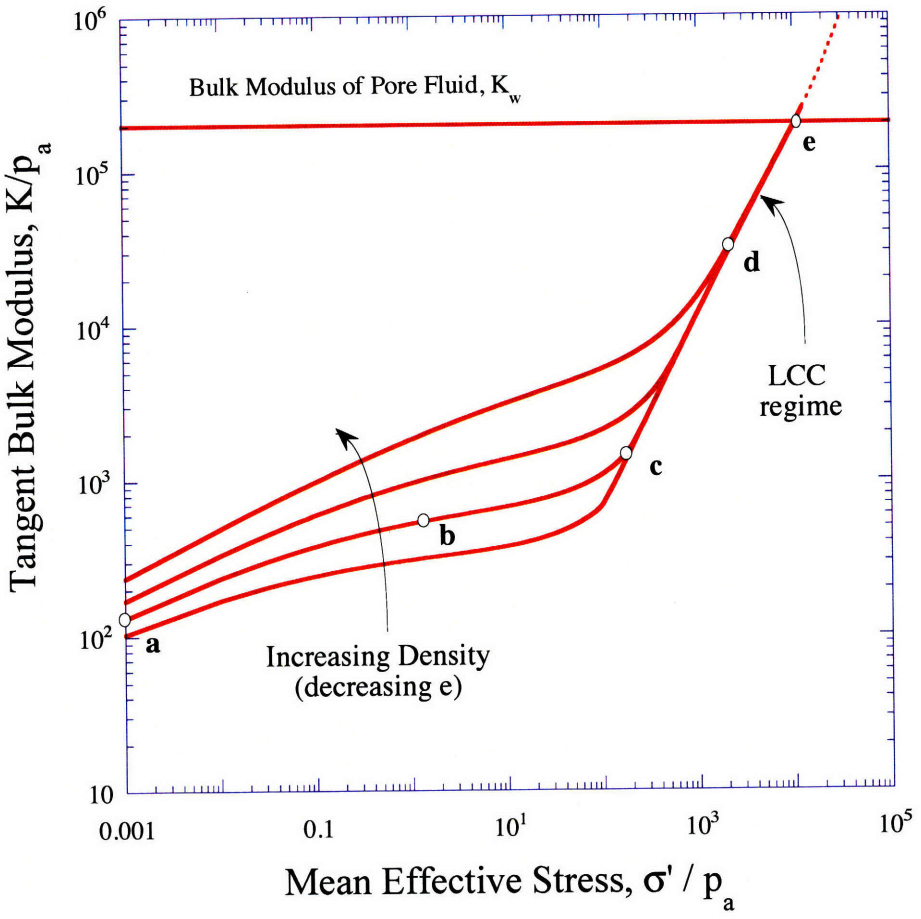

Figure 4-10: Conceptual representation of tangent bulk modulus during hydrostatic compression of freshly deposited cohesionless soils (after Pestana, 1994).

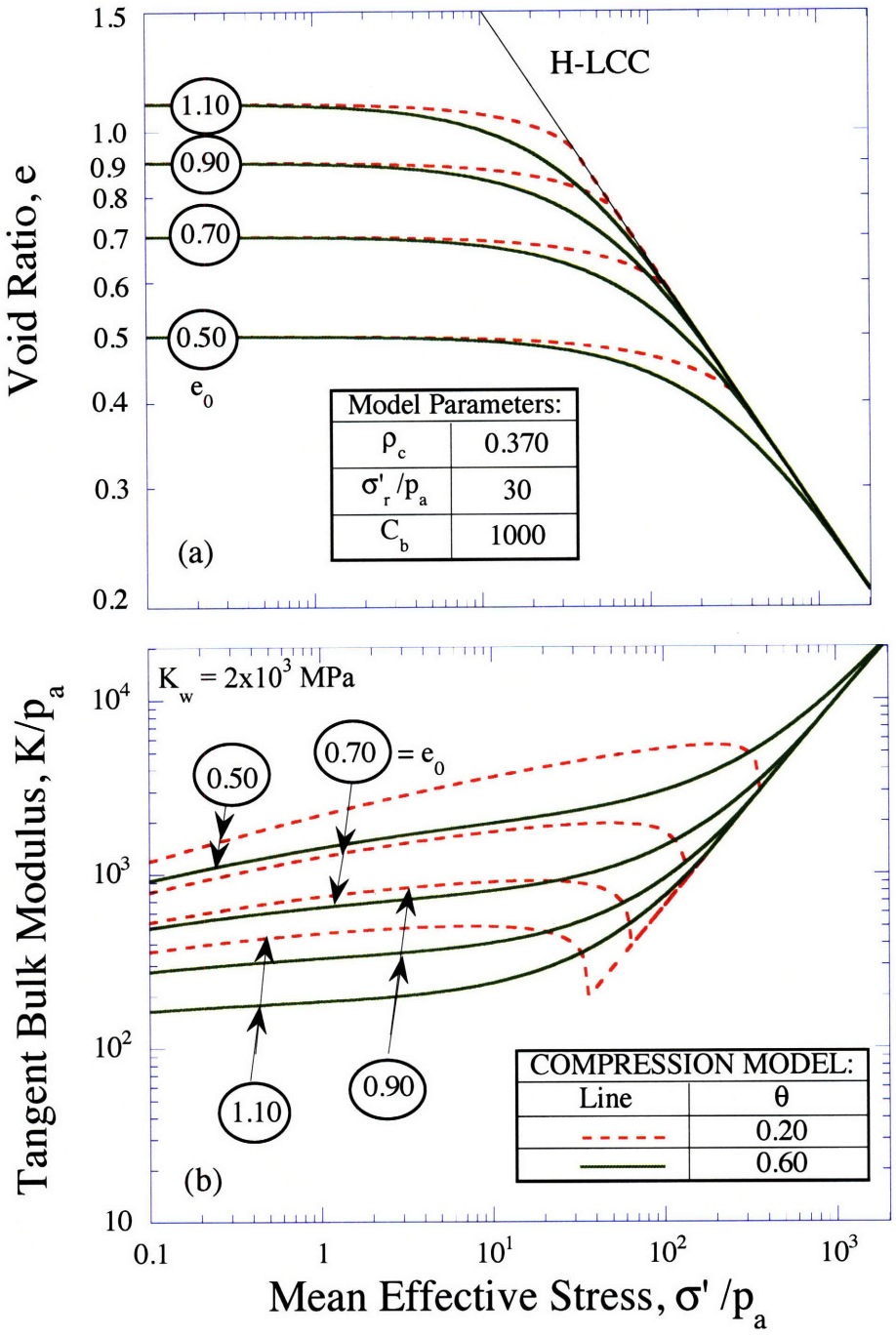

Figure 4-11: Effect of the parameter θ on the transitional region of the compression behavior: a) state space (upper graph) and b) tangent bulk modulus (lower graph); after Pestana, 1994.

Abbreviation	Sand name	Abbreviation	Sand name
Qtu	Uniform Ottawa S.	Ha	Hawaiian
Qtg	Graded Ottawa S.	Hk	Hokksund
Qzu	Ground Quartz	M	Mol
D	Ground Dolomite	MF	Manchester Fine
F	Ground Feldspar	P	Pennsylvania
CR	Chattahoochee R.	Q	Quiou
DB	Dog's Bay	SR	Sacramento R.
G	Glauconite	Ti	Ticino
HR	Ham River	To	Toyoura

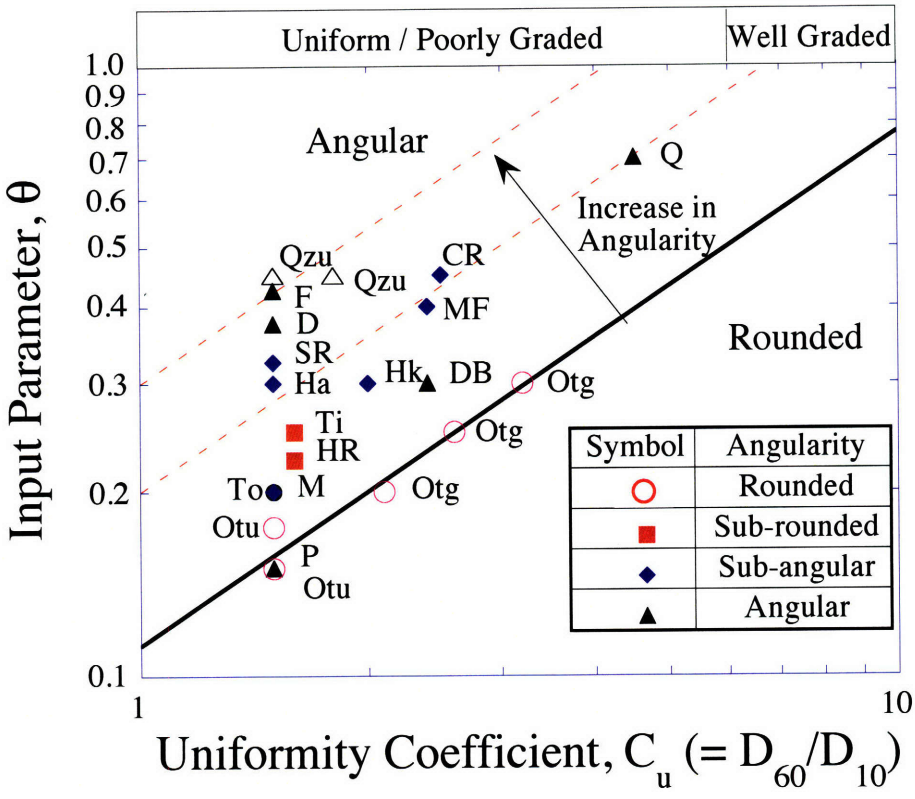

Figure 4-12: Effect of the particle angularity on the transition parameter θ (after Pestana, 1994).

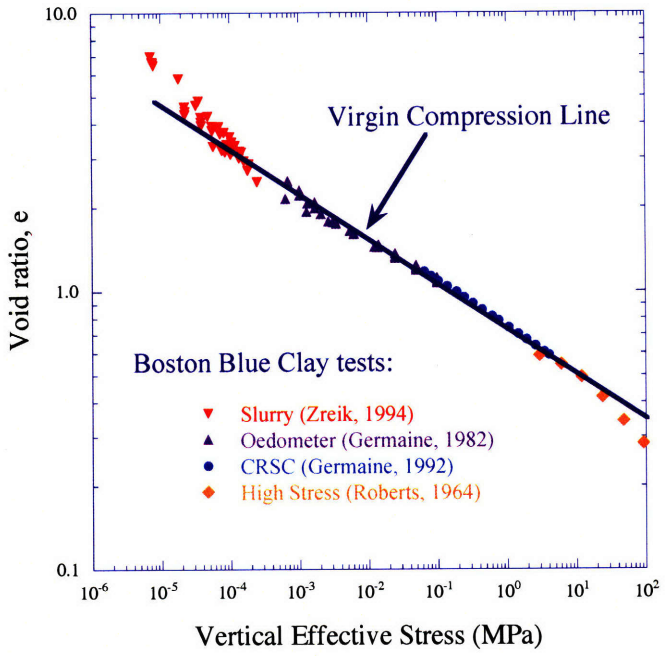

Figure 4-13: Virgin compression line for reconstituted Boston Blue Clay.

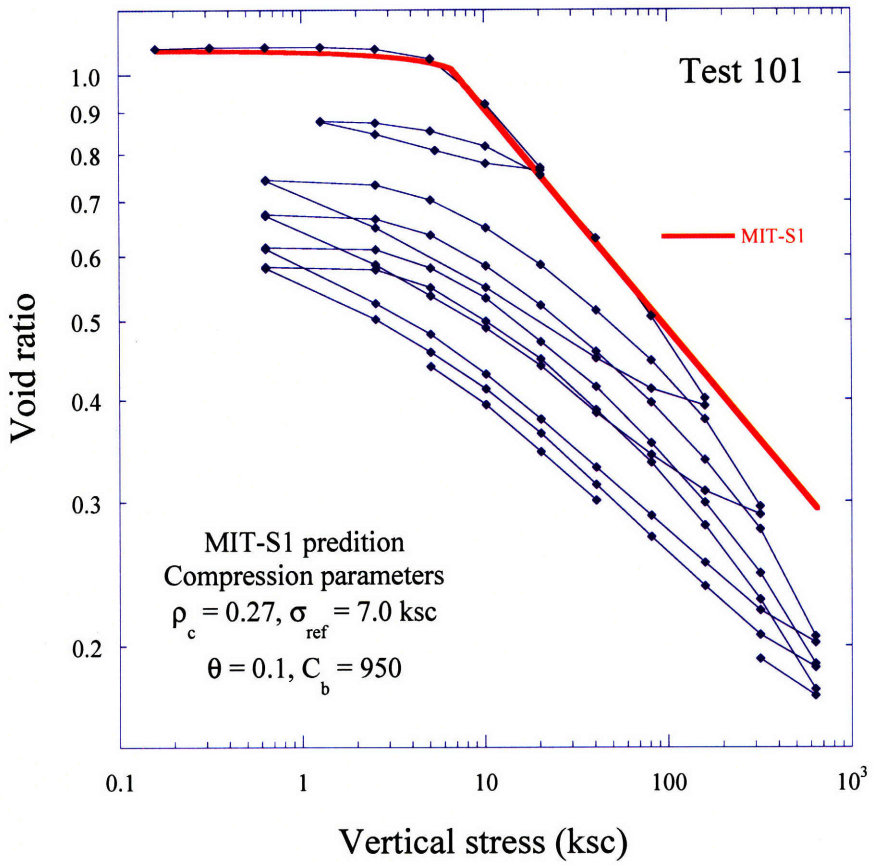

Figure 4-14: MIT-S1 prediction for the compression behavior of Old Alluvium. Input parameters fitted for stresses up to 100ksc.

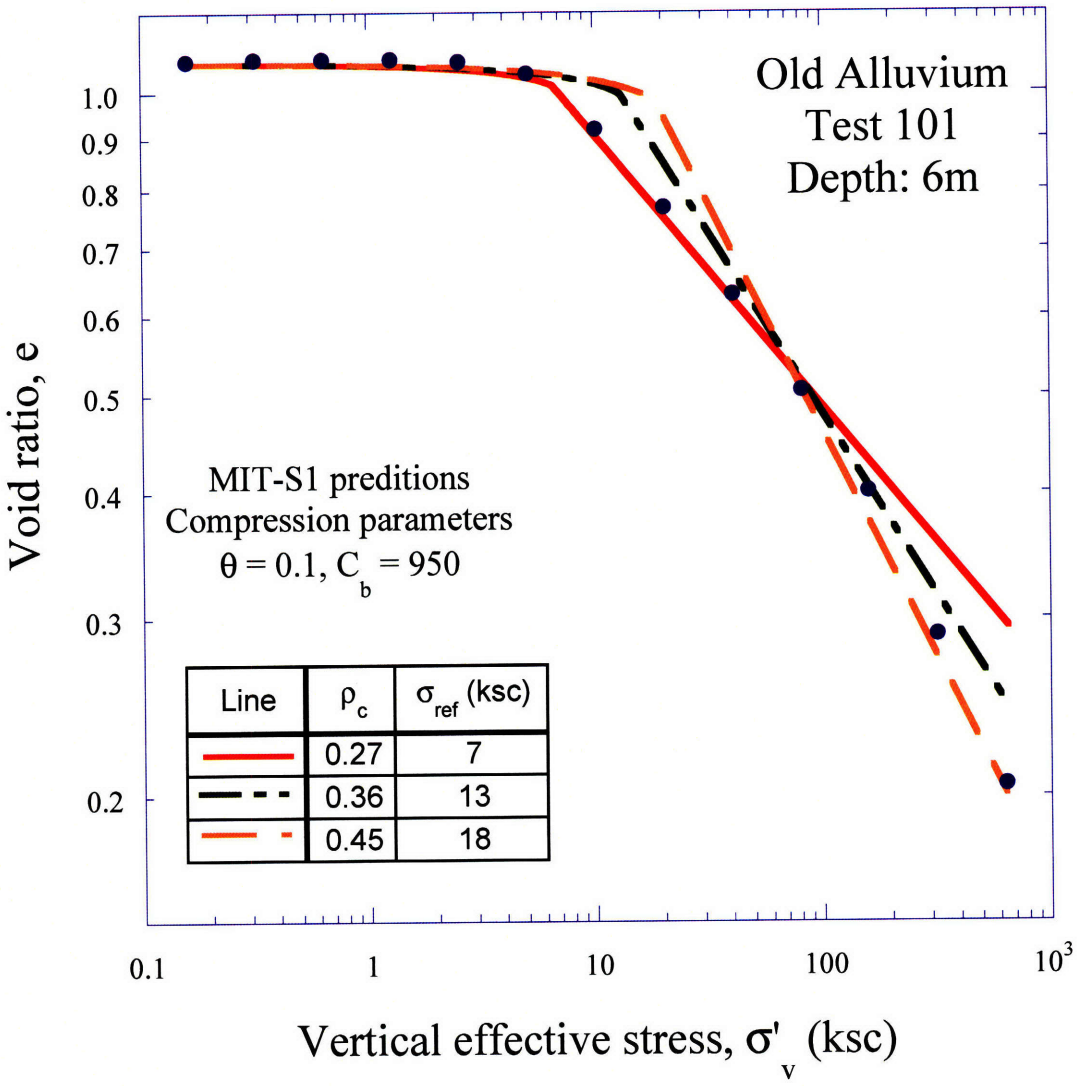

Figure 4-15: MIT-S1 prediction for the compression behavior of Old Alluvium. Input parameters fitted on the initial and final part, as well as an intermediate stage.

Abbreviation	Sand name	Abbreviation	Sand name
AP	Argille Plastique	MC	Mexico City Clay
BBC(n,r)	Boston Blue Clay	NwP	Newfoundland Peat
Bk	Bothkennar	NwS	Newfoundland Silt
CC	Chicago Clay	SFBM	San Francisco Bay Mud
DMp	Drammen (plastic)	SpK	Spestone Kaolin
DMl	Drammen (lean)	TCC	Tuy Cariaco Clays
EC	Empire Clay	WC	Weald Clay
KT	Kleinbelt Ton	WT	Wiener Tegel
LC	London Clay	I	Illite
LCT	Lower Cromer Till	K	Kaolinite
MG	Magnus Clay	Na/Ca-M	Montmorillonite

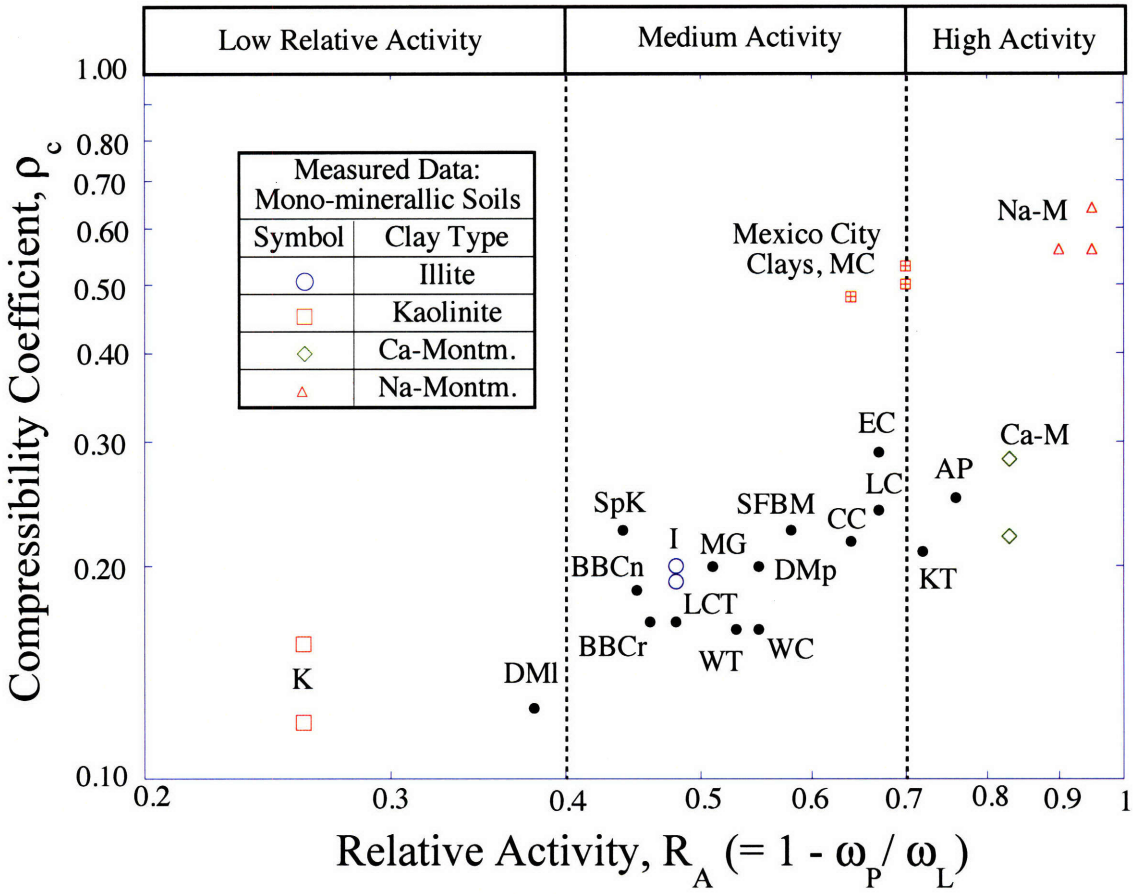

Figure 4-16: Correlation of the compression coefficient, ρ_c, and the relative activity, R_A (after Pestana, 1994).

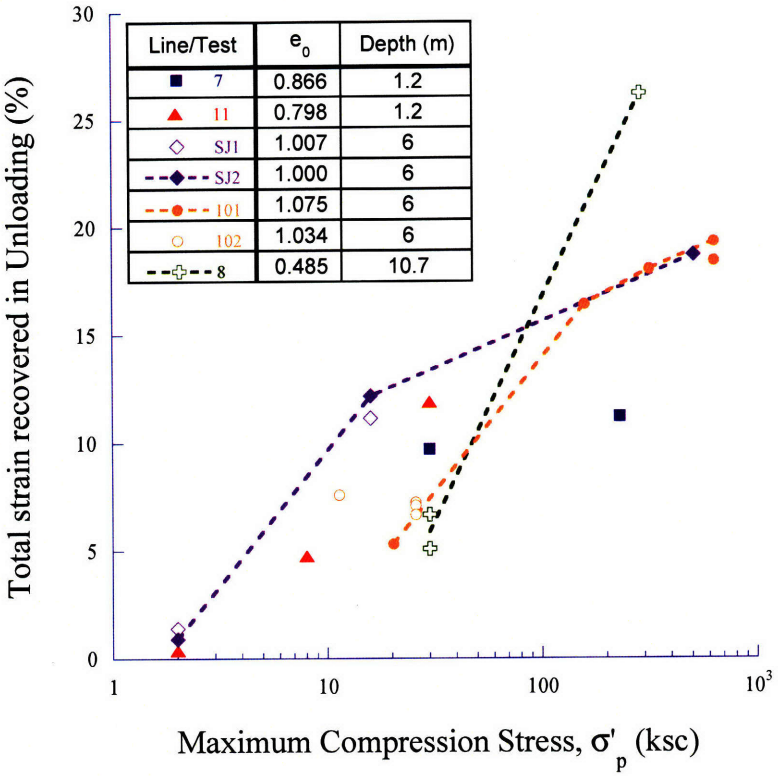

Figure 4-17: Total strain recovered during Unloading for all available compression tests on Old Alluvium. The dotted lines connect data from the same test (but different preconsolidation pressures).

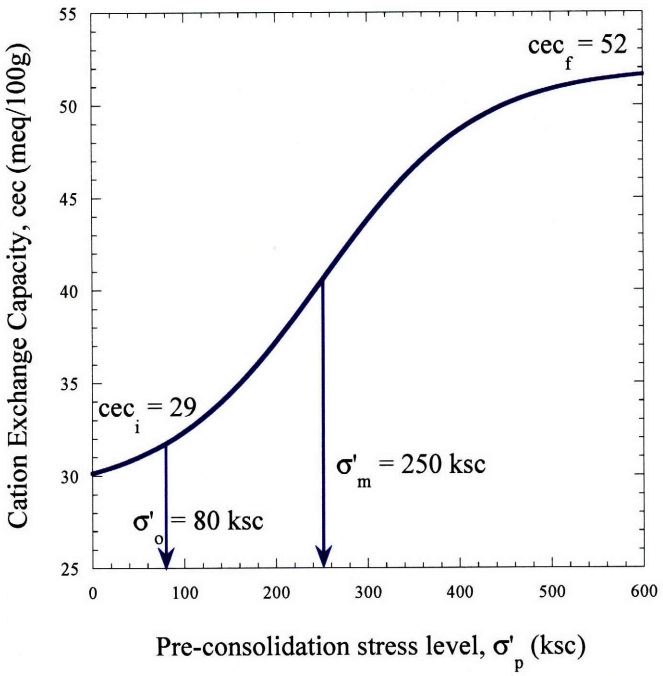

Figure 4-18: Prediction of Cation Exchange Capacity values for Old Alluvium during compression/structural breakdown, based on material from a depth of 6m (test 101).

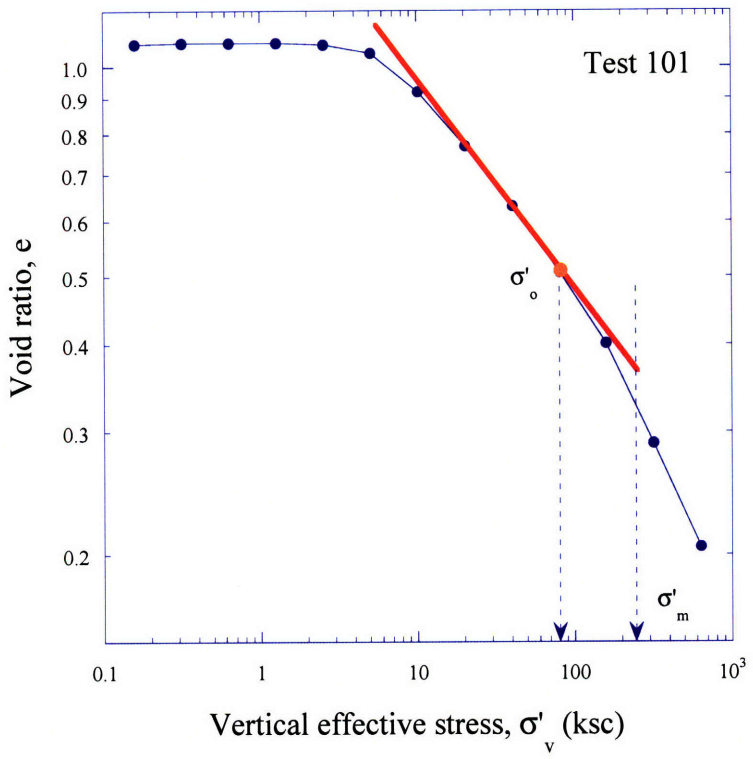

Figure 4-19: Example selection of parameters σ'_m and σ'_o from test 101

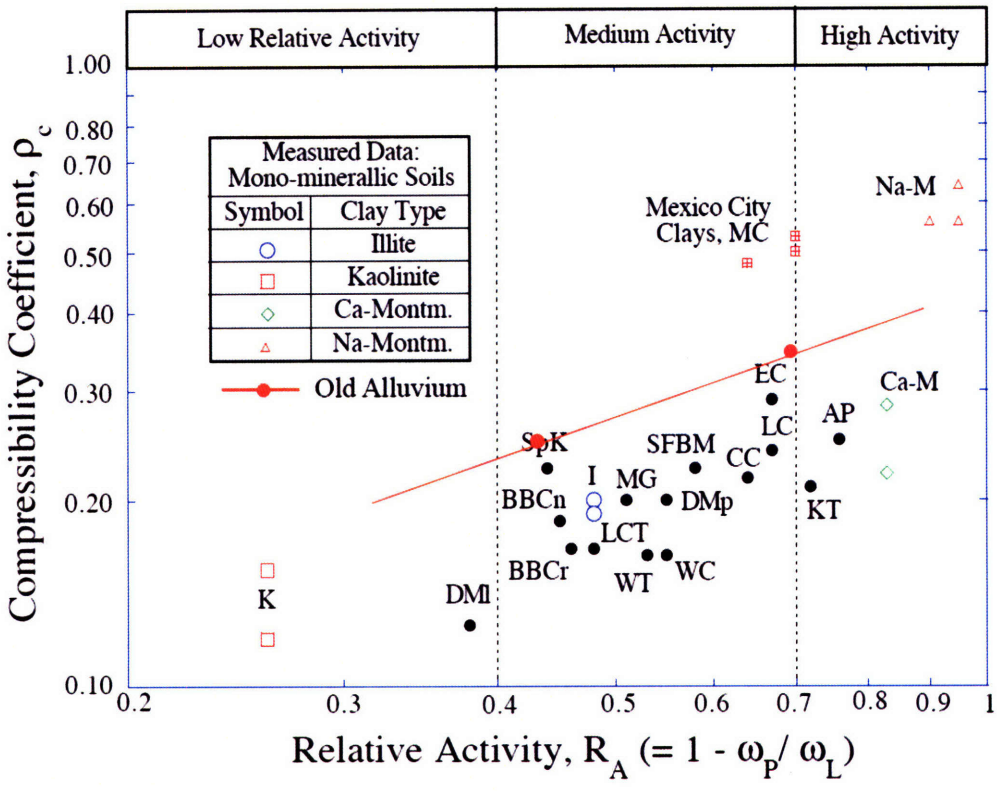

Figure 4-20: Relation between the compression coefficient, ρ_c, and the relative activity, R_A (after Pestana, 1994), with proposed relationship for the Old Alluvium.

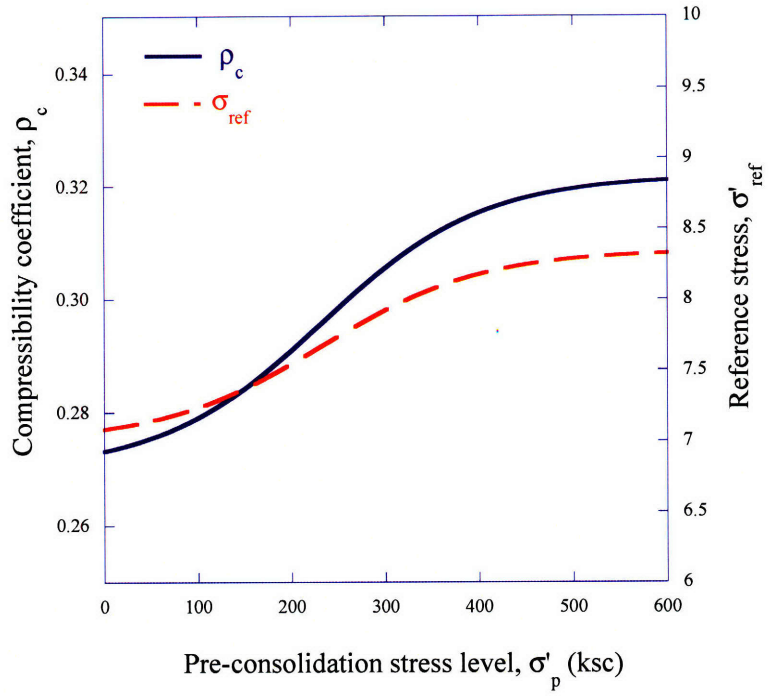

Figure 4-21: Prediction of the evolution of compressibility parameters ρ_c and σ_{ref} during compression and structural breakdown.

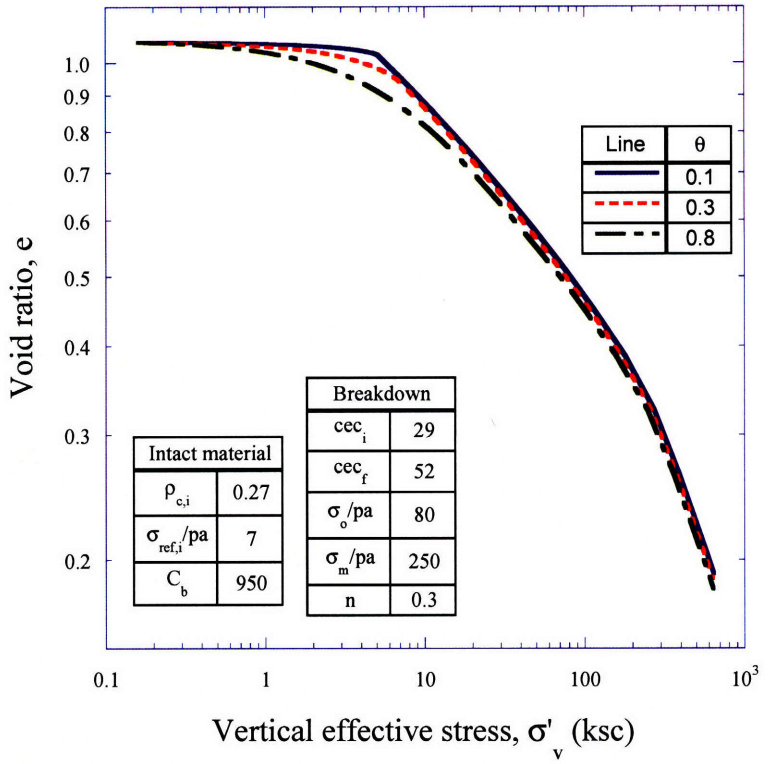

Figure 4-22: Effect of variation of input parameter θ on the first loading curve predictions.

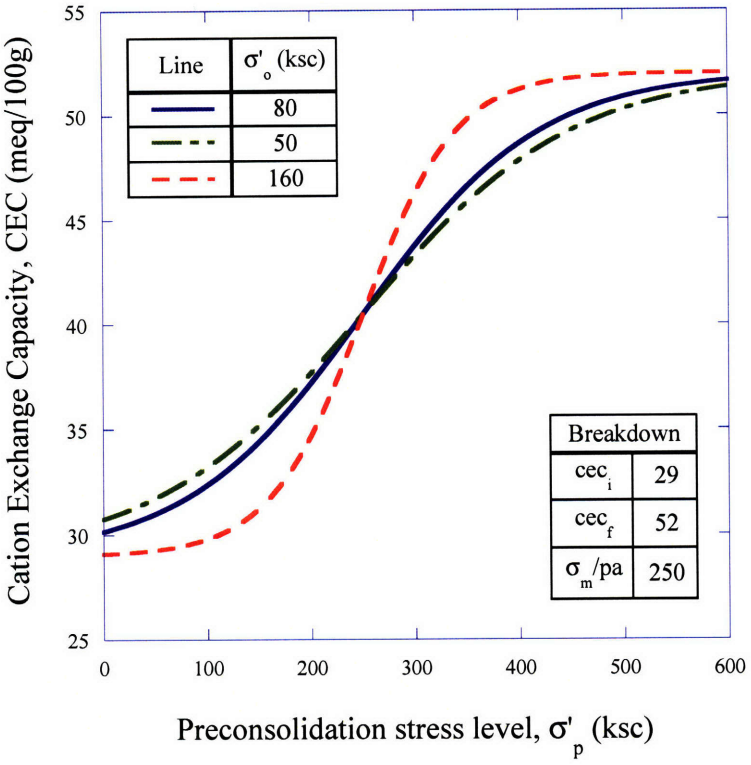

Figure 4-23: Effect of the input parameter σ'_o on the predictions for Cation Exchange Capacity.

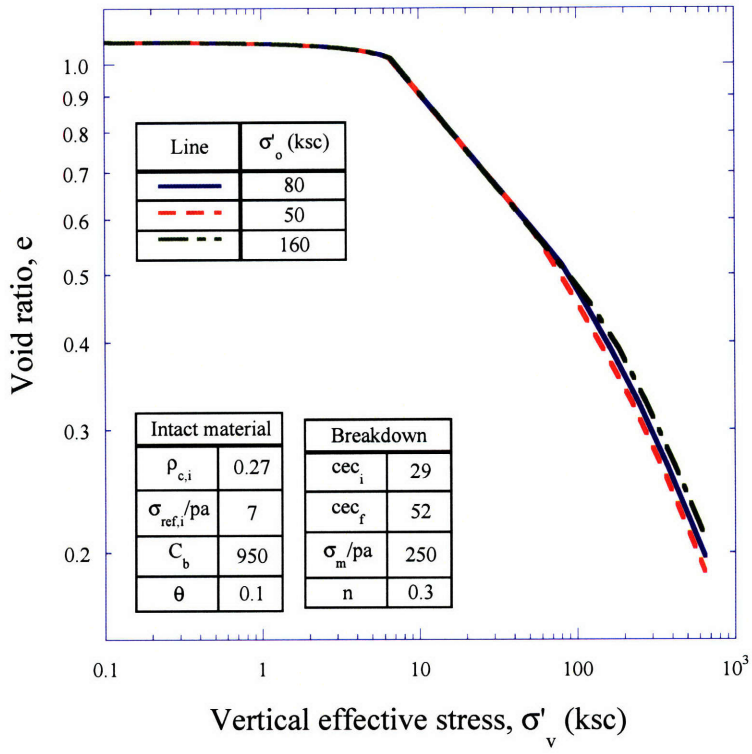

Figure 4-24: Effect of input parameter σ'_o on the predictions of the first loading compression curve.

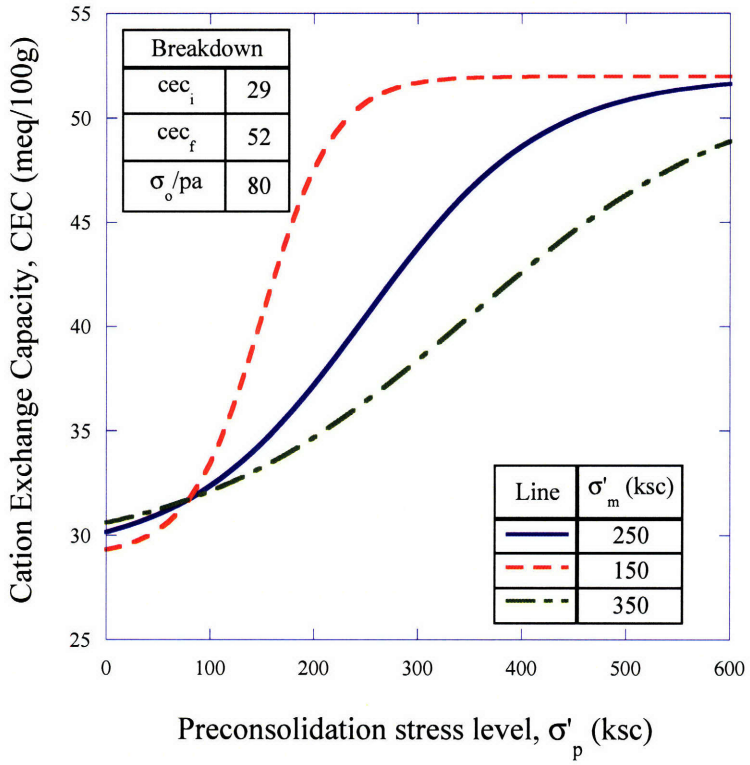

Figure 4-25: Effect of the input parameter σ'_m on the predictions for Cation Exchange Capacity.

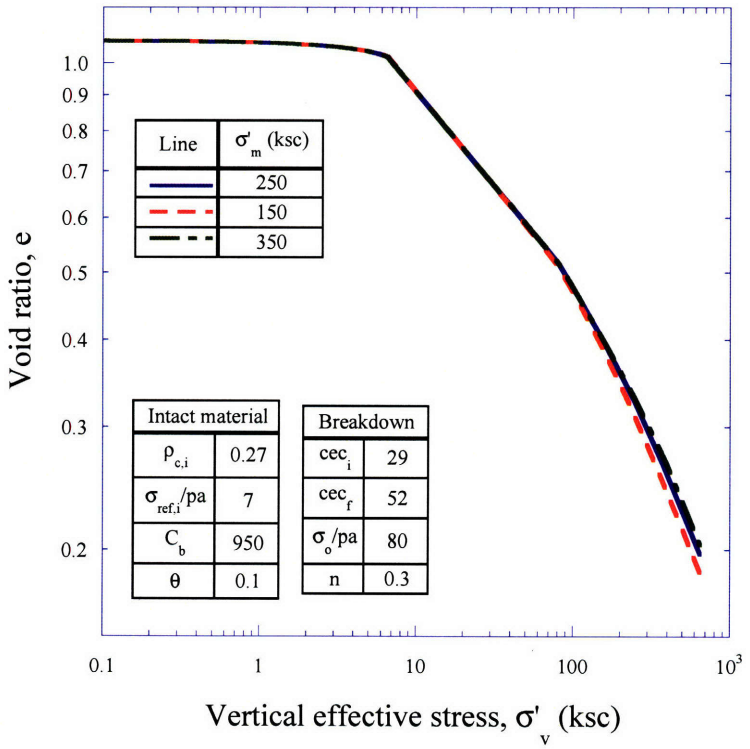

Figure 4-26: Effect of input parameter σ'_m on the predictions of the first loading compression curve.

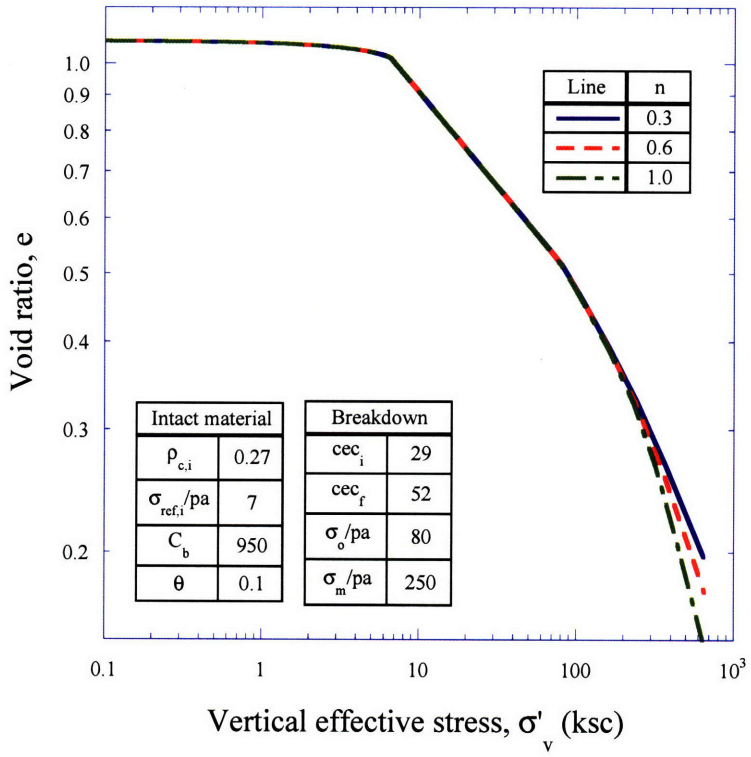

Figure 4-27: Effect of input parameter θ on the predictions of the first loading compression curve.

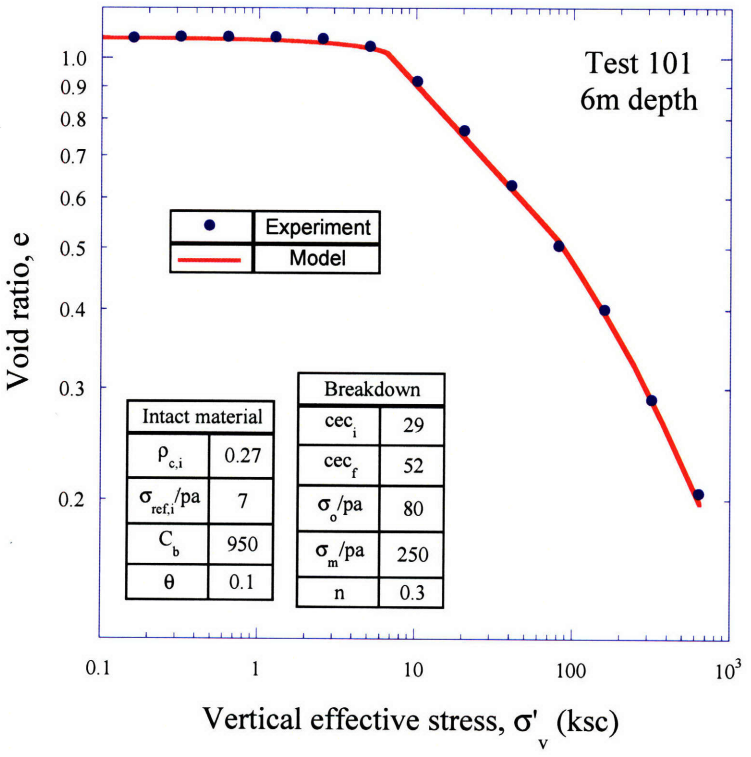

Figure 4-28: Compression model calibration for test 101 (depth 6m).

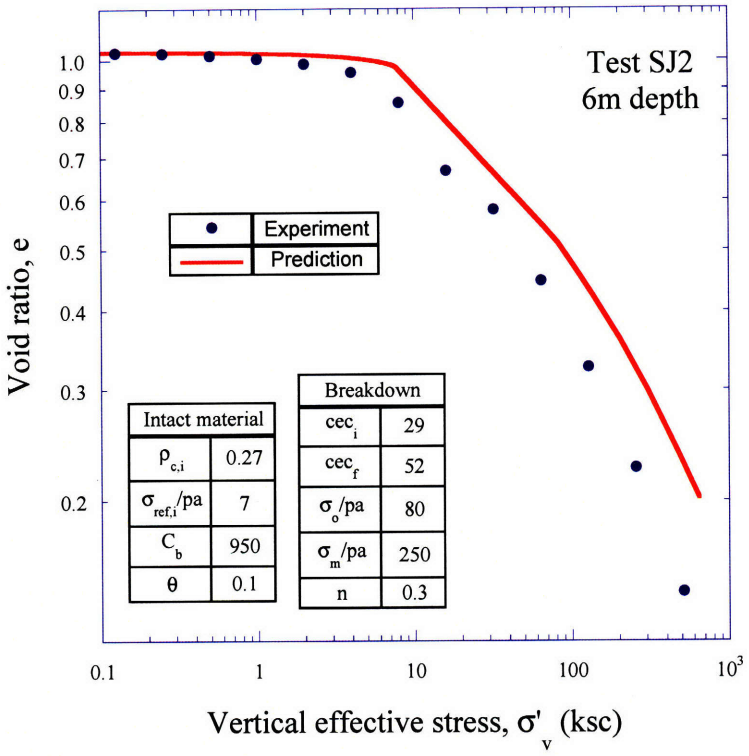

Figure 4-29: Compression model predictions for test SJ2 (depth 6m).

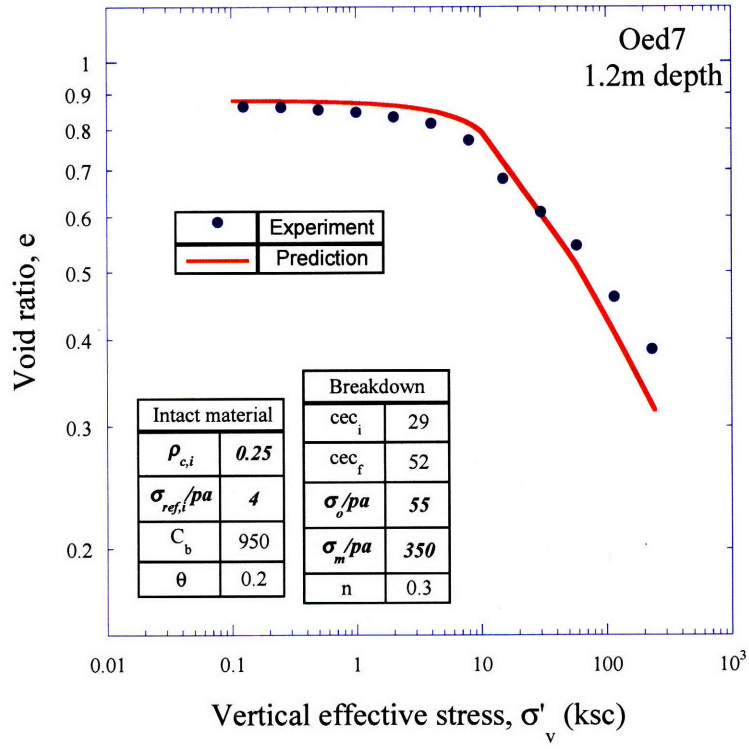

Figure 4-30: Compression model predictions for test oed7 (depth 1.2m).

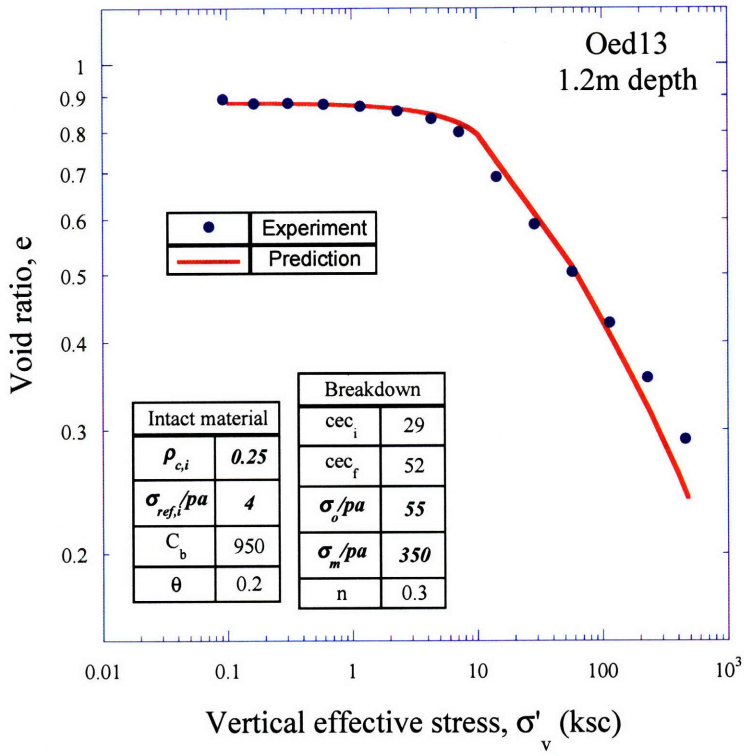

Figure 4-31: Compression model predictions for test oed13 (depth 1.2m).

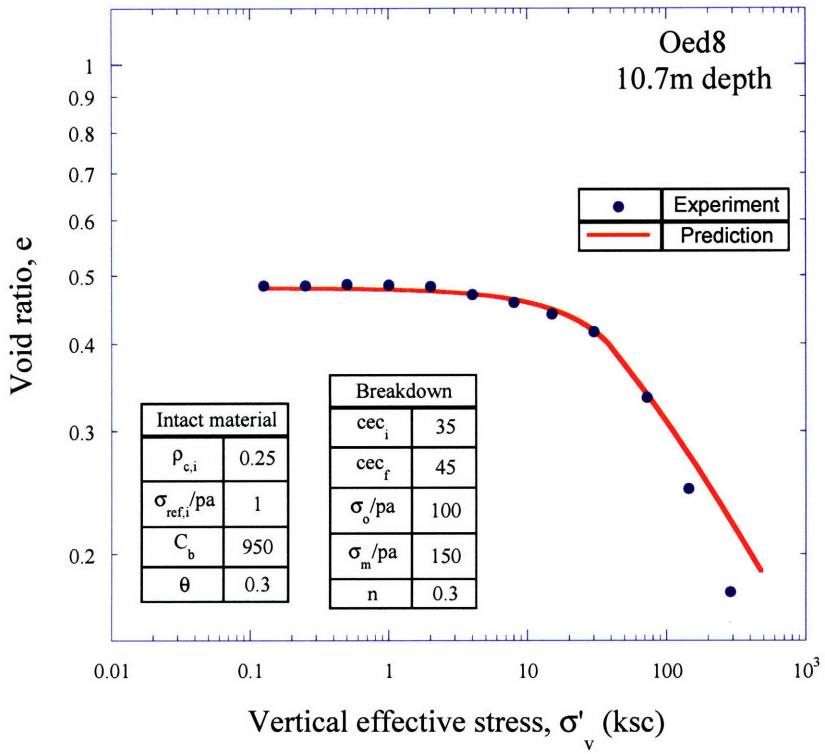

Figure 4-32: Compression model predictions for test oed8 (depth 10.7m).

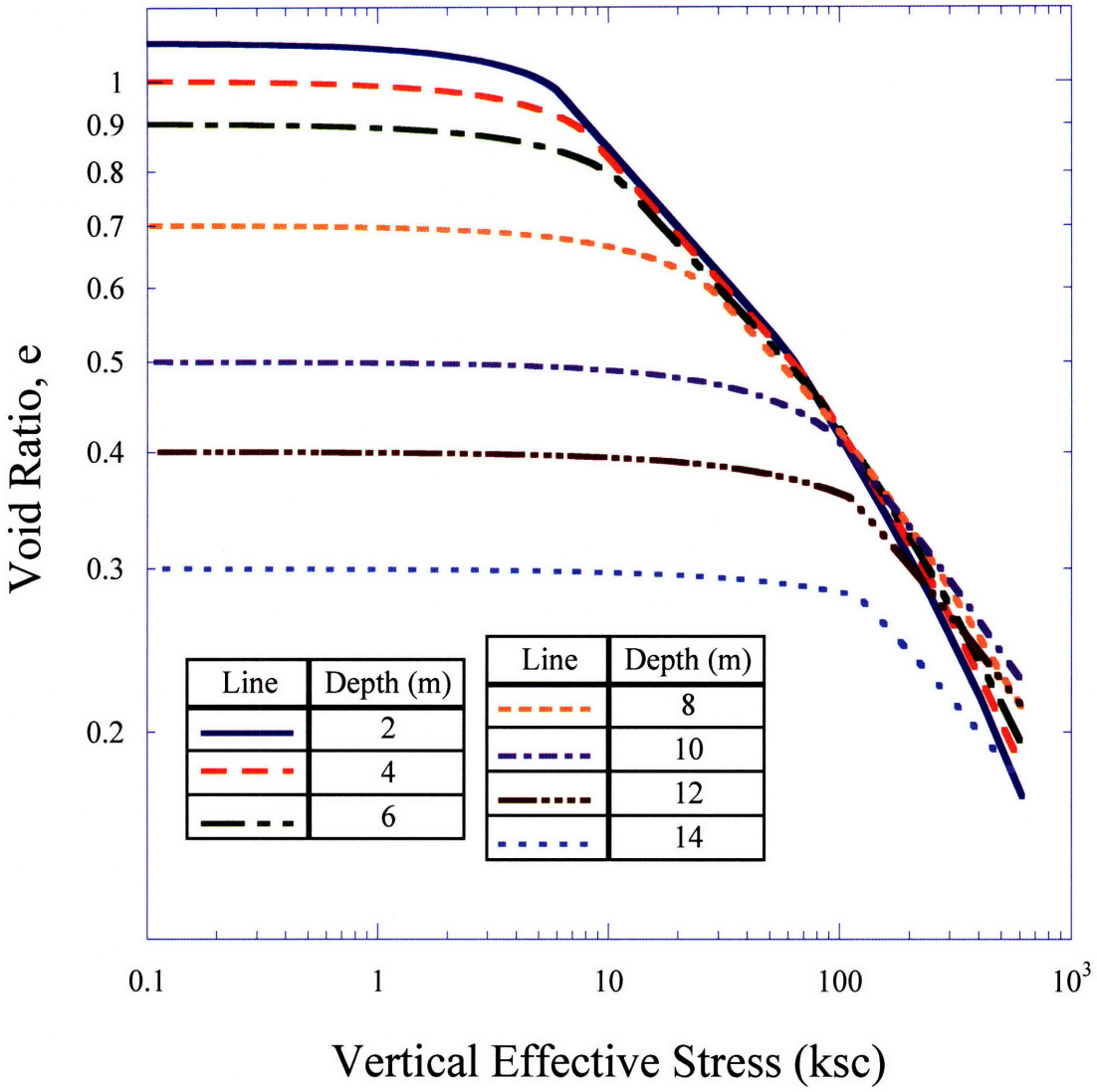

Figure 4-33: Predictions of the compression behavior of Old Alluvium for various depths. The input parameters for each depth are listed in Table 4-4.

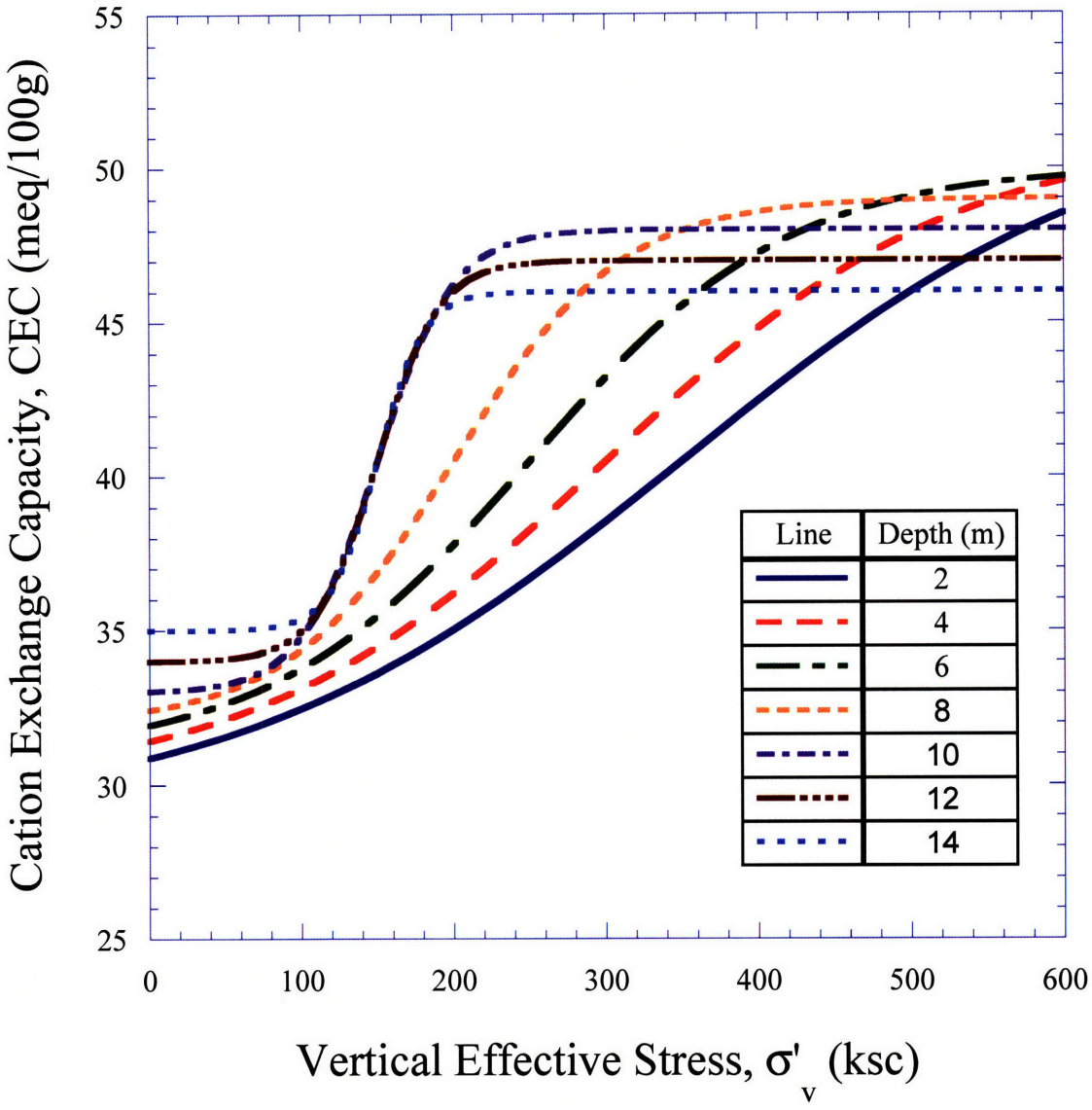

Figure 4-34: Evolution of the Cation Exchange Capacity during the compression tests simulated in Figure 4-33. The input parameters for each depth are listed in Table 4-4.

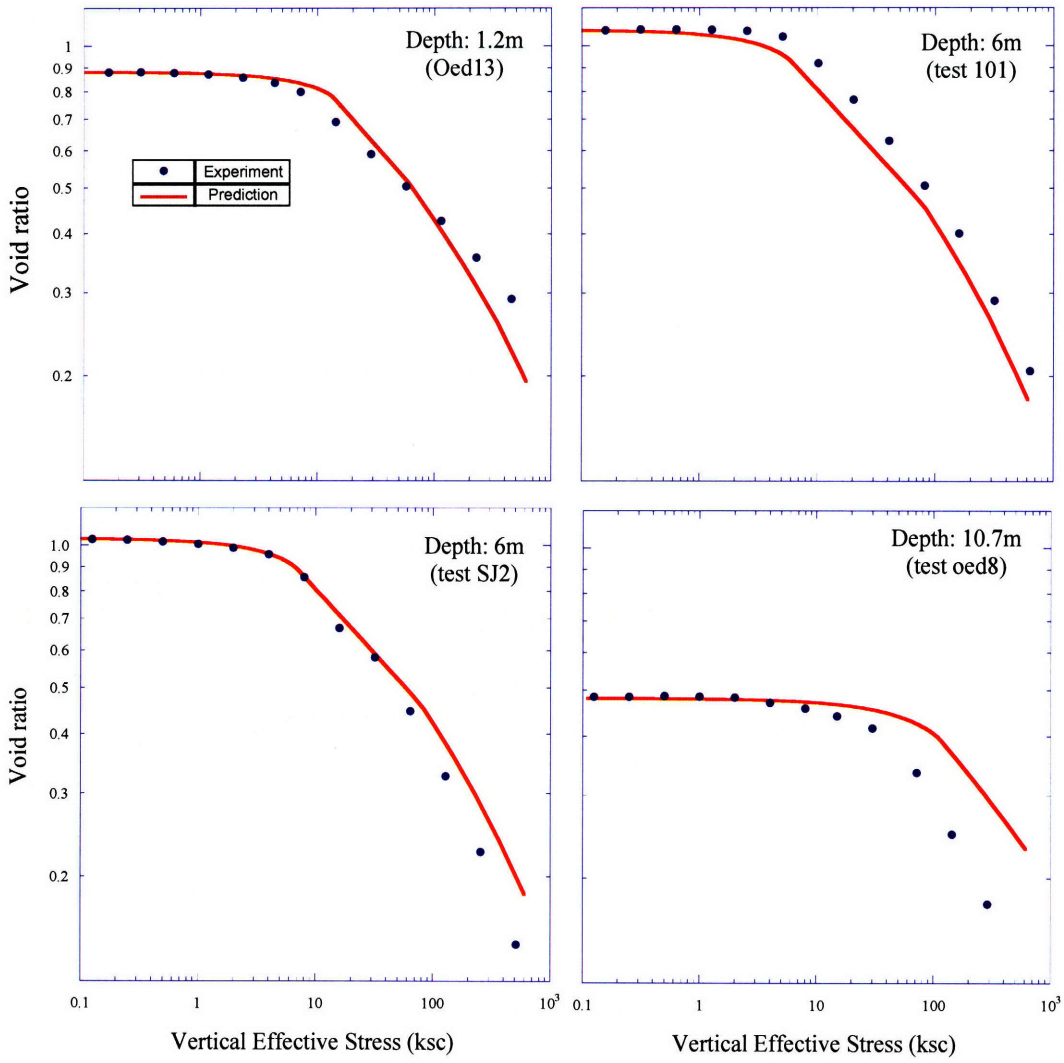

Figure 4-35: Comparison of measured compression data with predictions based on Table 4-4.

4.10 APPENDIX 4.I

Dvorkin et al (1991, 1994, 1099) proposed a method to obtain the normal and tangential stiffness of two cemented spheres. The method is based on the elastic theory (Timoshenko, 1970), and the cement layer is treated as an elastic foundation.

The main assumptions of the approach are:

- The contact region of the two grains is much smaller than the grain size.
- The cemented region is circular and axisymmetric to the line connecting the centers of the two grains.

Figure 4.I-1 shows the basic configuration and introduces some notation used in the equations below:

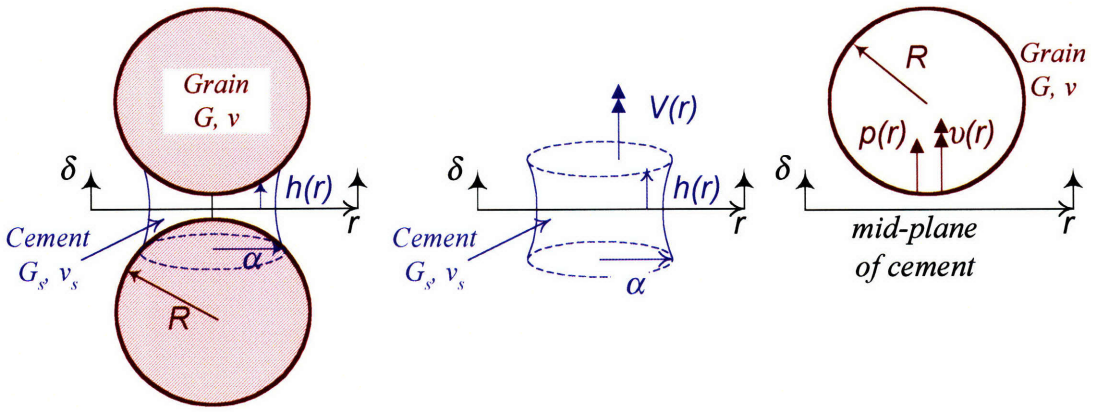

Figure 4.I-1: A pair of cemented grains.

Notation:

G, v: Shear modulus and poisson's ratio of the grain

G_s, v_s: Shear modulus and poisson's ratio of the cement

R: Radius of spherical grain

α: Radius of cement contact on grain

$0 \le r \le \alpha$: location on the cement/grain contact

$\upsilon(r)$: displacement of grain surface

p(r): normal stress on grain surface

V(r): displacement of cement at contact

δ: displacement of cement at mid-plane

h(r): local height of cement

The displacement of the grain surface is expressed as:

$$\upsilon(r) = f\left(G, \nu, \alpha, \int p(r)\right) \tag{4.I-1}$$

The normal stress on the grain is given by:

$$p(r) = f(G_c, \nu_c)\frac{V(r)}{h(r)} \tag{4.I-2}$$

and the displacement within the cement mass is expressed by:

$$\delta + V(r) = f_1(G, G_c, \nu, \nu_c) f_2(\int V(r)) \tag{4.I-3}$$

with

$$\delta = \upsilon(r) - V(r) \tag{4.I-4}$$

being the necessary consistency relationship.

In detail, equation 4.I-3 is written

$$\delta + V(r) = -\Lambda \int_0^{\pi} d\varphi \int_0^{r\cos\varphi + \sqrt{a^2 - r^2\sin^2\varphi}} \frac{V(\sqrt{r^2 + s^2 - 2rs\cos\varphi})}{R\left[\varepsilon + \frac{1}{2}\left(\frac{r^2}{R^2} + \frac{s^2}{R^2} - 2\frac{rs}{R^2}\cos\varphi\right)\right]} ds \tag{4.I-5}$$

with Λ being:

$$\Lambda = \frac{2G_c}{\pi G}\frac{(1-\nu)(1-\nu_c)}{1-2\nu_c} \tag{4.I-6}$$

Equation 4.I-5 can be solved using the Solve using Gauss-Legendre Quadrature method. Figure 4.I-2 shows the integrated normal stress at the grain-cement contact for the case of the cement being (a) softer or (b) harder than the grain.

With the distribution of normal stress known, the displacements can also be calculated. The effective bulk modulus of the system is then obtained by:

$$K_{eff} = \frac{G_c(1-\nu_c)}{1-2\nu_c}\frac{C(1-\phi)}{3(1+h(0))}\left(-\frac{k}{\delta}\right) \tag{4.I-7}$$

where C is the coordination number, ϕ the porosity and k is given by:

$$k = \int_0^{\alpha} \frac{V(r)r}{h(0) + r^2/2} dr \tag{4.I-8}$$

The shear bulk modulus follows as

$$G_{eff} = \frac{3}{5}K_{eff} + G_c \frac{3C(1-\phi)}{20(1+\varepsilon)}(-\frac{k}{\delta}) \qquad (4.I\text{-}9)$$

Parametric analyses conducted by the present author showed that the variation of elastic input parameters influences K_{eff} and G_{eff} individually, but not their ratio K_{eff}/G_{eff}.

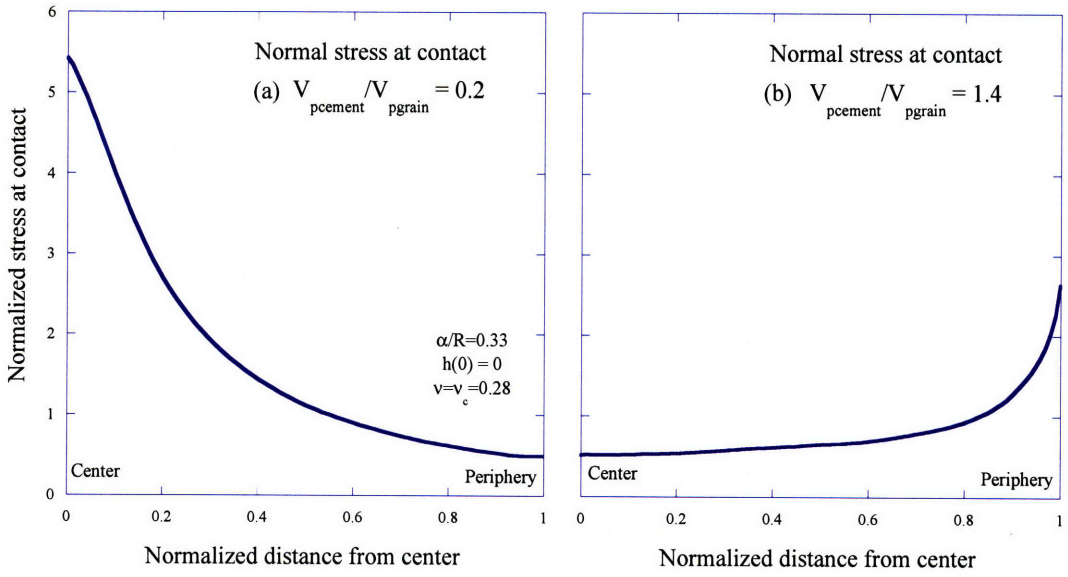

Figure 4.I-2: Integrated normal stress at the grain-cement contact for the case of the cement being softer (a) or harder (b) than the grain (based on Dvorkin, 1994).

In summary, the model provides an updated tangent and shear modulus for cemented granular materials. It requires the elastic properties of the constituents, some basic assumption on the contact geometry and a measure of porosity. It assumes that the grains are solid and that there is substantial amount of cementation to be considered a solid and continuous elastic foundation.

In the case of the Old Alluvium, the grains are not solid and the ESEM observations show that the cementation cannot always considered as uniform or continuous. Table 4.I-1 also demonstrates that there is a lot of uncertainty on the elastic properties of the cementation.

In order to estimate the effect of cementation in Old Alluvium, the following simplifying assumption were made:

- $v_c = 0.28$ and $G_c = 90GPa$
- Initial porosity is 0.52 (from Upper Clay tests)

- Coordination number C = 3 (due to the very open structure; the value is very low compare to 8 or 9 Dvorkin et al (1991) are assuming for sands).
- Because the grains are not necessarily compressible, it is also assumed that the displacement of the cement at contact is the same as at mid-plane.
- At cemented state: height of the cement at the center of the contact, h(0) = 0.4μm (estimated from ESEM pictures) and radius of the cemented area 0.3μm. After some breakdown of the cementation, h(0) = 0.05μm (estimated from ESEM pictures) and radius of the cemented area 0.1μm.

With these assumptions, the ratio of the effective bulk modulus of the cemented soil vs. the soil with destroyed cementation is close to 0.25 – which attributes a 25% increase in the bulk modulus due to cementation. However the ratio depends significantly on the cementation geometry assumed and cannot be used beyond a simple estimation.

Mineral	K (GPa)	G (GPa)	Poisson's ratio	Reference
Kaolinite poorly crystallized	44	22.1	0.29	Wang et al (2001)
Kaolinite well crystallized	47.9	19.7	0.32	Wang et al (2001)
Kaolinite	1.5	1.4	0.14	Woeber (Mavko et al, 1998)
Smectite ferruginous	9.3	6.9	0.20	Wang et al (2001)
Hematite	100.2	95.2	0.14	Hearmon (Mavko et al, 1998)
Hematite	154.1	77.4	0.28	Woeber (Mavko et al, 1998)
Hematite	206.6	91		Liebermann & Schrieber (1971)
Hematite	97	92		Schon
Hematite	206.6	91		Handbook of physical constants (1995; 1996)
Hematite		78.5	0.27	Carmichael (1961)
Goethite	?	?	?	
α Quartz	36-39	42-48	0.08	Mavko et al, 1998
β Quartz	56, 68	40-42		Mavko et al, 1998

Table 4.I-1: Elastic properties of cementing agents and clay minerals present in Old Alluvium.

References:

Ahrens T.J. (1995): A handbook of physical constants, Ahrens T.J. editor, American Geophysical Union

Carmichael C.M. (1961): "The magnetic properties of ilmenite–hematite crystals", Proceedings of the Royal Society of London, Series A 263, 508–530.

Clark S.P. (1996): A handbook of physical constants, Clark S.P. editor, Memoir, Geological Society of America, 97.

Liebermann R. C., Schreiber E. (1971): "Elastic properties of minerals, EOS, Transactions, American Geophysical Union, 52, 142-147.

Mavko G., Mukerji T., Dvorkin J. (1998): The rock physics handbook : tools for seismic analysis in porous media, Cambridge University Press.

Wang Z., Wang H., Cates M.E. (2001): "Effective elastic properties of solid clays", Geophysics, 66 (2), 428-440

Woeber A.F., Katz A., Ahrens T.J. (1963): "Elasticity of selected rocks and minerals", Geophysics, 658-663.

5 Swelling model

5.1 INTRODUCTION

Old Alluvium exhibits significant volumetric expansion upon unloading. Studies on the material microstructure (Chapter 2) revealed two main causes for this macroscopic behavior: (i) there is up to 20% (per weight) nontronite, an expansive mineral that belongs to the family of smectites; and (ii) nontronite is an in-situ tropical weathering product, and most probably the mineral sheets are initially found stacked in a parallel (face to face) configuration, with a local porous environment possibly rich in hydration cations. Measurements of the amount of adsorbed water (Zhang, 2002; Appendix 5.I) suggest that nontronite stacks are only minimally hydrated (with just one layer of water molecules between each mineral sheet).

Compression tests performed on specimens of Old Alluvium (Chapter 3) showed that the amount of recoverable volumetric expansion on unloading depends on the level of preconsolidation pressure. Higher preconsolidation leads to larger amounts of swelling strains. However, it was also observed that multiple unload-reload cycles from the same preconsolidation produce a response, which is largely reversible.

The swelling behavior of the Old Alluvium is controlled by the nature of the microstructure and strongly depends on the level of physicochemical changes induced by compressive stresses. The loading part of the compression model described in Chapter 4 was developed to account for such changes; the swelling model proposed in this Chapter is based on physicochemical and microstructural state variables that are related to the prior consolidation history.

The present chapter summarizes the predominant swelling mechanisms associated with clay minerals and reviews the main modeling approaches that have been proposed to describe the swelling behavior of expansive soils. It then details the formulation of a new swelling model, and discusses its predictive capabilities for the Old Alluvium and other materials with similar microstructural characteristics. Finally, it discusses the reloading response of the soil and proposes an approach to model the significant hysteresis in the largely reversible stress-strain response.

5.2 SWELLING MECHANISMS

5.2.1 Microstructure of a clay aggregation

In order to understand the mechanisms associated with the swelling of clays, it is necessary to associate them with the clay microstructure and the organization of the local pore space. Figure 5-1 shows a widely accepted structure for clay aggregates (Loret et al, 2002), which is also applicable to the microscale of the Old Alluvium (Chapter 2). Unit clay layers in parallel configuration are stacked together forming unit particles, or platelets. The number of layers in platelets depends on the clay mineral, the mode of formation, the ions present and the level of compaction, and it can range from 5 to 15 layers in Ca-Montmorillonites, or up to 1000 in compacted clays (i.e., up to 1μm thick) according to Loret et al. (2002). The interlayer or interlamellar space is filled with 1 to 4 water molecules (3Å to 12Å). This interlayer water, or "internally absorbed" water has substantially different properties from those of free water; it does not flow even when subjected to relatively high hydraulic gradients, and it deforms together with the solid part of clusters (Loret et al, 2002). Clay particles are separated by micropores, which are believed to contain free water; that is water that can be displaced by ordinary hydraulic gradients. At a larger scale, clay particles form groups or domains which, when aggregated, produce the macroscopic structure (ped) and define the macropores.

It is generally accepted that swelling is characterized by two regimes: at very low water contents, interlayer space absorbs water, until it is filled with three or four molecular water layers; this is referred to as crystalline swelling. After the interlamellar space has been saturated, water is adsorbed on the external surfaces of clay particles, producing osmotic swelling (Sposito & Prost, 1982). The following sections describe these processes in more detail.

5.2.2 Crystalline swelling

Crystalline swelling is considered to be driven by either a solvation or a hydration mechanism between the negatively charged clay surface, and its counter-ions[35] (Delville, 1991), Israelachvili (1992) and Sposito et al. (1999). It is however controversial which of the two is the dominant mechanism.

[35] A counterion is the ion that accompanies an ionic species in order to maintain electric neutrality.

Solvation is the process of attraction and association of molecules of a solvent with molecules or ions of a solute. In clays, the solvation mechanism arises due to the presence of the constraining geometry of clay sheet surfaces, and the presence of a cavity in this surface (Loret et al, 2002). Solvation forces are proportional to the difference in ionic density between the surface and the mid-plane of the interlamellar space (Israelachvili, 1991).

Hydration is the sorption of the first two to three water layers between the unit clay layers of the 2:1 dioctahedral series of alumino-silicate clays (i.e., interlayer or interlamellar sorption of water). Yong (1999) mentions that the entry of water molecules into the interlayer space due to their adsorption energy is thought to be greater than the attraction forces between the unit layers. A schematic representation of the hydration layer is shown in Figure 5-2.

The hydration of ions near the surfaces of the clay particles may contribute significantly to volume change, especially for dry compacted clays. For example, from a basal spacing d(001) = 0.95 to 1 nm for the anhydrous state, sorption or hydration is reported to increase the spacing to values between 1.25 and 1.9 nm, (Norrish, 1954, in Yong, 1999). Van Olphen (1977) also states that volume changes as high as 100 percent of the original volume of the dry clay can be obtained when four monolayers of water enter between the layers of a montmorillonite clay.

Yong (1999) associates the crystalline swelling with the matric potential, as the mechanism for sorption from very low water contents or from the anhydrous state is due not only to the presence of charge sites and exchangeable ions in the interlayers, but also to the attractions between water molecules and the polar surface groups[36].

In brief, regardless of whether hydration or sorption is the dominant mechanism, crystalline swelling depends on the nature of the clay sheets, and is capable of producing significant volume changes. The interlayer cations do not play a significant role in the crystalline swelling, given that the clay surfaces become directly hydrated, regardless of the nature of the cation. The significance of the interlayer cations lies in the fact that they control the fraction of layers that participate in the free (osmotic) swelling. The difference in swelling capacity between two expansive clays is due to the difference in the number of individual layers participating in the free swelling, rather than to a difference in the separation distance between the layers in the clay stacks.

[36] The study mainly focuses on montorillonites, but the author states that notronites also demonstrate similar swelling behavior.

5.2.3 Osmotic swelling and diffuse double layer

The second swelling mechanism, due to the adsorption of water on the existing external surfaces of the clay particles, is attributed to osmotic phenomena, and so to the diffuse electrical double layer.

Osmotic follows crystalline swelling. The number of water layers associated with the first mechanism varies between 2 to 3[37] and depends on the nature of the soil, the layer charge, the nature of interlayer cations, the properties of adsorbed liquid and the particle size. Expansion beyond this is described by double layer theory, which is introduced below. The change in swelling mechanism can be identified by the rate of ion dilution, which increases substantially after hydration to ~2-3 layers (Figure 5-3; Yong, 1999).

It is well known that isomorphous substitution in the crystal lattice of clays results in a negative charge at the clay surfaces, which attracts exchangeable cations present in the surrounding pore fluid. This causes a high electrolyte concentration in the vicinity of the clay surfaces and so the cations near the clay surfaces diffuse to equalize concentrations through the pore fluid. This tendency is restricted by the negative electric field that initially caused the cation concentration. The result of these two opposite forces produces an ion distribution adjacent to the clay particle, which forms a "diffuse double layer" (Bolt 1956; Tripathy et al, 2004; Mitchell & Soga, 2005). Figure 5-2 shows a schematic representation of the Double Layer.

Several theories have been proposed for the quantitative description of the Double Layer. The most widely used one was developed by Gouy (1910) and Chapman (1913) and has been frequently modified to include several aspects of the electro-physico-chemical interactions between the clay surfaces and the ion concentration in the pore fluid.

According to the Gouy-Chapman theory, the "thickness" of a single double layer is given by:

$$2d = \left(\frac{\varepsilon_0 \varepsilon kT}{2ne^2 v^2} \right)^{1/2} \tag{5.1}$$

where v is the ionic valence, e the electronic charge (1.602×10^{-19} C), n the ion concentration in the far field, ε the dielectric constant of the pore fluid, T the absolute temperature (^{0}K) , k Boltzmann's constant (1.38×10^{-23} J/^{0}K), and ε_0 the permittivity of the vacuum (8.854×10^{-12}

[37] Some report up to 4 layers of crystalline swelling (e.g. Saiyouri et al., 2000).

C^2/Jm). The theory assumes that the ions are point charges, which do not interact with one another, that the clay surface charge is uniformly distributed, that clay surface is a plate and much larger than the double layer (I-D conditions) and that the permittivity of the fluid is independent of position (Mitchell & Soga, 2005).

According to (5.1) the extent of the Double Layer is affected by the ion concentration in the pore fluid, the valence of these ions and also on the nature of the fluid and the temperature.

The diffuse double layer can be expected to be completely developed for clays in a slurry state (Tripathy et al., 2004). In all other cases that clay particles are close enough to force interaction between the two adjacent double layers. This interaction depends on the ion concentration of the midplane between the two clay platelets and results in the presence of an osmotic pressure at the midplane (Bolt, 1956). According to Gouy-Chapman theory the interacting force between two double layers can be derived from the ion concentration midway between the clay surfaces, which in turn is determined by the value of the electric potential. The repulsive pressure (Langmuir, 1938) is then given by the osmotic pressure at the mid-distance between the clay surfaces, with respect to the osmotic pressure of the equilibrium solution. Since the osmotic pressures depend on the ion concentration, the swelling pressure can be determined by the excess concentration at the mid distance between the clay surfaces.

Various authors have presented methods for calculating this osmotic pressure based on the Gouy-Chapman theory (Bolt, 1956; van Olphen, 1963; Sridharan & Jayadeva, 1982; Madsen & Mueller-Vonmoos, 1985). According to Madsen & Muller-Vonmoos (1985) for the same value of Cation Exchange Capacity, CEC, there is a unique relationship between the swelling pressure p_s, and the distance between the clay platelets; the swelling pressure, p_s, is given as a function of the electric potential, u, at the mid-distance between the clay surfaces:

$$p_s = 2nkT(\cosh u - 1) \tag{5.2}$$

where n is the ion concentration far from the clay surface, k the Boltzmann's constant and T the absolute temperature.

The electric potential is further related to the distance between the clay surfaces, 2d, through the following:

$$\chi d = 2\exp\left(-\frac{u}{2}\right)\left\{F_1\left(\exp(-u),\frac{\pi}{2}\right) - F_2\left(\exp(-u),\arcsin\exp(-(\frac{z-u}{2}))\right)\right\} \tag{5.3}$$

where $\chi = \left(\frac{8\pi n e^2 v^2}{\varepsilon kT}\right)^{0.5}$, z is the surface potential at the mid-distance between the clay surfaces, v the ion valence, ε the dielectric constant and e the unit electronic charge. F_1 and F_2 are the elliptic integrals of the first and second kind:

$$F_1(k,\phi) = \int_0^{\phi} \frac{d\theta}{\sqrt{1-k^2\sin^2\theta}}, \quad 0 < k^2 < 1 \tag{5.4}$$

$$F_2(k,\phi) = \int_0^{\phi} \sqrt{1-k^2\sin^2\theta}\, d\theta, \quad 0 < k^2 < 1 \tag{5.5}$$

Full details on the calculation of the osmotic pressure using this method are discussed in section 5.4.1.

Reported values of swelling pressures vary depending on the nature of the clay. Mesri et Olson (1971) report a swelling pressure p_s = 35ksc for montmorillonites, and Madsen & Mueller-Vonmoos (1985) refer to a maximum measured pressure p_s = 20ksc for Opalinum shale. Boergesson et al (1996) report pressures $p_s \leq$ 100ksc for bentonites while Tripathy et al (2004) found a maximum swelling pressure p_s = 400ksc for MX80 bentonite and less than 200ksc for Febex bentonite. It should be noted that these values are much smaller than the pressures associated with crystalline swelline. Seedsman (1987), for example reports that the pressure needed to reduce Na-montmorillonite from a two-layer to a one-layer hydration state is in the order of 700-1000 ksc (at 0°C), while the complete collapse of either Na- or Ca-montmorillonites requires pressures in excess of 3000 ksc.

The use of the double layer theory has several limitations, owing to many factors, which were summarized by Tripathy et al (2004) as follows: (*i*) poorly developed or partially developed diffuse double layer, (*ii*) deviation of soil structure and fabric from the parallel plate concept, (*iii*) surface hydration forces at close particle distances, (*iv*) direct mechanical effect of water in tension, (*v*) non-uniform size of clay plates, (*vi*) existence of electrical attractive forces, (*vii*) presence of multivalent cations, (*viii*) effect of ion size, (*ix*) anion adsorption, (*x*) particle size, and (*xi*) expulsion of diffuse double layer water in the case of application of high compressive stresses.

However, the double layer theory does provide a general framework that can quantify the physicochemical interactions between the clay surfaces and the surrounding pore fluid. Gens and Alonso (1992) note that it involves as input various of the parameters known to control the swelling behavior of clays.

5.2.4 Further mechanisms

Saiyouri et al (2000) argue that in the cases when large particles exist originally in the clay (due to compaction for instance), saturation of the interlamellar space can cause splitting of the particles, which produces new surfaces available for osmotic swelling (Figure 5-4). As evidence, they present results of X-Ray analyses for specimens of the Fourges-Cahaignes clay[38], which show that particles of the clay are composed of about 100 layers for low values of the water content, but of as little as 10 layers when the water content increases (Figure 5-5). Unfortunately, there are few quantitative data, regarding the structure of the water, the transport phenomena and the microscopic mechanisms associated with this separation of layer groups into different particles.

5.2.5 Hysteresis

Crystalline swelling is considered hysteretic and there are various experimental results which confirm the hypothesis; for example Fu et al. (1990) and Huang et al. (1994) report hydration/dehydration cycles with more than 10Å hysteresis observed (12.5% strain of 1-D parallel layered stack).

Likos (2004) reports wetting/drying cycles of Na-smectite (initially oven-dried) with up to 9.75% irrecoverable deformation (Figure 5-6). Figure 5-7 further shows that axial deformation is greater during drying than for the same value of humidity during wetting (more water is retained during drying than is adsorbed during wetting). The figure also illustrates a double-step hydration mode often documented for swelling clays. Likos (2004) interprets the step portions of the curve as the transition from one hydration state to the other and the flat parts as the regimes for a particular hydrate state. However, since the basal spacing is obtained from humidity controlled XRD tests, Chipera (1997), argues that the stepwise form of hydration/dehydration curve may be an artifact of fitting the defraction data.

[38] Fourges-Cahaignes clay, a smectite-kaolinite clay.

Fu et al (1990), explain the observed hysteresis based on the silica structure and turbostratic arrangement of clay layers[39]. They postulate that hysteresis between adsorption and desorption occurs because the orderliness of the system is not reversible; and some of the orderliness gained during adsorption is not lost until last stages of desorption.

Yong (1975) also suggests that the observed hysteresis between drying and wetting of clays is due to particle rearrangement, and hence will always be present, since there is always an opportunity for rearrangement during swelling and shrinking.

Verburg & Baveye (1995), looking mainly in quasi-crystal formations, discuss that there are activation energy barriers that need to be overcome for platelet collapse or separation, which prevent instantaneous collapse or separation of the platelets.

It is not clear whether hysteresis at the microscopic scale can be directly associated with the hysteresis observed macroscopically in materials like the Old Alluvium during swelling/reload cycles. Boergesson et al (1996) also observed a significant hysteresis during swelling-compression tests on bentonite (Figure 5-8), but did not propose an underlying mechanism.

5.3 SWELLING MODELS

5.3.1 Common formulations within constitutive models

The most widely used models for the compression behavior of clayey soils (Casagrande, 1936; Schofield & Wroth, 1968) assume that volume changes during unloading are non-linear but elastic. They predict a linearized response in e-logσ' space, even though the measured behavior is always non-linear in this space, and the swelling slope depends on the amount of unloading:

$$de = C_s d(\log \sigma'_v) \tag{5.6}$$

$$de = \kappa d(\ln \sigma') = \kappa \frac{d\sigma'}{\sigma'} \tag{5.7}$$

[39] Turbostratic is a type of crystalline structure where the basal planes have slipped sideways relative to each other, causing the spacing between planes to be greater than the ideal. In the clay microstructure, the silicate tetrahedra rotate causing the surface network of oxygens to assume ditrigonal symmetry, which does not allow the layers to fit together in any regular or periodic way; therefore they rotate/translate to obtain the best fit possible. As a result, the degree of disorder is relatively high (after Fu et al, 1990).

where C_s or κ are material properties, usually defined by the swelling slope over one log cycle of stress, σ'_v and σ' are the vertical and mean effective stress, respectively.

However, the study of expansive clays and the design of buffer materials for applications such as nuclear waste confinement have developed the need for a more accurate representation of the swelling mechanisms. The following paragraphs summarize the most recent approaches proposed from various modeling disciplines.

5.3.2 Swelling within the MIT-S1 model

Pestana (1994) recognized that the unloading behavior of cohesive soils involves both the recovery of elastic energy stored at particle contacts (as in cohesionless soils), and physicochemical factors that affect the osmotic pressures and hence, the double layer thickness. Therefore, he proposed volume changes during unloading can be described by[40]:

$$d\varepsilon^e = \left(\frac{e}{1+e}\right)\left(\frac{1}{C_b}\left(\frac{\sigma'}{p_a}\right)^{2/3} + D(1-\xi^r)\right)\frac{d\sigma'}{\sigma'} \tag{5.8}$$

where C_b, D, and r are material constants, and $\xi = \frac{\sigma'}{\sigma'_{max}}$ (stress ratio).

In equation (5.8) the first term, $\frac{1}{C_b}\left(\frac{\sigma'}{p_a}\right)^{2/3}$ is loosely based on Hertz contact theory and is equivalent to expressions used to model cohesionless soils. The constant C_b controls the stiffness of the soil immediately following the load reversal and was discussed in Chapter 3.

The second term in equation (5.8), $D(1-\xi^r)$, aims to capture the physicochemical phenomena that affect volumetric expansion in clays, by controlling the double layer thickness. However, the material constants D and r are empirically derived from measured unloading data. D represents the maximum slope of the swelling line in loge-logσ' space (at high overconsolidation ratios) and r controls the shape of the swelling lines and is fitted at intermediate OCR values. Higher values of r result in more strain recovery at a given stress ratio ξ.

[40] Equation (5.8) is written here for hydrostatic unloading.

Figure 5-9 presents results of parametric calculations that show the effect of D and r to the predictions of the swelling model. Higher D values result in increased volumetric strain recovery at large OCR values (i.e., smaller stress ratio, ξ), while r controls the rate of strain accumulation at intermediate OCR values.

5.3.3 Hydration and double layer considerations

Likos & Lu (2006), consider a simple microstructural geometry of parallel expandable clay sheets, related the change in the interlayer void ratio e_{IL} to the separation distance between two layers, 2δ:

$$\Delta e_{IL} = \frac{2\delta}{\tau} \tag{5.9}$$

where τ is the thickness of the mineral sheet. However, the microstructural deformations upscale directly to the macroscopic ones, as the total void ratio e is the sum of the interlayer(IL) and the interparticle (IP) one:

$$\Delta e = \Delta e_{IP} + \Delta e_{IL} \tag{5.10}$$

Saiyouri et al (2000) proposed the use of the model of Pons et al (1981), which interrelates the number of layers per particle and the interlayer distances with their corresponding probabilities of occurrence. This approach allows the estimation of the interlayer sizes in the hydrated clay, based on the probability of one to four layers of water molecules occurring in the inter-clay layer spaces (as calculated by the Pons' model). Hence, the approach concentrates on volumetric changes due to crystalline swelling, and it is assumed that beyond hydration and splitting of the particles, the interlayer distances increase linearly with the log of the decreasing stress.

Murad (1999) has formulated a much more elaborate model of hydration that takes into account the thermo-physico-chemical interaction between the adsorbed water phase, the clay surface and the surrounding pore space. The model introduces a generalized thermodynamical pressure that depends on mechanical as well as chemical gradients and a modified effective stress

principle that depends on the hydration stresses. Homogenization schemes are then used to upscale to the soil macrostructure. Apart from its theoretical value, this type of approach entails a substantial number of constitutive assumptions and requires much more extensive procedures for parameter estimation (Loret et al, 2002).

Komine & Ogata (1999, 2003, 2004) proposed a revision of the Gouy-Chapman diffuse double layer theory, which considers the presence of more than one cations:

$$p_s = \frac{1}{CEC} \sum_{\substack{i=Na^+,Ca^{++} \\ K^+,Mg^{++},etc}} [exc_i\{(f_r)_i - (f_a)_i\}] \, (kPa) \tag{5.11}$$

where p_s is the calculated swelling pressure between two montmorillonitic layers, CEC the Cation Exchange Capacity of the montmorillonite, exc_i the exchange capacity of cation i (different than the Cation Exchange Capacity of the clay), $(f_r)_i$ the repulsive force between two parallel montmorillonitic layers caused by cation i, and $(f_a)_i$ the repulsive force between two parallel montmorillonitic layers caused by cation i. The repulsive force f_r is calculated from the classic double layer theory, while the calculation of the attractive force, f_a, is based on London's theory (Van der Waals force). Therefore, the influence of the various exchangeable cations is incorporated by the weighted average of repulsive/attractive forces caused by these cations.

In order to relate the microstructural double layer calculations (half distance between the montmorillonite mineral layers) with the macroscopic strains of the bentonite/buffer material, the authors introduced a new state variable, the "swelling volumetric strain of montmorillonite", which is based on the mass percentages of swelling and non-swelling constituents:

$$\varepsilon_{sv}^{*} = \left(e_0 + \frac{\varepsilon_{s\max}}{100}(e_0+1)\right)\left(1+\left(\frac{100}{C_m}-1\right)\frac{\rho_m}{\rho_{nm}}+\left(\frac{100}{\alpha}-1\right)\frac{100}{C_m}\frac{\rho_m}{\rho_{sand}}\right)100\% \tag{5.12}$$

$$e_0 = \frac{\rho_{solid}}{\rho_{d0}} - 1 \tag{5.13}$$

$$\rho_{solid} = \frac{\dfrac{100}{C_m}\dfrac{100}{\alpha}\rho_m}{\left(1+\left(\dfrac{100}{C_m}-1\right)\dfrac{\rho_m}{\rho_{nm}}+\left(\dfrac{100}{\alpha}-1\right)\dfrac{100}{C_m}\dfrac{\rho_m}{\rho_{sand}}\right)} \; (Mg/m^3) \tag{5.14}$$

where ε_{smax} is the maximum swelling strain of buffer and backfill materials (%), e_0 is the initial void ratio of the materials, C_m is the mass (percent) content of montmorillonite in the bentonite, ρ_{d0} is the initial dry density of the material (Mg/m^3), ρ_m is the particle density of the montmorillonite (Mg/m^3), ρ_{nm} is the particle density of the component minerals other than montmorillonite (Mg/m^3), ρ_{sand} is the particle density of the sand (Mg/m^3), and α is the mass percent content of bentonite in the materials.

It should be noted that based on SEM observations, the authors assume that the expanding layers fill the voids between the bentonite particles. The proposed model is very useful for the design of buffer systems, where the mass percentage and densities of the various constituents, as well as the present cations are known and can be controlled. Application in natural clays requires various assumptions on the properties of the clay and fluid constituents. More importantly, the upscaling of microscopic deformations to macroscopic strains requires that the swelling minerals eventually occupy all of the interparticle pore space, as illustrated in Figure 5-10.

5.3.4 Plastic macroscopic deformations due to reversible microstructural strains

Alonso & Alcoverro (2002) associated the potential microstructural expansivity of a soil with debonding[41]. As discussed in Chapter 4, the objective of their research was to model the swelling of clayey shales, that contain expandable clay stacks initially restricted by the encircling rock mass. The model has two components, one at the macro level and one at the micro level.

At the micro level, bonding evolves as an exponential function of strain:

$$b = b_i e^{-h_1 \int |de_v^p| - h_2 \int |de_s^p|} \tag{5.15}$$

where b_i is the initial amount of bonding, $\varepsilon_v^p, \varepsilon_s^p$ the plastic (macroscopic) volumetric and deviatoric strains respectively and h_1, h_2 input parameters fitted to describe the rate of bond degradation. An example of the evolution of bonding for various levels of bind degradation is shown in Figure 4.6.

[41] When a clay soil becomes bonded while under stress, it has the potential to swell, once the stress is removed and the bonds break. From this perspective, swelling is not an exclusive behavior of materials that contain active clay minerals, but can occur even in granular soils (Fernández & Santamarina, 2001).

The microscopic volume strains depend on the mean effective stress, and the amount of bonding. This is formulated by introducing a dependence of a microstructural stiffness to bonding:

$$e_m = e_{m0} - \kappa_m(b)\ln\frac{\sigma'}{\sigma'_{\max}},\ (\sigma' \le \sigma'_{\max}) \tag{5.16}$$

where σ'_{max} is a confining stress beyond which no microstructural deformations are expected, e_{m0} is the microscopic void ratio corresponding to this stress, and κ_m the microstructural stiffness coefficient given by:

$$\kappa_m(b) = \kappa_{mfd}\left(1 - \frac{b}{b_0}\right) \tag{5.17}$$

with κ_{mfd} corresponding to the fully damaged state and b_0 to the fully bonded state. These microscopic swelling strains are reversible.

At the macro-scale, the debonding associated with the volumetric expansion is an irreversible mechanism. The authors establish that plastic strains develop during unloading and hence, postulate a second yield surface associated with the irreversible macroscopic swelling strains.

In order to translate the reversible micro-strains to the plastic macroscopic strains, Alonso et al (1992, 1998) introduced the notion of interaction functions, based on the assumption that plastic deformations are a function of the microstructural deformations, $d\varepsilon_m$, the current confining stress, σ', and the current yield stress in compression (or preconsolidation pressure), σ^*_{ob}:

$$\varepsilon_v^p = \varepsilon_m f\left(\frac{\sigma'}{\sigma^*_{ob}}\right) \tag{5.18}$$

f is the "transfer" or "interaction" function, given by:

$$f = f_0 + f_1\left(1 - \frac{\sigma'}{\sigma^*_{ob}}\right)^{n_D} \tag{5.19}$$

This transfer function is controlled by three additional input constants, f_0, f_1, and n_D, which control the influence of micro-strains on the macrostructure. These parameters are selected based on the available swelling data; for example, f_0 is selected so that the calculated behavior fits the

swelling curve immediately upon load reversal, while n_D controls the effect of the unloading stress ratio σ'/σ'_{ob}, and so is selected at lower stress levels.

In equation (5.19) the ratio σ'/σ^*_{ob} is a measure of the degree of openness of the macrostructure relative to the applied stress state. Low values imply a dense packing of the material, and hence a higher degree of interaction is expected between the microstructural swelling and the macrostructural plastic strains.

The notion of "interaction functions" was first introduced by Alonso (1998) and Alonso et al. (1999). In the general case, a function for loading and a different one for unloading were implemented in the Barcelona Expansive Model to express irrecoverable macroscopic strains due to suction cycles. Alonso and Alcoverro (2002) applied the idea to bonded materials with expansive microstructures, and so used only one such function, in the unloading part of the model. The potential of the transfer functions lies in the fact that they can simulate various degrees of micro-macro interaction. This is illustrated in Figure 5-11, which concentrates on the unloading part of the Barcelona Expansive Model and shows the case of strong and of weak interactions. In order to achieve a strong interaction between the micro strains and the macroscopic deformations, the transfer function is fitted to increase substantially as the stress ratio, σ'/σ^*_{ob} decreases, and hence, significant macroscopic volumetric strains are observed (solid line in Figure 5-11). In contrast, a small change in the value of the interaction function results in minimum interaction between the micro and macro scale, and so the macroscopic strains remain relatively small (dashed line in Figure 5-11). This mechanical law is also able to model the invasion of macropores induced by the microstructural expansion, when high confinement conditions prevail (as reported by Komine and Ogata, 2004), by considering negative values of the interaction function (Alonso et al., 1999). In this case, the positive (expansive) microscopic strains are translated into negative macroscopic deformations, and hence, the macroscopic void ratio decreases (the macropores are filled).

Within the framework of a generalized model for unsaturated expansive materials, Sánchez et al (2005) further proposed a formulation to include thermo-hydro-mechanical phenomena in the prediction of swelling strains. As in prior formulations from the Barcelona group (Alonso et al., 1998, 1999, 2002), microstructural strains are elastic and volumetric:

$$\dot{\varepsilon}_{vm} = \frac{\dot{\hat{p}}}{K_m} = \frac{\dot{p}}{K_m} + \chi \frac{\dot{s}}{K_m} \tag{5.20}$$

where p is the mean stress, $\hat{p} = p + \chi s_t$ is the microstructural effective stress, $s_t = s + s_0$ is the total suction, s_0 the osmotic suction, s the matric suction, $\chi > 0$ a constant, and K_m the microstructural bulk modulus given by:

$$K_m = \frac{e^{-\alpha_m \hat{p}}}{\beta_m} \quad or \quad K_m = \frac{(1+\bar{e}_m)}{\kappa_m}\hat{p} \tag{5.21}$$

where α_m, β_m, e_m and κ_m are additional input parameters, the latter probably corresponding to a reference microstructural void ratio/stiffness (Alonso, 2002). These microstructural strains are considered to modify the global arrangement of aggregates in an irreversible way, through a transfer function of the kind proposed by Gens & Alonso (1992) and Alonso (1998).

5.3.5 Chemo-mechanical coupling

Loret et al (2002) proposed modeling the clay swelling phenomena by chemo-mechanical coupling. Their approach introduces various species (clay particles, absorbed and adsorbed water, salt in absorbed water) within the fluid and solid phase of the material, and models the transfer of species driven by mechanical and chemical potentials. This is illustrated by equation (5.22), which expresses the Clausius-Duhem inequality as a sum of three contributions, associated with mechanical work (D_1), mass transfer (D_2) and diffusion (D_3):

$$\begin{aligned}
&\delta D_1 = -\delta\Psi + \sigma : \delta\varepsilon + \sum_{k,K} \mu_{kK}\delta m_{kK} \geq 0 \\
&\delta D_2 / \delta t = -(\mu_{wS} - \mu_{wW})\hat{\rho}^{wS} - (\mu_{sS} - \mu_{sW})\hat{\rho}^{sS} \geq 0 \\
&\delta D_3 / \delta t = -\nabla\mu_{wW} \cdot M_{wW} - \nabla\mu_{sW} \cdot M_{sW} \geq 0 \\
&\delta D = \delta D_1 + \delta D_2 + \delta D_3
\end{aligned} \tag{5.22}$$

where Ψ is the free energy per unit initial volume, μ_{kK} the potential of species k in phase K, m_{kK}, the corresponding masses, M_{kK} the mass flux, and $\hat{\rho}^{kK} = \delta m_{kK}^{reactive} / \delta t$; k∈ {water, salt, clay} and K∈ {Solid, Water fluid}.

Equation (5.22) forms the basis for the chemo-mechanical coupling, which is built within the well-known elastoplastic framework of Modified Cam Clay. The modified yield surface depends

(in addition to the preconsolidation pressure) on the chemical potential of the water in the micro-structure:

$$f = f(\bar{p}, q, \bar{\mu}_{wS}, tr\varepsilon^{pl}) = \frac{q^2}{M^2 \bar{p}} + \bar{p} - p_c$$
$$M = M(\bar{\mu}_{wS}),\ \ p_c = p_c(\bar{\mu}_{wS}, tr\varepsilon^{pl}) \tag{5.23}$$

where $\bar{p}, \bar{\mu}_{wS}$ are the effective values of the mean stress and the chemical potential of the microstructural water respectively.

The model does not distinguish between crystalline and osmotic swelling. Figure 5-12 shows the application of the model to chemical loading of Ponza bentonite (diMaio, 1996). The chemical loading is achieved by addition of salt (potential increase) or flooding with distilled water (potential decrease) and results in a step change of the void ratio (point A to B or point C to D), and modification of the parameters λ, κ of the MCC model. In the first case (Figure 5-12a), the chemical loading is induced at low stresses and results in significant immediate volume change and subsequent compression with modified slope $\lambda_{\text{NaCl-saturated}}$. In the second case (Figure 5-12b), the soil compressibility is initially $\lambda_{\text{distilled-water}}$, until salt is added at $\bar{p} = 1000kPa$. This figure illustrates that the model successfully captures the changes in compressibility and swelling index observed during variations in pore fluid salinity.

5.3.6 Chemo-poromechanical approaches

Dormieux et al (1995) developed a macroscopic poromechanical model, which incorporates the results of double layer theory. They consider 3 phases: the soil skeleton, the free water in the connected porosity and the electrolyte in solution; and 2 structural levels: and the macrostructure, and the microstructure, which includes groups of clay layers in parallel configuration, surrounded by the electrolytic solution (Figure 5-13).

At the macroscale, the state equations are expressed following the Clausius-Duhem inequality:

$$\underline{\underline{\sigma}} : \underline{\underline{\dot{\varepsilon}}} + \mu^e \dot{m}^e + \mu^w \dot{m}^w - \frac{d\Psi}{dt} \geq 0 \tag{5.24}$$

where ψ is the volume density of the total free energy, $\underline{\underline{\sigma}}$ is the total stress tensor, $\underline{\underline{\varepsilon}}$ the strain tensor, μ^e & μ^w the chemical potentials of the electrolyte and water respectively, and m^e, m^w the corresponding masses.

At the microscale, the characteristic length of the double layer is given by equation (5.1), and the osmotic pressure in the midplane between two clay layers is

$$\Pi^{sw} = kT(n^+(0) + n^-(0) - 2n^e_\infty) \tag{5.25}$$

with

$$\frac{\partial}{\partial n^e_{eq}}(\Pi^{sw}) = 2kT\left(\frac{\partial}{\partial h}(\lambda h) - 1\right) \tag{5.26}$$

where n(0) is the concentration of ions in the midplane, n^e_∞ the electrolyte concentration in the solution outside the clay system, n^e_{eq} the electrolyte concentration in an equivalent solution[42], $\lambda = n^e / n^e_{eq}$, and h the distance between 2 clay layers. (k is Boltzman's constant and T the absolute temperature)

With e being the macroscopic void ratio, the authors relate the microscale deformations h to the macroscale with

$$h = \frac{1}{\rho^s S_m} e \tag{5.27}$$

which requires only the knowledge of the specific surface of the clay layers, S_m, and the density of the solids, ρ^s.

The modeling approach has been refined since (for example, Dormieux et al, 2003). Of interest is also the research by Lemarchand et al (2005) which derives the pressures generated by the confined volumetric expansion of micro-constituents, as a function of the micro and macro-scale stiffnesses, the mass of the constituents, and the porosity.

Appendix 5.II presents an effort to set up a poromechanical model for the Old Alluvium, considering it as a double porosity system (Berryman, 2002). The major difficulty of the application of such models on the Old Alluvium is posed by the need of upscaling, hence the use

[42] Solution not subjected to any electric field and in thermodynamic equilibrium with the pore fluid in the associated elementary volume.

of homogenization methods that require knowledge of the mass and elastic properties of the various micro-constituents. Furthermore, it is challenging to distinguish a "matrix" material within the microstructure of the Old Alluvium, in contrast to concrete materials or clay buffers (c.f., Dormieux et al., 2006).

5.4 PROPOSED MODEL

It has been extensively discussed that the behavior of the Old Alluvium is controlled significantly by physicochemical changes that occur in the microstructure. According to Double Layer theory, swelling depends on the exposed Specific Surface Area of the clay minerals (mainly of nontronite) and the Cation Exchange Capacity. In the intact state of Old Alluvium, the strongly positive Fe-oxide cations and the base cations present in the micro-pores provide sufficient (positive) charges to equilibrate the negatively-charged clay surfaces. As a result, they mask Double Layer development, even when distilled water enters the micro-porous environment. However, when the iron oxides disaggregate from the clay surfaces, their negative charge is released and hence the swelling capability is recovered.

Since the above mechanisms depend on the level of mechanical disaggregation or on the stress history in a compression test, the amount and rate of volumetric expansion also depends on the preconsolidation stress level. While no extra breakage occurs, the physicochemical activity remains unaltered, so the swelling pattern remains the same even if after various unload-reload cycles.

The model proposed here uses electric double layer theory to predict swelling strains with Cation Exchange Capacity as the main state variable that controls the volumetric expansion. Hence, it links directly the swelling behavior to the level of destructuration caused by the compression loading.

5.4.1 Calculation of swelling pressures

The swelling pressures are calculated according to the double layer theory, following the method proposed by Madsen and Mueller-Vonmoos (1985).

The method requires estimation of:

- the valence of ions in the double layer, v

- the ion concentration of the pore water away from the clay surfaces, n (ions/cm^3)
- the surface charge of clay, D (m^2/gr), which depends on the Cation Exchange Capacity, CEC (meq/100g), and the specific surface area, SSA, of the clay.

Additional constants needed are Boltzmann's constant, k = 1.38x10^{-16}erg/K, the dielectric constant of water, $\varepsilon = 80$, the electric charge, e = 4.8x10^{-10} esu[43] and the absolute temperature, (assume 20^{0}C = 293 ^{0}K).

The basic equation for the double layer describes the variation of the electric field strength (electric potential ψ) at a distance x from the clay surface as a function of the local density of charge:

$$\frac{d^2\psi}{dx^2} = \frac{8\pi nev}{\varepsilon}\sinh\left(\frac{ve\psi}{kT}\right) \tag{5.28}$$

Substituting $y = \frac{ve\psi}{kT}$, $z = \frac{ve\psi_0}{kT}$, $\chi = \left(\frac{8\pi ne^2v^2}{\varepsilon kT}\right)^{0.5}$, *and* $\xi = \chi x$, with ψ_0 the potential at the surface:

$$\frac{d^2y}{d\xi^2} = \sinh y \tag{5.29}$$

At the mid-distance between the clay surfaces (d), the field strength is zero, and the electric potential is ψ_d, or normalized

$$u = \frac{ve\psi_d}{kT} \tag{5.30}$$

The first integration of (5.29) gives, with boundary conditions: x = d; y = u; and $\frac{dy}{d\xi} = 0$:

$$\frac{dy}{d\xi} = -(2\cosh y - 2\cosh u)^{0.5} \tag{5.31}$$

The second integration of (5.29) gives, for y$\in$ {z,u} and x$\in$ {0,d}:

$$\int_z^u (2\cosh y - 2\cosh u)^{-0.5}\,dy = -\int_0^d d\xi = -\chi d \tag{5.32}$$

[43] esu: electrostatic unit of charge.

So, finally, the mid distance, d, is calculated using elliptic integrals:

$$\chi d = 2\exp\left(-\frac{u}{2}\right)\left\{F_1\left(\exp(-u),\frac{\pi}{2}\right) - F_2\left(\exp(-u),\arcsin\exp(-(\frac{z-u}{2}))\right)\right\} \tag{5.33}$$

where F_1 and F_2 are the elliptic integrals of the first and second kind:

$$F_1(k,\phi) = \int_0^{\phi} \frac{d\theta}{\sqrt{1-k^2\sin^2\theta}}, \quad 0 < k^2 < 1 \tag{5.34}$$

$$F_2(k,\phi) = \int_0^{\phi} \sqrt{1-k^2\sin^2\theta}\, d\theta, \quad 0 < k^2 < 1 \tag{5.35}$$

On the other hand, the osmotic pressure, p_{sw}, depends on the ion concentration and can be calculated from the excess concentration at the mid-distance, d:

$$p_{sw} = 2nkT(\cosh u - 1) \tag{5.36}$$

Therefore, for a given value of surface charge, a unique relationship can be established between the swelling pressure, p_{sw} and the distance 2d between the clay layers (double layer thickness) through the following steps:

1. For various values of the electric potential at the mid-distance, u, the surface potential z, can be calculated from (5.31):

$$\cosh z = 0.5\left(\frac{dy}{d\xi}\right)_0^z + \cosh u, \quad with \quad \left(\frac{dy}{d\xi}\right)_0 = \frac{4\pi evD}{\varepsilon kT\chi} \tag{5.37}$$

where $D = \frac{e}{A}$, $A = \frac{SSA}{CEC}$

2. then the mid-distance d can be calculated through equation (5.33) (elliptic integrals), as a function of u, z and χ.

3. On the other hand, the swelling pressure, p_{sw} can be calculated as a function of u from equation (5.36).

4. Hence, for the same values of u, the values of the swelling pressure p_s, and the corresponding double layer thickness, d, are calculated.

Figure 5-14 shows the results obtained (p_{sw}, d) for a series of CEC values ranging between 10 - 100 meq/100g.

For values of the Cation Exchange Capacity varying between 20 and 200 meq/100g (typical range of values for soils, the relationship between the swelling pressure, p_{sw} and the double layer half thickness, d can be closely approximated by a power law function:

$$p_{sw} = a_{sw} d^{b_{sw}} \tag{5.38}$$

where a_{sw} and b_{sw} are two coefficients related to the CEC:

$$a_{sw} = -2530.3 + 2303 \log(CEC) \tag{5.39}$$

$$b_{sw} = -0.669 - 0.723 \log(CEC) \tag{5.40}$$

Figure 5-15 shows that indeed equations (5.38) to (5.40) provide a close fit to the theoretically calculated osmotic pressure values.

5.4.2 Swelling model

At the microscale, the double layer expansion results in a volumetric strain, ε_{DL}, which can be calculated from the change in thickness, d, of the double layer:

$$d\varepsilon_{DL} = \frac{d(d)}{d_i} \tag{5.41}$$

where d_i is the initial double layer thickness of the clay stacks (the amount of adsorbed water present in the microstructure).

Substituting d in equation (5.41) from equation (5.38), the volumetric strains can be expressed as a function of the confining stress:

$$d\varepsilon_{DL} = \frac{1}{d_i} \frac{1}{a_{sw} b_{sw}} \left(\frac{\sigma'}{a_{sw}} \right)^{\frac{1}{b_{sw}} - 1} d\sigma, \quad or$$
$$d\varepsilon_{DL} = \frac{1}{d_i a_{sw}^{1/b_{sw}} b_{sw}} \frac{d\sigma}{\sigma^{1-1/b_{sw}}} \tag{5.42}$$

Equation (5.42) reveals a microstructural bulk modulus that depends only on physicochemical forces, as it is directly related to Cation Exchange Capacity, through coefficients a_{sw} and b_{sw}:

$$\frac{1}{K_{DL}} = \frac{1}{d_i a_{sw}^{1/b_{sw}} b_{sw}} \frac{1}{\sigma^{1-1/b_{sw}}} \tag{5.43}$$

It is assumed that the expansion of the double layer contributes only to volumetric strains. The assumption is justified by the observed random orientation of the clay platelets in the microstructure (Zhang, 2002).

Therefore, it is proposed that the volumetric changes at the micro-scale are expressed at the macro-scale through the addition to the elastic bulk modulus of a physicochemical term related to equation (5.43):

$$\frac{1}{K} = \frac{1}{K_H} + \frac{1}{K_{DL}} \Rightarrow$$

$$\frac{1}{K} = \left[\frac{\sigma'}{\left(\frac{e}{1+e}\right)\frac{1}{C_b}\left(\frac{\sigma'}{p_a}\right)^{2/3}} \right]^{-1} + \left[s(d_i a_{sw}^{1/b_{sw}} b_{sw}) \left\langle \left(\frac{\sigma'}{p_{swi}}\right)^{n_T} \right\rangle_{\sigma' \le p_{swi}} \sigma' \left(\frac{\sigma'}{p_a}\right)^{-1/b_{sw}} \right]^{-1} \tag{5.44}$$

where K_H is a term based on Hertzian contact theory, which controls the stiffness of the soil immediately following the load reversal, and K_{DL} the proposed physicochemical term that takes into account the swelling at the microscale.

Some additional parameters and variables are present in equation (5.44):

- p_{swi} is the swelling pressure that corresponds to the initial double layer thickness of the clay stacks, for the value of the Cation Exchange Capacity corresponding to the current preconsolidation pressure.

$$p_{swi} = a_{sw}(d_i)^{b_{sw}} = f(CEC) \tag{5.45}$$

  where d_i can be estimated by measurements of the adsorbed water present (see Appendix 5.I). Hence it marks the development of the double layer deformations at the microscale. Note that this swelling pressure is also a function of the Cation Exchange Capacity of the soil.

- The parameter s accounts for the amount of expansive minerals present in the microstructure. The parameter is required by the original double layer theory, because the electric potential

depends on the ratio of Cation Exchange Capacity to the mineral Specific Surface Area (i.e., variable, D, in the Madsen & Mueller-Vonmoos (1985) formulation, equation (5.37)). The parameter s can also provide some correction to predictions at low stress levels, where measurements may actually overestimate the initial Cation Exchange Capacity of the soil, due to unavoidable destruction of the soil structure.

Figure 5-16 illustrates the role of the parameter, s, on the computer macroscopic swelling behavior. Greater amounts of expansive clay minerals lead to larger volumetric strains. The magnitude of s can be fitted to the observed data for one unloading cycle, at high values of the stress ratio σ'/σ'_p ($p_{swi} < \sigma' < \sigma'_p$).

- The term $\left(\frac{\sigma'}{p_{swi}}\right)^{n_T}$, *for* $\sigma' \leq p_{swi}$, translates the swelling strains of the micro-scale to the macroscopically observed deformations, therefore it controls the degree of interaction between the micro and the macrostructure. It serves as a transfer function similar to that proposed by Alonso (1998) and analogous to the term $(1-\xi)^r$ of the MIT-S1 model. The major difference introduced in the current formulation is that this term is only contributing to the macroscopic behavior for $\sigma' \leq p_{swi}$. The intensity of the interaction is controlled by parameter n_T, which can be fitted to the measured data of one unloading cycle at low stress levels ($\sigma' < p_{swi}$). Figure 5-17 shows calculation of the swelling response for $n_T = 0 - 2.0$. Smaller values of n_T generate a higher degree of interaction between the micro and the macro-structures.

As discussed in 5.3.2, the MIT-S1 model (Pestana, 1994) introduces an additional term in the soil stiffness during unloading, which depends on 2 empirically fitted parameters, D, r, and the stress ratio $\xi = \frac{\sigma}{\sigma_{rev}}$. Within the MIT-S1 formulation, the bulk modulus is expressed as (equation (5.8)):

$$\frac{1}{K}=\left[\frac{\sigma'}{\left(\frac{e}{1+e}\right)\frac{1}{C_b}\left(\frac{\sigma'}{p_a}\right)^{2/3}}\right]^{-1}+\left[\frac{\sigma'}{\left(\frac{e}{1+e}\right)D(1-\xi^r)}\right]^{-1} \tag{5.46}$$

Comparison of equation (5.46) with (5.44) illustrates that the proposed physicochemical term has a form similar to the empirical term used by MIT-S1. However, in the new formulation, the term is a power function of the stress, $\sigma^{1-1/b_{sw}}$ (with b_{sw}(cec)), which is the result of the underlying double layer theory. In addition, the empirical parameter, D, is now defined as a function of the current Cation Exchange Capacity of the soil. Finally, the stress ratio $\xi=\frac{\sigma}{\sigma_{rev}}$, which expresses the effect of the "distance" from the reversal point, is substituted by the transfer function $\left(\frac{\sigma'}{p_{swi}}\right)^{n_T}$, relating to the underlying swelling pressure in the micro-structure.

5.4.3 Model application for the Old Alluvium

One of the main characteristics of the compression model developed in Chapter 4 is the use of Cation Exchange Capacity as a state variable that evolves with the structural breakdown. Every stress level on the Limiting Compression Curve, and hence every potential reversal point is associated with a CEC value. Hence, upon load reversal, the swelling model is activated with parameters a_{sw}, b_{sw} automatically assigned according to the current CEC value.

The model requires 3 input parameters: s, n_T and the initial double layer thickness, $2d_i$. As discussed above, d_i can be estimated based on measurements of the amount of water adsorbed in the microstructure (Appendix 5.I). s and n_T are then fitted to an unloading branch of test 101 (at σ'_p = 640ksc – Figure 5-18).

Figure 5-19 shows the predicted volumetric expansion for test 101 for the other levels of preconsolidation pressures, σ'_p = 317 ksc, 158ksc, and 20ksc. The predictions agree well with the measured data, although they seem to be dependent on the corresponding preconsolidation pressure. This dependency on the level of compression is only related to the associated variation of the Cation Exchange Capacity during loading, since this is the same sample on which the model was calibrated. The rate of evolution of CEC with applied stress, and hence its value at

each preconsolidation stress level is controlled by the input parameter σ'_m, (section 4.6) which it was shown to have little influence on the predicted compression behavior but significant impact on the values of CEC at intermediate stress levels (Figure 4-26). Figure 5-21 illustrates that changing the value of parameter σ'_m, from 250ksc to 150ksc, (therefore forcing the CEC to increase within a smaller stress range) achieves a much better prediction of the recovered volumetric strains for all unloading cycles, with minimal effect on the compression model.

Figure 5-19 also shows that the model overpredicts the recovered strain at low preconsolidation pressures. This can reflect an overestimation of the Cation Exchange Capacity at low stresses (due to unavoidable damage associated with the measurement technique). It can also be linked to the particle splitting mechanism discussed by Saiyouri et al, (2000): parameter s, which is associated with the surfaces that are available to swell, was fitted at high stresses, after particle splitting had taken place; hence it does not correctly represent the material at low stresses, where splitting has not yet taken place. Figure 5-21 indeed shows that a smaller value of s would provide a better fit at $\sigma'_p = 20$ ksc.

Specimen SJ2 was obtained from the same depth as 101, hence its response should be well described by the same set of input parameters. Figure 5-22 illustrates that the model captures very well the volumetric expansion from 540ksc, and as expected slightly overpredicts the volume recovered from 20ksc.

Specimen oed7 was obtained from a shallower depth (1.2m compared to 6m for 101 and SJ2). Because the mineralogical analyses available for the calibration of parameters were performed on block samples from an intermediate depth (4m), the same input values for s, n_T and d_i are used. Figure 5-23 shows that again the model describes well the observed expansion form high stress levels (240ksc), and overpredicts the volumetric expansion from low stresses.

Specimen oed8 was obtained from a greater depth (10.7m) in Middle Zone. Mineralogical analyses on material from a depth of 13.7m (Zhang, 2002) showed that there is less nontronite present. Therefore, s should be lower. On the other hand, because of the denser initial state of the material, more interaction between the micro and macro structure should be expected. Hence the value of n_T should be smaller. From adsorbed water measurements it was estimated that $2d_i \approx$ 10.5Å (Appendix 5.I). Figure 5-24 shows that with the described expected variation of input parameters, the model can generally describe the overall observed behavior and the magnitude of

the volume expansion. It should be noted though that the bucket sample used to obtain the mineralogical characteristics for oed8 (10.7m depth) was obtained from a higher depth (13.7m) and hence it is possible that it was not representative of the conditions at the vicinity of Block B1 (from depth 10.7m).

5.4.4 Predictions through the weathering profile of Old Alluvium

As discussed in section 4.7.2, Old Alluvium is a tropical in-situ weathered soil, and hence is characterized by spatial variability that is not always consistent with depth. However, the degree of weathering decreases generally with depth, and so certain assumptions can be made regarding vertical variations in the swelling model input parameters:

- The smectitic minerals (i.e. nontronite) are the result of the in-situ weathering, their presence is expected to decrease with depth, as weathering becomes less intense. This has also been observed in the mineralogical analyses (Zhang, 2002). Hence, parameter s is expected to decrease with depth.
- The structure of the soil is more open at the top parts of the profile, due to the weathering action. Therefore, as the depth increases, the porosity decreases and the microstructural strains resulting from the expansion of platelets have a higher impact on the macroscopic strains. Hence, parameter n_T is expected to decrease with depth (i.e., lower values of n_T correspond to higher interaction).

Based on the above discussion, and the available tests from depths 1.2m, 6m and 8m, the input parameters are varied with depth as shown in Table 4-4. A simple linear mode of change is assumed. Note that due to lack of consistent data on the initial double layer thickness, d_i is considered the same (d_i=6.5Å) for all depths.

Figure 5-25 plots complete predictions for the load – unload behavior of Old Alluvium at various depths. The model describes the breakdown of soil structure and the associated increase of compressibility during loading, and upon load reversal, it predicts the volumetric expansion as a function of the Cation Exchange Capacity of the expansive minerals present in the microstructure. Highly weathered material from small depths compresses significantly and, when unloaded, produces very large volumetric expansion. Less weathered soil from larger depths has a higher yield strength, smaller compressibility, and smaller amount of expansive smectitic minerals, but the microstructural swelling has a stronger effect on the macroscopic response.

Furthermore, Figure 5-26 shows the volumetric expansion predicted above for 2 levels of preconsolidation pressure, σ'_p = 60ksc and 600ksc. The figure clearly illustrates how the amount of disaggregation and the evolution of compressibility affect the recovered volumetric strains. At the level of σ'_p=60ksc little disaggregation has taken place, and so all samples compress to similar void ratios and produce the same volumetric expansion. After significant compression however, (σ'_p = 600ksc), the highly weathered material from the most shallow depths compresses the most, and exhibits the largest amount of volumetric recovery, while the less weathered material from higher depths is less compressible and exhibits a reduced capacity for volumetric recovery during unloading.

Finally, based on the selection of input parameters in Table 4-4, Figure 5-27 compares the overall behavior described by the model with the available data from each depth. Clearly, a less accurate description of the compression affects the unloading behavior, but overall the model succeeds in capturing the main characteristics of Old Alluvium: increasing compressibility and significant volumetric expansion as loading disaggregates the material.

5.4.5 Application of the swelling model to other clayey materials

In this section the proposed model is employed to predict the behavior of clayey materials other than the Old Alluvium. The formations examined are some clayey Shales, and Todi Clay. Mineralogical information and the assumed input parameters for these materials are summarized in Table 5-2. As discussed in Chapter 3, these clayey shales include stacks of expansive clay minerals and so are believed to have similar microstructural characteristics with the Old Alluvium. The main purpose of this application is to evaluate the strength, flexibility and limitations of the proposed formulation. It is noted that in this section only the swelling part of the model is examined, as the compression mechanisms associated with the discussed materials are not comparable to those of Old Alluvium.

Figure 5-28 shows data from the compression behavior of intact Pierre Shale. The Shale contains 12-40% Montmorillonite and Fe/Mn cementation (Diaz and Fernando, 1987; Tourtelot, 1962). According to some literature observations (Diaz and Fernando, 1987) the clay stacks are believed to be initially hydrated to 1-2 layers of water, and so the assumed initial double layer

thickness, $2d_i$ = 16Å. The figure shows that with input parameters s, n_T within the range discussed for the Old Alluvium the model can describe well the observed behavior.

Figure 5-29 shows data and the model application for intact Bearpaw Shale. The Shale contains 50% clay minerals (Diaz and Fernando, 1987). In this case, an increased interaction between the microstructure and the macrostructure seems to describe better the measured data (a lower value of n_T = 0.3 fits the measured data better).

Figure 5-30 shows the compression response of intact Fort Union Shale and the corresponding model description. The formation has lower plasticity index than Pierre or Bearpaw Shales, and hence, a value of s lower than in Pierre Shale is selected. In addition, it is assumed that there is similar degree of micro-macro interaction with Pierre Shale.

Cucaracha Shale (Figure 5-31) exhibits a swelling index comparable to the compression one at load reversal. However, an increased cation exchange capacity value at load reversal and a proper degree of interaction between the microstructure and the macrostructure are capable of describing the observed data.

Todi Clay (Figure 5-32) is a medium plastic clay with a small clay content (3-5% clay fraction), which is believe to have a microstructure (Leroueil, 2001; Calabresi & Scarpelli, 1985). As illustrated in Figure 5-32, the clay exhibits a very high volumetric expansion. It can be observed that the rate of volume expansion increases substantially at a stress level of 0.2 ksc. This behavior may at first look similar to the response of the Old Alluvium (or the clayey Shales). However, the stress range of this observed behavior is very low (an order of magnitude smaller than the values of the initial swelling pressure that would mark the onset of double layer swelling). Indeed, the proposed model captures well the expansive behavior up to the level of 0.2 ksc, but is unable to predict the rapid volume recovery beyond this stress level (solid line on Figure 5-32). It is possible that the observed change reflects a splitting mechanism of the clay stacks to smaller particles, as discussed by Saiyouri et al (2000), especially in this case where the level of stresses in quite low. Such a mechanism would lead to more external surfaces being available for the development of double layer expansion, and hence increase the amount of the observed volumetric recovery. Indeed, the model can fit the observed behavior only by assuming a microstructural change, because, if there were a significant splitting of clay particles, the value of parameter s, which is related to the amount of available expansive minerals, would increase

substantially. The dashed line on Figure 5-32 illustrates the effect of changing the value of s from 0.2 to 0.88[44].

In general, the above examples illustrate that the proposed model has the flexibility to describe the swelling behavior of different clayey soils, because it represents the underlying physical mechanism of double layer expansion and requires input directly related to the microstructure and main physicochemical characteristics of the materials.

5.5 DISCUSSION ON RELOADING

The experimental data on Old Alluvium (Chapter 3), and especially tests 101 and SJ2 have shown that reloading is characterized by an extensive amount of hysteresis (Figure 5-33). However, the soil seems to maintain a memory of the preconsolidation stress (the stress at load reversal at the beginning of unloading), and repeating-unloading reloading cycles follow the same pattern of volumetric expansion and contraction.

Such large hysteresis has been also observed in other smectitic soils; for example, the bentonites studied by Boergesson et al (1996), as shown in Figure 5-8. As discussed in section 5.2.5, adsorption and desorption of water onto the clay surfaces exhibits significant hysteretic characteristics. However, no clear evidence exists to link this hysteresis in the microscopic scale with the hysteresis observed macroscopically.

It is hypothesized that the large volumetric expansion causes irrecoverable strains. In the microscale, this is supported by the mechanism of particle splitting, proposed by Saiyouri et al (2000). Seedsman (1987) expects that deformations on the crystalline scale could lead to local failure of the surrounding fabric. Murray and Quirk (1990) also observed a system of intercluster cracks, in general larger than 200Å, and attributed them to an irreversible formation of separate particles. Yield in expansion has been postulated by Leroueil and Vaughan (1990) and Vaughan (1997) in a study of yield behavior of overconsolidated clays. Alonso & Alcoverro (2002) also introduced a second yield stress associated with unloading.

[44] It should be noted that s is a constant input parameter n the proposed model. Its value is changed here to illustrate the discussed microstructural changes.

In Old Alluvium, the stacks of clay minerals are found randomly oriented within the structure of the aggregates. Double layer expansion leads to increase of the volume occupied by the clay platelet groups, and so to dislocation of the neighboring aggregates and quartz grains at the macro-scale. This is illustrated by the drawing in Figure 5-34. Upon reloading, loading would need to re-arrange the quartz particles and aggregates, before further crushing would be induced. Alonso (1998) postulated a similar scenario for expansive clays, arguing that during unloading the clay layers expand and the macropores increase due to the macrostructural configuration, while during reloading particles reduce in size, but higher pressures are needed to re-arrange the material. This mechanism illustrated in Figure 5-35, which shows how wetting and drying can lead to different macrostructural deformations: wetting leads to adsorption of water by the clay minerals and subsequent expansion of the clay particles, which creates additional macroscopic void spaces, while drying shrinks the clay particles.

Based on the above discussion, it is proposed that the reloading response of the Old Alluvium is characterized by elastoplastic strains. Reloading rearranges the particles dislocated during unloading. However, further crushing only takes place beyond the preconsolidation pressure of the unload-reload cycle. Hence, the Limiting Compression Curve (ρ_c and σ'_{ref}) associated with this preconsolidation pressure can serve as the reference for the reloading response. The proportion of plastic to elastic strains required to reach this reference LCC depends on the amount of volumetric expansion, since the higher the expansion, the more disorder is caused in the macrostructure.

Within the elastoplastic compression model proposed in Chapter 4, the rate of transition to the target limit behavior is expressed by parameter θ. It is hence proposed that the response during reloading can be described with the elastoplastic compression model, where ρ_c and σ'_{ref} are the values that correspond to the LCC associated with the preconsolidation pressure of the unload-reload cycle, and θ varies as a function of the volume recovery:

$$\theta = \theta_p + a_{rl} \exp\left(b_{rl}(e - e_p)\right) \tag{5.47}$$

where a_{rl} and b_{rl} are coefficients that are selected based on the available reload data, e_p the void ratio at the preconsolidation stress level, and θ_p the value of θ at the preconsolidation stress level.

According to Pestana, (1994), for stresses far below the range of crushing, the ratio, $\beta = \frac{\rho_c \theta}{(\sigma'_r / p_a)}$ is a dimensionless material constant. Hence, for the case of evolving compressibility characteristics, the value of θ_p at any preconsolidation stress level can be obtained by:

$$\frac{\theta_p}{\theta_i} = \frac{\rho_{c,i}}{\rho_{c,p}} \frac{\sigma'_{r,p}}{\sigma'_{r,i}} \tag{5.48}$$

where index (i) denotes the initial values of the parameters and (p) the values at the current preconsolidation stress (crushing stress level).

It is rational to expect that the significant expansion of aggregates would result in a decrease of the soil's overall stiffness; upon the load reversal following unloading, C_b should be lower; its value should also depend of the amount of volume expansion. There are no data to support any such law of C_b evolution, hence here a simple linear relationship is proposed:

$$C_b = \left[1 - (e - e_p)\right] C_{bp} \tag{5.49}$$

where again (p) denotes the values at the preconsolidation stress level.

An application of the discussed approach for the Old Alluvium is shown in Figure 5-36. Parameters a_{rl} and b_{rl} are selected based on the unload-reload cycle of test 101 at σ'_p = 640ksc. The figure shows the resulting response for other preconsolidation pressures of test 101 and also for test SJ2. Even though the proposed approach is based on a high degree of speculation, it describes well the hysteresis observed during the compression tests, and the overall reversibility of the unload-reload cycles.

Figure 5-37 plots the reloading response for various degrees of volumetric expansion according to the proposed approach, and illustrates how the state variables θ and C_b evolve during unloading. The predictions reflect the principles discussed above, however it is difficult to evaluate them without relevant experimental data. Multiple reloading cycles from various levels of overconsolidation ratios and elastic measurements (e.g., bender element tests) are required to better understand the unloading-reloading behavior and hence, model it properly.

5.6 SUMMARY

This chapter presented the formulation of a new swelling model, which is based on the electric double layer theory and aims to describe the volumetric expansion behavior of materials characterized by the presence of swelling minerals in their microstructure.

The model depends on the Cation Exchange Capacity at load reversal, which is a direct measure of the physicochemical status of the soil. It requires as input an estimation of the amount of expandable minerals in the microstructure, and of the degree of initial hydration of the clay mineral stacks. In addition, the formulation uses a transfer function to account for the interaction between the microstructural double layer changes and the observed macro-scale deformations. The function also depends on the degree of initial clay hydration and on a third parameter that controls the amount of micro-macro interaction.

The new model has a structure similar to the swelling model in MIT-S1. However, the main coefficients have a physical basis from the double layer theory and are closely associated with the physicochemical characteristics of the soil, using Cation Exchange Capacity as a key state variable that evolves with crushing of the Old Alluvium.

Comparison of the model predictions with the available unloading data showed that the formulation is able to describe very well the volumetric expansion at a range of preconsolidation stresses.

Beyond Old Alluvium, the model has the potential to describe more generally the unloading behavior of clayey materials that include stacks of expandable (clay) minerals, because it is built on the double layer theory, and it depends on some measure of the physicochemical characteristics of the soil. Indeed, it was successfully applied to other materials such as some clayey shales and certain clays.

Finally, it was proposed to describe the reloading response as an elastoplastic compression of the particles that have been dislocated and expanded (in the case of the aggregates) during unloading. The approach uses the Limiting Compression Curve of the preconsolidation stress level as a tangent limit state and varies the degree of elastoplastic transition to this LCC depending on the amount of volumetric expansion experienced during the unloading. However, the reloading behavior is poorly understood and further testing is required.

5.7 REFERENCES

Alonso E, Vaunat J, Gens A. (1999): "Modelling the mechanical behavior of expansive clays", Engineering Geology, 54, 173–183.

Alonso E. (1998): "Modelling expansive soil behaviour", Proceedings of the 2nd International Conference on Unsaturated Soils, Beijing, China, 2, 37-70.

Alonso E.E., Alcoverro J. (2002): "Swelling and Degradation of Argillaceous Rocks", Proceedings of the 3rd International Conference on Unsaturated Soils, Recife, Brazil, 3, 951-969.

Alonso, E.E., Gens A., Josa A. (1990): "A constitutive model for partially saturated soils", Géotechnique, 40 (3), 405-430.

Banks D.C., Strohm W.E., DeAngulo M., Lutton R. (1975): "Study of Clay Shale Slopes along the Panama Canal", Technical Report S-70-9, Report 3 of a Series, U.S. Army Engineer Waterways Experiment Station, Vioksburg, Mississippi.

Berryman J.G. (2002): "Extension of poroelastic analysis to double porosity materials: new technique in microgeomechanics", Journal of Engineering Mechanics, 128 (8), 840-847.

Berryman J.G., Wang H.F. (1995): "The elastic coefficients of double porosity models for fluid transport in jointed rock", Journal of Geophysical Research, 100, 24611-24627.

Boergesson L., Karnland O. and Johannesson L.E. (1996): "Modelling of the physical behaviour of clay barriers close to water saturation", Engineering Geology 41, 127–144.

Bolt G. H. (1956): "Physico-chemical analysis of the compressibility of pure clays", Géotechnique, 6 (2), 867-93.

Calabresi G., Scarpelli G. (1985): "Effects of swelling caused by unloading in overconsolidated clays", Proceedings 11th ICSMFE, 2, 411-414.

Casagrande A. (1936): "Characteristics of cohesionless soils affecting the stability of slopes and earth fills", Journal of Boston Society of Civil Engineers, 23 (1), 13-32.

Chapman D.L. (1913): "A contribution to the theory of electro-capillarity", Philosophical Magazine, 25, 475–481.

Chipera S.J., Carey J.W., Bish D.L. (1997): "Controlled humidity XRD analyses: Application to the study of smectite expansion/contraction", Advances in X-Ray analysis, 39, 713-722.

Delville A. (1991): "Modeling the clay–water interface", Langmuir 7, 547–555.

Di Maio C. (1996): "Exposure of bentonite to salt solution: osmotic and mechanical effects", Géotechnique, 46 (4), 695-707.

Di Maio C., Santoli L., Schiavone P. (2004): "Volume change behaviour of clays: the influence of mineral composition, pore fluid composition and stress state", Mechanics of Materials 36, 435–451.

Diaz C., Fernardo A. (1987): "An experimental investigation of the engineering behavior of natural shales", PhD Thesis, University of Illinois at Urbana-Champaign.

Dormieux L., Barboux P., Coussy O., Danglia P. (1995): A microscopic model of the swelling phenomenon of a saturated clay", European Journal of Mechanics and Solids, 14 (6), 981-1004.

Dormieux L., Lemarchand E., Coussy O. (2003): "Macroscopic and Micromechanical Approaches to the Modelling of the Osmotic Swelling in Clays", Transport in Porous Media 50, 75–91.

Dormieux L., Lemarchand E., Sanahuja J. (2006): "Comportement macroscopique des matériaux poreux à microstructure en feuillets", C. R. Mecanique 334, 304–310

Fernández, A., Santamarina, C. (2001): "The effect of cementation on the small strain parameters of sand". Canadian Geotechnical Journal, 38 (1), 191-199.

Fleming R.W., Spencer G.S., Banks D.C. (1970): "Empirical study of behavior of clay shale slopes", NCG Technical Report No 15 (2 vols.), U.S. Army Engineer Nuclear Cratering Group, Livermore, California.

Fu M.H., Zhang Z.Z., Low P.F. (1990): "Changes in the properties of a montmorillonite-water system during the adsorption and desorption of water: hysteresis", Clay and Clay Minerals, 38 (5), 485-492.

Gens, A., Alonso, E. (1992): "A framework for the behavior of unsaturated expansive clays", Canadian Geotechnical Journal, 29, 1013-1032

Gouy G. (1910): "Electric charge on the surface of an electrolyte", Journal of Physics, 4 (9), 457.

Huang W.L., Bassett W.A., Wu T.C. (1994): "Dehydration and rehydration of montmorillonite at elevated temperatures monitored using synchrotron radiation", American Mineralogist, 79, 683-691.

Israelachvili J. (1991): Intermolecular and surface forces, Academic Press, London, UK.

Komine H., Ogata N. (1999): "Experimental study on swelling characteristics of sand-bentonite mixture for nuclear waste disposal", Soils and Foundations, 39 (2), 83-97.

Komine H., Ogata N. (2003): "New equations for swelling characteristics of bentonite-based buffer materials", Canadian Geotechnical Journal, 40 (2), 460-475.

Komine H., Ogata N. (2004): "Predicting Swelling Characteristics of Bentonites", Journal of Geotechnical and Geoenvironmental Engineering, 130 (8), 818 – 829.

Langmuir I. (1938): "The role of attractive and repulsive forces in the formation of tactoids, thixotropic gels, protein crystals and coacervates", Journal of Chemical Physics, 6, 873-896.

Lemarchand E., Dormieux L., Ulm F.J. (2005): "Micromechanics investigation of expansive reactions in chemoelastic concrete", Philosophical Transactions of the Royal Society A, 363, 2581–2602

Leroueil S. (2000): "Contribution to Round Table: Peculiar aspects of structured soils", The Geotechnics of Hard Soils – Soft Rocks, Evangelista & Picarelli (editors), Balkema, 1669-1678.

Likos W.J. (2004): "Measurement of Crystalline Swelling in Expansive Clay", Geotechnical Testing Journal, 27 (6), 1-7.

Likos W.J., Lu N. (2006): "Pore-Scale Analysis of Bulk Volume Change from Crystalline Interlayer Swelling in Na^+ and Ca^{2+} Smectite", Clays and Clay Minerals, 54 (4), 515-528.

Loret B., Hueckel T., Gajo A. (2002): "Chemo-mechanical coupling in saturated porous media: elastic-plastic behavior of homoionic expansive clays", International Journal of Solids and Structures, 39, 2773-2806.

Madsen F.T., Mueller-Vonmoos M. (1985): "Swelling pressure calculated from mineralogical properties of a Jurassic opalinum shale, Switzerland", Clays and Clay Minerals, 33 (6), 501-509.

Mesri G., Olson R.E. (1971): "Consolidation characteristics of montorillonite", Géotechnique, 21 (4), 341-352.

Mitchell J.K., Soga K. (2005): Fundamentals of Soil Behavior, John Wiley & Sons, New York, N.Y, 3rd edition.

Murad M.A. (1999): "Thermomechanical model of hydration swelling in smectitic clays: I two-scale mixture-theory approach, II three-scale inter-phase mass transfer: homogenization and computational validation", International Journal of Numerical and Analytical Methods in Geomechanics, 23, 673-719.

Murray R.S., Quirk J.P. (1990): "Intrinsic failure and cracking of clay", Soil Science Society of America Journal, 54 (4), 1179–1184.

Norrish K. (1954): "The swelling of montmorillonite", Faraday Society, London, Discussions 18, 353–359.

Pestana J.M. (1994): "A unified constitutive model for clays and sands", Sc.D thesis, Massachusetts Institute of Technology, Cambridge, MA.

Peterson R. (1958): "Rebound in Bearpaw shale", Geologic Society of America, Bulletin, 69, 1113-1124.

Picarelli L. (1991): Discussion on the paper: "The general and congruent effects of structure in natural soils and weak rocks" by S. Leroueil and P.R. Vaughan, Géotechnique, 40 (2), 281-284.

Picarelli L., Olivares L., DiMaio C., Urcioli G. (2000): "Properties and behaviour of tectonized clay shales in Italy", The Geotechnics of Hards Soils Soft Rocks, Balkema, 1211-1214.

Pinyol N. (2008): Personal communication.

Pons C.H., Rousseaux F., Choubar D. (1981): "Utilisation du rayonnement synchrotron en dillusion aux petits angles pour l' étude du gonflement des smectites. I: Etude du système eau-montmorillonite-Na en fonction de la température", Clay Minerals, 16, 23-42.

Saiyouri N., Hicher P.Y., Tessier D. (2000): "Microstructural approach and transfer water modelling in highly compacted unsaturated swelling clays", Mechanics of Cohesive-Frictional Materials, 5, 41-60.

Sánchez M., Gens A., Guimaraes L.N., Olivella S. (2005): "A double structure generalized plasticity model for expansive materials", International Journal of Numerical and Analytical Methods in Geomechanics, 29, 751 – 787.

Schofield A., Wroth C.P. (1968): Critical State Soil Mechanics, McGraw Hill, London.

Seedsman R.W. (1987): "Strength implications of the crystalline and osmotic swelling of clays in shales", International Journal of Rock Mechanics, Mineral Sciences and Geomechanics, Abstracts, 24 (6), 357-363.

Sposito G., Prost R. (1982): "Structure of water adsorbed on smectites", Chem. Rev., 82 (6), 552–573.

Sposito G., Skipper N.L., Sutton R., Park S.-H., Soper A.K., Greathouse J.A. (1999): "Surface geochemistry of the clay minerals", Proceedings of the National Academy of Science, USA, 96, 3358–3364.

Sridharan A., Jayadeva M.S. (1982): "Double layer theory and compressibility of clays", Géotechnique, 32 (2), 133-144.

Tourtelot H.A. (1962): "Preliminary investigation of the geologic setting and chemical composition of the Pierre Shale, Great Plains Region, U.S. Geol. Surv. Prof. Pap., 390.

Tripathy S., Sridharan A., Schanz T. (2004): "Swelling pressures of compacted bentonites from diffuse double layer theory", Canadian Geotechnical Journal, 41, 437-450.

van Olphen H. (1963): "An introduction to clay colloid chemistry: for clay technologists, geologists and soil scientists", Interscience, New York.

van Olphen H. (1977): "An Introduction to Clay Colloid Chemistry", Interscience Publications, New York.

Vaughan P. (1997): "Engineering behavior o weak rocks: some answers and some questions", Geotechnical Engineering of Hard Soils-Soft Rocks, Balkema, 1741-1765.

Verburg K., Baveye P. (1995): "Effect of cation Exchange hysteresis on a mixing procedure in the study of clay suspensions", Note, Clays and Clay minerals, 43 (5), 637-640.

Verwey E.J.W., Overbeek J.T.G. (1948): "Theory of the stability of lyophobic colloids", Elsevier, Amsterdam.

Yong R.N. (1999a): "Soil suction and soil-water potentials in swelling clays in engineered clay barriers", Engineering Geology 54, 3–13.

Yong R.N. (1999b): "Overview of modeling of clay microstructure and interactions for prediction of waste isolation barrier performance", Engineering Geology 54, 83–91.

Yong R.N., Warkentin B.P. (1975): "Soil properties and behaviour", Elsevier, New York.

Zhang, G. (2002): "Laboratory Characterization of a Highly Weathered Old Alluvium in San Juan, Puerto Rico", PhD thesis, MIT, Cambridge, MA.

Parameter	2m	4m	6m	8m	10m	12m	14m
C_b	950	950	950	950	950	950	950
θ	0.2	0.22	0.24	0.26	0.28	0.3	0.32
$\rho_{c,i}$	0.28	0.275	0.27	0.265	0.26	0.255	0.25
$\sigma_{ref,i}$/pa	5.5	5	4.5	4	3.5	3	2.5
cec_i	29	(29) 30	31	32	33	34	35
cec_f	52	(52) 51	50	49	48	47	(45) 46
σ'_o/pa	60	70	80	90	100	110	120
σ'_m/pa	350	300	250	200	150	150	150
n	0.3	0.3	0.3	0.3	0.3	0.3	0.3
s	0.85	0.8	0.75	0.7	0.65	0.6	0.55
n_T	0.6	0.55	0.5	0.45	0.4	0.35	0.3
d_i (Å)	6.5	6.5	6.5	6.5	6.5	6.5	6.5
Void Ratio	1.1	1.0	0.9	0.7	0.5	0.4	0.3

To account for the presence of cementation C_{bi} = 1200 at stress levels below the yield point.

Table 5-1: Complete selection of input parameters with depth, for the Old Alluvium

Material	w_l (%)	I_p (%)	Clay fraction	Cementation	Hydrated layers	e_0	Assumed input parameters			
							$2d_i$ (Å)	s	n_T	CEC_p (meq/100g)
Pierre Shale	36-113	113	12-40% montm.	Fe/Mn Oxide	1-2	0.84	16	0.75	0.55	45
Bearpaw Shale	80-150	140	50% clay	-	2-3	0.62	20	0.2	0.3	25
Fort Union Shale	89	69		-	1-2	0.55	16	0.5	0.53	25
Cucaracha Shale	-	-	-	-	1-2	0.56	16	0.25	0.4	35
Todi Clay	57.9	28.1	3-5% clay	-	1-2	0.51	16	0.2	0.6	25

Table 5-2: Mineralogical properties and assumed input parameters for the clayey materials discussed in 5.4.5.

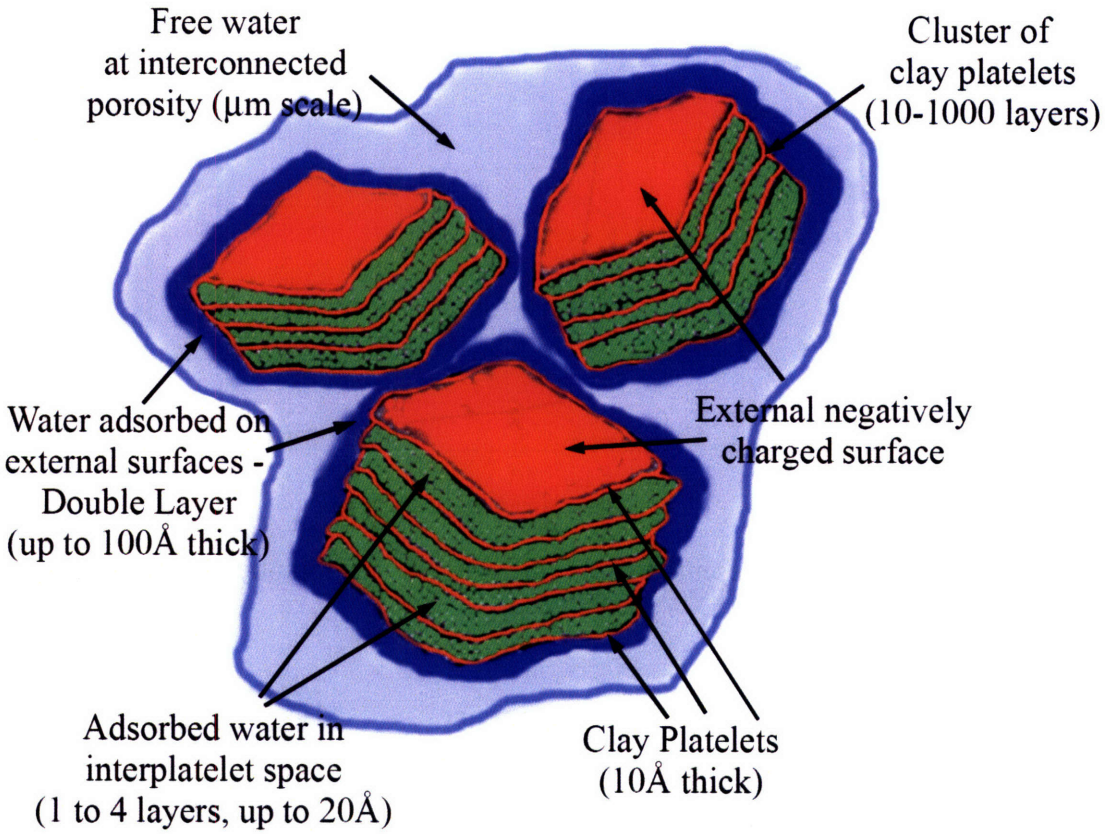

Figure 5-1: Representation of clay microstructure (after Loret et al, 2002).

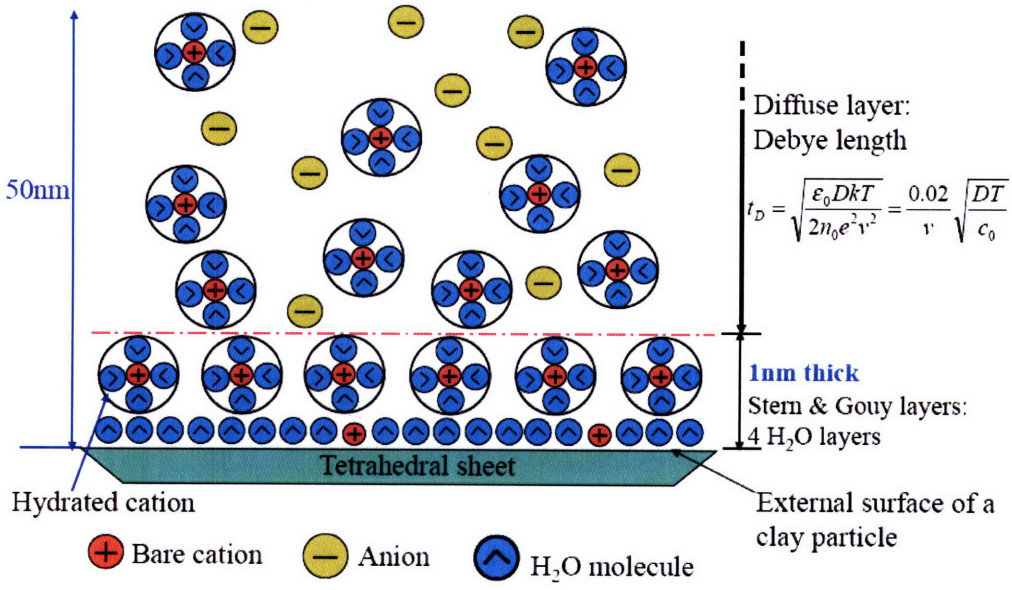

Figure 5-2: Schematic representation of the hydrated layer and the diffuse double layer (Zhang, personal communication).

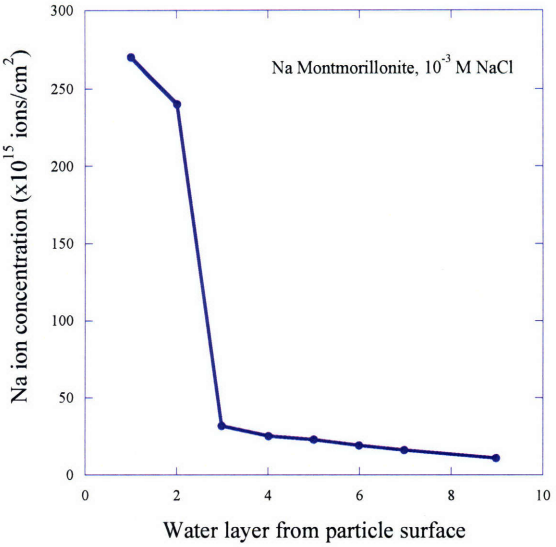

Figure 5-3: Theoretical representation of dilution of ions plotted against the number of adsorbed/absorbed water layers (Yong, 1999).

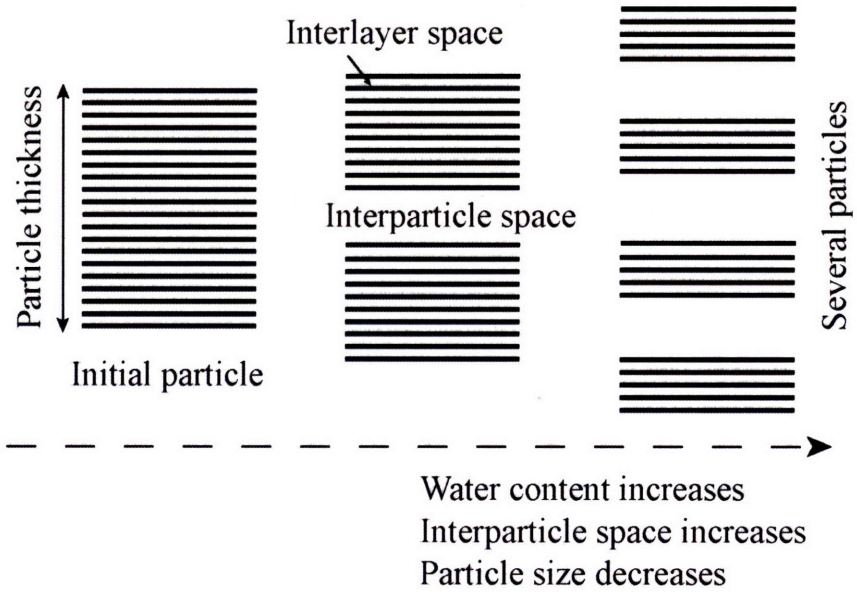

Figure 5-4: Schematic representation by Saiyouri et al (2000) of clay particle splitting due to saturation of the interlayer space.

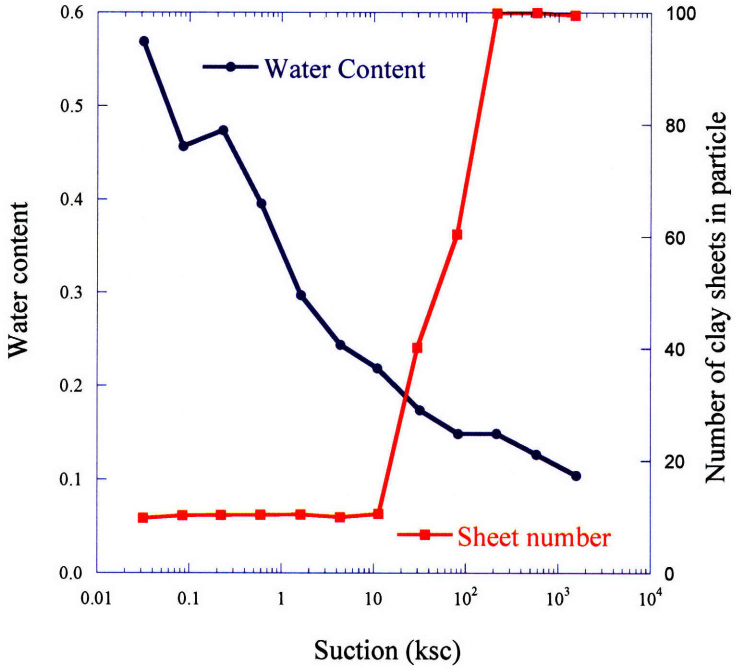

Figure 5-5: Result of X-Ray analyses reported by Saiyouri et al (2000) showing the estimated number of clay sheets per particle related to the amount of water uptake by the clay microstructure (about 100 layers for low values of the water content, but as little as 10 layers when the water content increases).

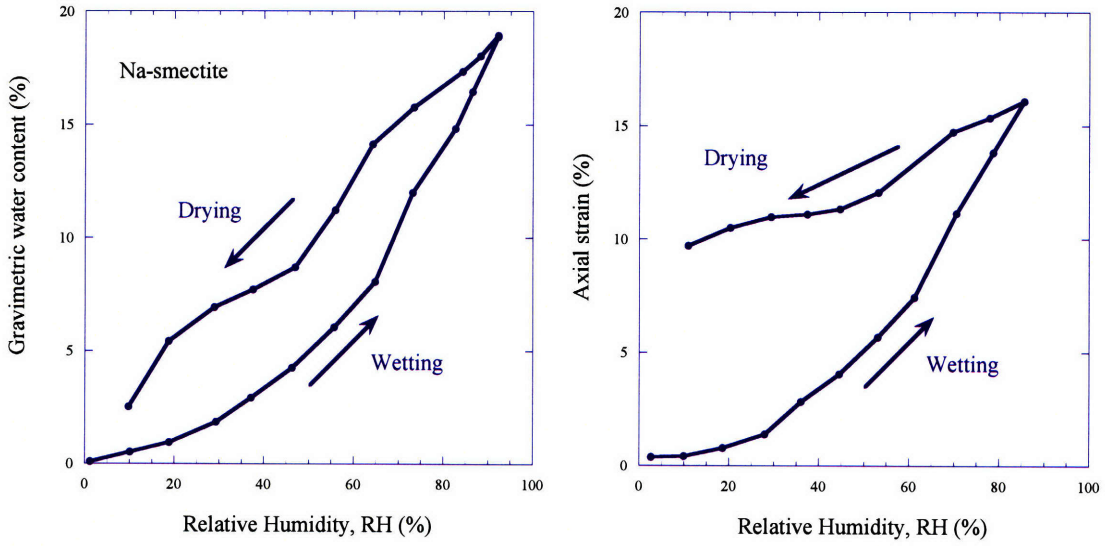

Figure 5-6: Wetting and drying cycle on Na smectite showing hysteretic behavior and 9.75% residual strain (Likos, 2004).

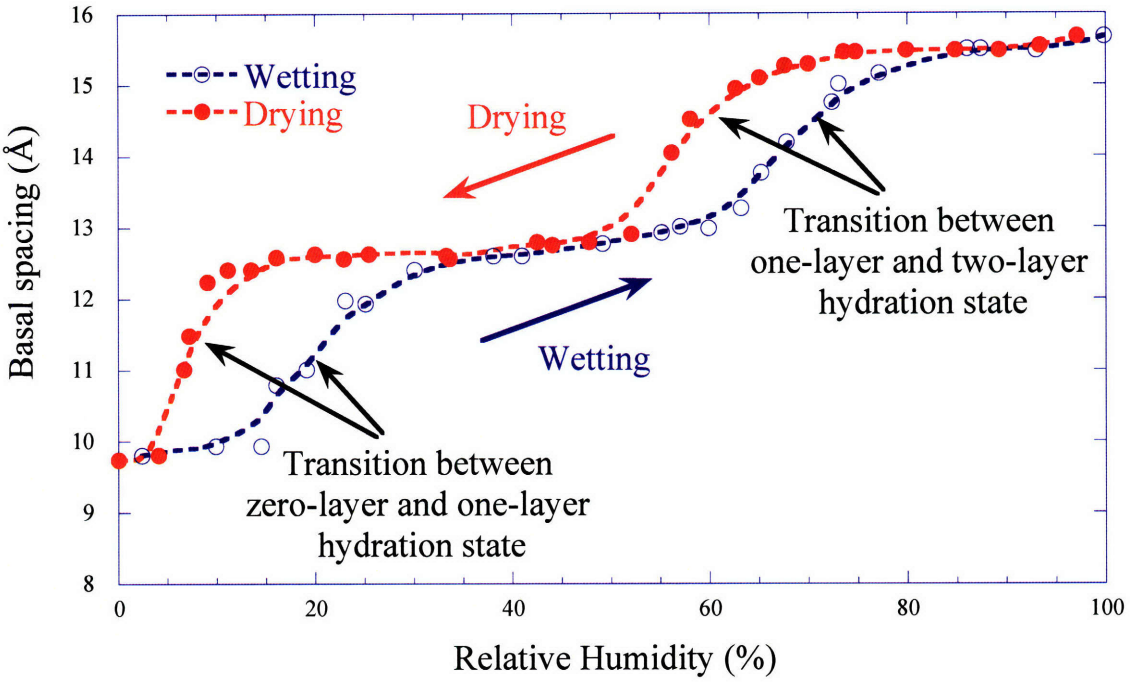

Figure 5-7: Measured basal spacing for Na-smectite as a function of the relative humidity during wetting and drying (Likos, 2004, after Chipera et al, 1997).

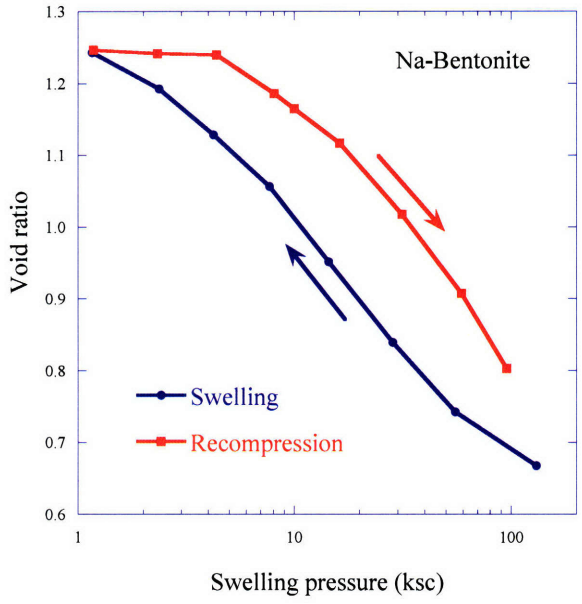

Figure 5-8: Swelling-compression oedometer test on Na-bentonite showing significant hysteresis between the unloading and the reloading curve (after Boergesson et al, 1996).

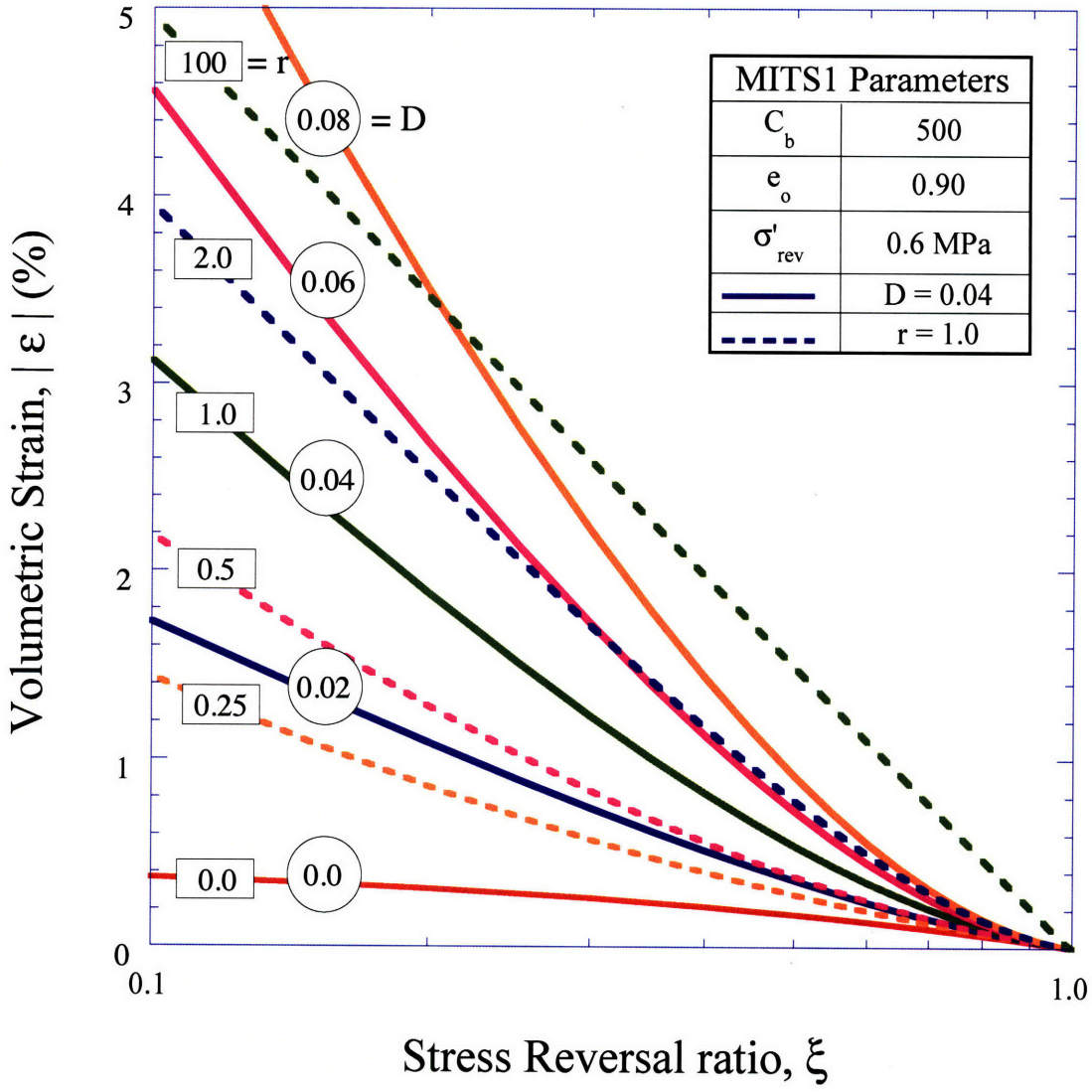

Figure 5-9: Parametric analyses on the input parameters D and r of the MIT-S1 formulation (Pestana, 1994).

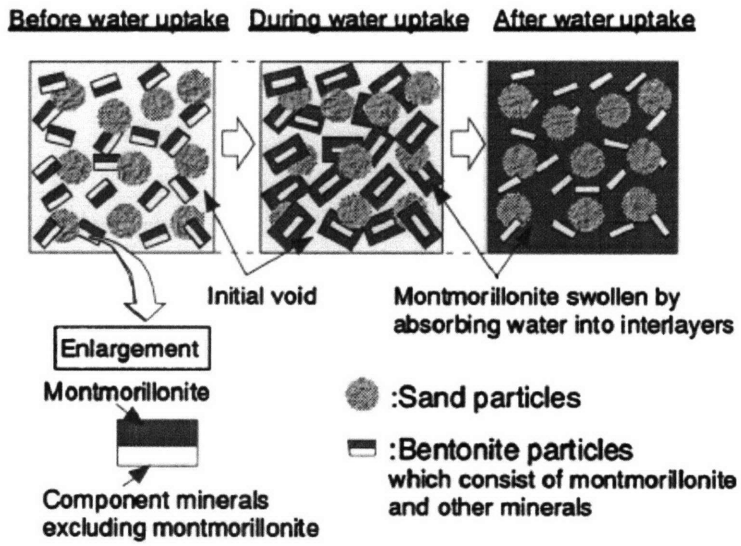

Swelling pressures with swelling deformation restricted

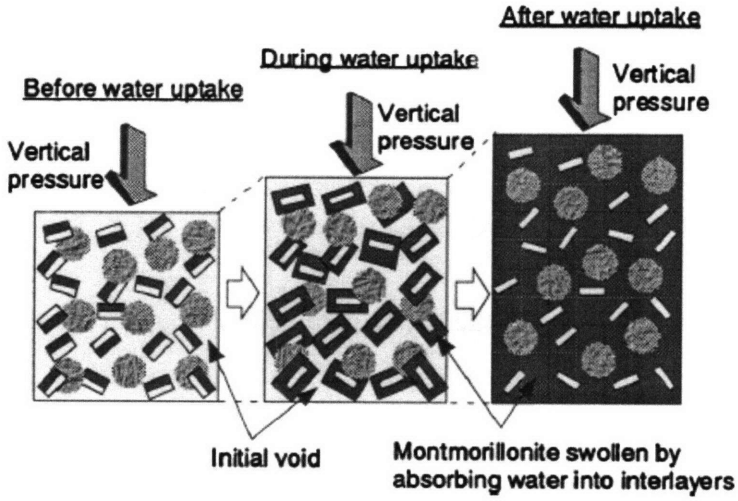

Swelling deformation at constant vertical pressure

Figure 5-10: Illustration of the process of swelling behavior of buffer materials, for the case restricted deformation (top) and constant vertical pressure (unrestricted deformation, bottom), after Komine and Ogata, 2004.

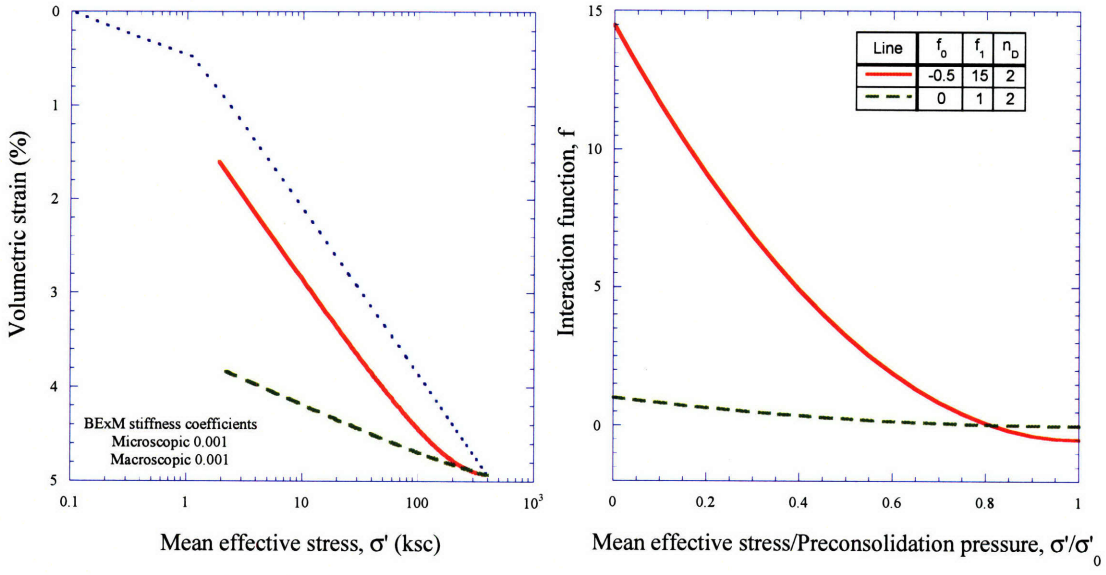

Figure 5-11: Example of the effect of the interaction function proposed by the Barcelona group (BExM) for the case of unloading. The solid line shows a much stronger interaction between the microstrains and the macroscopic expansion (Pinyol, 2008).

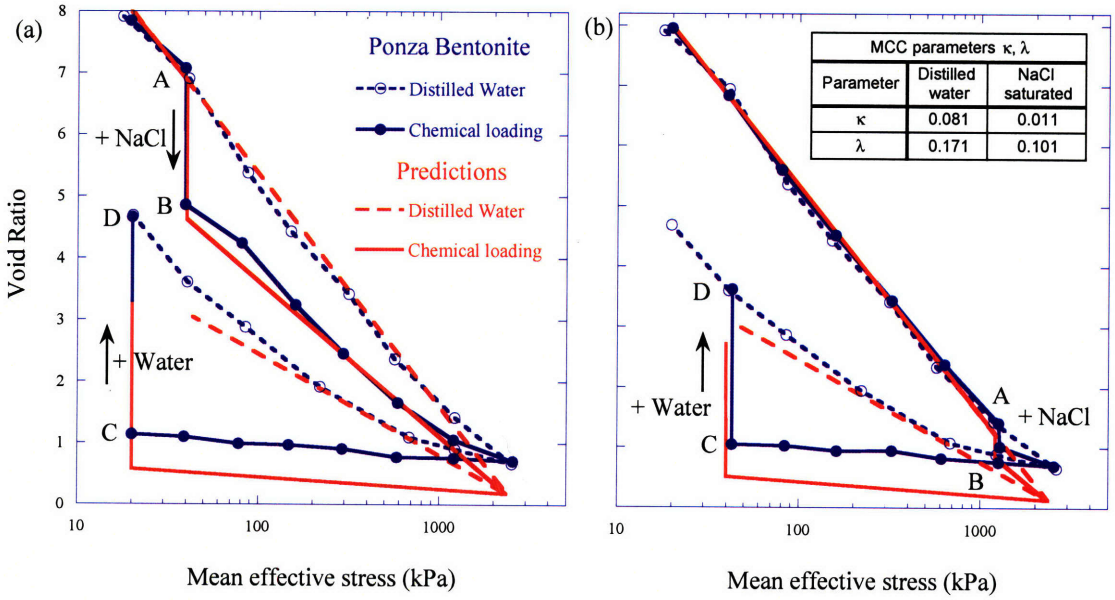

Figure 5-12: Application of the chemo-mechanical model proposed by Loret et al (2002) to chemical loading on Ponza bentonite (diMaio, 1996). Dashed lines correspond to pure mechanical loading with distilled water, while solid lines correspond to chemical loading (addition of NaCl and or distilled water, as noted).

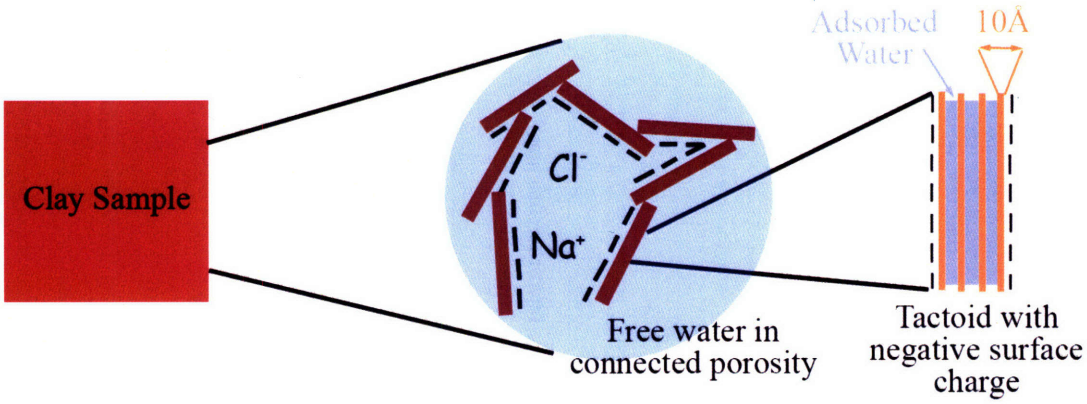

Figure 5-13: Macro- and micro-structural representation of an expansive clay (Dormieux et al, 1995).

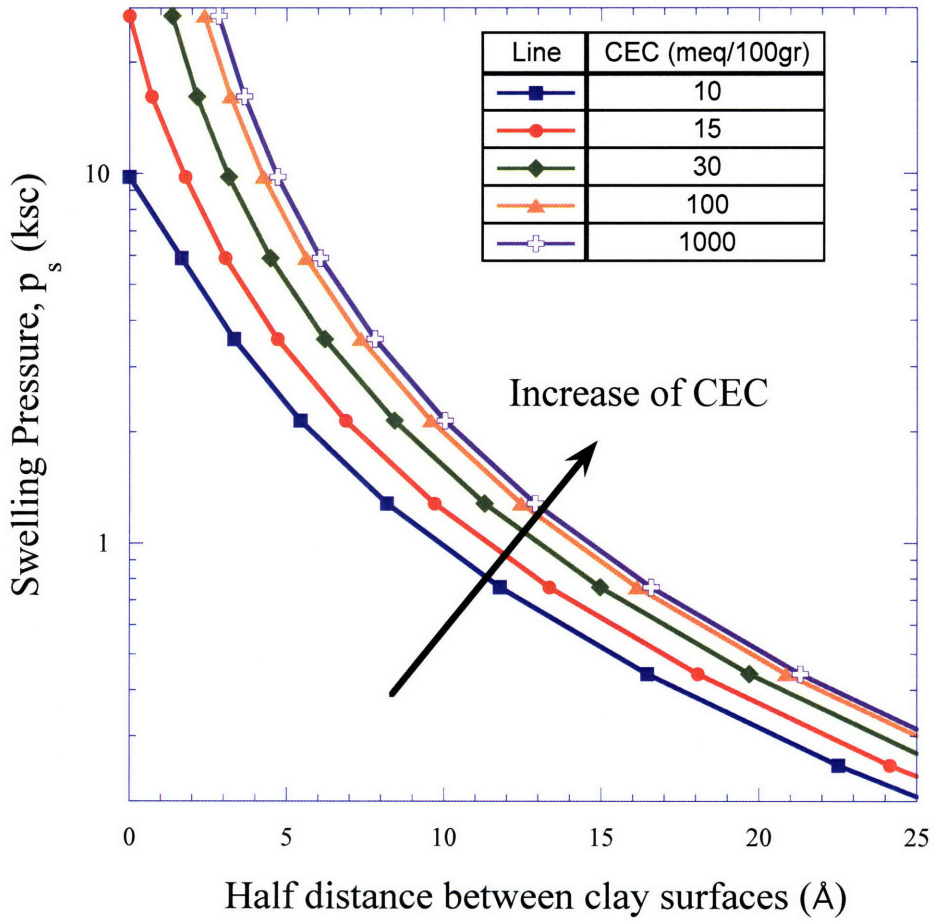

Figure 5-14: Prediction of swelling pressure from thickness of double layer, based on method proposed by Madsen & Mueller-Vonmoos, 1985.

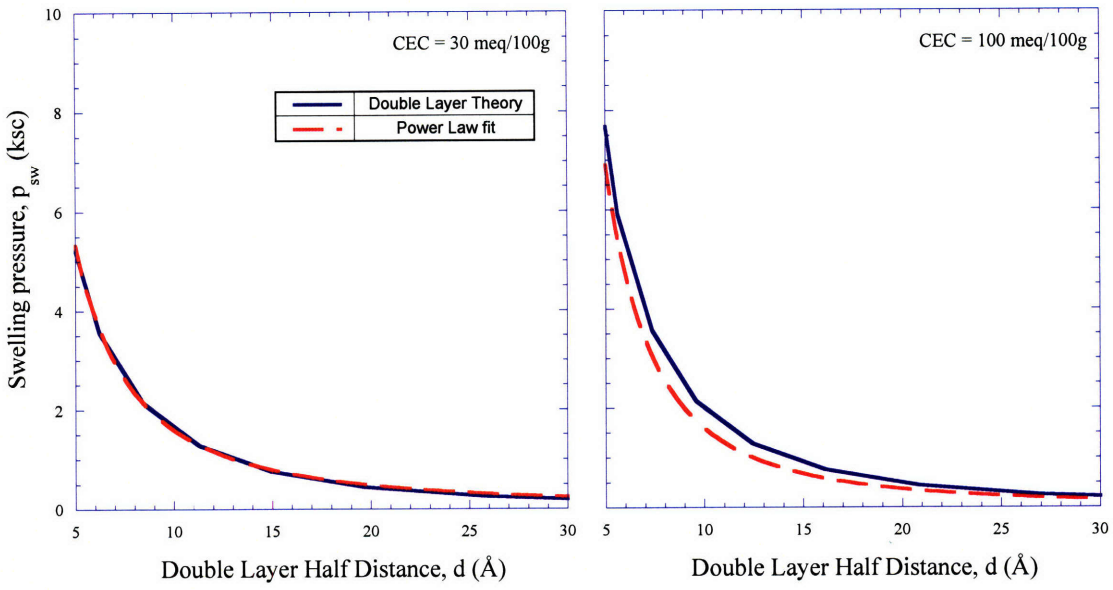

Figure 5-15: Comparison of swelling pressure predictions between double layer theory and power law fit, for CEC values of 30 and 100 meq/g.

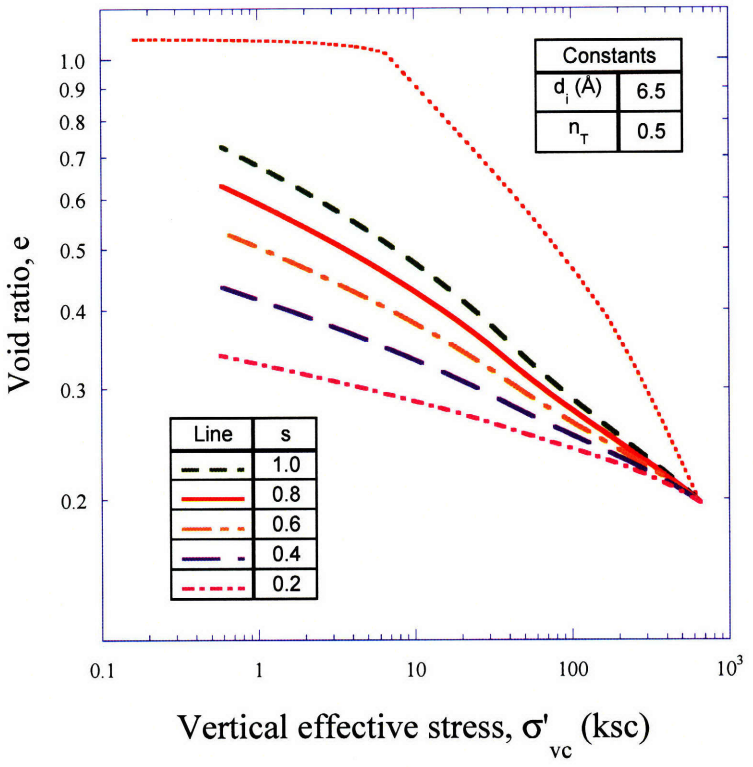

Figure 5-16: Parametric analysis on parameter s of the swelling model.

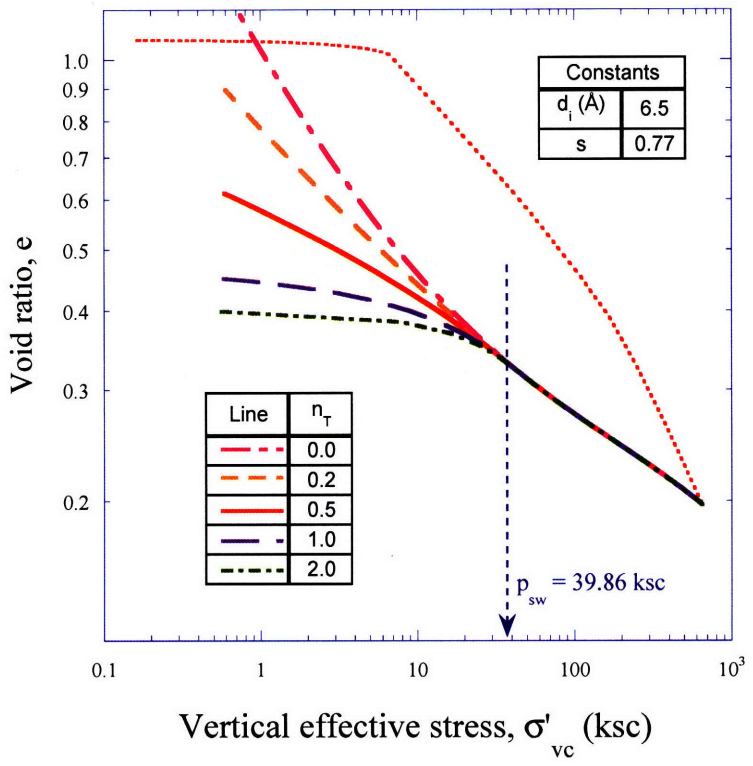

Figure 5-17: Parametric analysis on parameter n_T of the swelling model.

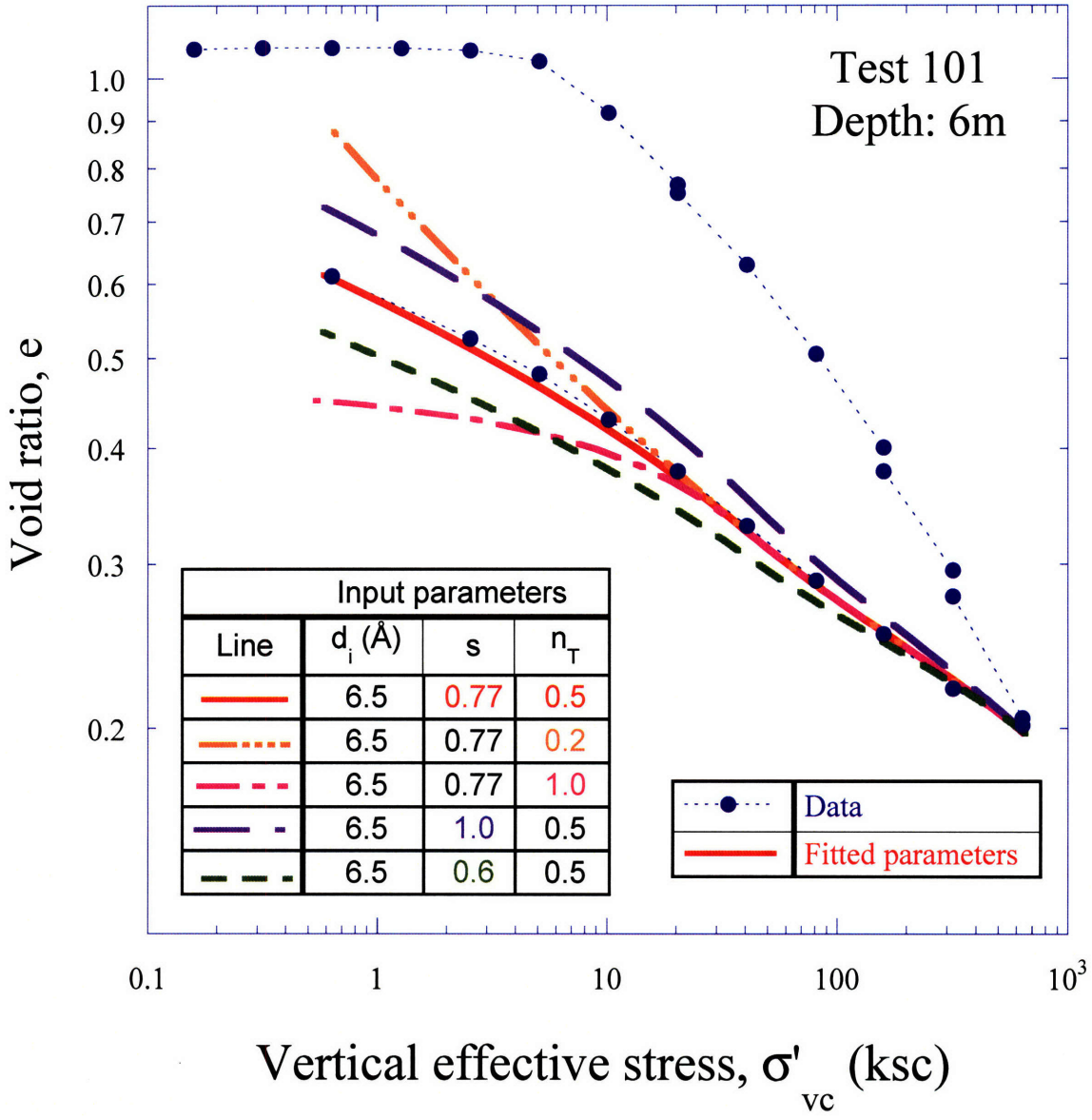

Figure 5-18: Selection of input parameters s and n_T from test 101 observed data .

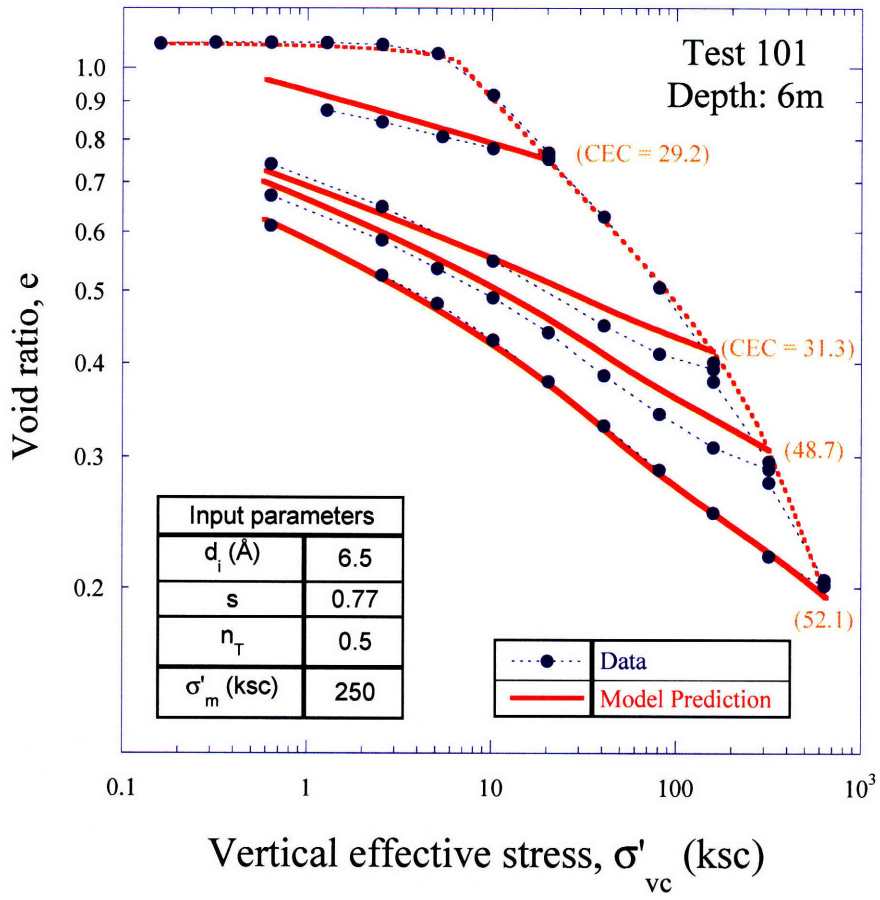

Figure 5-19: Predictions of the unloading behavior of Old Alluvium (test 101), for preconsolidation pressures σ'_p = 317 ksc, 158ksc, and 20ksc. The values of state variable CEC are noted next to each reversal point.

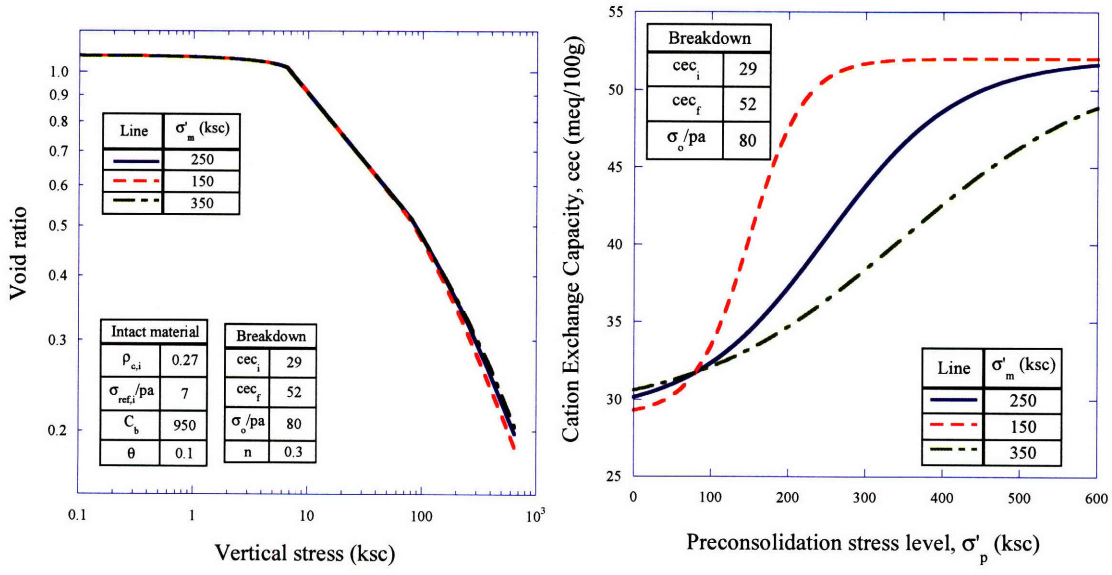

Figure 5-20: Effect of input parameter σ'_m on the predictions of the first loading compression curve and on predictions of the evolution of Cation Exchange Capacity.

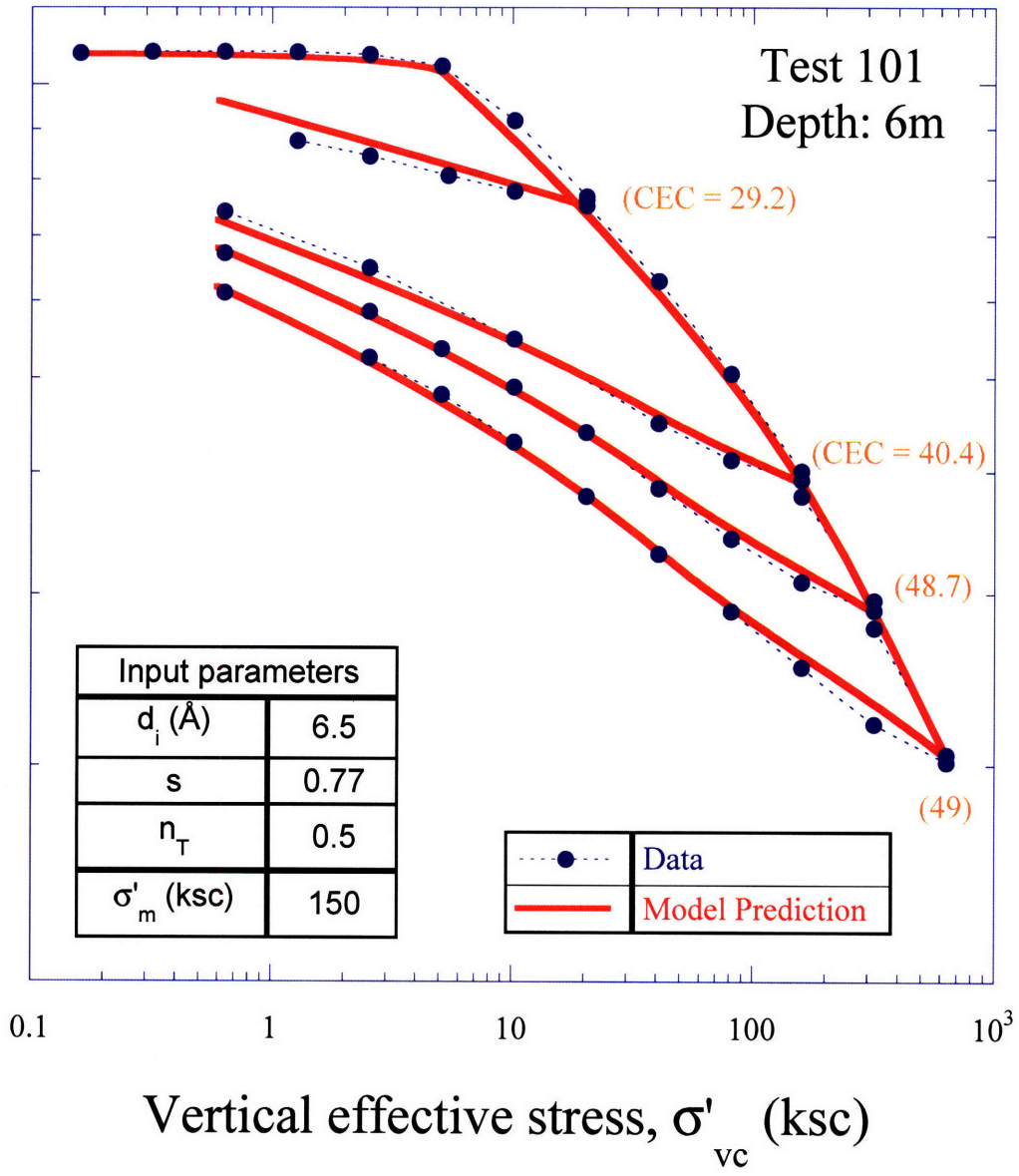

Figure 5-21: Predictions of the unloading behavior of Old Alluvium (test 101), with re-evaluation of input parameter σ'_m.

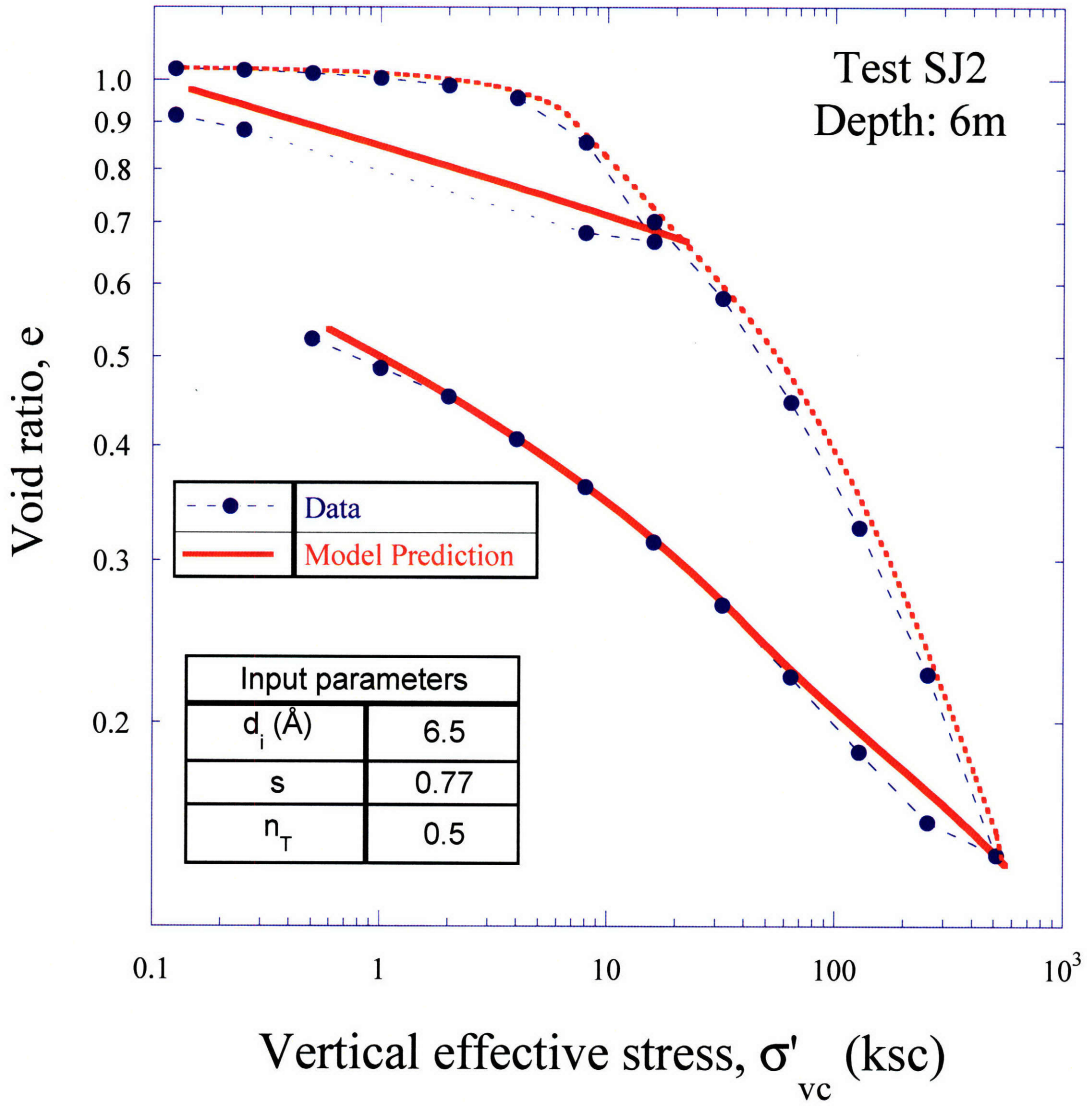

Figure 5-22: Model prediction for the unloading behavior observed in test SJ2.

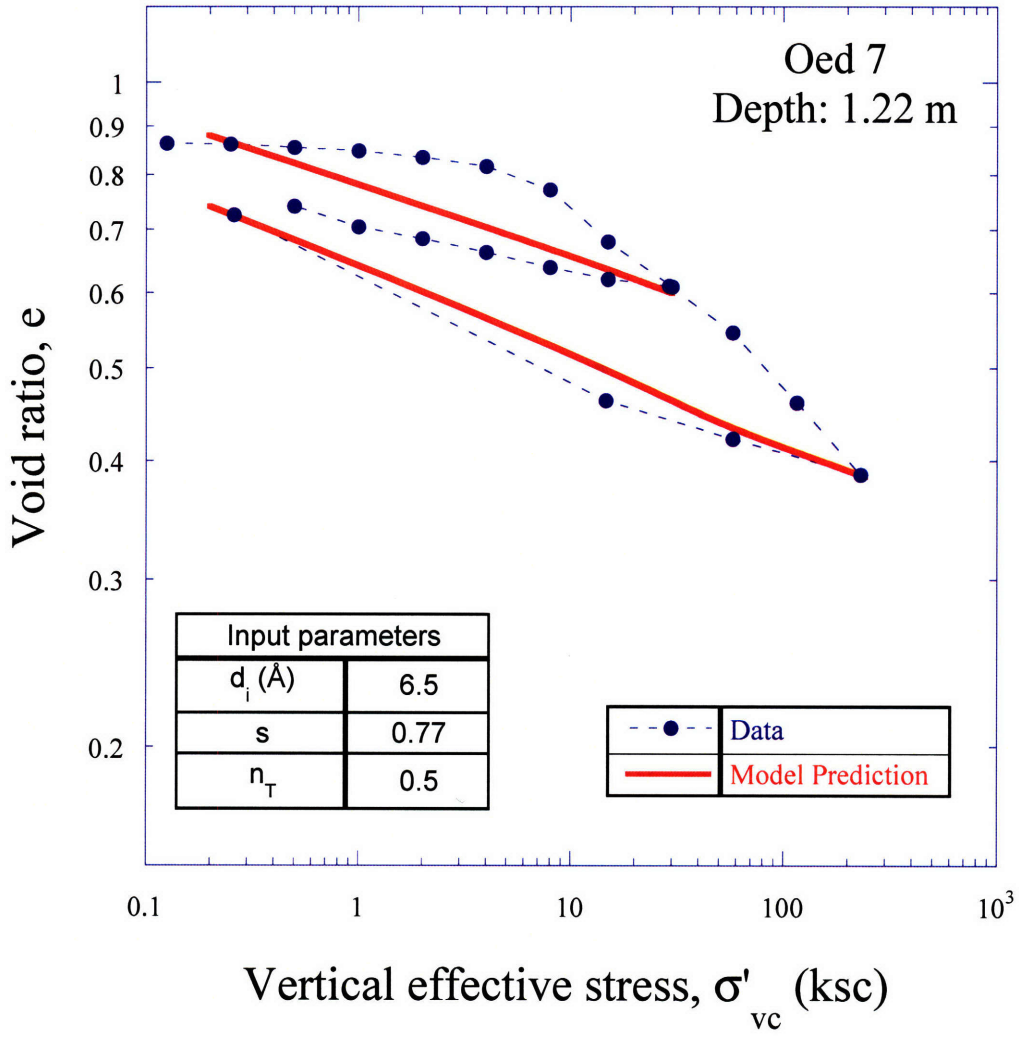

Figure 5-23: Model prediction for the unloading behavior observed in test Oed7.

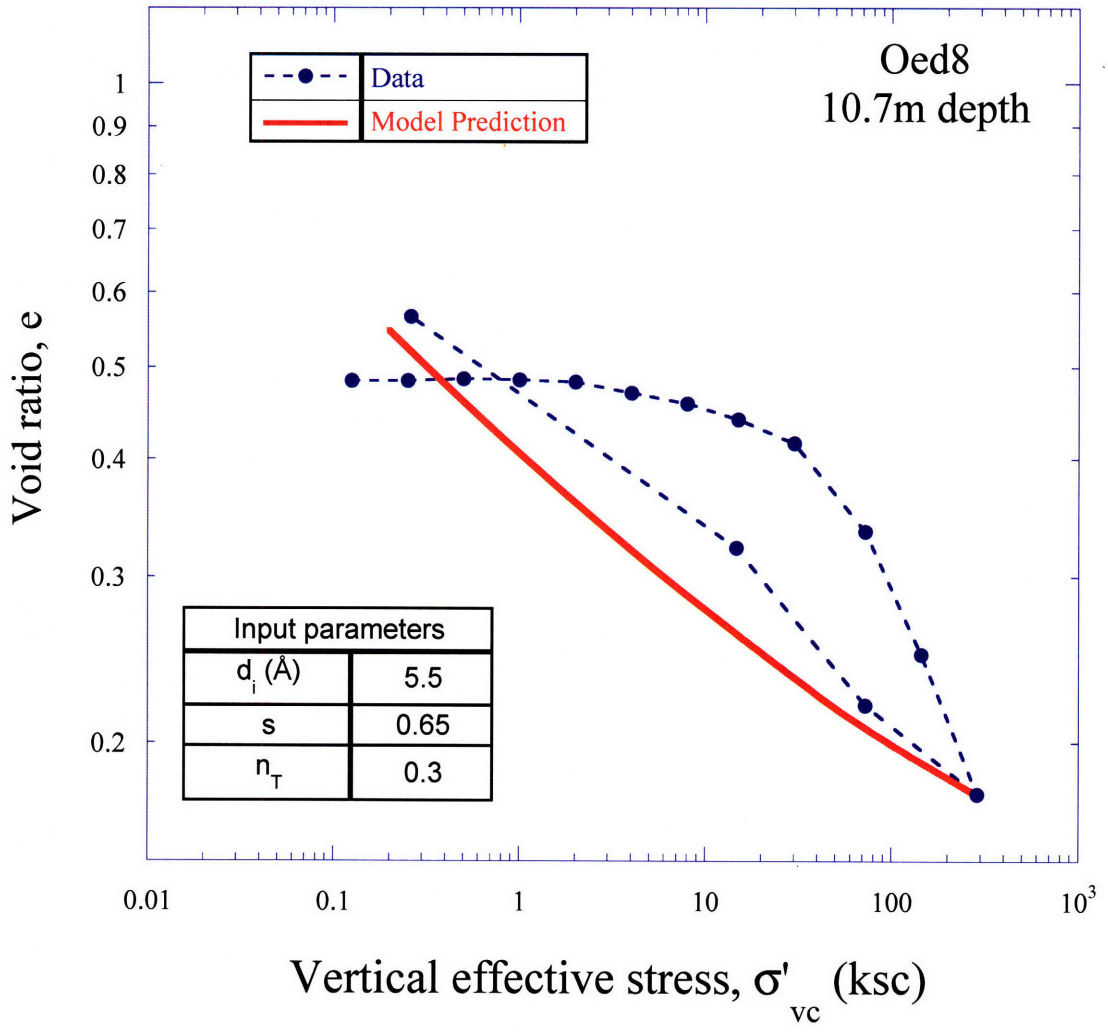

Figure 5-24: Model prediction for the unloading behavior observed in test Oed8 (Middle Zone).

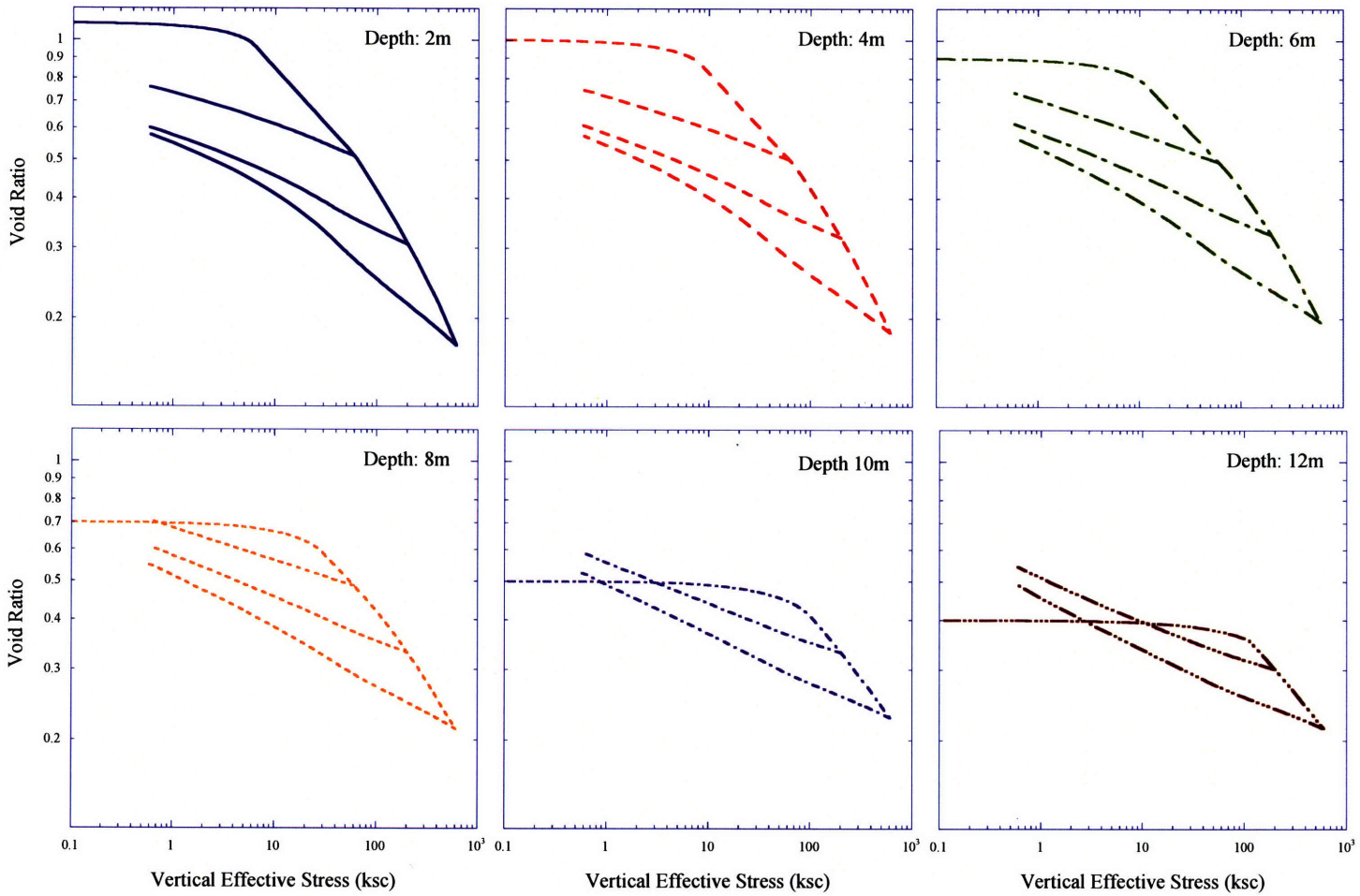

Figure 5-25: Predictions of the load-unload behavior at various depths in the Old Alluvium. The input parameters for each depth are listed in Table 4-4.

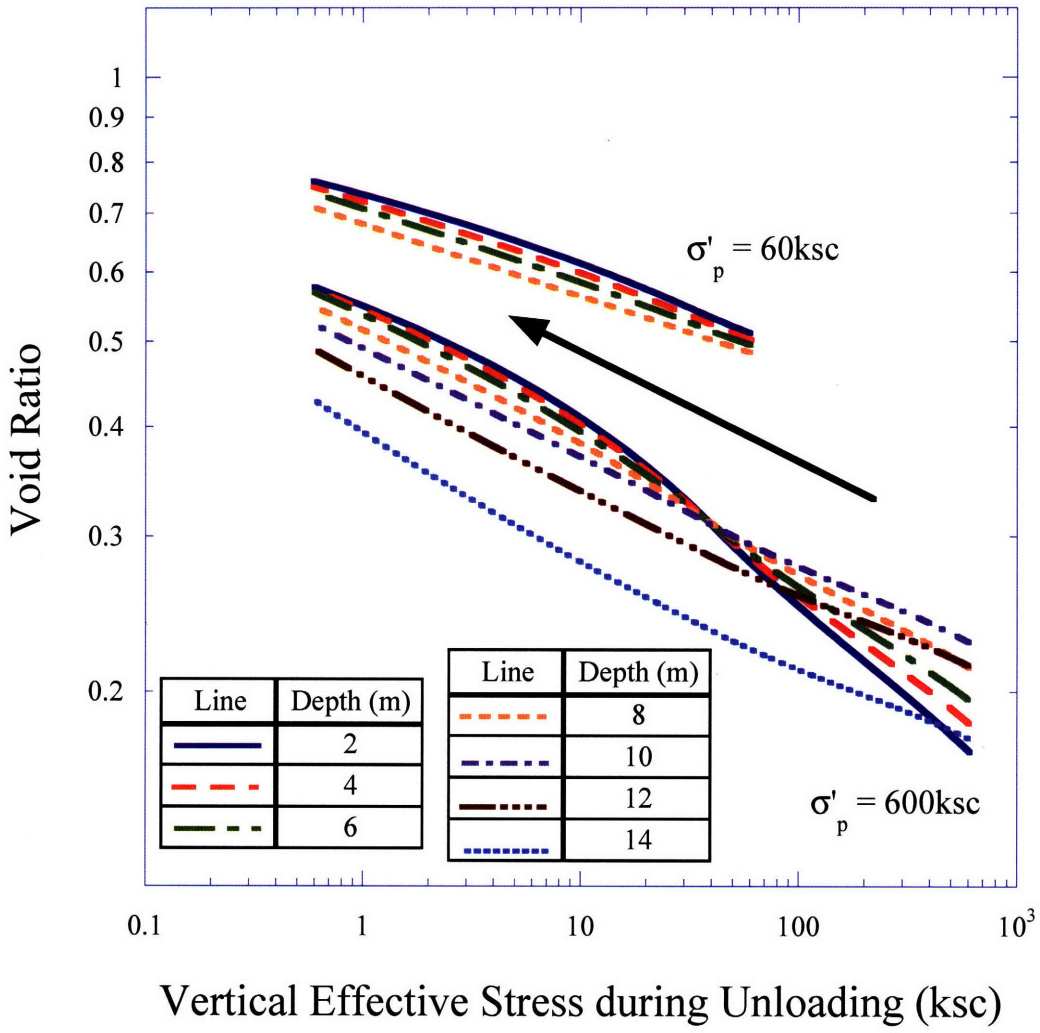

Figure 5-26: Predicted volumetric expansion for various depths and 2 levels of preconsolidation pressure. Input parameters are listed in Table 4-4.

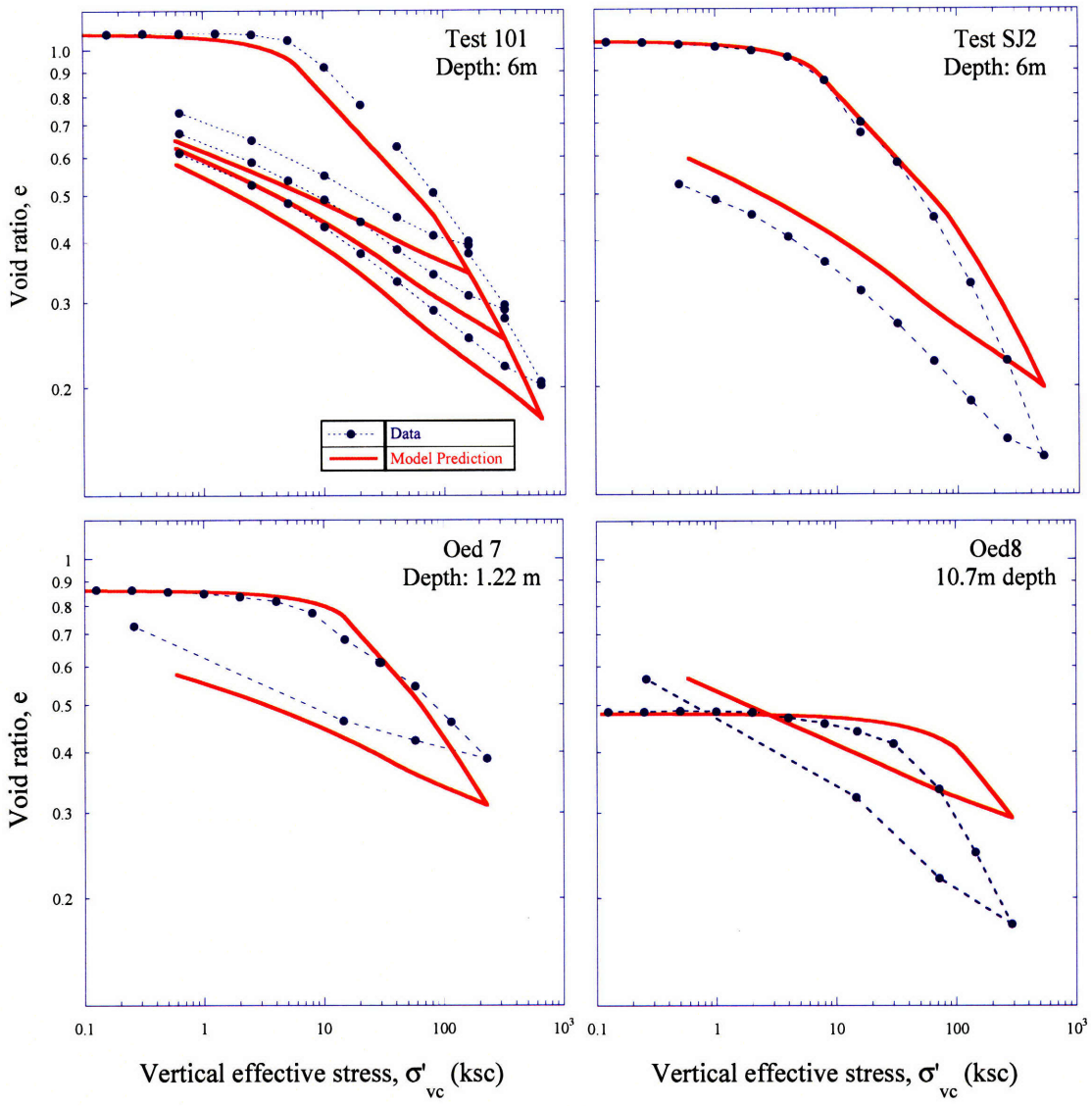

Figure 5-27: Model description of available compression tests on Old Alluvium, with input parameters from Table 4-4.

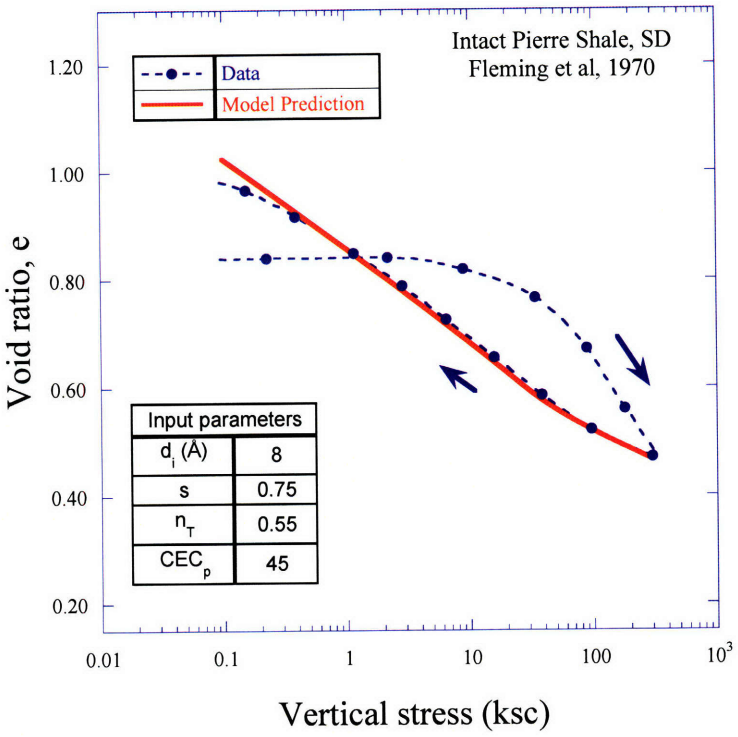

Figure 5-28: Experimental data (Fleming et al, 1970) and model prediction for intact Pierre Shale.

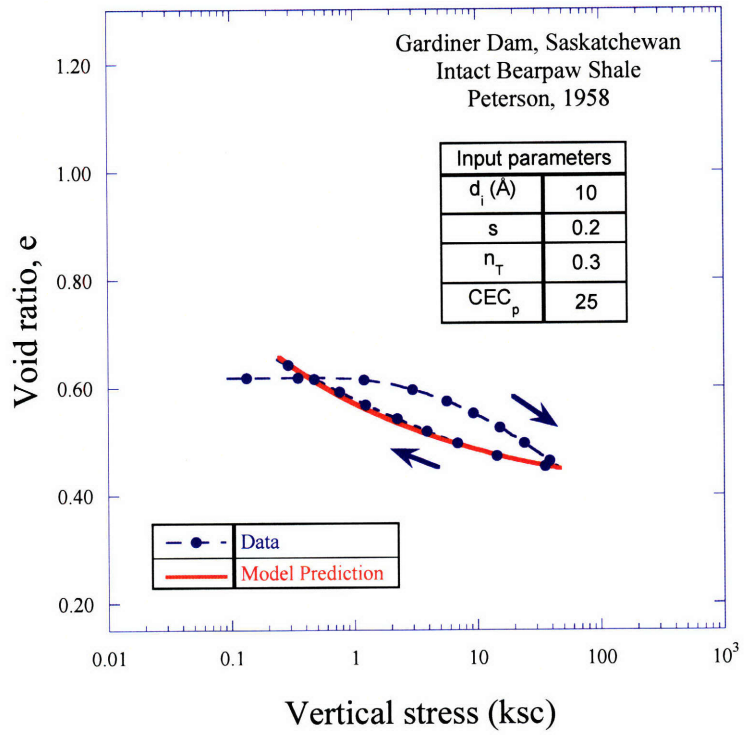

Figure 5-29: Experimental data (Peterson, 1958) and model prediction for intact Bearpaw Shale.

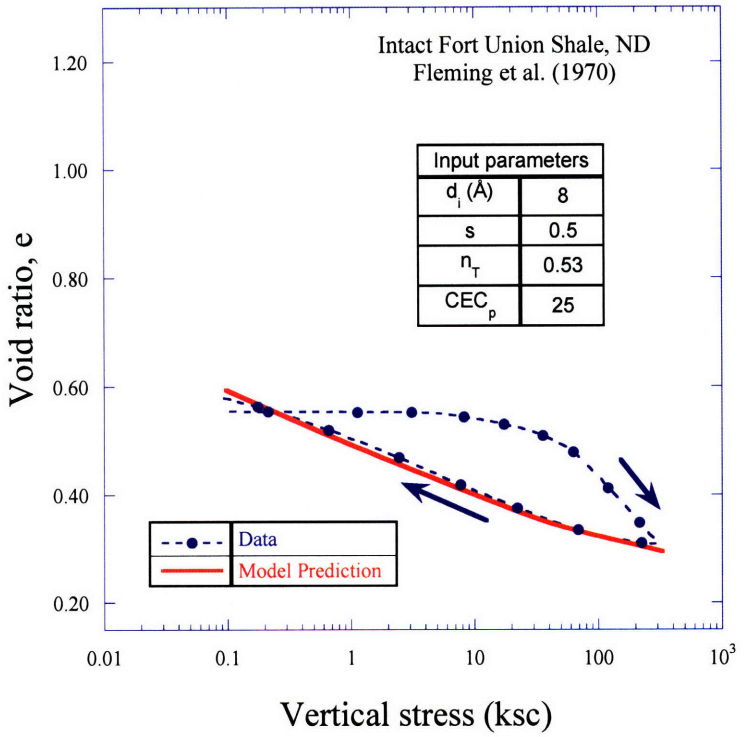

Figure 5-30: Experimental data (Fleming et al, 1970) and model prediction for intact Fort Union Shale.

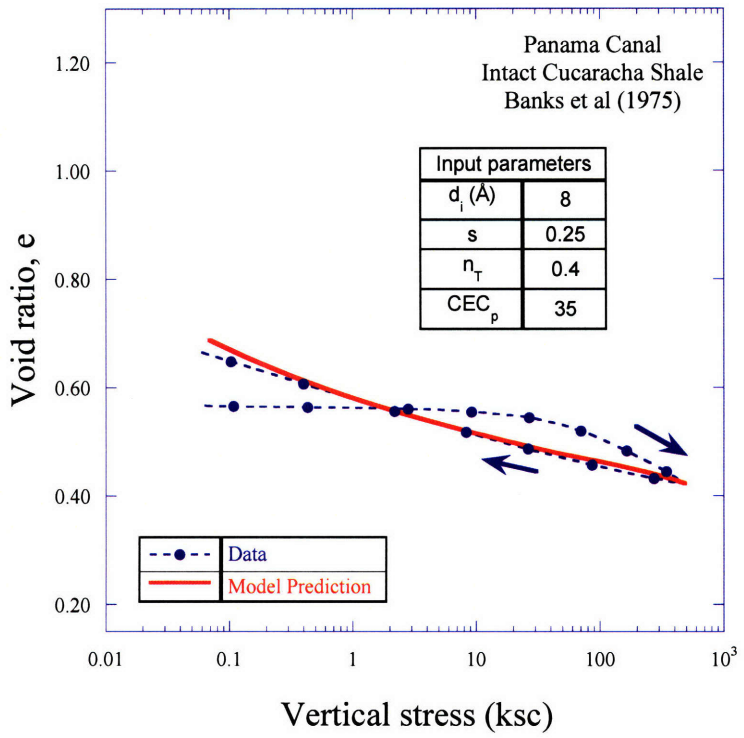

Figure 5-31: Experimental data (Banks et al, 1975) and model prediction for intact Cucaracha Shale.

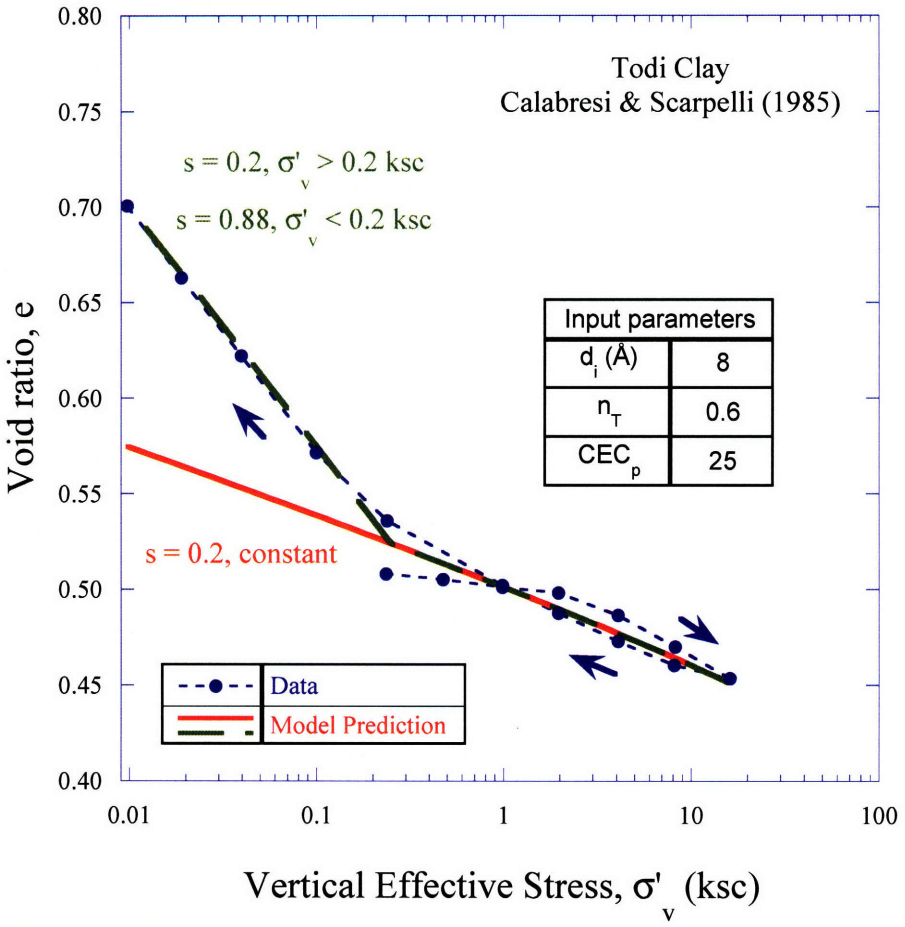

Figure 5-32: Experimental data (Calabresi & Scarpelli, 1985) and model prediction for Todi Clay.

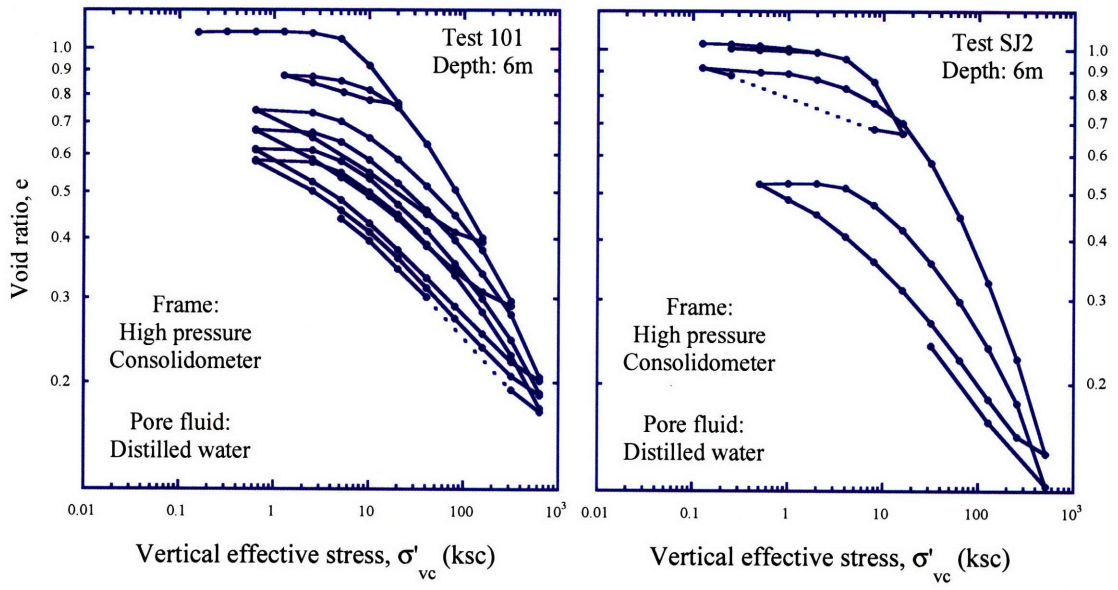

Figure 5-33: Compression data from multiple unload-reload cycles on Old Alluvium.

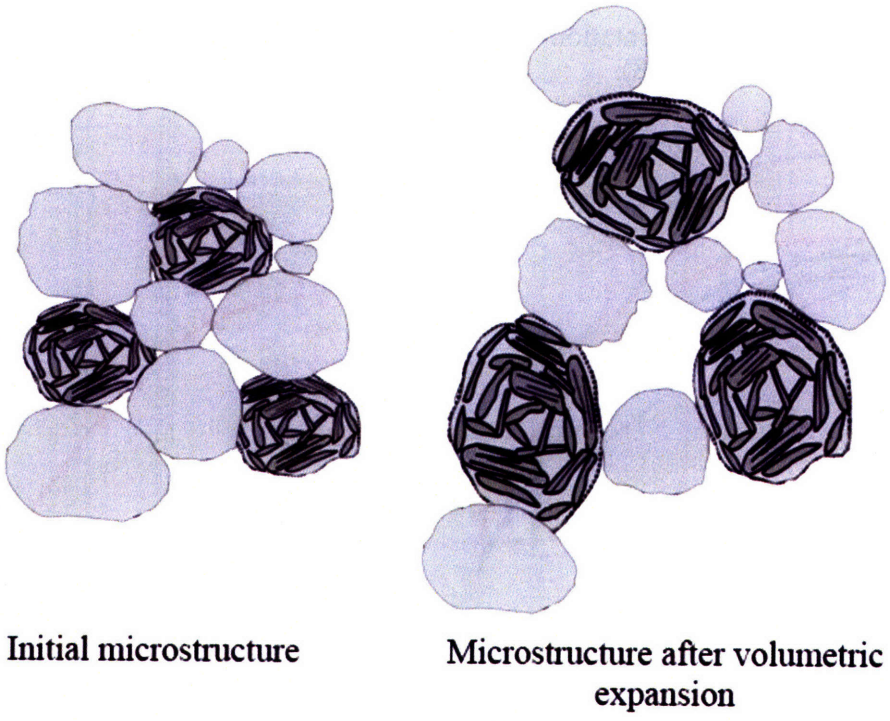

Figure 5-34: Schmematic drawing illustrating the microstructure of Old Alluvium before and after volumetric expansion.

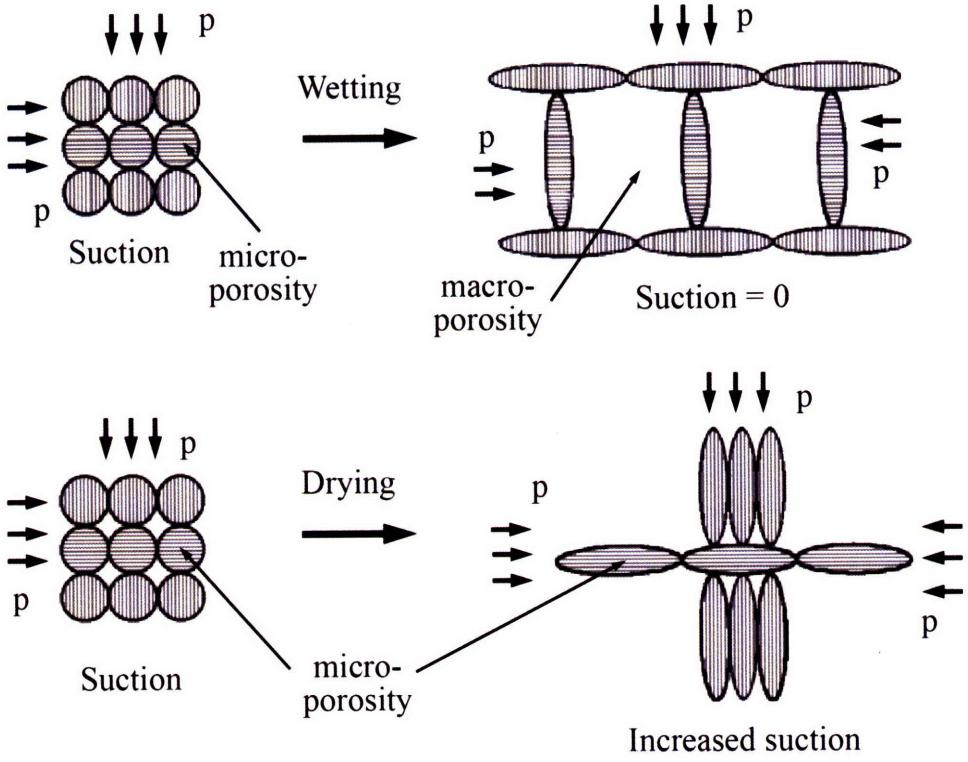

Figure 5-35: Schematic representation of the effect of wetting and drying on the clay microstructure (after Alonso, 1998).

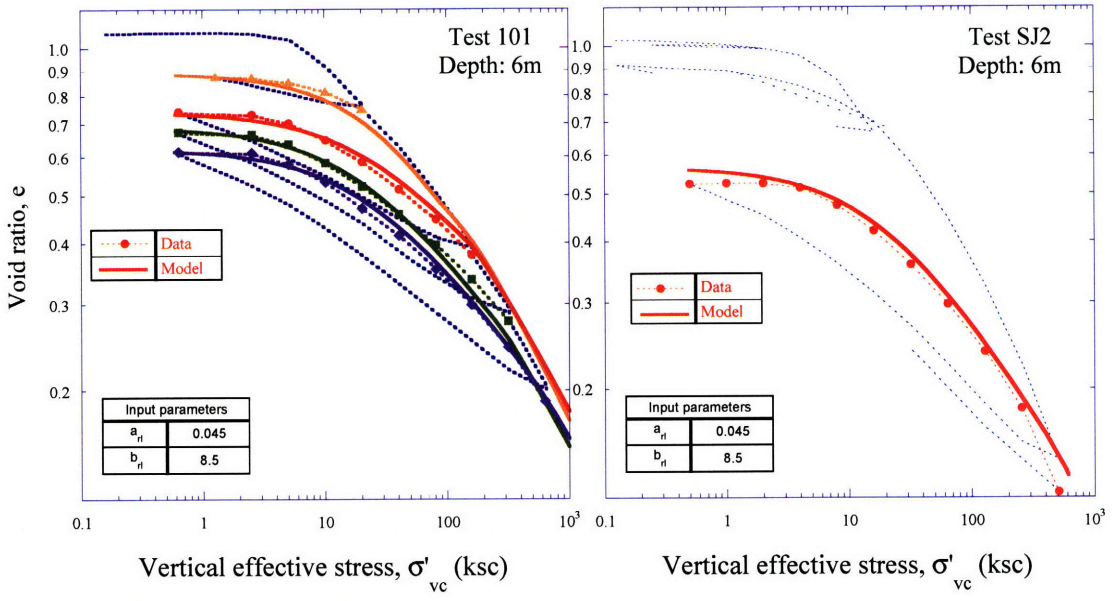

Figure 5-36: Description of reloading response for Old Alluvium, at depth 6m.

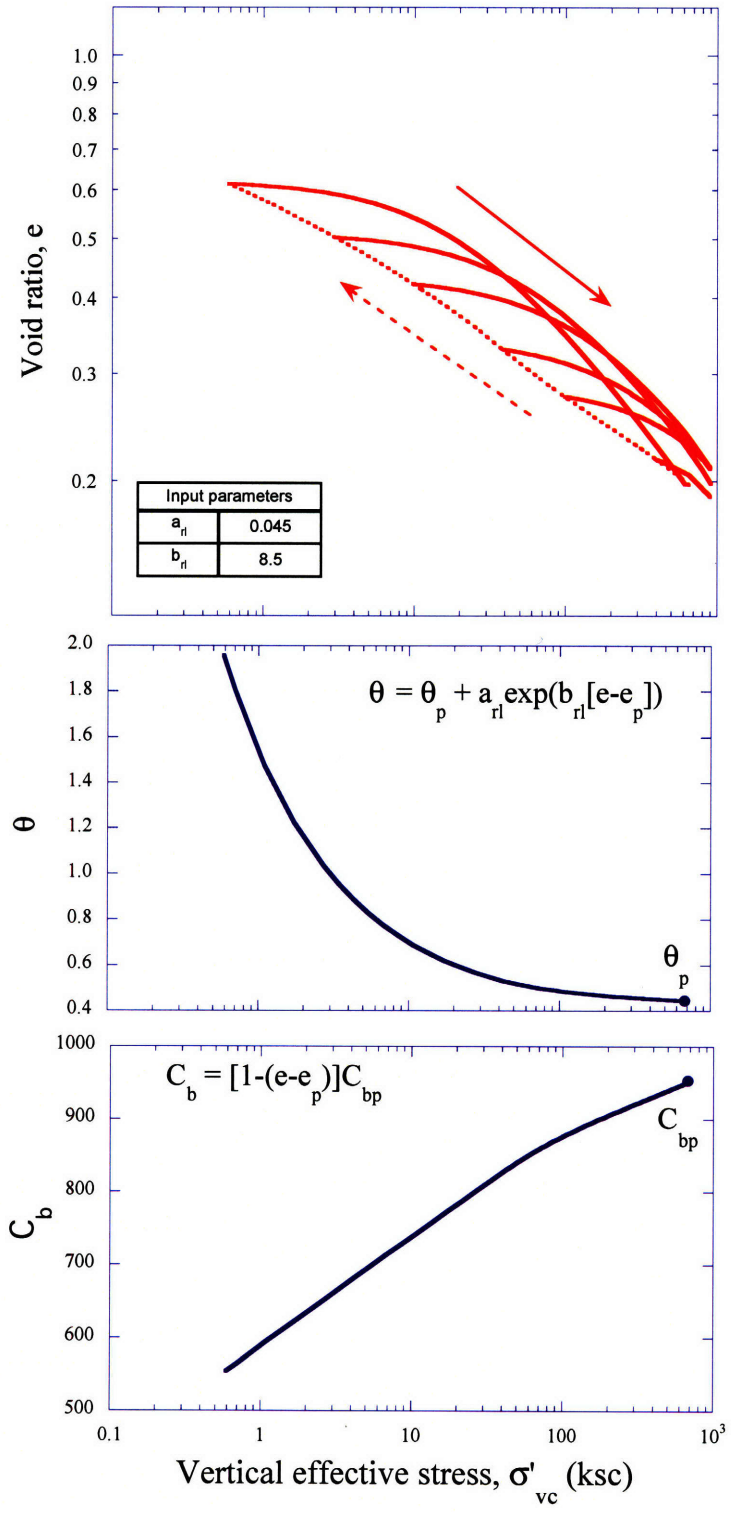

Figure 5-37: Description of reloading response for various degrees of volumetric expansion and corresponding evolution of state parameters θ and C_b.

5.8 APPENDIX 5.I: NONTRONITE AND ADSORBED WATER

a. Nontronite:

Smectite mineral layers are 2:1 phyllosilicate sheets. Depending wheter the isomorphous substitution is taking place in the octahedral (Gibbsite/Brucite) vs. the tetrahedral (silica) sheet, different minerals in the family of smectites are obtained. Nontronite is the result of substitution of Al for Si in the tetrahedral sheet and Fe for Al in the octahedral sheet. Montmorillonite on the other hand, is the result of substitution of Mg for Al in the octahedral sheet only (no substitution in the tetrahedral sheet).

b. Adsorbed water and degree of initial clay hydration

The thickness of the water initially adsorbed on the clay surfaces, and hence the degree of hydration of the clay sheets at the intact structure can be estimated by measurements of the fractions of clay minerals and associated water in the microstructure. Table 5.I-1 summarizes the fractions found in air-dried samples of Upper Clay and Middle Zone samples (Zhang, 2002). The table also reports the density values assumed for each mineral.

	UC Fraction (wt. %)	MZ Fraction (wt. %)	Density (g/cc)
Adsorbed Water	12.43	8.39	1.3
Kaolinite	29.46	21.01	2.62
Nontronite	17.65	11.98	2.3
Illite	-	2.75	2.4
Montmorillonite	-	2.05	2.3

Table 5.I-1: Clay and adsorbed water fractions in the microstructure of the Old Alluvium (Zhang, 2002)

The amount of water adsorbed on the clay surfaces is estimated by calculating the relative volumes of the swelling constituents (nontronite and montmorillonite), based on the clay layer geometry illustrated in Figure 5.I-1. The calculations are summarized in Table 5.I-2. The thickness of the adsorbed water is 12Å for the Upper Clay, and 10.5Å for the Middle Zone.

	Upper Clay		Middle Zone	
	Adsorbed Water	Nontronite	Adsorbed Water	Nontronite Montmorillonite
Mass (g) in 100g	12.43	17.65	8.39	11.98+2.05
Density (g/cc)	1.3	2.3	1.3	2.3 / 2.35
Volume (cc) in 100g	9.56	7.67	6.45	5.2+0.87=6.07
Corresponding thickness (Å) for unit area	9.6	t = 12 [=9.6(9.56/7.67)]	9.6	t = 10.5 [=9.6(6.45/6.07)]

Table 5.I-2: Summary of the calculations for the estimation of the initial hydration of the swelling clay minerals.

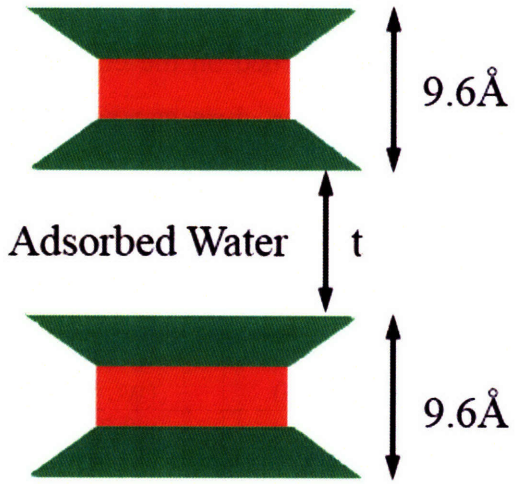

Figure 5.I-1: Schematic geometry of clay layers and associated adsorbed water.

5.9 APPENDIX 5.II: DOUBLE POROSITY SYSTEMS: AN ELASTIC APPROACH

Berryman (2002, 1995) developed a double porosity poroelastic analysis technique for "microgeomaterials". With his technique, and for systems containing two porosities and two types of solid constituents, exact results for all but one of the macroscopic geomechanical constants are derived. The constant missing is taken as the overall drained bulk modulus of the system, which is assumed known or measured independently.

In his thought experiment, Berryman considers a composite porous medium with two distinct types of porous solids, one considered as storage and the other as transport porosity (Figure 5.II-1).

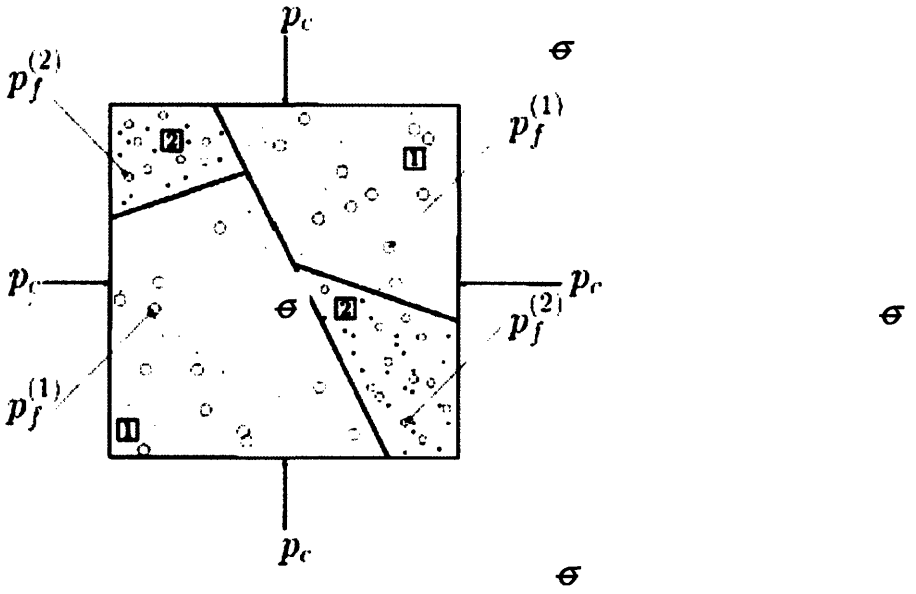

Figure 5.II-1: Berryman's composite porous medium (Berryman, 2002).

Each porous system (i) occupies a volume fraction v^i and has its own drained elastic modulus K^i, skeleton elastic modulus K_s^i, porosity ϕ^i, and subsequently, Biot coefficient b^i, and Skempton coefficient B^i. In addition, there is an overall drained modulus K, and equivalent Biot coefficients b^I, b^{II}, and skeleton moduli N_{ij}.

It is set that $\delta\sigma_m = \delta\sigma_m^{(1)} = \delta\sigma_m^{(2)}$ and expressions for $\delta\sigma_m, \delta p^{(1)}, \delta p^{(2)}$ are sought such that the system is spatially uniform, or self similar, or, in other words, $\delta\varepsilon = \delta\varepsilon^{(1)} = \delta\varepsilon^{(2)}$.

For the general case of all the constituents having a certain degree of compressibility, the system response can be summarized in the following equations:

$$\sigma_m = K\varepsilon - b^I p^{(1)} - b^{II} p^{(2)} \tag{5.II-1}$$

$$\frac{m^{(1)} - m_0^{(1)}}{\rho_{fl}^{(1)}} = b^I \varepsilon + \frac{1}{M_{11}} p^{(1)} + \frac{1}{M_{12}} p^{(2)} \tag{5.II-2}$$

$$\frac{m^{(2)} - m_0^{(2)}}{\rho_{fl}^{(2)}} = b^{II} \varepsilon + \frac{1}{M_{21}} p^{(1)} + \frac{1}{M_{22}} p^{(2)} \tag{5.II-3}$$

where $b^{I,II}$ are the equivalent Biot coefficients and M_{ij} the overall Biot moduli:

$$b^I = b^{(1)} \frac{K - K^{(2)}}{K^{(1)} - K^{(2)}} \tag{5.II-4}$$

$$b^{II} = b^{(2)} \frac{K - K^{(1)}}{K^{(2)} - K^{(1)}} \tag{5.II-5}$$

$$\frac{1}{M_{11}} = \frac{\upsilon^{(1)} b^{(1)}}{B^{(1)} K^{(1)}} - \left(\frac{\upsilon^{(1)}}{K^{(1)}} + \frac{\upsilon^{(2)}}{K^{(2)}} - \frac{1}{K} \right) \left(\frac{b^{(1)} K^{(2)}}{K^{(1)} - K^{(2)}} \right)^2 - \frac{1}{K} (b^I)^2 \tag{5.II-6}$$

$$\frac{1}{M_{22}} = \frac{\upsilon^{(2)} b^{(2)}}{B^{(2)} K^{(2)}} - \left(\frac{\upsilon^{(1)}}{K^{(1)}} + \frac{\upsilon^{(2)}}{K^{(2)}} - \frac{1}{K} \right) \left(\frac{b^{(2)} K^{(1)}}{K^{(1)} - K^{(2)}} \right)^2 - \frac{1}{K} (b^{II})^2 \tag{5.II-7}$$

$$\frac{1}{M_{12}} = \frac{1}{M_{21}} = \frac{b^{(1)} b^{(2)}}{(K^{(1)} - K^{(2)})^2} \left(K - \upsilon^{(1)} K^{(1)} - \upsilon^{(2)} K^{(2)} \right) \tag{5.II-8}$$

and

$$b^{(i)} = 1 - \frac{K^{(i)}}{K_s^{(i)}} = 0 \tag{5.II-9}$$

$$B^{(i)} = \frac{\frac{1}{K^{(i)}} - \frac{1}{K_s^{(i)}}}{\frac{1}{K^{(i)}} - \frac{1}{K_s^{(i)}} + \phi_0^{(i)} \left(\frac{1}{K_f} - \frac{1}{K_\phi^{(i)}} \right)} \tag{5.II-10}$$

Note that the porous materials are assumed microhomogeneous ("Gassmann materials"), and so $K_\phi^{(i)} = K_s^{(i)}$.

Considering now the case of incompressible fluid,

$$\frac{\rho_t^{fl}}{\rho_0^{fl}} = 1 + \frac{p}{K_{fl}} \overset{K_{fl} \to \infty}{\Rightarrow} \rho_t^{fl} = \rho_0^{fl} \tag{5.II-11}$$

so

$$\frac{m^{(i)} - m_0^{(i)}}{\rho_{fl}^{(i)}} = \phi^{(i)} - \phi_0^{(i)} \tag{5.II-12}$$

and the system behavior can be described by:

$$\sigma_m = K\varepsilon - b^I p^{(1)} - b^{II} p^{(2)} \tag{5.II-13}$$

$$\phi^{(1)} - \phi_0^{(1)} = b^I \varepsilon + \frac{1}{N_{11}} p^{(1)} + \frac{1}{N_{12}} p^{(2)} \tag{5.II-14}$$

$$\phi^{(2)} - \phi_0^{(2)} = b^{II} \varepsilon + \frac{1}{N_{21}} p^{(1)} + \frac{1}{N_{22}} p^{(2)} \tag{5.II-15}$$

where now (5.II-16)

$$\frac{1}{N_{11}} = \frac{\upsilon^{(1)} b^{(1)}}{K^{(1)}} - \left(\frac{\upsilon^{(1)}}{K^{(1)}} + \frac{\upsilon^{(2)}}{K^{(2)}} - \frac{1}{K} \right) \left(\frac{b^{(1)} K^{(2)}}{K^{(1)} - K^{(2)}} \right)^2 - \frac{1}{K} (b^I)^2 \tag{5.II-17}$$

$$\frac{1}{N_{22}} = \frac{\upsilon^{(2)} b^{(2)}}{K^{(2)}} - \left(\frac{\upsilon^{(1)}}{K^{(1)}} + \frac{\upsilon^{(2)}}{K^{(2)}} - \frac{1}{K} \right) \left(\frac{b^{(2)} K^{(1)}}{K^{(1)} - K^{(2)}} \right)^2 - \frac{1}{K} (b^{II})^2 \tag{5.II-18}$$

$$\frac{1}{N_{12}} = \frac{1}{N_{21}} = \frac{b^{(1)} b^{(2)}}{(K^{(1)} - K^{(2)})^2} \left(K - \upsilon^{(1)} K^{(1)} - \upsilon^{(2)} K^{(2)} \right) \tag{5.II-19}$$

Coefficients N_{12}, N_{21} obviously control the coupling of the two porous systems. In order to have a distinct double porosity material, this coupling should be minimum. Setting $1/N_{12} = 1/N_{21} = 0$,

$$\frac{1}{N_{12}} = \frac{1}{N_{21}} = 0 \Rightarrow K = \upsilon^{(1)} K^{(1)} + \upsilon^{(2)} K^{(2)} \tag{5.II-20}$$

Equation (5.II-20) provides an expression for the overall drained modulus K as a function of the local moduli $K^{(i)}$ and the volume fractions $\upsilon^{(i)}$ of the porous systems (mixture rule).

Micromechanics derivation.

Following Berryman's thought model, consider a volume Ω consisting at the micro-level of two independent porous materials (Figure 5.II-2).

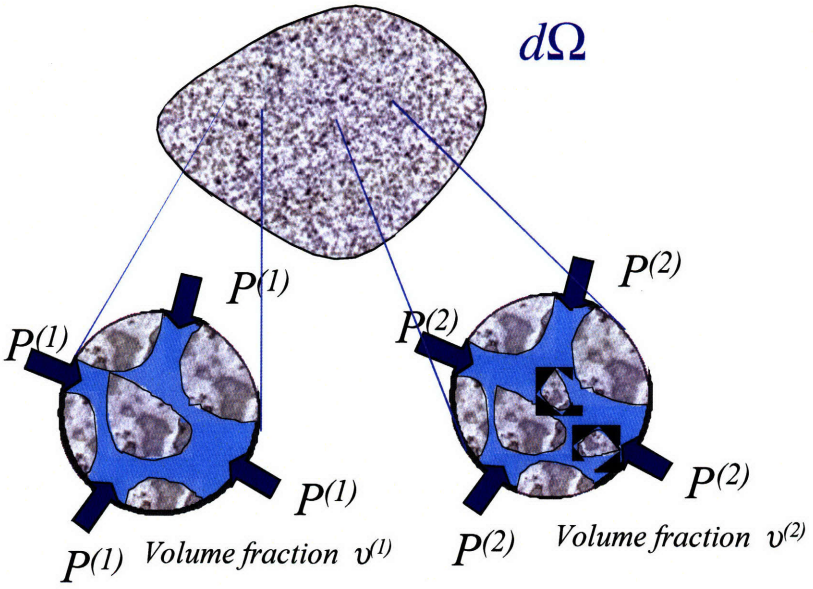

Figure 5.II-2: Volume $d\Omega$ with two porous systems at the micro-level.

Each porous system, in the micro-level, is described by the standard poroelastic equations:

$$\sigma_m^{(i)} = K^{(i)}\varepsilon - b^i p^{(i)} \tag{5.II-21}$$

$$\phi^{(i)} - \phi_0^{(i)} = b^i\varepsilon + \frac{1}{N^i} p^{(i)} \tag{5.II-22}$$

Upscaling can be done using a homogenization process, where the macroscopic stress Σ_m is the volume average of the local stresses σ_m and the macroscopic strain E_m is connected to the local strains ε through a localization factor A^v, which is obtained from an appropriate scheme (for example Mori-Tanaka):

$$\Sigma_m = <\sigma_m>_V \tag{5.II-23}$$

$$\varepsilon = A^v E_m \tag{5.II-24}$$

Considering further that the pressure does not change over scales and that the porosity can simply be upscaled with the corresponding volume fractions,

$$(\phi - \phi_0)_L^{(i)} = \upsilon^{(i)}(\phi - \phi_0)^{(i)} \tag{5.II-25}$$

equation (II.22) can be rewritten as

$$(\phi - \phi_0)_L^i = b_L^i \mathrm{E}_m + \frac{1}{N_L^i} p^{(i)} \tag{5.II-26}$$

or

$$\phi^{(1)} - \phi_0{}^{(1)} = b^I \mathrm{E}_m + \frac{1}{N^I} p^{(1)} \tag{5.II-26(a)}$$

$$\phi^{(2)} - \phi_0{}^{(2)} = b^{II} \mathrm{E}_m + \frac{1}{N^{II}} p^{(2)} \tag{5.II-26(b)}$$

where

$$b_L^i = b^i A^v \upsilon^i \tag{5.II-27}$$

$$N_L^i = \frac{N^i}{\upsilon^i} \tag{5.II-28}$$

Therefore, it is concluded from micromechanics that there should be no coupling between the two porosities.

I-D Think model for double porosity systems.

Following the above research, an appropriate 1-D think model for poroelastic systems of dual porosity should be able to represent equations (5.II-13)-(5.II-15). Further imposed condition of $1/N_{12} = 1/N_{21} = 0$ for double porosity systems will provide an extra relationship for the model's elastic moduli.

Figure 5.II-3 shows such a 1-D think model. There are two porous spaces, space (1) characterized by porosity $\phi^{(1)}$ and porous space (2), characterized by porosity $\phi^{(2)}$. Porosity (2) is in series with porous space (1), connected with a control spring H and coupled to the system {porous space (1); spring K_0} with spring M. The macroscopic stress is σ_m, the macroscopic strain is ε, and the elasticity of the skeleton is represented by the spring K_s. Finally, there is a yield mechanism (ε_p), essential for the further developments of the model, but which will be deactivated in the present analysis since only elastic systems are considered.

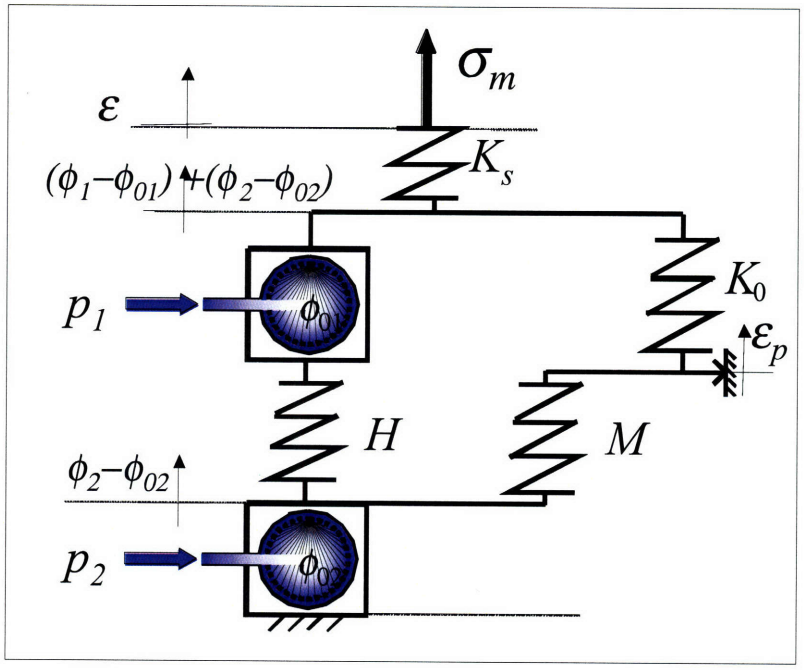

Figure II.3: 1-D Think Model for elastic double porosity systems.

Dissipation of this system is given by (5.II-29):

$$dD = \sigma_m d\varepsilon + p_1 d\phi_1 + p_2 d\phi_2 - d\Psi \geq 0 \tag{5.II-29}$$

with the free energy being:

$$\Psi = \frac{1}{2}K_s\left(\varepsilon - (\phi^{(1)} - \phi_0^{(1)}) - (\phi^{(2)} - \phi_0^{(2)})\right)^2 + \frac{1}{2}K_0\left((\phi^{(1)} - \phi_0^{(1)}) + (\phi^{(2)} - \phi_0^{(2)}) - \varepsilon_p\right)^2 + \frac{1}{2}M\left(\varepsilon_p - (\phi^{(2)} - \phi_0^{(2)})\right)^2 + \frac{1}{2}H\left((\phi^{(1)} - \phi_0^{(1)}) - (\phi^{(2)} - \phi_0^{(2)})\right)^2 \tag{5.II-30}$$

With $\sigma_m = \frac{\partial \Psi}{\partial \varepsilon}, p^{(1)} = \frac{\partial \Psi}{\partial \phi^{(1)}}, p^{(2)} = \frac{\partial \Psi}{\partial \phi^{(2)}}$, and ignoring the yield mechanism, the state equations of the system are given by the following equations:

$$\sigma_m = K\varepsilon - b^{(1)}p^{(1)} - b^{(2)}p^{(2)} \tag{5.II-31}$$

$$(\phi^{(1)} - \phi_0^{(1)}) = b^{(1)}\varepsilon + \frac{1}{N_{11}}p^{(1)} + \frac{1}{N_{12}}p^{(2)} \tag{5.II-32}$$

$$(\phi^{(2)} - \phi_0^{(2)}) = b^{(2)}\varepsilon + \frac{1}{N_{21}}p^{(1)} + \frac{1}{N_{22}}p^{(2)} \tag{5.II-33}$$

with

$$b^{(1)} = \frac{2H + M}{4K_0H + K_0M + 4K_sH + K_sM + HM}K_s \tag{5.II-34}$$

$$b^{(2)} = \frac{H}{4K_0H + K_0M + 4K_sH + K_sM + HM}K_s \tag{5.II-35}$$

$$\frac{1}{N_{11}} = \frac{K_0 + K_s + H + M}{4K_0H + K_0M + 4K_sH + K_sM + HM} \quad (5.II\text{-}36)$$

$$\frac{1}{N_{22}} = \frac{K_0 + K_s + H}{4K_0H + K_0M + 4K_sH + K_sM + HM} \quad (5.II\text{-}37)$$

$$\frac{1}{N_{12}} = \frac{K_0 + K_s - H}{4K_0H + K_0M + 4K_sH + K_sM + HM} \quad (5.II\text{-}38)$$

It can be easily seen that equations (31)-(33) are essentially the same with target equations (13)-(15). Furthermore, imposing $1/N_{12} = 1/N_{21} = 0$:

$$H = K_s + K_0 \quad (II.39)$$

Double porosity theory and Old Alluvium.

The discussed poromechanical approach was considered for Old Alluvium, since it can offer a thermodynamically accepted way to model the physicochemical changes in the clay micro-porosity. However, the model requires knowledge of the mass volume fractions of the various micro-constituents as well as their elastic properties. Furthermore, it assumes the existence of a continuous "matrix" material. These assumptions do not appear to describe the observed micro-structure and hence, this approach has not been pursued further in this thesis.

6 Summary, Conclusions and Recommendations

6.1 SUMMARY AND CONCLUSIONS

This thesis has proposed a new constitutive model, which is capable of describing the compression behavior of soils with a complex microstructure that evolves due to the application of external loading.

The thesis has contributed in the study of tropical and/or weathered soils in the following:

- A better understanding of how some aspects of mechanical macroscopic behavior can be affected by geological formation processes and weathering mechanisms.

  In the Old Alluvium the macrostructure of the intact soil does not interact with the expansive clay minerals because of the salinity of the micro-porosity and the local aggregation of oxides. Hence the isolation of the two scales is not purely mechanical, but rather physicochemical. In this case, the breakdown of the soil structure can be the result of both mechanical damage and electro-chemical changes facilitated by the mechanical damage. Microstructural characteristics such as the orientation of clay minerals, the salinity of the adsorbed water, the nature and amount of aggregated cations are a direct consequence of the geologic formation and weathering processes and can play a very important role on the macroscopic response of the soil.
- The appreciation that a reference state, as established by Burland (1990) for bonded soils, may not be unique for structured but weathered soils.

  In such soils, breakdown is the result of both mechanical and chemical changes. Because the electro-chemical changes are affected by the mechanical loads, the structural degradation depends on the applied loading path, hence there may be various reconstituted states.
- The formulation of a modeling approach that does not refer to a reconstituted state, but rather varies the compressibility parameters in order to reflect changes in the soil structure and mineralogical content.

  The model introduces the Cation Exchange Capacity (CEC) as a state variable that maintains information of the clay activity in the microstructure. This offers a way to account for such changes as the revelation of active clay minerals or the variation of their surface

properties. Therefore, a link is established between the macroscopic compressibility and physicochemical processes that occur in the microstructure. Furthermore, since Cation Exchange Capacity is monotonically increasing in these tests, it provides a suitable measure of accumulation of plastic strains due to degradation (increased compressibility).

- The introduction of a swelling model that depends directly on the physicochemical characteristics of the soil and can accommodate the evolution of these characteristics during a loading cycle, due to macroscopic mechanical or chemical loading.

The model derives from the double layer theory, and so is related to double layer swelling in the microstructure. As it depends on the Cation Exchange Capacity at load reversal, it is able to vary according to the microstructural changes during compression loading. The formulation has a similar structure with previous swelling models (e.g. MIT-S1). However, the main coefficients are not input parameters that are fitted on experimental unloading data, but variables that are derived directly from the physicochemical characteristics of the soil (Cation Exchange Capacity).

The new formulation requires input parameters that are related to:

- the compression characteristics of the intact soil
- the stress levels along which the structural changes take place
- the Cation Exchange Capacity of the intact soil and the CEC after disaggregation (obtained for example by chemical treatment)
- an estimation of the amount of expandable minerals in the microstructure,
- the degree of initial hydration of the clay mineral stacks.
- the degree of interaction between the micro and the macro structure

The parameters can be determined directly through standard laboratory measurements in oedometer tests. Comparison of the model predictions with the available compression data on the Old Alluvium showed that the formulation is able to describe very well both the response to compressive loads and the volumetric expansion of the specific tropical soil.

The proposed formulation is not specific to the Old Alluvium. The ability of the formulation to trace changes in the microstructure, and link both the compressibility and the swelling response to the evolution of the soil's physicochemical properties applies to the modeling of materials with evolving physicochemical characteristics in the microstructure.

Such soils are encountered in many parts of the world. Other Old Alluvium formations are found is South-East Asia, for example in Singapore (Shirlaw et al, 2000). But a tropical climate is not a necessary condition. Clayey materials with stacks of expandable (clay) minerals exhibit similar dependence on mechanical and physicochemical factors. In addition, many clays are reported to have analogous observed behavior. Rampello (1991) reports that in the case of Todi clay, destructuration similar to that caused by compression could also be reached by drying the soil. Cotecchia & Chandler (1998) also discuss that the carbonate bonding of Pappadai clay can be significantly reduced by drying. Finally, data compiled by Bertuccioli & Lanzo (1993) on several Italian clays illustrates that their clay fraction increases considerably after mechanical disaggregation (Figure 6-1a) and that the clays exhibit significant volumetric expansion (Figure 6-1b).

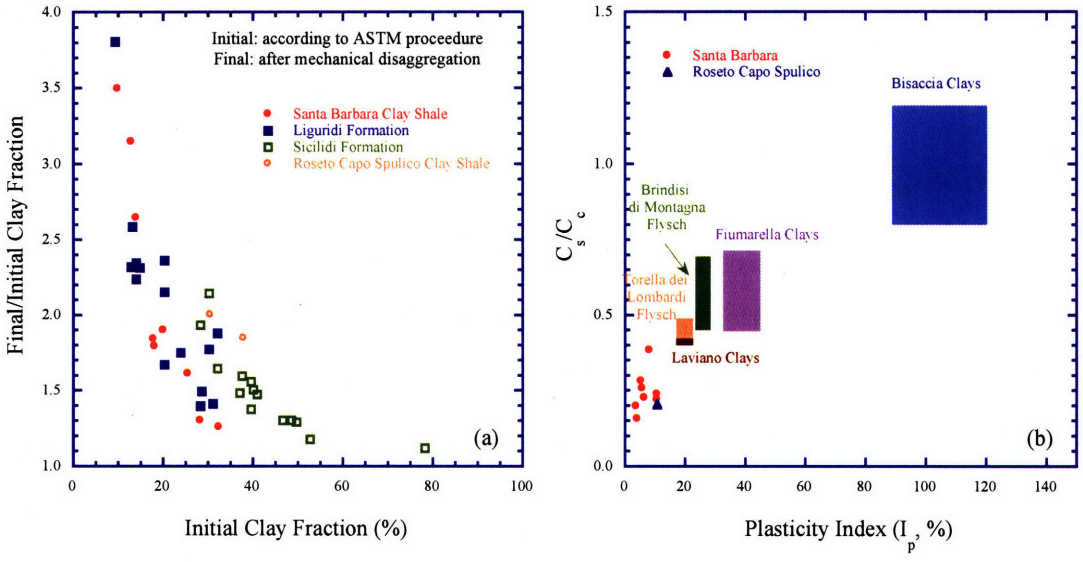

Figure 6-1: Mechanical properties of structurally complex Italian clays: (a) Influence of treatment procedures on clay fraction (b) Ratio of Swelling to Compression coefficient (after Bertuccioli & Lanzo, 1993)

The presence of these materials has significant engineering implications:

- Even if they show a high initial hydraulic conductivity, they may not be used as filters or other permeable functional fills (e.g., back fill for retaining walls), because construction processes such as compaction will destroy any cementation bonding, and reveal the high swelling potential.
- They may, however, be suitable to be used as impermeable barriers after sufficient structure breakdown.
- In excavations, tunneling, preloading and surcharging (unloading related constructions) much larger expansive deformations should be expected, since construction may damage the intact structure, and reveal the soil's swelling potential.
- Exposure of the soil to environmental conditions (at excavation walls or tunnel faces) can induce air drying and hence, deterioration of the soil structure
- The time required for the completion of consolidation will be much larger than calculated with the initial coefficient of consolidation, since the later may change significantly under construction loading.

Therefore, the proposed modeling approach can benefit the understanding of soil behavior and the construction practice in more than one geographical regions.

6.2 RECOMMENDATIONS

Recommendations for further research can be discussed in two main directions: (a) research related to Old Alluvium in Puerto Rico and the proposed model, and (b) study of weathered tropical materials.

As far as Old Alluvium is concerned, further experimental work is required to validate the proposed formulation and further expand it:

- There isn't yet a complete understanding of the behavior of Old Alluvium during reloading. It is not clear why the soil exhibits such a significant hysteresis and to what extend this is connected to hysteresis observed in the micro-scale during adsorption and desorption of water by the clay mineral stacks. Furthermore, it is surprising that despite the large volumetric

expansion and the hysteretic behavior, unload-reload cycles appear to be reversible and repeatable. In order to better understand the soil behavior, a series of compression tests is needed that would include reloading from different stages of the unloading curve, and further unloading from intermediate levels of reloading. Microscopy observations from various stages of the unload/reload cycles could also offer valuable insight.

- Measurements of the Cation Exchange Capacity values at different degrees of mechanical disaggregation during loading would provide a better understanding of the microstructural changes and validate the proposed model for the evolution of clay activity.
- Elastic deformations seem to be small and cannot be observed directly from the macroscopic strains measured in the existing oedometer tests. Bender element measurements at load reversal from various levels of disaggregation are required to provide a better understanding of the changes in elastic properties.
- Beyond the compression behavior, there are very few indications on how the Old Alluvium would respond to shear loading. Systematic testing is required to understand how the changes induced during compression would affect the shear behavior of the soil. In order to establish the evolution of effective stress envelope with the degree of disaggregation, multiple tests are needed for each level of mechanical breakdown. In addition, the opposite interaction should be studied. The application of shear loading (not necessarily up to failure) will induce disaggregation and changes in the soil microstructure. Therefore, shear loading is expected to affect the compressibility of the material and probably alter significantly its swelling characteristics. Such behavior is evident in field observations that report dramatic increase of the soil plasticity during advance of a TBM (Whittle & Bernal, 1993 for the Old Alluvium in Puerto Rico; Chiam et al, 2003 for the Old Alluvium in Singapore).
- Finally, it has been discussed that drying induces irreversible damage on the Old Alluvium. The behavior of the soil should hence be studied during repeated wetting and drying cycles, with the objective to develop a more complete formulation for partially saturated states.

With the experience gained from the study of the Old Alluvium in Puerto Rico, the next logical step is to study the Old Alluvia of SE Asia. Construction in the uplands of Singapore has encountered an Old Alluvium with similar deposition and weathering history as the one in Puerto Rico. Mineralogical and microstructural analyses will confirm the suspected similarities and an

experimental program including Cation Exchange Capacity measurements and a high pressure compression test with unloading cycles will enable the application of the proposed model to the Old Alluvium in Singapore.

More generally, soils with complex microstructural characteristics have not been systematically studied and more effort is required to understand and properly model their behavior:

- It is very important to develop techniques to measure soil properties, such as the Cation Exchange Capacity, or the Specific Surface Area without disrupting the structure, as this would result in differences in the obtained values. The ability to observe the structure at various stages of disintegration would also provide significant insight. Cotecchia & Chandler (1998), for example, obtained SEM observations of Pappadai clay by compressing to the different stress levels, quickly unloading (with the oedometer cell emptied of water) and then freezing the dried sample and gold coating it.
- Furthermore, weathered tropical soils are characterized by significant spatial variability. Void ratio alone is not sufficient to establish a characteristic profile of the soil properties. Systematic experimental testing on many samples from a three-dimensional grip within the soil is required to relate the spatial variability with easily measured soil characteristics, such as the Atterberg limits, and hence to formulate a consistent parameter selection with depth.
- Experiments are needed to study the rate and temperature effects on weathered structured soils. It is possible that differences in the applied strain rate would alter the disaggregation path and hence lead to different end states. On these lines, Rocchi et al (2003) have proposed an approach that takes into account the interaction between destruction processes and strain rate effects. However, few experimental observations exist to enable a good understanding of the behavior (Leroueil, 2000)
- Biological effects on soil compressibility and the mechanical behavior should also be considered, especially for soils in the tropics (Barksdale & Blight, 1997). Gates et al (1998), for example, report some dependence of the swelling pressure and deformations of iron bearing smectites on the presence of autotrophic bacteria that use iron in the absence of carbon to produce energy.

- A lot of the tropical weathered soils exist above the groundwater table, therefore the effect of negative pore pressures and suction are important. In soils with microstructure similar to the Old Alluvium, characterized by micro-aggregation and micro-scale pore spaces, changes in the relative humidity can be sufficient to induce disaggregation and changes in the macroscopic compressibility (Oldecop & Alonso, 2001). Therefore, the nature of environmental loading (pattern of rainfall for example) can be significant.
- The understanding of the behavior of weathered soils with complex microstructure can lead to the development of simple techniques to identify them in the field. This will certainly benefit construction in tropical areas. Such procedures can be the measurement of Atterberg limits not only in the natural state but also after a specific mincing time, or air-drying. If increase in plasticity were observed, study of the microstructure would be required.

6.3 REFERENCES

Barksdale R.D., Blight G.E. (1997): "Compressibility and settlement of residual soils", Chapter 8 in Mechanics of Residual Soils, G.E. Blight, Balkema

Bertuccioli P., Lanzo G. (1993): "Mechanical properties of two Italian structurally complex clay soils", Geotechnical Engineering of Hard Soils – Soft Rocks, Anagnostopoulos et al (editors), Balkema, 383-389.

Chiam S.L., Wong K.S., Tan T.S., Ni Q., Khoo K.S., Chu J. (2003): "The Old Alluvium", Underground Singapore 2003 Engineering Geology Workshop.

Cotecchia F., Chandler R.J. (1998): "One-dimensional compression of a natural clay: Structural changes and mechanical effects", The Geotechnics of Hard Soils – Soft Rocks, Evangelista & Picarelli (editors), Balkema, 103-114.

Gates W.P., Jaunet A.M., Tessier D., Cole M. A., Wilkinson H. T., Stucki J. W. (1998): "Swelling and texture of iron bearing smectites reduced by bacteria", Clays & Clay Minerals, 46 (5), 487–497.

Leroueil S. (2000): "Contribution to Round Table: Peculiar aspects of structured soils", The Geotechnics of Hard Soils – Soft Rocks, Evangelista & Picarelli (editors), Balkema, 1669-1678.

Oldecop L.A., Alonso E.E. (2001): "A model for rockfill compressibility", Géotechnique, 51 (2), 127-139.

Rampello S. (1991): "Some remarks on the mechanical behavior of stiff clays: the example of Todi clay", Proceedings of the international workshop on experimental characterization and modeling of soils and soft rocks, Napoli, 131-190.

Rocchi G., Fontana M., Da Prat M. (2003): "Modeling of natural soft clay destruction processes using viscoplasticity theory", Géotechnique, 53 (8), 729–745.

Shirlaw J.N., Hencher S., Zhao J. (2000): "Design and construction issues for excavation and tunneling in some tropically weathered rocks and soils", Proceedings of the GeoEng2000cInternational Conference on Geotechnical, Geological Engineering, Melbourne, Australia.

Whittle A.J., Bernal J. (2003): "Stacked Drift Construction of a Large Cavern in Weathered Alluvium", Proceedings of the Soil and Rock America Conference, MIT, Cambridge MA, 2315-2322.